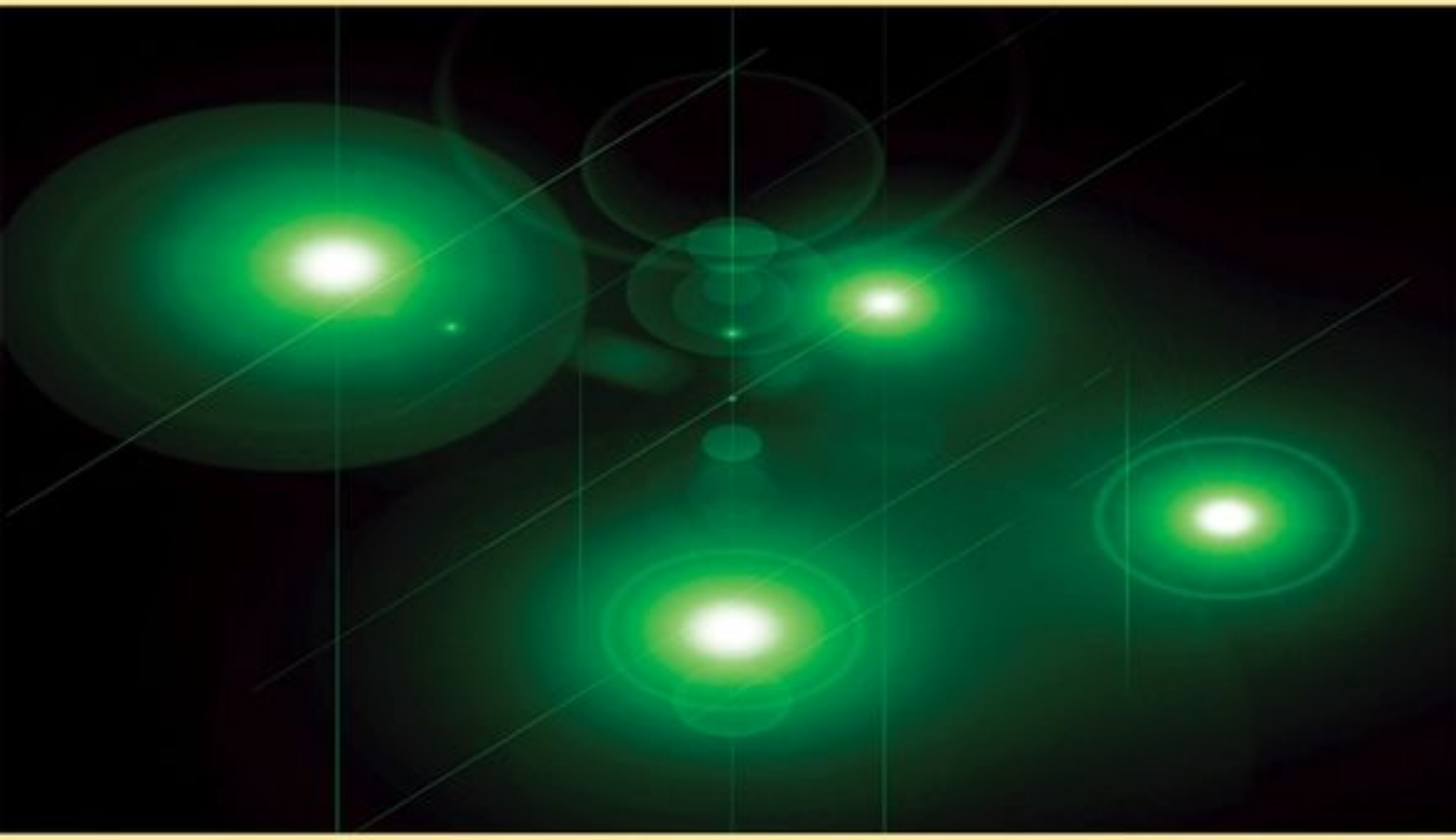

Photonic Waveguides

Azzedine Boudrioua

iSTE

WILEY

This page intentionally left blank

Photonic Waveguides

This page intentionally left blank

Photonic Waveguides

Theory and Applications

Azzedine Boudrioua

Series Editor
Pierre-Noël Favennec

ISTE

WILEY

First published in France in 2006 by Hermes Science/Lavoisier entitled *Optique intégrée théorie et applications* © LAVOISIER, 2006
First published in Great Britain and the United States in 2009 by ISTE Ltd and John Wiley & Sons, Inc.

ISTE Ltd
27-37 St George's Road
London SW19 4 EU
UK

www.iste.co.uk

John Wiley & Sons, Inc.
111 River Street
Hoboken, NJ 07030
USA

www.wiley.com

Library of Congress Cataloging-in-Publication Data

Boudrioua, Azzedine.
[Optique intégrée. English]
Photonic waveguides : theory and applications / Azzedine Boudrioua.
p. cm.
Includes bibliographical references and index.
ISBN 978-1-84821-027-1
1. Integrated optics. 2. Photonics. I. Title.
TA1660.B68 2009
621.36'93--dc22

2009005091

British Library Cataloguing-in-Publication Data
A CIP record for this book is available from the British Library
ISBN: 978-1-84821-027-1

Printed and bound in Great Britain by CPI/Antony Rowe, Chippenham and Eastbourne.

Table of Contents

This page intentionally left blank

Foreword

The various properties of light are the basis of many applications in sectors as varied as biology, metrology and telecommunications. Control of the propagation of light is not easy to achieve; photons, like electrons, do not easily obey and cunning must be used to obtain the desired effect. As with electrons, we need to carry out optical signal processing for data transmission and treatment. For this it is important to control the photons at different levels: their generation and detection, as well as their propagation in the matter.

In recent decades, optics has escaped from the tradition which used the propagation in open space, by using optical fibers and integrated optical components. The use of optical fibers has allowed control of the propagation of spatially confined light, without notable losses of power at long distances. The use of photon properties opens the door for many devices. Treatment of the visible signal is designated to integrated optical devices due to the use of photon properties. As for electronic integrated circuits, there will be on the same "chip" optical functions either of emission or of photo-detection with their electronic monitoring circuit and all the optical connectors between components. These photonic integrated circuits must allow good fabrication reproducibility and, moreover, are adapted to collective fabrication in great numbers.

Waveguides of integrated optics constitute one of the most important elements in the building of all-optical technology. Thanks to the work undertaken in parallel by theorists, Maxwell's equations, technologists and experimenters, the fabrication and characterization of integrated optics components has taken great steps towards really miniaturized integrated optics and there is more to come. To improve the performances of integrated optics in the treatment of the signals as well as in the optical switching systems, it is necessary to modify and create new two-dimensional or three-dimensional guiding structures controlled on a micrometric or even on a nano-metric scale.

This book by Azzedine Boudrioua is interested particularly in waveguides of integrated optics. Certain works cover one particular aspect, theory or characterization. This book covers all the aspects of waveguides, from theoretical descriptions to fabrication and applications. This book on integrated optics gives the state of the art of this area of optics, developed a few decades ago but still under development, especially with the appearance of photonic crystals. The work is not only limited to the linear aspect of waveguides; indeed a chapter is dedicated to non-linear effects in waveguides, and another focuses on electro-optical effects and the devices using these effects. The book ends with a chapter on photonic crystals. This chapter, written as an introduction to these new components, provides the reader with an understanding of components controlled on a nano-metric scale, which belong to the field of the nanotechnologies.

Boudrioua's objective was to produce an explanatory, accessible work for researchers and students that would provide a good starting point for those interested in acquiring knowledge in the field of integrated optics. From my point of view, the present work filled this objective perfectly. To my knowledge there are few works covering all of the subjects described in this work at the time of publication, and there is no doubt that it will become a well used reference.

Frédérique de Fornel
Director of research at CNRS
University of Bourgogne

Acknowledgments

The existence of this book is a happy corollary of a profitable exchange of ideas with Mrs Frederique de Fornel (Director of Research at the CNRS, University of Dijon) at the time of a visit to her very friendly company between Valence and Dijon in November 2003, after having taken part in the National Days of Guided Optics (JNOG 2003). I would like to express here my gratitude for and recognition of the encouragement and support that she gave me.

I also testify my gratitude to Mr Pierre Noël Favennec, who followed the development of this project with much patience. His availability, kindness, assistance and encouragement touched me greatly. He did everything to make this project become reality.

It is sometimes providential meetings that positively influence the path of a person. It was thus here with the meetings with Mrs Frederique de Fornel and Mr Pierre Noël Favennec.

This work would probably never have been conceived without the contribution of my colleague and friend Régis Kremer (Lecturer at the University of Metz) with whom I have shared all these years of research. A tremendous recognition to Régis; he never failed in his support and his encouragement especially in the difficult moments spent together. My most cordial thanks also go to his wife Sylvie Kremer (Lecturer at the University of Metz) for the second reading of the manuscript. These same thanks are extended to Ahmed Brara (Doctor of Mechanics of Materials and Director of Research) who helped me to make this manuscript readable. The many discussions with my friend Ahmed were of great importance to me.

For clarity, the preparation of this book required the utilization of various PhD theses manuscripts which I have had the opportunity to supervise these past years.

For this reason, all PhD students who have allowed the use of passages or figures from their manuscripts are also warmly thanked.

Azzedine BOUDRIOUA

Introduction

For ten years, optical telecommunications have had spectacular success, thanks to the explosion of the Internet. This spectacular development is the fruit of a great research and development effort in the field of guided optics, which led to the improvement of the performances of optical fibers. Appearing at the same time was the need to develop optical and optoelectronic components with a planar technology, able to generate, detect, modulate or commutate light, using waveguiding structures. This field of investigation is called integrated optics.

The research and developments undertaken in these two fields (guided and integrated optics) made it possible to provide on the market, optoelectronic components of any kind at low cost. Consequently, other applications in various fields were also developed.

As a matter of fact, today the use of optics includes strategic fields like space, military fields and also fields in everyday life like data storage (CD and DVD), medicine and unsuspected sectors like the car industry.

In a competitive way, the advent of nano-photonics is pushing the limits of photonic system miniaturization to scales lower than the wavelength. Ultimately, the 20^{th} century was the century of electronics, and the 21^{st} century will probably be the century of photonics. The basic idea supporting the use of the photon rather than the electron comes from the very high optical frequencies (200 THz), which allow a very broad bandwidth and offer an unequaled data transmission capacity.

Although optics is a very old science, its major improvements were made during the last quarter of the century. The first work on optics is from the School of Alexandria, Euclid (325-265 BC). However, the reform of optics was undertaken by the Muslim scientists of the medieval period with, at their head Al-Kindi (801-873) and especially Ibn Al-Haytham known under the name of Alhazen (965-1040). This

famous scientist truly created the foundation of modern optics with his experimental approach to the propagation of light. He, indeed, introduced experimentation into physics and provided the basis for understanding the luminous phenomena and the control of light propagation (reflection and refraction).

The heritage of this eminent scientist was transmitted to us through his major book "Kitab Al-Manazir" (*The Book of Vision*) which was translated into Latin and distributed throughout western countries at the beginning of the 13th century. This book was used as a reference until the 17th century and influenced work on optics of the majority of renaissance period scientists. The first philosopher who studied and diffused Ibn Al-Hyatham's work was his enthusiastic disciple Roger Bacon (1214-1292). He was aware of the importance of the Muslim heritage in the fields of science and philosophy. The science historian Gerard SIMON wrote:

> *Roger Bacon was the first to know the Optics of Alhazen (Ibn Al-Haytham) very well... he contributed to its diffusion and he particularly built on it his own work on optics, the Perspective and Multiplication Specierum* (towards 1260-1265)*... he thus accurately followed the analysis of the role of light, the description of the eye, theory of perception and the study of reflection and refraction formulated by Alhazen*. [Adding:] *Kepler renews optics (Paralipomena AD Vitellionem) around 1604 thanks to reading Alhazen and Witelo*.

D.C. Lindgerg emphasizes that Roger Bacon and Johannes Kepler were without any doubt the best disciples of Alhazen (*Optics & Photonics News*, 35 (2003)).

If the revolution of the concepts relating to light sometimes took several centuries, the explosion of telecommunications in the 1980s allowed optics to become a major technology in our everyday life.

Over the last few decades, the approach based on fundamental research and the development of new concepts has been transformed into research and development for new optical products in order to fulfill the increased demand of integrated optoelectronic components in particular for optical telecommunications.

Thus, optics have progressed and moved through four generations: conventional optics, micro-optics, integrated optics and more recently nano-optics (nano-photonics). From optical components of laboratory dimensions (meter and centimeter), research was directed towards micro-optics, particularly with the advent of optical fiber and laser diodes which made it possible to miniaturize photonic systems. Thereafter, integrated optics introduced the concept of integrated optical circuits by similarity to the integrated circuits in micro-electronics. This technology

made it possible in many cases to be released from the limitations imposed by the use of light for signal processing.

The concept of "integrated optics" was introduced for the first time by S.E. Miller in 1960 from Bell Laboratories (USA). The approach suggested by Miller consisted of creating on the same substrate, passive and active components for light generation and treatment. The basic element of this type of circuit is the waveguide.

Finally, in the continuity of the idea suggested for the first time by the physicist R. Feynman in 1959, who spoke about the concept "Smaller, Faster, Cheaper", for which the emergent idea was the possibility of handling matter on an atomic and molecular scale in order to conceive and produce sub-micrometric components and systems, there thus appeared the concept of nanotechnology, which became a new challenge for scientific research around the world. In this nano-scale world, the photon is also building its own realm. Thus, nano-photonics actually make it possible to develop new optical components for light generation and treatment based on new paradigms (such as photonic crystals).

Progress in the previously mentioned research fields is incontestably determined by the fabrication and characterization of structures making it possible to manipulate the photon. Among them is the optical waveguide which constitutes the basic element of any integrated optical circuit. In optics, the waveguide plays the same role as the electric conductor (wire) for electronics.

This progress also requires important work regarding the materials and technology to be used. Similar to the development of electronics, the engineering of materials took several decades to develop adequate materials to carry out reliable and effective optoelectronic components. For example, lithium niobate ($LiNbO_3$) is a major dielectric material. It has been used for many years for the fabrication of optoelectronic components for optical signal processing. The use of this material in the form of optical waveguides made it possible in many cases to be released from the limitations related to the use of bulk crystals.

The objective of this book is to provide researchers and students undertaking studies at a Master's level with a teaching aid to understand the basis of integrated optics. This book is a synthesis of theoretical approaches and experimental techniques necessary for the study of the guiding structures. It is based in particular on the research tasks undertaken in this field by the author for about 15 years.

The originality of this book comes from the fact that the ideal models are often accompanied by the experimental tools and their setting to characterize the studied phenomenon. The marriage of the theory and the experiment make the comprehension of the physical phenomena simple and didactic.

The structure of this book is organized into six chapters. Chapter 1 gives the theory of optical waveguides, particularly reporting the study of planar and channel waveguides.

In Chapter 2, the principles of waveguide fabrication techniques are discussed and a review of materials for integrated optics is also reported.

Chapter 3 describes the experimental techniques used for the characterization of guiding structures. The technique of prism coupling – m-line spectroscopy – is described and discussed from theoretical and experimental points of view. The second part of this chapter is devoted to optical losses within the guides, with on the one hand, the presentation of the physical origin of losses and on the other hand, experimental techniques to measure these losses.

The non-linear optical effects in waveguides are covered in Chapter 4. This chapter focuses on second order phenomena and more specifically the second harmonic generation of light.

Chapter 5 is dedicated to the electro-optic effect in waveguides. This chapter covers the electro-optic modulation and its applications in the field of optical telecommunications.

Chapters 4 and 5 present the two theoretical and experimental aspects. The various devices used for the non-linear optical characterization and electro-optics of waveguides are also discussed further.

Finally, Chapter 6 is designed like an introduction to photonic crystals. The photonic crystals are a great part of nano-photonics, which takes an increasingly important place in photonic technologies. This new approach to manipulate the photon will probably provide the ideal solution for allowing integrated optics to make an important technological leap. This chapter is written as an introduction to this field and is far from exhaustive.

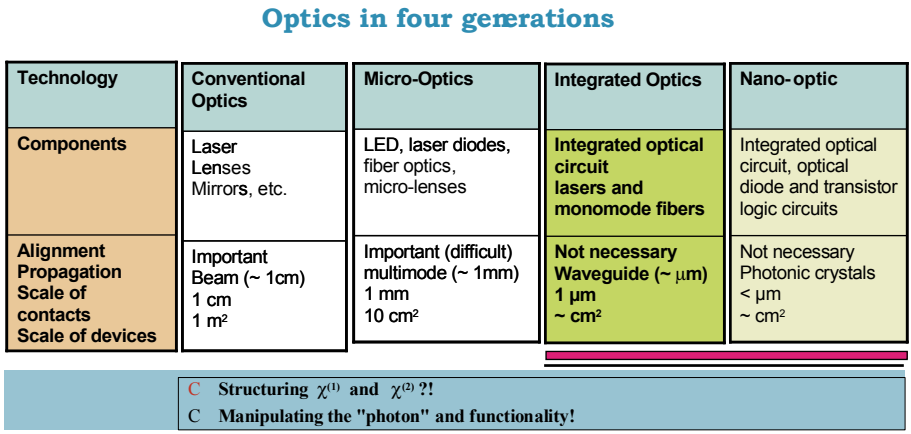

Figure 1. *Summary of the evolution of optics*

This page intentionally left blank

Chapter 1

Optical Waveguide Theory

Optical waveguides are structures with three layers controlling light confinement and propagation in a well defined direction inside the central layer (Figure 1.1).

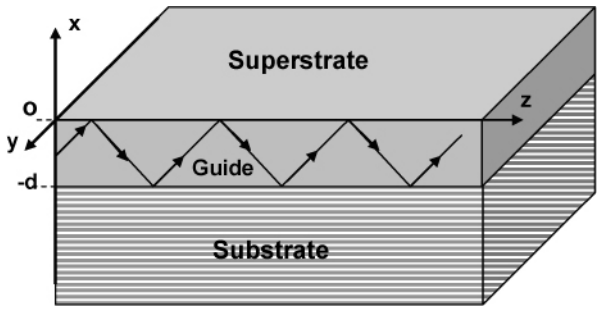

Figure 1.1. *Planar optical waveguide*

Light confinement is carried out by successive total reflections on the two interface guides – substrate and guide – superstrate.

Light propagation is governed by an interference phenomenon which occurs inside the guide between two waves; one of them undergoes two successive total reflections. For a better understanding of the guided wave propagation, we will recall the main principles of these two phenomena, total reflection and interference, inside a transparent plate with parallel faces.

1.1. Principles of optics

1.1.1. *Total reflection phenomenon*

Let us consider an interface separating two mediums 1 and 2, which are dielectric, lossless, homogenous and isotropic with refractive indices n_1 and n_2, respectively. An electromagnetic wave propagates from 1 to 2 with an angle of incidence θi related to the normal of the interface (Figure 1.2).

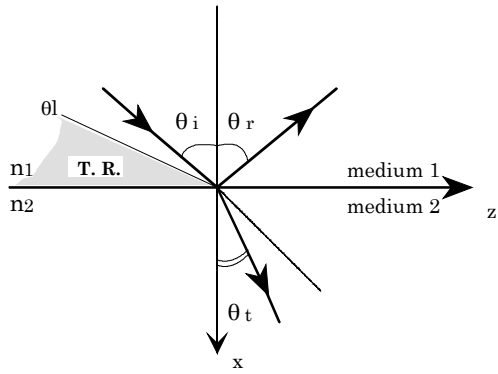

Figure 1.2. *Reflection on an interface (medium 1/medium 2)*

The electric field of the incident wave is given by:

$$\vec{E}_i = \vec{\mathrm{E}}_{\mathrm{i0}} \exp \mathrm{i}(\mathrm{n}_1 \vec{k}_i \vec{r} - \omega t) \qquad [1.1]$$

with: $\vec{k}_i \vec{r} = k\left(x \cos \theta_i + z \sin \theta_i\right)$ [1.2]

$\vec{k} = k\vec{u} = \dfrac{2\pi}{\lambda}\vec{u}$ is the wave vector in the vacuum (λ: wavelength in the vacuum) and E_{i0} is the incident wave amplitude. The electric fields of the reflected and transmitted waves can be written:

$$\vec{E}_r = \vec{\mathrm{E}}_{\mathrm{r0}} \exp \mathrm{i}(\mathrm{n}_1 \vec{k}_r \vec{r} - \omega t) = \vec{\mathrm{E}}_{\mathrm{r0}} \exp i\left(n_1 k\left(-x \cos \theta_r + z \sin \theta_r\right) - \omega t\right) \qquad [1.3]$$

$$\vec{E}_t = \vec{\mathrm{E}}_{\mathrm{t0}} \exp \mathrm{i}(\mathrm{n}_1 \vec{k}_t \vec{r} - \omega t) = \vec{\mathrm{E}}_{\mathrm{t0}} \exp i\left(n_1 k\left(x \cos \theta_t + z \sin \theta_t\right) - \omega t\right) \qquad [1.4]$$

In addition, refraction law is given by:

$$n_1 \sin\theta_i = n_2 \sin\theta_t \qquad [1.5]$$

$$\text{Therefore, } \sin\theta_i = \frac{n_2}{n_1}\sin\theta_t \qquad [1.6]$$

In the case of $n_1 > n_2$, there is an incident angle θ_l, as:

$$\sin\theta_l = \frac{n_2}{n_1} \qquad [1.7]$$

For $\theta_i > \theta_l$, the incident wave is totally reflected into medium 1 (total reflection) and the angle θ_t of the transmitted wave is complex [Bor 1999, War 1988]:

$$\begin{aligned}\cos\theta_t &= \left(1-\sin^2\theta_t\right)^{1/2} = \left(1-\left(\frac{n_1}{n_2}\right)^2 \sin^2\theta_i\right)^{1/2} \\ &= \frac{i}{n_2}\left(n_1^2\sin^2\theta_i - n_2^2\right)^{1/2} = i\chi\end{aligned} \qquad [1.8]$$

From [1.4], the transmitted wave can be written as:

$$\exp j\left(\vec{k}_t\vec{r}-\omega.t\right) = \exp j\left(k_{zt}z-\omega t\right)\exp\left(-\chi.x\right) \qquad [1.9]$$

This wave propagates in the Oz direction with an amplitude exponentially decreasing in the Ox direction. This is called an evanescent wave. Also, according to Fresnel's formulae, the considered wave undergoes a phase shift compared to the incident wave, given by [Bor 1999]:

$$\Phi_{TE} = 2artg\left[\frac{{n_1}^2\sin^2\theta_i - {n_2}^2}{{n_1}^2 - {n_1}^2\sin^2\theta_i}\right]^{1/2} \text{ (TE incident wave)} \qquad [1.10]$$

$$\Phi_{TM} = 2artg\left[\left(\frac{n_1}{n_2}\right)\left(\frac{{n_1}^2\sin^2\theta_i - {n_2}^2}{{n_1}^2 - {n_1}^2\sin^2\theta_i}\right)\right]^{1/2} \text{ (TM incident wave)} \qquad [1.11]$$

Relations [1.9] and [1.10] will be used throughout this chapter in order to study the propagation of guided waves. Note that evanescent waves have been experimentally investigated and they are currently utilized in the field of integrated optics. A similar phenomenon appears at the interface between a dielectric and a metallic layer generating, under specific conditions, a surface plasmon [Rae 1997].

1.1.2. *Parallel-face plate*

Let us consider a transparent plate with parallel faces (Figure 1.3), with refractive index n and a thickness d, placed in air (index = 1). We will focus on the calculation of the difference of the optical path (δ) between the first two rays transmitted throughout the plate (the same approach can be applied for the first two reflected rays).

$$\delta = [SOABCR_2] - [SOAHR_1] \qquad [1.12]$$

We can easily show that δ is given by:

$$\delta = 2nd\cos\theta \qquad [1.13]$$

where θ is the propagation angle within the plate.

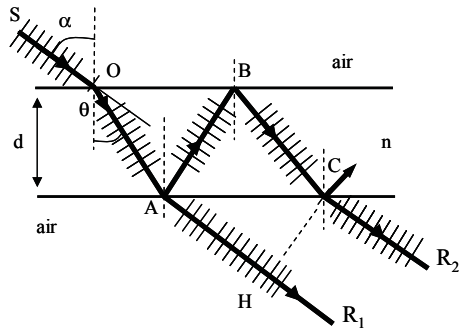

Figure 1.3. *Interference between two rays transmitted by a parallel face plate with a thickness d and a refractive index n*

In these conditions the parallel-face plate introduces a phase shift between the two rays R_1 and R_2 given by the following relation:

$$\varphi = 2ndk\cos\theta = \frac{4\pi}{\lambda}nd\cos\theta \qquad [1.14]$$

The latter is at the origin of the interference between the two rays R_1 and R_2. The transmitted rays are parallel, thus the interference phenomenon is located at infinity. However, we can observe the interference fringes in the Fresnel's field on a screen placed at the focal distance of a convergent lens [Bor 1999, War 1988, Rae 1997, Sal 1991].

To summarize, when a plane wave propagates, two kinds of phase mismatches can be considered: the first is due to total reflection, and the second could be due to a difference in the optical path.

1.2. Guided wave study

1.2.1. *General description*

Let us consider the case of three mediums with a central layer of refractive index n, surrounded by two layers of indices n_s and n_a called the substrate and superstrate respectively.

Light confinement in such a structure (waveguide) is based on a total reflection (TR) phenomenon on the interfaces (n-n_s) and (n-n_a). Thus, two critical angles θ_{c1} and θ_{c2} can be defined as:

$$\sin\theta_{c1} = \frac{n_a}{n}$$
$$\sin\theta_{c2} = \frac{n_s}{n} \qquad [1.15]$$

if $n > n_s > n_a$, then $\theta_{c1} < \theta_{c2}$. We can distinguish three situations related to the propagation angle θ:

– $\theta < \theta_{c1}$: air modes (if $n_a = 1$)

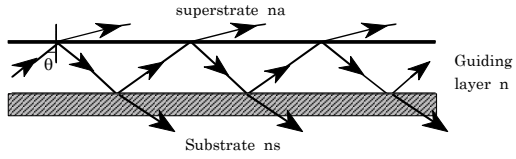

Figure 1.4. *Air modes*

In this case, the total reflection conditions are not satisfied on the two interfaces, and there is no confinement of the light. Light propagates as substrate-superstrate radiation modes. We will reconsider the concept of modes in the continuation of this chapter.

– $\theta_{c1} < \theta < \theta_{c2}$: substrate modes

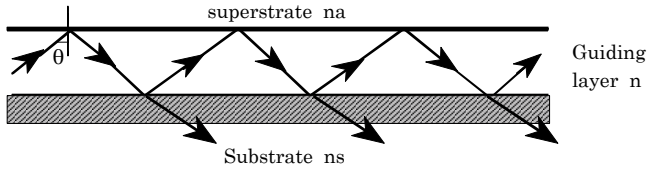

Figure 1.5. *Substrate modes*

The total reflection of the light is carried out only on the interface guide-superstrate (air). A part of the light is refracted through the interface guide-substrate. These are substrate modes.

– $\theta > \theta_{c2}$: guided modes

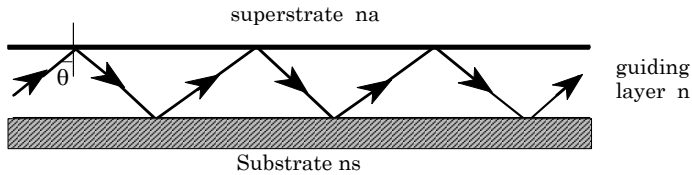

Figure 1.6. *Guided modes*

In this situation, light is in total reflection on the two interfaces, guide-superstrate and guide-substrate, remaining confined between them. These are well confined guided modes. Radiation and substrate modes are called leaky modes, and have been discussed by several authors [Mar 1969, DIN 1983]. They can be used to characterize the optical properties of planar waveguides.

In the rest of this chapter, we will be interested only in the guided modes which theoretically allow light propagation without loss in the guiding layer, and play a very important role in integrated optics.

So far we have only considered structures with a guiding zone of a constant refractive index. We will, however, also be interested in waveguides having a central zone whose index varies. In addition, the index profile of the guiding layer (n) enables us to distinguish two types of waveguides:

– the step index waveguide, where the refractive index remains constant throughout the guiding layer depth x (Figure 1.7a), thus we can write: n = constant; and

– the graded index waveguide, where the refractive index varies throughout the guiding layer depth x (Figure 1.7b). Therefore, we can write: n = n(x).

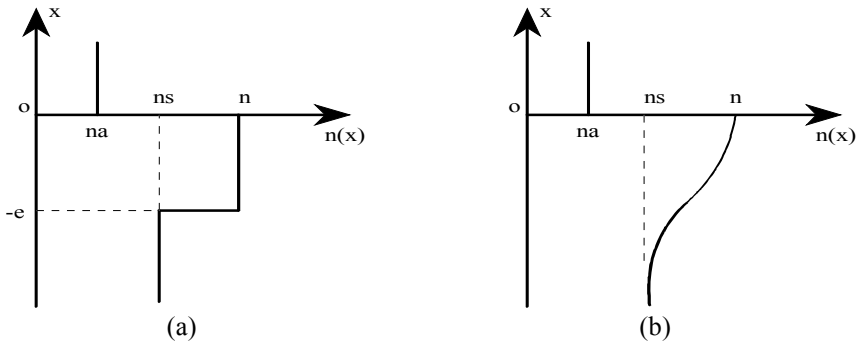

Figure 1.7. *(a) Step index waveguide, (b) graded index waveguide*

1.2.2. *Step index planar waveguide*

1.2.2.1. *Guided modes dispersion equation*

1.2.2.1.1. Optic-ray approach

A planar waveguide is characterized by parallel planar boundaries with respect to one direction (x) and is infinite in extent in the other directions (y and z). The refractive indices of the superstrate, the guiding layer and the substrate are n_a, n and n_s respectively.

Let us consider a plane wave propagating in the Oz direction. In the optic-ray approach, light propagation is carried out by the superposition of several plane waves being propagated in zigzags, between the two interfaces (n, n_a) and (n, n_s), in the Oz direction (Figure 1.8). The light ray is defined as the direction of the optical energy flux (direction of the Poynting vector).

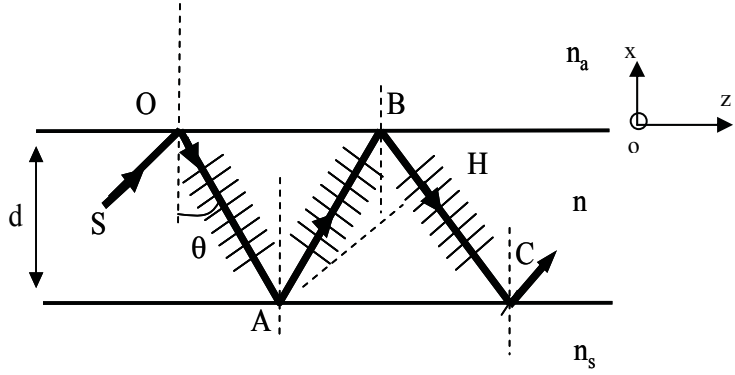

Figure 1.8. *Propagation in zigzags within a planar waveguide*

This situation is similar to that of the parallel-face plate presented in the previous section. Phase mismatch for such a wave between the points A and H (see Figure 1.8) is composed of three terms: phase mismatch $\Delta\phi$, due to the difference in optical paths; and the two phase mismatches, which are due to the total reflection on the two interfaces, $\Phi_{(n,na)}$ and $\Phi_{(n,ns)}$, with:

$$\Delta\phi = 2ndk\cos\theta = \frac{4\pi}{\lambda} nd\cos\theta \qquad [1.16]$$

and $\Phi_{(n,na)}$ and $\Phi_{(n,ns)}$ given by expressions [1.10] and [1.11].

In order to maintain light propagation within the guiding layer, it is important that light undergoes constructive interference. For that, the total phase mismatch should be a multiple of 2π. Therefore, we can write the following guided mode dispersion equation:

$$2ndk\cos\theta - \Phi_{(n,n_a)} - \Phi_{(n,n_s)} = 2m\pi \qquad [1.17]$$

m: integer ≥ 0
d: thickness of the guiding layer
k: wave number ($2\pi/\lambda$)

Equation [1.17] can also be written as:

$$2kd\sqrt{\left(n^2 \quad N_m^2\right)} \quad \Phi_{(n,n_a)} + \Phi_{(n,n_s)} + 2m\pi \qquad [1.18]$$

$N_m \quad n\sin\theta_m$

$$\Phi_{(n,n_j)} \quad arctg \left[\left(\frac{n}{n_j}\right)^{2\rho}\left(\frac{\left(N_m^2 \quad n_j^2\right)}{\left(n^2 \quad N_m^2\right)}\right)^{1/2}\right] \qquad [1.19]$$

$$\rho = \begin{cases} 0 & \text{TE polarization} \\ 1 & \text{TM polarization} \end{cases} \qquad [1.20]$$

On the one hand, equation [1.18] indicates that light propagates within a medium of a refractive index $n\sin\theta$ called the effective index, N_m. On the other hand, equation [1.18] imposes discrete values of θ related to different values of m. These values determine the set of guided modes of the structure.

Relation [1.18] is called the guided mode dispersion equation. It represents the condition to be satisfied in order to confine light within the guiding layer. It is a resonant condition indicating that the wave phase in A and H is the same modulus 2π [Nis 1989, Tie 1970, Tie 1977, Mur 1999, Mar 1991, Yar 1973].

However, it is clear that the optic-ray approach does not allow the determination of the guided mode electric field distribution. For that, it is necessary to consider the Maxwell's equation approach.

1.2.2.1.2. Maxwell's equation approach

In this section, we will develop the theoretical study of light propagation within a planar waveguide starting from Maxwell's equations. This study will lead us to the guided mode dispersion equation as well as the distribution of the electromagnetic field in the guide.

The waveguide is formed by three dielectric mediums that are homogenous, isotropic, linear and lossless. The magnetic permeability is considered as constant μ_0. Light propagates in the Oz direction, and the structure is taken as infinite with invariant properties in the Oy direction. Solving this problem consists of finding out solutions for Maxwell's equations that satisfy the boundary conditions imposed by the structure.

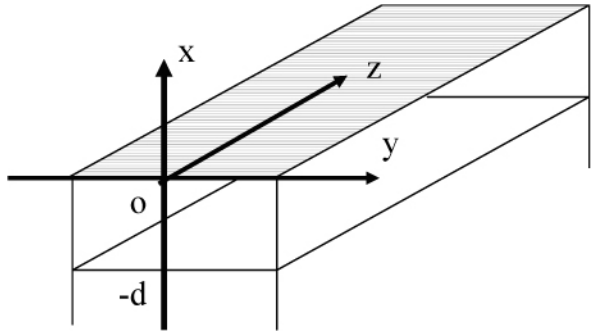

Figure 1.9. *Schematic planar optical waveguide*

The electromagnetic wave within every medium of such a structure is given by the following Maxwell's equations:

$$\vec{\nabla} \wedge \vec{E} = -\mu_0 \frac{\partial \vec{H}}{\partial t}$$
$$\vec{\nabla} \wedge \vec{H} = \varepsilon_0 n^2 \frac{\partial \vec{E}}{\partial t} \qquad [1.21]$$

$$\vec{\nabla}\vec{E} = 0$$
$$\vec{\nabla}\vec{H} = 0 \qquad [1.22]$$
$$\vec{B} = \mu_0 \vec{H} \quad \text{and} \quad \vec{D}=\varepsilon\vec{E}$$

with:

- $\vec{E}$: electric field vector;
- $\vec{B}$: magnetic field vector;
- $\vec{H}$: magnetic induction vector ;
- $\vec{D}$: electric displacement vector.

The solutions take the form:

$$\vec{E} = \vec{E} \exp i(\omega t - \vec{k}\vec{r}) = \vec{E} \exp i(\omega t - \beta z)$$
$$\vec{H} = \vec{H} \exp i(\omega t - \vec{k}\vec{r}) = \vec{H} \exp i(\omega t - \beta z) \qquad [1.23]$$

As the structure is infinite in the Oy direction, the problem has no dependence on y ($\frac{\partial}{\partial y} = 0$).

An electromagnetic field can be considered as a sum of two polarized fields TE and TM, corresponding to a TE (Transverse Electric) wave with $\vec{E}$ parallel to Oy and a TM (Transverse Magnetic) wave where $\vec{H}$ is transverse. Then, from Maxwell's equations, it can be written that:

$$\begin{cases} \dfrac{\partial^2 E_y}{\partial x^2} + \left(k^2 n^2 - \beta^2\right) E_y = 0 \\ H_x = -\dfrac{\beta}{\omega \mu_0} E_y \\ H_z = -\dfrac{1}{i\omega\mu_0} \dfrac{\partial E_y}{\partial x} \end{cases} \quad \text{TE modes} \qquad [1.24]$$

$$\begin{cases} \dfrac{\partial^2 H_y}{\partial x^2} + \left(k^2 n^2 - \beta^2\right) H_y = 0 \\ E_x = -\dfrac{\beta}{\omega \mu_0} H_y \\ E_z = -\dfrac{1}{i\omega\mu_0} \dfrac{\partial H_y}{\partial x} \end{cases} \quad \text{TM modes} \qquad [1.25]$$

Note that the previous separation in TE and TM modes can be performed in the case of a planar optical waveguide with a refractive index n(x) which depends on one transverse coordinate only.

Generally speaking, we have to solve the following Helmholtz's equation:

$$\frac{\partial^2 F}{\partial x^2} + \left(k^2 n^2 - \beta^2\right) F = 0 \qquad [1.26]$$

with: $F = E$ or H depending on the light polarization.

It is necessary to solve the previous equation in the three mediums, n, n_s and n_a.

TE modes

Equation [1.26] can be written for the three layers as:

$$\frac{\partial^2 E_y}{\partial x^2} - q^2 E_y = 0 \quad \text{medium } n_a \qquad [1.27]$$

$$\frac{\partial^2 E_y}{\partial x^2} + h^2 E_y = 0 \quad \text{medium n} \qquad [1.28]$$

$$\frac{\partial^2 E_y}{\partial x^2} - p^2 E_y = 0 \quad \text{medium } n_s \qquad [1.29]$$

$$\text{with: } \begin{aligned} q^2 &= \beta^2 - k^2 n_a^2 \\ h^2 &= k^2 n^2 - \beta^2 \\ p^2 &= \beta^2 - k^2 n_s^2 \end{aligned} \qquad [1.30]$$

β is the propagation constant given by: $\beta = kN = kn\sin\theta$ (N is the guided mode effective index).

The guiding condition imposes the existence of a sinusoidal solution within the central layer n ($h^2 \geq 0$), with evanescent waves into mediums n_a and n_s (q^2 and $p^2 \geq 0$) [Nis 1989, Tie 1970, Tie 1977, Mur 1999, Mar 1991, Yar 1973]. So:

$$kn \geq \beta \geq \text{kns} \geq kn_a$$

The electric field E_y has the general form:

$$E_y(x) = \begin{cases} C\exp(-qx) & 0 \leq x \leq \infty \\ A\cos(hx) + B\sin(hx) & -d \leq x \leq 0 \\ D\exp[p(x+d)] & -\infty \leq x \leq -d \end{cases} \qquad [1.31]$$

where A, B, C and D are constants that can be determined by matching the boundary conditions which require the continuity of E_y and H_z. Note that for $\vec{D}$ and $\vec{B}$ the continuity conditions concern their normal components. Thus, at the interfaces (n, n_a) and (n, n_s), we can write:

$$E_y\Big|_n = E_y\Big|_{n_a}$$

$$\frac{\partial E_y}{\partial x}\Big|_n = \frac{\partial E_y}{\partial x}\Big|_{n_a} \qquad [1.32]$$

$$E_y\Big|_n = E_y\Big|_{n_s}$$

$$\frac{\partial E_y}{\partial x}\Big|_n = \frac{\partial E_y}{\partial x}\Big|_{n_s} \qquad [1.33]$$

These conditions allow us to write previous equations [1.31] in the following form:

$$E_y(x) = \begin{cases} C\exp(-qx) & 0 \le x \le \infty \\ C\left[\cos(hx) - (q/h)\sin(hx)\right] & -d \le x \le 0 \\ C\left[\cos(hd) + (q/h)\sin(hd)\right]\exp\left[p(x+d)\right] & -\infty \le x \le -d \end{cases} \qquad [1.34]$$

$\vec{H}$ can be determined from equations [1.23].

The equation system allows us to determine the electric field profile of each guided mode propagating within the structure. However, it is necessary to determine the constants C and β. For this we use the derivative continuity of the electromagnetic field in the guide. After simplification, we can find:

$$\tan(hd) = \frac{p+q}{h - \frac{pq}{h}} \qquad [1.35]$$

This relation can be transformed into:

$$dh = \arctan\left(\frac{q}{h}\right) + \arctan\left(\frac{p}{h}\right) + m\pi \qquad [1.36]$$

where m is an integer ≥ 0. This defines the guided mode order.

(For the previous calculation, we can use: $\tan(a+b) = \dfrac{\tan(a)+\tan(b)}{1-\tan(a)\tan(b)}$)

Equation [1.36] represents the TE guided mode dispersion equation. By replacing p, q and h in [1.35], we obtain equation [1.17] previously described during consideration of the optic-ray approach.

Finally, we need to determine the constant C in order to obtain a complete description of the guided modes travelling within the structure. For that, we use the normalization condition [Yar 1973]. Calculation shows that [Vin 2003]:

$$C_m = 2h_m \left[\frac{\omega\mu_0}{|\beta_m| \left(d + \frac{1}{q_m} + \frac{1}{p_m} \right) \left(h_m^2 + q_m^2 \right)} \right]^{1/2} \qquad [1.37]$$

As an example, the solutions of the problem are schematically displayed on the following figure.

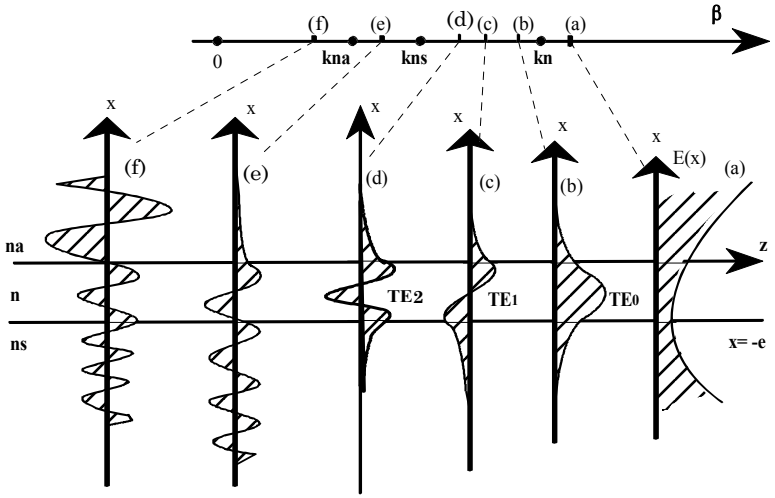

Figure 1.10. *Guided mode electric field distribution in a planar optical waveguide structure: (a) represents an unacceptable physical solution because $k^2n^2 - \beta^2 < 0$ in the three mediums; (b), (c) and (d) represent the electric field distribution of well guided modes ($TE_{0..}$); (e) represents a substrate mode – the optical energy is well confined at the interface (n,na) but it varies sinusoidally in the substrate; (f) shows the electric field distribution of a radiation mode, $k^2n^2 - \beta^2 > 0$ in the three mediums – this is an oscillatory solution in the three mediums (free extension outside the guide)*

TM modes

In this case, we have:

$$\vec{H} = (0, H_y, 0) \text{ and } \vec{E} = (E_x, 0, E_z) \quad [1.38]$$

Helmholtz's equation can be written as:

$$\frac{\partial^2 H_y}{\partial x^2} + \left(k^2 n^2 - \beta^2\right) H_y = 0 \quad [1.39]$$

As with TE modes, we can show that the magnetic field H is given by:

$$H_y(x) = \begin{cases} -(h/\bar{q})C\exp(-qx) & 0 \le x \le \infty \\ C\left[-(h/\bar{q})\cos(hx) + \sin(hx)\right] & -d \le x \le 0 \\ -C\left[(h/\bar{q})\cos(hd) + \sin(hd)\right]\exp\left[p(x+d)\right] & -\infty \le x \le -d \end{cases} \quad [1.40]$$

Thus, the continuity of E and H gives the following TM guided mode dispersion equation:

$$\tan(hd) = \frac{h(\bar{p} + \bar{q})}{h^2 - \bar{p}\bar{q}} \quad [1.41]$$

with: $\bar{p} = \dfrac{n^2}{n_s^2} p$ and $\bar{q} = \dfrac{n^2}{n_a^2} q$.

Equation [1.41] can be easily transformed as:

$$dh = \arctan\left(\frac{q}{h}\frac{n}{n_a}\right) + \arctan\left(\frac{p}{h}\frac{n}{n_s}\right) + m\pi \quad [1.42]$$

As previously shown, by replacing p, q and h in [1.42], we find the modal equation [1.16] reported above. The normalization condition gives:

$$C_m = 2\sqrt{\frac{\omega\varepsilon_0}{\beta_m d_{eff}}} \qquad [1.43]$$

with:

$$d_{eff} \equiv \frac{\bar{q}^{-2} + h^2}{\bar{q}^{-2}}\left[\frac{d}{n_c^{\,2}} + \frac{q^2 + h^2}{\bar{q}^{-2} + h^2}\frac{1}{n_c^2 q} + \frac{p^2 + h^2}{\bar{p}^{-2} + h^2}\frac{1}{n_3^2 p}\right] \qquad [1.44]$$

The dispersion equation makes it possible to connect in a transcendent way the optogeometric parameters of the guiding structure (the guide index n and its thickness d), with the propagation constants β_m of the guided modes. The propagation constant $\beta_m = kN_m$ and, therefore, the effective index N_m ($N_m = n\sin\theta_m$), characterize, particularly, the guided modes of order m (discrete aspect of N_m given by the equation of dispersion). The effective index is an important parameter in the characterization of optical planar waveguides owing to the fact that it constitutes the directly measurable parameter. The index of the guiding layer must be taken higher than the indices of the two surrounding layers. This defines the guiding properties of the structure and constitutes the basic element for waveguide fabrication.

The thickness of the guiding layer is also an essential parameter as it determines the optical properties of the guide, in particular the number of guided modes. These aspects will be evoked and discussed in the following chapters. However, we will focus on the influence of these parameters, in particular the guide thickness on the optical properties of the structure.

1.2.2.2. *Cut-off thickness*

Using dispersion equations [1.35] and [1.42] for TE and TM modes, respectively, it is possible to study the effective index N_m variation as a function of the waveguide thickness for different guided modes order m (the substrate and superstrate indices selected are constant). Results are displayed on Figures 1.11a and 1.11b.

It can be noted that the effective index of a guided mode m increases according to the thickness variation and tends towards its maximum value N (free propagation). The minimal value $N_m = N_s$ corresponds to a thickness below which

the mode *m* cannot exist in the guide. This thickness is known as the cut-off thickness for the *m* mode. It can be calculated starting with the dispersion equations previously reported. We find:

$$d_c(TE) = \frac{m\pi + \arctan\left(\frac{n_s{}^2 - n_a{}^2}{n^2 - n_s{}^2}\right)^{1/2}}{k\left(n^2 - n_s{}^2\right)^{1/2}} \qquad [1.45]$$

$$d_c(TM) = \frac{m\pi + \arctan\left[\left(\frac{n}{n_a}\right)^2\left(\frac{n_s{}^2 - n_a{}^2}{n^2 - n_s{}^2}\right)^{1/2}\right]}{k\left(n^2 - n_s{}^2\right)^{1/2}} \qquad [1.46]$$

Moreover, equations [1.46] and [1.47] allow us to calculate the guided modes number supported by the waveguide structure. For this it is necessary to find the guided mode order which corresponds to a guide cut-off thickness similar to the guide thickness considered. Thus, we can write [Hun 1985]:

$$\begin{aligned} nbr_m &= 1 + m_{\max} \\ &= 1 + IP\left\{\frac{1}{\pi}\left[kd\left(n^2 - n_s{}^2\right)^{1/2} - artg\left(\left(\frac{n}{n_a}\right)^{2\rho}\left(\frac{n_s{}^2 - n_a{}^2}{n^2 - n_s{}^2}\right)^{1/2}\right)\right]\right\} \end{aligned} \qquad [1.47]$$

where *IP* is the integer part, and ρ is 0 for TE and 1 for TM.

According to Figures 1.12a and b, we see that the number of modes proportionally varies versus the thickness, and rather exponentially according to the variation of structure index. Finally, let us note that for a symmetric waveguide (optical fiber) the fundamental mode (m=0) always exists because it has a cut-off thickness equal to zero.

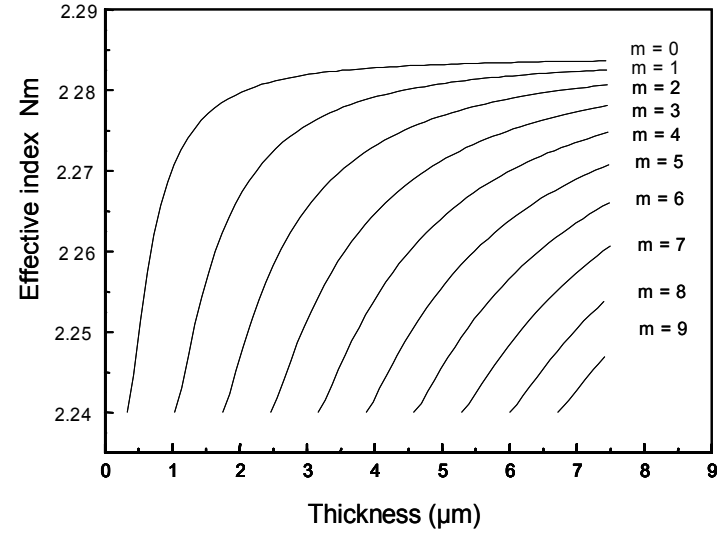

(a)

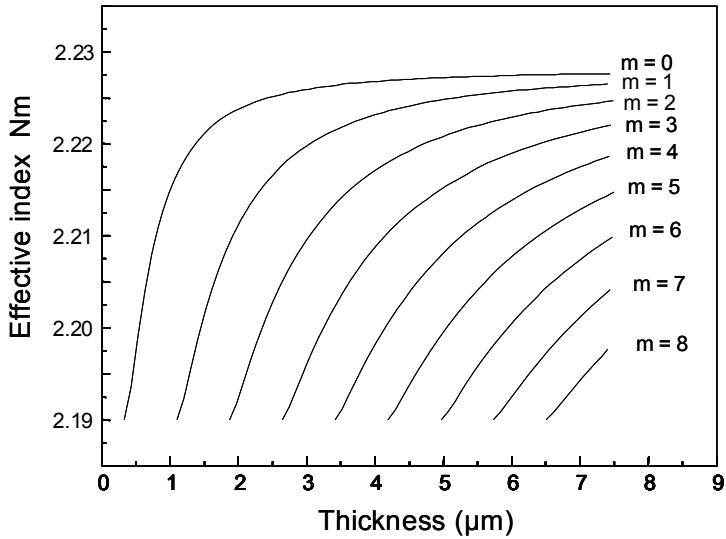

(b)

Figure 1.11. *Cut-off thickness for guided modes: (a) TE and (b) TM; for an $LiNbO_3$ planar waveguide (n=2.224, n_s=2.19 and n_a =1 at λ= 632 nm)*

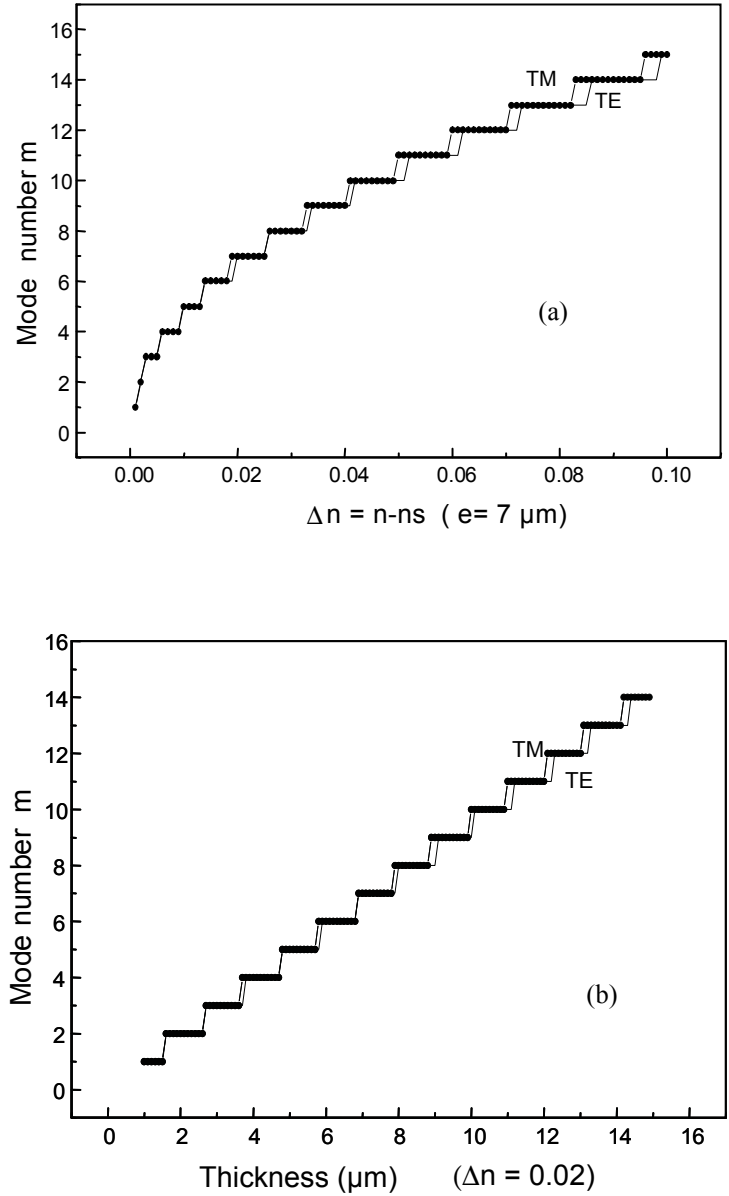

Figure 1.12. *(a) Influence of the index variation n on the number of modes m; and (b) influence of the thickness on the number of modes m*

1.2.2.3. *Effective thickness*

As indicated above, the case of a step planar waveguide is easy to discuss. Light propagation is completely described by dispersion equations [1.35] for TE and [1.42] for TM. As a matter of fact, the optic-ray undergoing internal total reflection penetrates into the substrate and the superstrate, as indicated in Figure 1.13, interacting with the guiding structure through the evanescent waves created during successive total reflections. From that point of view, light travels within a new structure with a different thickness called the guide effective thickness [Hun 1985].

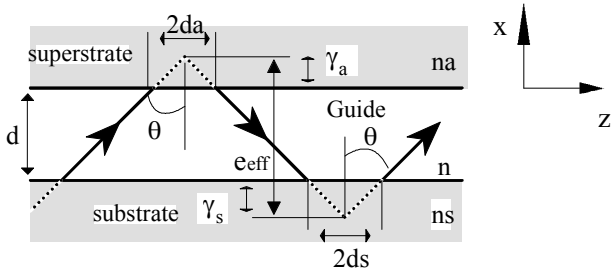

Figure 1.13. *Optic-ray propagation in zigzags: showing the Goos-Hänchen shift and the effective thickness*

The guide effective thickness can be written as:

$$d_{eff} = d + \gamma_a + \gamma_s \qquad [1.48]$$

with:

$$\gamma_i = \begin{cases} k_0^{-1}\left(N_m^{\,2} - n_i^2\right)^{-1/2} & \text{TE} \\ k_0^{-1}\left(N_m^{\,2} - n_i^2\right)^{-1/2}\left(\dfrac{N_m^{\,2}}{n_i^2} + \dfrac{N_m^{\,2}}{n^2} - 1\right)^{-1} & \text{TM} \end{cases} \qquad [1.49]$$

i= a,s

This effective thickness corresponds to the thickness seen by the guided mode m which is propagated in the guiding structure. The penetration depths of the guided mode into the superstrate and the substrate are given by $1/\gamma_a$ and $1/\gamma_s$, respectively (see Figure 1.13). Consequently, light undergoes a lateral displacement of $2d_s$ and $2d_a$ on the two interfaces x = 0 and x = -d, respectively. These displacements are due

to the total reflection and are known as the Goos-Hänchen effect. They are given by the following expression:

$$d_i = \frac{1}{\gamma_i}\tan\theta = \frac{1}{\gamma_i}\frac{N_m}{\left(n^2 - {N_m}^2\right)^{1/2}} \qquad i= a,s \qquad [1.50]$$

The Goos-Hänchen effect, due to total reflection at a dielectric interface, is a specific situation where the optic-ray behaves differently from the wave vector $\vec{k}$; this is similar behavior to an anisotropic medium which will be described in the following sections.

Finally, note that the effective thickness also depends on the mode order.

1.2.3. *Graded index planar waveguide*

The majority of the active waveguides used in integrated optics particularly for electro-optic modulation, are based on graded index waveguides. This type of waveguide is more difficult to treat because the refractive index varies versus the guide thickness (n = n(x)). According to [1.26], the TE wave equation for such a guide is:

$$\frac{\partial^2 E_y}{\partial x^2} + \left(k^2 n^2(x) - \beta^2\right)E_y = 0 \qquad [1.51]$$

Solving this equation is a hard task. Its analytical solution exists only for specific index profiles (linear, exponential, etc). Nevertheless, this equation can be solved by using approximate methods such as:

– a multilayer approach;
– optic-ray approximation; or
– the WKB method.

These methods are currently employed because of their simplicity.

In the following sections, we will only focus on optic-ray and WKB methods. They correspond to the optic-ray and Maxwell's equation approaches previously utilized in the study of the step index waveguide.

1.2.3.1. *Optic-ray approximation*

This consists of considering a set of layers of low thickness, where the refractive index can be considered as constant. Thus, the refraction index distribution is expressed in the following form:

$$n(x) = n_s + \Delta n f\left(\frac{x}{d}\right) \qquad [1.52]$$

n_s: substrate index;

$f(x/d)$: decreasing monotonous function of x;

$0 < f(x/e) < 1$;

d: the guide thickness.

The maximum value of n is $(n_s + \Delta n)$ at the waveguide surface. The optic-ray trajectory within the guide can be approached by a combination of small segments corresponding to a propagation distance Δz [Nis 1989, Tie 1070]. The wave vector diagram is displayed in Figure 1.14.

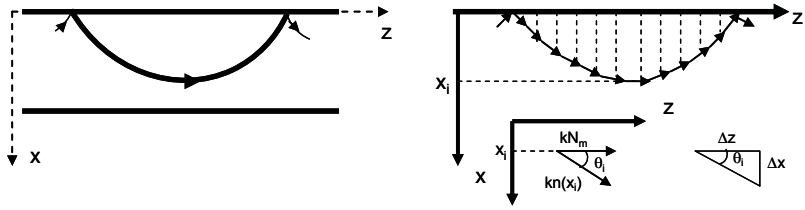

Figure 1.14. *Optic-ray trajectory in a graded index waveguide*

Note:

$$\theta_i = \arccos\left(\frac{N_m}{n(x_i)}\right) \qquad [1.53]$$

The angle θ_i gradually varies as it depends on $n(x)$.

The previous equation emphasizes that $\theta_i = 0$ for $n(x_i) = N_m$. This allows us to determine the maximal penetration depth x_t, for which the light undergoes a total reflection. This point x_t is called the turning point and the depth x_t is considered as the waveguide effective thickness.

The phase variation over a distance equal to Δx_i is given by:

$$\Delta\Phi_i = kn(x_i)\cos\theta_i \Delta x_i = k\left(n^2(x_i) - {N_m}^2\right)^{1/2} \Delta x_i \qquad [1.54]$$

The propagation of light as a guided mode within such a structure implies that the total phase variation should be an integer m multiple of 2π. Thus, we obtain:

$$\sum_i \Phi_i - 2\Phi_{(n,n_a)} - 2\Phi_t = 2m\pi \qquad [1.55]$$

$$\sum_i \Phi_i = 2k\int_0^{x_t} \left(n^2(x) - {N_m}^2\right)^{1/2} dx$$

with $\Phi_{(n,n_a)}$: phase mismatch at the interface (n, n_a) [1.56]

Φ_t: phase mismatch at the turing point

Relation [1.55] represents the guided mode dispersion equation. To simplify this relation and by considering that $\Delta n << n_s$, we can show that [Tie 1977, Tie 1974]:

$$\begin{aligned} 2\Phi_{(n,n_a)} &= \pi \\ 2\Phi_t &= \frac{\pi}{2} \end{aligned} \qquad [1.57]$$

In these conditions, the guided modes dispersion equation becomes:

$$2k\int_0^{x_t} \left(n^2(x) - {N_m}^2\right)^{1/2} dx = \left(2m + \frac{3}{2}\right)\pi \qquad [1.58]$$

The normalization of this relation can be performed by considering:

$$n^2(x) = {n_s}^2 + \left(n^2 - {n_s}^2\right) f\left(\frac{x}{d}\right) \qquad [1.59]$$

and $V = kd\sqrt{(n^2 - {n_s}^2)}$.

Therefore, we can write:

$$2V\int_0^{\xi_t}\sqrt{f(\xi)-b}\,d\xi=\left(2m+\frac{3}{2}\right)\pi \qquad [1.60]$$

with:

$$\xi=\frac{x}{d}$$
$$\xi_t=\frac{x_t}{d} \qquad \text{and} \qquad b=f\left(\xi_t\right) \qquad [1.61]$$

The normalized dispersion equation [1.61] can be numerically solved by considering a specific function of $f(\xi)$.

For instance, for the $LiNbO_3$ waveguide fabricated by Ti diffusion, the index profile function is an exponential [Tie 1974]:

$$f(\xi)=\exp\left(-\xi^2\right) \qquad [1.62]$$

In this case, the waveguide cut-off thickness can be found by taking $b = 0$ in equation [1.61]. By considering $x_t \to \infty$ for cut-off points and utilizing the following known integral:

$$\int_0^{\infty}\sqrt{\exp\left(-\xi^2\right)}d\xi=\sqrt{\frac{\pi}{2}} \qquad [1.63]$$

we deduce the normalized cut-off thickness:

$$V_m=\sqrt{2\pi}\left(m+\frac{3}{4}\right) \qquad [1.64]$$

From the study previously reported, we note that this method can be applied to any guide with a graded index. However, it does not take into account the electromagnetic field distribution of the guided mode. For the distribution of the electromagnetic field determination, WKB seems to be more appropriate. It carries out a treatment of the problem starting from Maxwell's equations, this will be the subject of the following section.

1.2.3.2. *WKB method*

This method was developed by Wentzel, Kramers and Brillouin (hence the name WKB) to solve problems of variable potentials in quantum mechanics [Tie 1977, Lan 1960]. However, it is merely applicable to refractive index profiles with smooth variation. The equation to be solved is similar to Schrödinger's equation for quantum mechanics:

$$\frac{\partial^2 F(x)}{\partial x^2} + \left(k^2 n^2(x) - \beta^2\right) F(x) = 0 \qquad [1.65]$$

$F(x)$ is the amplitude of the electric field $\vec{E}$.

The propagation constant β, eigenvalue of the previous equation, belongs to the interval [kn_{max} , kn_{min}]. Thus, we can distinguish two main parts in the index profile:

– values of x corresponding to $k^2 n^2(x) - \beta^2 > 0$, where an oscillatory solution exists; and

– values of x corresponding to $k^2 n^2(x) - \beta^2 < 0$, where the solution is exponential (an evanescent wave).

Therefore, the index profile contains one point x_t for which: $kn(x_t) = \beta$.

That point corresponds to the turning point as previously mentioned. Within the oscillatory part, we can consider:

$$F(x) = A(x)\exp(i\Phi(x)) \qquad [1.66]$$

Equation [1.66] becomes:

$$\frac{d^2 A}{dx^2} - \left(\frac{d\Phi}{dx}\right)^2 A + i\left[2\frac{d\Phi}{dx}\frac{dA}{dx} + \frac{d^2\Phi}{dx^2}A\right] + \left[k^2 n^2(x) - \beta^2\right]A = 0 \qquad [1.67]$$

Then, we can write:

$$\frac{d^2A}{dx^2} - \left(\frac{d\Phi}{dx}\right)^2 A + \left[k^2 n^2(x) - \beta^2\right] A = 0 \qquad \text{(a)}$$

and [1.68]

$$2\frac{d\Phi}{dx}\frac{dA}{dx} + \frac{d^2\Phi}{dx^2} A = 0 \qquad \text{(b)}$$

WKB approximation consists of neglecting the term of $\frac{d^2A}{dx^2}$ in equation [1.69a]. As a matter of fact, this is equivalent to the optic-ray approximation:

$$\left(\frac{d\Phi}{dx}\right)^2 = k^2 n^2(x) - \beta^2 \qquad [1.69]$$

This relation is the "eikonal" equation, a basic concept of ray optics. It describes the evolution of a optic-ray in a medium with a graded index given by:

$$k^2 n^2(x) - \beta^2 \qquad [1.70]$$

By taking: $g(x) = \frac{d\Phi}{dx}$ [1.71]

equation [1.69b] becomes:

$$2g\frac{dA}{dx} + \frac{dg}{dx} A = 0 \qquad [1.72]$$

Two solutions can be considered:

$$- \frac{dg}{dx} = \frac{dA}{dx} = 0 \qquad \forall x \qquad [1.73]$$

then, $g(x) = const$. In other words: $k^2 n^2(x) - \beta^2 = const.$

This case represents a step index planar waveguide (for such a guide WKB approximation is an exact solution). This emphasizes why the optic-ray approach yields the same results as using the Maxwell's equation treatment.

Equation [1.68b] becomes:

$$\frac{1}{A}\frac{dA}{dx} = -\frac{1}{2.g}\frac{dg}{dx} \qquad [1.74]$$

Thus:

$$A(x) = \frac{C}{\sqrt{\frac{d\Phi}{dx}}} \qquad [1.75]$$

where C is a constant.

The oscillatory solution can therefore be given by:

$$F(x) = \frac{C'}{\sqrt{\frac{d\Phi}{dx}}} \exp\left[i \int_0^{x_t} \frac{d\Phi}{dx} dx - \rho \right] \qquad [1.76]$$

C' and $\rho = const$

The real part of interest is:

$$F(x) = \frac{C'}{\sqrt{\frac{d\Phi}{dx}}} \cos\left(\int_0^{x_t} \left(k^2 n^2(x) - \beta^2\right)^{1/2} dx - \rho \right) \qquad [1.77]$$

Note that $F(x)$ contains a singular point corresponding to $k^2 n^2(x) = \beta^2$, i.e. the turning point. At this point, we cannot neglect the term $\frac{d^2 A}{dx^2}$ in equation [1.68a].

To solve this problem, in the WKB approximation approach, the index profile used is "linear" around the turning point. This ensures the continuity between the oscillatory and the evanescent wave solutions. Beyond the turning point, the solution is exponential, and is not of interest for the current study. As an example, Figure 1.15 displays the electric field distribution for the mode m=0 and m=1.

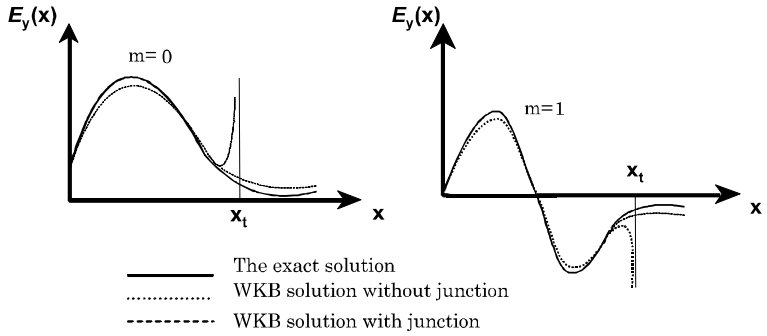

Figure 1.15. *Schematic solutions of graded index planar waveguide*

Finally, for an arbitrary index profile $n(x)$ and by using the continuity conditions of the electric field E, we can obtain the general expression of the dispersion equation:

$$\int_0^{x_t}\left(k^2n^2(x)-\beta^2\right)dx-\Phi_{(n,na)}-\Phi_{(n,ns)}=m\pi \qquad [1.78]$$

with:

$$n(x_t)=\beta \qquad [1.79]$$

To summarize, it is worth noting that starting from a given index profile n(x), the WKB approximation makes it possible to determine the propagation constants β_m. However, the mathematical expression of the electric field is less obvious and consists of the locally valid connection of solutions. Nevertheless, the WKB method seems to be adapted for index profile waveguides with weak variation.

1.3. Channel waveguides

Generally, the majority of the components used in integrated optics utilize channel waveguides. In these guiding structures, light is confined in two directions which considerably improves the component performances with the increase of matter-light interaction. However, the conditions of light propagation in such a structure are more difficult to study than in the planar waveguide. In addition,

guided modes are known as hybrid modes. They are quasi-TE or quasi-TM, as will be presented in this section.

The basic channel waveguide structure consists of a guiding region surrounded on all sides by a low index medium. As with planar waveguides, step index waveguides and graded index guides are distinguished using refractive index variation in the area where energy is confined. The analysis of these last structures is generally carried out using a variational formalism [Fer 1981, Wal 1985] which leads to rather complex and expensive calculations.

In the framework of this book, we will only focus on the study of step index channel waveguides where several resolution methods can be used.

As an example, Figure 1.16 displays a schematic channel waveguide.

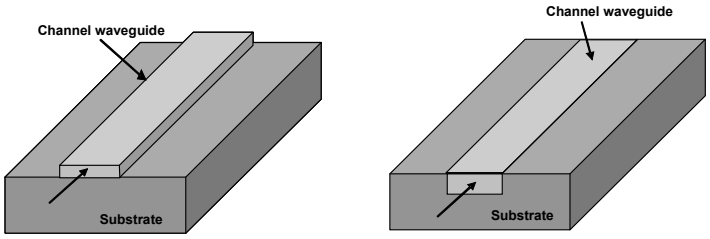

Figure 1.16. *Basic rectangular waveguide*

In the case of ridge structures, different materials can be used. This applies to thin films deposited on low index substrate. We focus on a general structure as displayed in Figure 1.17.

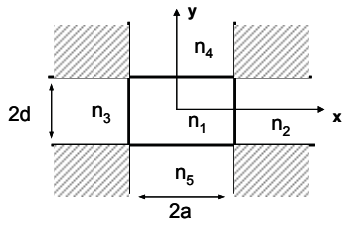

Figure 1.17. *Cross-section of a rectangular waveguide*

The guiding properties of such structures are generally given by the two 2D distributions of the electric field within the guiding region as well as the determination of the propagation constants of guided modes.

The exact solution of the wave equation for this guide is extremely complicated and has not been determined yet. Therefore, it is necessary to employ numerical resolutions and approximation methods. The most important methods are the effective index method, the finite difference method and the finite element method [Rac 1984]. Note that Marcatili [Mar 1969], for the first time, derived an approximate solution of rectangular waveguides. The key assumption made in Marcatili's method consists of separating variables in order to solve the wave equation in Cartesian coordinates for regions 1-5 of Figure 1.17.

In the context of this work, we will limit ourselves to the presentation of the effective index method which applies to the majority of the configurations. The reader will be able to find more details of the other methods in many references [Fre 1981, Wal 1996, Rac 1984, Mar 1969, Bae 1992].

The most current approximation consists of considering well confined guided modes so that there is a very weak penetration of the electric field into the four areas constituting the "gladding" which surrounds the guiding region. Moreover, we can consider that the field penetrates even more slightly in the four corners (hatched areas of Figure 1.17). In this case, the field in these areas is regarded as zero. This approximation will be at least correct for the modes far from their cut-off frequencies.

1.3.1. *Effective index method*

Let us consider a channel waveguide displayed in Figure 1.17. The index profile of the guiding region is $n(x,y)$. It does not depend on z, the propagation direction.

In these conditions, the guided mode electric field travelling in the Oz direction is given by:

$$\vec{E}(x,y,z) = E(x,y)e^{\,i\beta z}\vec{u} \qquad [1.80]$$

where β is the propagation constant.

It is easy to show (as for planar waveguides) that the electric field $\vec{E}(x,y)$ is a solution for the following wave equation:

$$\nabla_{xy}^2 E + \left(k^2 n^2(x,y) - \beta^2\right)E = 0 \qquad [1.81]$$

where k is the wave number.

In this approximation, we assume that the electric field E is given by the product of two fields:

$$E(x,y) = F(x,y)G(x) \qquad [1.82]$$

$F(x,y)$ is taken to slightly vary versus x so that:

$$\frac{\partial F(x,y)}{\partial x} \approx 0 \qquad [1.83]$$

The substitution of [1.82] in equation [1.81] (Helmoltz's) gives:

$$F(x,y)\frac{d^2G}{dx^2} + 2\frac{\partial F(x,y)}{\partial x}\frac{dG(x)}{dx} + G(x)\left[\frac{\partial^2 F(x,y)}{\partial x^2} + \frac{\partial^2 F(x,y)}{\partial y^2}\right] \qquad [1.84]$$
$$+ \left(n^2k^2 - \beta^2\right)F(x,y)G(x) = 0$$

By taking into account [1.83], this relation can be simplified:

$$\frac{1}{G}\frac{d^2G}{dx^2} + \frac{1}{F}\frac{\partial^2 F}{\partial y^2} + \left(n^2k^2 - \beta^2\right) = 0 \qquad [1.85]$$

At this level of calculations, we introduce an effective index $N_{\text{eff}}(x)$ yielding the following expressions:

$$\frac{1}{F}\frac{\partial^2 F}{\partial y^2} + n^2k^2 = k^2 N_{eff}^2(x) \qquad [1.86]$$

$$\frac{1}{G}\frac{d^2G}{dx^2} - \beta^2 = -k^2 N_{eff}^2(x) \qquad [1.87]$$

These two equations are essential for the effective index method. From [1.86], we determine the effective index N_{eff} and the field $F(x,y)$. The obtained value of N_{eff} is then used in equation [1.87] in order to determine the propagation constant β and

the field distribution $G(x)$. Finally, equation [1.82] allows us to obtain the modal field of the guide.

The previous analysis indicates that the effective index method consists of substituting the channel waveguide problem by that of two orthogonal planar waveguides. One of them is in the x direction and the other is in the y direction, as reported in the following figure.

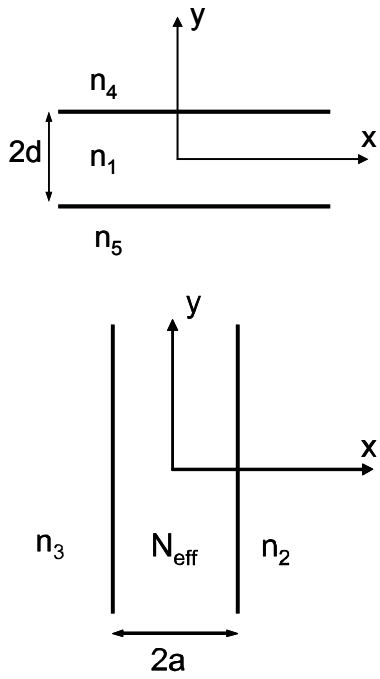

Figure 1.18. *Decomposition of channel waveguides in two planar waveguides*

In contrast to a planar waveguide case, there are not guided modes that are strictly TE or TM. We speak about quasi-TE or quasi-TM modes. In addition, it should be noted that the effective index N_{eff} in equation [1.86] can be calculated for two polarizations TE and TM. The analysis of the quasi-TE modes is carried out according to the following sequence: we calculate the effective index N_{eff} and F(x, y) of structure 1. The value of N_{eff} found makes it possible to calculate the propagation constants as well as the G(x) function of structure 2. From the point of view of polarization: for a polarization quasi-TE, we carry out a calculation for a TE polarization in the case of structure 1 and a TM polarization in the case of structure 2. For the quasi-TM modes, the calculation sequences are reversed.

Note that for the analysis of structures 1 and 2 separately, we use the same approaches discussed in the preceding sections. In other words, we can use the dispersion equation of guided modes already presented or the WKB method in case of a graded index waveguide.

The errors of the effective index method are basically connected with equation [1.83] (approximation of slight variation). However, it gives quite accurate results particularly in the case of well confined guided modes (far from the cut-off). To improve the accuracy of this method, a number of modifications have been suggested. The most important one is the azimuthal effective index and the dual effective index reported in [Mar 1988, Cha 1986].

1.4. Light propagation in anisotropic media

From an optical point of view, materials can belong to three large families: isotropic materials, uniaxial materials and biaxal materials. The isotropic materials, due to their symmetry, have the same properties in all the directions of space. They have a single refractive index noted n. The uniaxial materials have two indices because they present a center of symmetry. Their indices are noted n_o (ordinary index) and n_e (extraordinary index). The biaxal materials present three different indices and thus have different properties in all the directions of space. Their indices are noted n_x, n_y, n_z.

In this section, we will concentrate on the case of uniaxial materials. The latter belong to tetragonal, trigonal or hexagonal systems. For such a material with the optical axis along the Oz, we can write:

$n_x = n_y = n_o$ ordinary index.

$n_z = n_e$ extraordinary index.

In addition, if $n_o < n_e$ the crystal is considered positive uniaxial, otherwise it is a negative uniaxial material. For example, $LiNbO_3$ is a positive uniaxial crystal.

Generally, the problems of anisotropy appear at the time of the study of the thin films for integrated optics. As a matter of fact, during thin film growth, it is not certain that the optical axis is in accordance with the required direction. Moreover, we systematically do not know its orientation after the film deposition.

Let us consider the case of a planar waveguide in the form of dielectric, homogenous and uniaxial (with indices n_o and n_e) thin film. The substrate and superstrate refractive indices are n_s and n_a, respectively. The direction of the guiding layer optical axis is given by two angles θ and φ and the incidence plane is taken parallel to xOz (Figure 1.17).

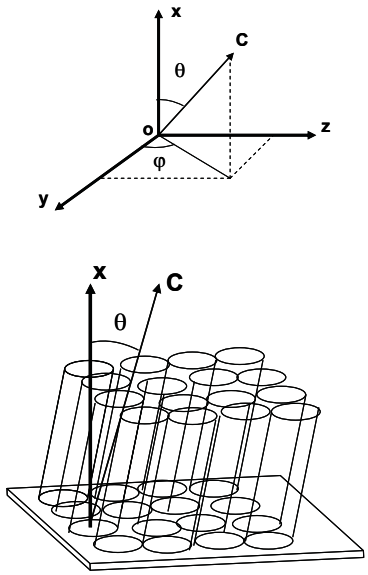

Figure 1.19. *Model of a tilted structure with an angle φ*

In order to solve the problem of the guided mode propagation in such a structure theoretically, two cases should be considered: the first is the case of a well oriented guide and the second one is that of a tilted structure.

In the first case, we consider a simple structure whose optical axis is well directed either in the xOz plane ($\varphi = 90°$) or in the yOz plane ($\theta = 90°$, $\vec{c} \perp \vec{x}$). This problem can be solved by using Maxwell's equations that have already been pointed out. It is shown that we obtain TE and TM modes depending on the state of polarization of the guided wave and its direction of propagation compared to the optical axis [Kad 1989, Par 1984].

For example, let us consider the case where the optical axis is in the plane of incidence which coincides with the xOz plane. In this configuration, whatever the orientation of the optical axis, the TE wave always sees the same ordinary index n_o. The dispersion equation is that of TE modes presented above. However, the propagation of a TM wave is influenced by the orientation of the optical axis in the plane of incidence because its electric field has two components. The dispersion equation is, then, slightly modified compared to that of TM modes presented in section 1.2.2. The use of Maxwell's equations and the boundary conditions show that this equation can be written in the following way:

$$\frac{2\pi d}{\lambda}\frac{n_o n_e}{n_j^2}\sqrt{(n_g^2 - N_m^2)} = \Phi'_{(n,n_a)} + \Phi'_{(n,n_s)} + m\pi \qquad [1.88]$$

$$\Phi'_{(n,n_j)} = arctg\left[\left(\frac{n_o n_e}{n_j^2}\right)\sqrt{\frac{\left(N_m^2 - n_j^2\right)}{\left(n_j^2 - N_m^2\right)}}\right] \qquad [1.89]$$

$$n_g^2 = n_o^2 \sin^2\theta + n_e^2 \cos^2\theta \qquad [1.90]$$

where θ is the angle between the optical axis and the normal to the surface.

Under these conditions, starting from TE modes and by using the dispersion equation in the same manner as the isotropic case, we determine the ordinary index n_o and the thickness d of the guiding layer. The dispersion equation of TM modes becomes a transcendent equation with two unknown factors n_e and θ. Thus, two values of the effective indices are sufficient to obtain these parameters. However, the accuracy of n_e and θ determination depends on the precision of the effective indice measurements as well as n_o and d calculations [Kad 1989].

Note that in the case of materials with strong birefringence, this method makes it possible to accurately determine the ordinary and extraordinary indices as well as the orientation of the optical axis of the guiding layer.

In the second case of a tilted structure, the optical axis $\vec{c}$ has an unspecified orientation given by the two angles θ and φ. In this case, guided modes are not strictly TE or TM but rather hybrid modes whose analysis requires a calculation that we will not develop here. The reader can consult the following references [Par 1984, Hor 1994, Flo 1994, Wan 1996, Jan 1996].

1.5. Bibliography

[Bae 1992] Baets B., Kaczmarski P. and Vankwikelberge P., "Design and modelling of passive and active optical waveguide devices", J. H. Marsh and R. M. De La Rue (eds.), *Waveguide Optoelectronics*, 21-71 (1992).

[Bor 1999] Born M. and Wolf E., *Principles of Optics*, Cambridge University Press; 7th edition (1999).

[Cha 1986] Chang K.S., "Dual effective index method for the analysis of rectangular dielectric waveguide", *Applied Optics*, 25(13), 2169-2174 (1986).

[Din 1983] Ding T.-N. and Garmine E., "Measuring refractive index and thickness of thin films: a new technique", *Appl. Opt*., 22(20), 3177- 3181 (1983).

[Fer 1981] Fereiral L.G., Pudensi M.A.A., "Waveguiding in a dielectric medium varying slowly in one transverse direction", *J. Opt. Soc. Am*., 71(11), 1377-1380 (1981).

[Flo 1994] Flory F., Albrand G., Endelema D., Maythaveekulchai N., Pelletier E., Rigneault H., "Guided-wave characterization techniques for the comparison of properties of different optical coatings", *Opt. Eng*., 33(5), 1669 (1994).

[Jan 1996] Janchen H., Endelema D., Kaiser N. And Flory F., "Determination of the refractive indices of highly biaxial anisotropic coatings using guided modes", *Pure Appl. Opt*., 5, 4056-415 (1996).

[Hor 1994] Horowitz H., Mendes S.B., "Envelope and waveguide methods: a comparative study of PbF_2 and CeO_2 birefringent films", *Appl. Opt*., 33(13), 2659-2663 (1994).

[Hun 1985] Hunsperger R.G, *Integrated Optic: Theory and technology*, Springer-Verlag, 2nd edition, (1985).

[Kad 1989] Kadad I., Réalisation et etude de guides d'ondes optiques plans en Nitrure d'Aluminium par pulverisation magnetron réactive, PhD Thesis, University of Saint-Etienne (1989).

[Lan 1960] Landau L.D. and Lifshitz E.M., *Quantum Mechanics*, Pergamon Press (1960).

[Mar 1969] Marcatili E. A.J., "Dielectric rectangular waveguides and directional couplers for integrated optics", *Bell Syst. Tech. J*., 48, 2071-2102 (1969).

[Mar 1988] Marcatilli A.J. and Hardy A.A., "The azimutal effective index method", *IEEE Journal of Quantum Electronics*, QE-24(5), 766-774 (1988).

[Mar 1969] Marcuse D., "Mode conversion caused by surface imperfections of a dielectric slab waveguide", *Bell Syst. Tech. J*., 48, 3187-3215 (1969).

[Mar 1991] Marcuse, D., *Theory of Dielectric Optical Waveguides*, Academic Press, New York, 2nd edition, (1991).

[Mur 1999] Murphy, E.J., *Integrated Optical Circuits and Components, Design and Applications*, Marcel Dekker, New York (1999).

[Nis 1989] Nishihara H., Haruma M. and Suhara T., *Optical Integrated Circuits*, McGraw-Hill Professional (1989).

[Par 1984] Parriaux O. and Cochet F., "Characterization method of birefringent films by guided optical waves", *Opt. Lett*., 9, 484-487 (1984).

[Rac 1984] Rachman B.M.A., Davies J.B., "Finite-element analysis of optical and microwave waveguide problems", *IEEE Trans. on Micrwave Theory and Tech.*, MTT-32, 20-26 (1984).

[Rae 1997] Raether H., in G. Hass, M.H. Francombe and R.W. Hoffman's (Eds) *Physics of Thin Films, Advances in Research and Development*, Academic Press, New York, 9, 145-261 (1997).

[Sal 1991] Saleh B.E.A. and Teich M.C., *Fundamentals of Photonics*, series in pure and applied optics, John Wiley & Sons (1991).

[Tie 1970] Tien P.K. and Ulrich R., "Theory of prism-film coupler and thin-film light guides", *J. Opt. Soc. Am*., 60, 1325- 1337 (1970).

[Tie 1974] Tien P.K., Riva-Sanseverino S., Martin R.J., Ballman A.A. and Brown H., "Optical waveguide modes in single crystal-line $linbo_3$-$litao_3$ solid solution films", *Appl. Phys. Lett*., 24, 503-506 (1974).

[Tie 1977] Tien P.K., "Integrated optics and new wave phenomena in optical waveguides", *Rev. of Modern Physics*, 49 (2), 361- 410 (1977).

[Vin 2003] Vincent B., Conversion de frequencies dans les guides d'ondes fabriqués par implantation ionique dans les cristaux périodiquement polarises, PhD Thesis, University of Metz (2003).

[Yar 1973] Yariv A., "Coupled-mode theory for guided wave optics", *IEEE J. of Quantum Electronics*, 9(9), 919-933 (1973).

[Wal 1985] Walpita L.M., "Calculation of approximate propagation characteristics of any given two-dimensional optical waveguide", *Electronics Letters*, 21(23), 1075-1076 (1985).

[Wan 1996] Wang H., and Hurtado-Ramos J., "Guided waves in thin films consisting of tilted columns deposited on anisotropic substrates: excited by a birefringent coupler", *Pure Appl. Opt.*, 5, 239-250 (1996).

[War 1988] Ward L., *The Optical Constant of Bulk Materials and Films*, series on optics and optoelectronics, Adam Hilger (1988).

This page intentionally left blank

Chapter 2

Optical Waveguide Fabrication Techniques

In Chapter 1, we stated that the characteristics and the use of optical waveguides mainly depend on the index profile of the guiding layer which must be higher than those of the two surrounding layers. Consequently, to obtain a guiding structure, it is necessary to micro-structure the refractive index creating a central layer whose index is higher than those of the two adjacent layers. This principle is at the foundation of all the optical waveguide fabrication techniques, of which we will describe the most current in this chapter. These techniques can be classified into two families:

– deposition techniques, consisting of deposition of high index thin film onto a low index substrate; and

– substitution techniques, where the principal is to create a high index region in a substrate by introducing new atoms.

The basic criteria behind the choice of one technique rather than another are:

– the thickness and indices of the guiding layer;

– losses of the structure;

– purity of material and its optical axes;

– the stability of the process and the layer obtained;

– the reproducibility of the technique;

– the cost of the technique and interest of material.

In this chapter, we describe the principal techniques of planar waveguide fabrication, and provide some information on channel waveguides. The list of these techniques is not exhaustive and only the most current will be presented [Nis 1989].

2.1. Optical waveguide fabrication techniques

2.1.1. *Thin film deposition techniques*

The study of waveguides in the form of thin films continues to cause considerable interest. The advantage of thin films is that they enable us to carry out an even monolithic or hybrid integration compatible with already existing semiconductor technology. However, thin film need to be competitive on the level of cost and performance compared with bulk materials.

Many techniques have already been used for the realization of active or passive planar waveguides in the form of thin films. In general, it is difficult to say which technique is the best. This seems to depend on the practical application concerned.

In particular, we note the problems of the surface roughness which can cause detrimental optical losses due to diffraction. It is necessary to solve these problems before any practical use of the film can be made. Therefore, we need to undertake studies on the fabrication procedure, and optimize the deposition parameters. The goal of this endeavor would be to find a compromise between the thickness and the roughness of the surface.

2.1.1.1. *Spin coating technique*

This technique consists of depositing a thin layer of polymer on a substrate [Pau 1986]. Initially, a drop of polymer solution is deposited on the substrate (see Figure 2.1). This drop is then spread out over the surface of the substrate by rotation. After the deposition, the film generally undergoes a thermal process to ensure its adhesion to the substrate.

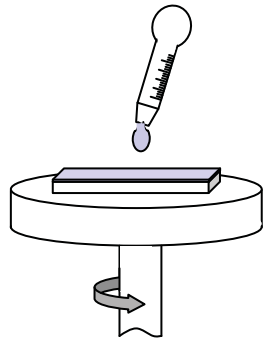

Figure 2.1. *Principle of the spin coating technique*

This technique is simple, not very expensive and does not require sophisticated technical tools. However, the purity and the homogenity (in terms of thickness) of the layer obtained must be carefully considered.

2.1.1.2. *Chemical vapor deposition (CVD) technique*

The technique previously described is a method of physical deposition. The chemical vapor deposition method consists of creating chemical reactions between gases and depositing the products resulting from the reaction onto a substrate [Lee 1986]. These chemical reactions are produced under various conditions. Deposition at high temperature and under atmospheric pressure is used, in particular, to fabricate optical fibers and perform waveguides on glass [Hua 2004] (in this case they are transparent oxides which are deposited after the reaction or combustion of oxygen with halides). The CVD can also be used to create thin layers on ferroelectric materials [Swa 1992]. As it allows the deposition of several types of thin films CVD is largely used in the semiconductors industry as a component fabrication process. There are several alternatives to the CVD technique depending on deposition conditions. The HTCVD (high temperature chemical vapor deposition) technique [Kon 1996] is used if the substrate is heated at very high temperature; while LTCVD (low temperature chemical vapor deposition) [Aha 1991] is used at low temperature or at room temperature. If an organometallic precursor is used, then we refer to MOCVD (metal-organic chemical vapor deposition) [Lee 1998]. Finally, in the case of plasma, the PECVD (plasma enhanced chemical vapor deposition) process is used [Ely 2001].

2.1.1.3. *Sol-gel technique*

The sol-gel technique is recognized as one of the simplest methods of thin film deposition. It gives high quality layers with low cost [Yan 1994], and is used to deposit crystallized thin layers on substrates of glass. This technique consists of polymerizing in the form of gel, a solution containing the components to be deposited and an organic solvent. After annealing, an inorganic oxide is obtained at the end of the reaction. This method makes it possible to obtain layers from 100 to 500 nm. Thicker layers can be achieved by successive depositions. Although this technique is easy to perform and requires relatively cheap material, it requires good control of the deposition conditions which can, if they are not sufficiently managed, generate constraints and thus cracks and thickness variations in the layer obtained [Bah 1998].

2.1.1.4. *Epitaxial growth*

This is very often used to produce active waveguides for integrated optics, in particular for optical systems such as the optical modulators and switches. This technique [Fei 1996] consists of growing a crystalline thin layer on a substrate starting from a material whose cell parameters and/or structure is similar to that of

the substrate. This technique is often used to produce waveguides of semiconductor materials, such as ZnO [Shi 1980], InP [Nag 1997] or GaN [Dub 1995]. However, dielectric materials can also be synthesized, such as for example, $LiNbO_3$ or $LiTaO_3$ [Fuk 1974] for electro-optic modulation applications.

2.1.1.5. *Pulsed laser deposition (PD)*

Pulsed laser deposition enables the growth of film in a reactive atmosphere (oxygen) [Wil 2000]. Its principal advantage lies in its capacity to restore in film the stoechiometry and the chemical composition of the target. This technique is thus particularly relevant for the complex material growth of oxides such as bi, tri or tetra metallic compounds. The judicious choice of the temperature and the nature of the substrate can lead to films of good structural quality being able to reach the perfect epitaxy of the deposition. The experimental device for laser ablation is composed mainly of a laser and an enclosure of ablation (Figure 2.2). The latter contains several supports of various diameters allowing coupling with accessories: target and substrate holders, pressure gauges, the pumping system, the gas introduction system, manipulators and visualization holes.

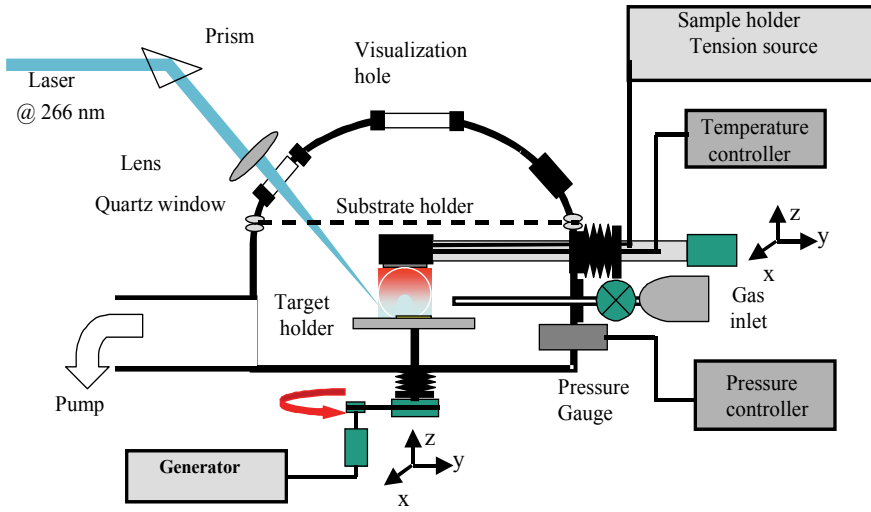

Figure 2.2. *Principle of thin film deposition by using pulsed laser deposition (PD) (reproduced courtesy of EMillon)*

The interaction processes between the target and the ablation laser, which influence the morpho-structural quality of the layers, are strongly conditioned by the laser characteristics: energy per unit must be sufficient to achieve the top of the threshold of ablation, the wavelength of the radiation must correspond to the absorption range of the material and the pulse duration of sufficiently short impulse (a few nanoseconds) to limit the thermal phenomenon of the diffusion process in the target [Che 2001].

2.1.1.6. *Magnetron sputtering*

This technique consists of bombarding a target with ions, in order to tear off the target ions that are to be deposited onto the substrate [Kad 1989] (Figure 2.3). The argon ions, created by the high voltage excitation, tear off the target compounds to be deposited on the surface of the substrate. This technique allows the deposition of all types of simple or complex, conducting or dielectric materials. It also allows deposition onto any type of conducting or dielectric substrate [Kad 1989, Dog 1999].

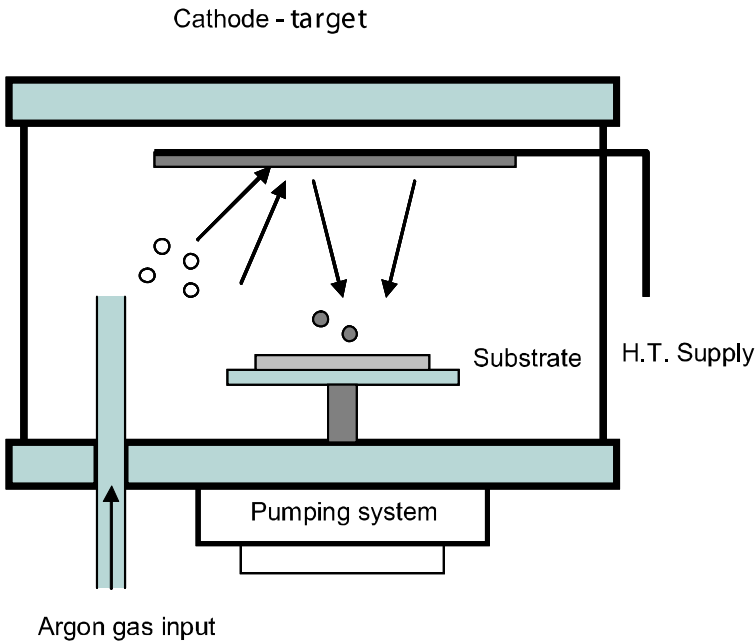

Figure 2.3. *Magnetron sputtering principle*

Note that magnetron sputtering can be performed under a DC or a radio frequency (rf) voltage.

2.1.2. *Substitution techniques*

This family of techniques is based on the introduction of ions into a substrate to locally vary its refractive index. These techniques produce graded index waveguides and they are used, especially, with crystals such as ferroelectric materials.

2.1.2.1. *Exo-diffusion*

The exo-diffusion is among the first methods being used for waveguide fabrication. It was developed by J.P. Kaminow and I.R. Careuthers in 1973 [Kam 1973]. In the implementation of this technique, a thin layer with high index is created by extraction from the substrate surface of certain elements belonging to its composition. The process is performed under particular temperature and pressure conditions. In $LiNbO_3$, the lithium oxide (Li_2O) is extracted from the surface using a heat treatment of 1,000°C over several hours in a vacuum or under oxygen atmosphere, thus causing an increase in the extraordinary index [Kam 1973].

2.1.2.2. *Ionic diffusion*

This technique has been extensively used over the last few decades. It was developed by R.V. Schmidt and I.P. Kaminow [Sch 1974] following observations concerning the occupation of the interstices in the $LiNbO_3$ crystal caused by Ti atoms, and also the substitution of Nb^{5+} by titanium. Ionic diffusion consists of diffusing into the substrate a material deposited on its surface, under particular temperature and pressure conditions (850–1,150°C), thus, creating a thin layer with a high index. The various steps of this process are indicated in Figure 2.4.

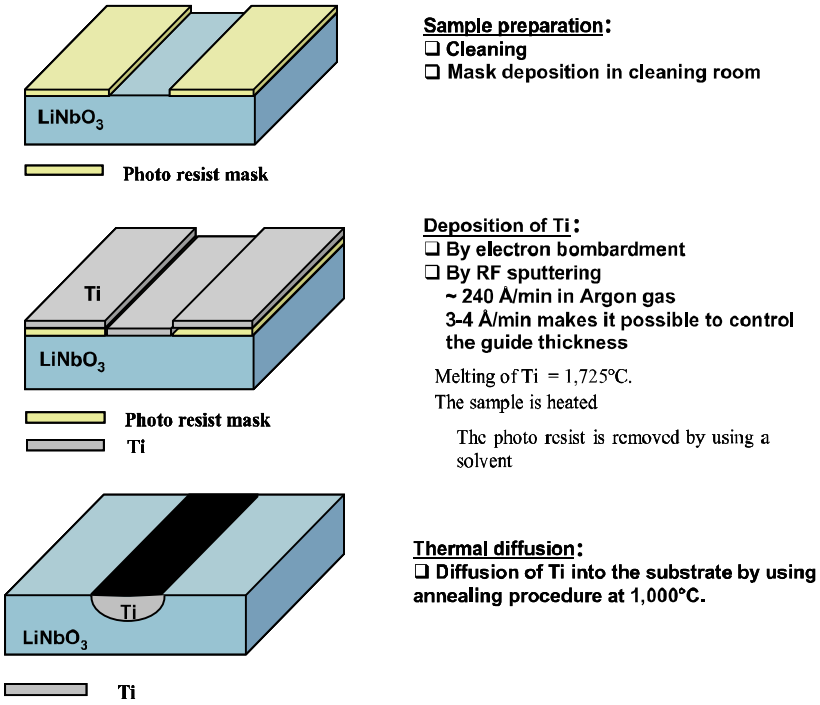

Figure 2.4. *Waveguide fabrication process in $LiNbO_3$ using Ti diffusion*

In $LiNbO_3$, for example, several species of atoms, such as Mg, Ni, Zn, Fe, Co, Cr, V and Ti, can be diffused [Jac 1982, Abo 1993]. The diffusion of Ti can be carried out at a temperature of 1,000°C over several hours at a given pressure. The diffusion of Li can be carried out under vapor atmosphere in a closed tube which is half-closed to avoid the problems of exo-diffusion on the surface. In addition, this protocol makes it possible to directly obtain channel guides by adding a photolithography process into the clean room. It should be noted that the deposition of Ti layer is carried out using the electrons bombardment technique or by the radio frequency magnetron sputtering method. This constraint is dictated by the melting point of Ti which is about 1,725°C.

Figure 2.5 shows a typical temperature profile of Ti diffusion into $LiNbO_3$. The temperature is about 1,000°C, which is reached in 30 min. The Ti diffusion requires 4 to 6 hours to obtain a layer of Ti from 400 to 600 Å. Generally, this diffusion continues for 1 hour in an atmosphere of O_2 to compensate for the oxygen losses in lithium niobate. Cooling down to the ambient temperature can take between 15 and

20 minutes. Lastly, the annealing atmosphere plays an important role in the waveguide optical properties obtained.

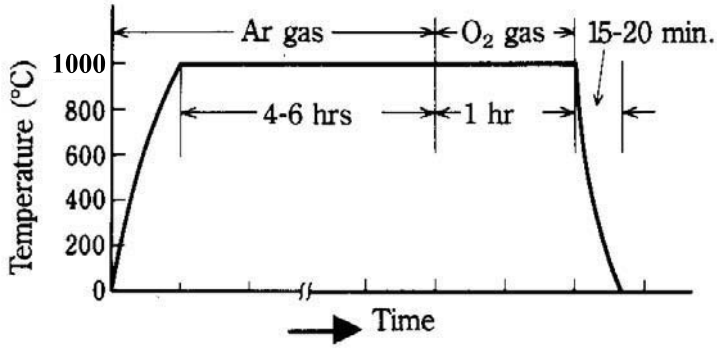

(a)

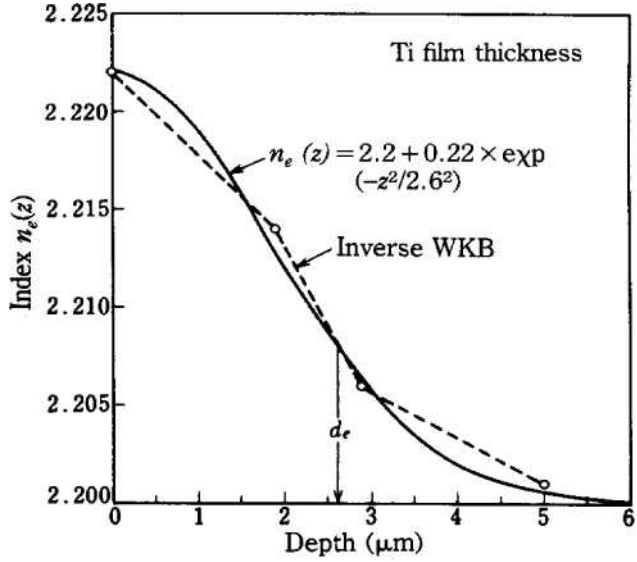

(b)

Figure 2.5. *(a) Typical temperature profile for titanium diffusion, and (b) index profile of a titanium diffusion guide (from Nishihara et al. 1989)*

Generally, this technique leads to an increase in the ordinary and extraordinary indices of the diffused layer and obtained waveguides of good optical quality. In addition, the characteristics of the diffused guides can be controlled by an accurate management of the experimental conditions, in particular the concentration of ions which generally has a Gaussian profile.

2.1.2.3. *Ionic exchange*

This is currently one of the most developed techniques. It was created by J L Jackel *et al.* [Jac 1980], particularly to fabricate guides by protonic exchange in $LiNbO_3$. The work of Spillman *et al.* [Spi 1983] must also be mentioned, which made it possible for the first time to produce guides in $LiTaO_3$ by protonic exchange.

The ionic exchange consists of introducing the substrate into a bath of acid in order to carry out an exchange between the ions of the bath and those of the substrate (see Figure 2.6). The immersion of a sample of $LiNbO_3$ in a molten salt of $AgNO_3$ around 360°C during several hours, produces an exchange of the ions Ag^+ and Li^+ causing a growth of the extraordinary index [Jac 1980, Spi 1983, Kor 1996]. Other ions can also be exchanged, such as Ti^+ and Li^+. Nevertheless, waveguides fabricated by exchange of ions in $LiNbO_3$ proved to be difficult to reproduce. For this reason many works turned to the exchange of protons which arouses today more and more interest. These studies highlighted that the guides obtained have good optical qualities but that their non-linear properties seem to be somewhat faded [Lau 1992, Bor 1993]. Other materials can also be used. For example, the exchange of potassium ions by protons in a crystal of KTP ($KTiOPO_4$) makes it possible to obtain effective waveguides [Ris 1996, Roe 1993].

From the optical point of view, the exchange of protons causes a growth of the extraordinary index n_e and a slight decrease of the ordinary index n_o. Consequently, the guides obtained support only TM modes. Guiding structures were carried out at the same time in crystals of $LiNbO_3$ z-cut or x-cut with losses lower than 0.5 $dB.cm^{-1}$ [Pas 2002]. In addition, a post-fabrication annealing is generally applied to the sample in order to improve the optical properties of the guiding area.

Finally, waveguides produced by exchange of protons, comparatively, have a better resistance to optical damage than those fabricated by Ti diffusion. From the technological point of view, the characteristics of the guide depend mainly on three parameters: concentration of the bath, the temperature and duration of the exchange (see Figures 2.7 and 2.8 below).

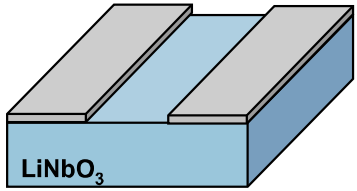

Sample preparation:
- ❑ Cleaning
- ❑ Mctallic mask of (Al, Ta).

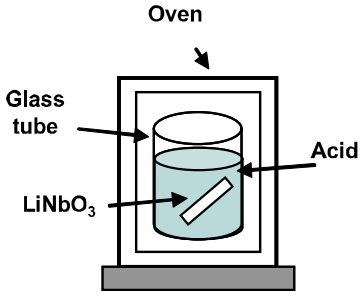

Emersion into an acid bath:
- ❑ Benzoic: C_6H_5COOH.

Temperature: 120-250 °C
Time: 15 -90 min

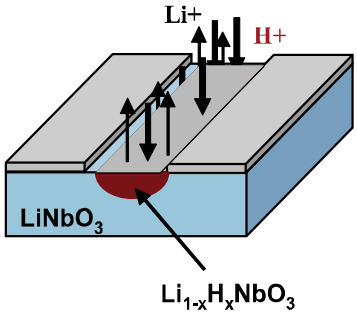

☞ **Exchange of Li+ by H+ : $Li_{1-x}H_xNbO_3$**

Thermal annealing:
- ❑ Temperature ~ 350 °C
- ❑ Time: several hours
- ❑ Atm.: air

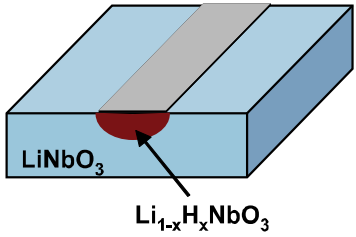

Figure 2.6. *Ion exchange (H)+in lithium niobate*

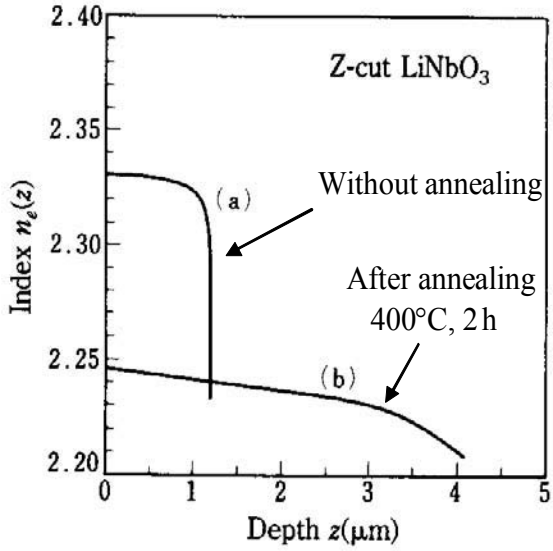

Figure 2.7. *Typical index profile of a H^+:$LiNbO_3$ (z-cut) waveguide*

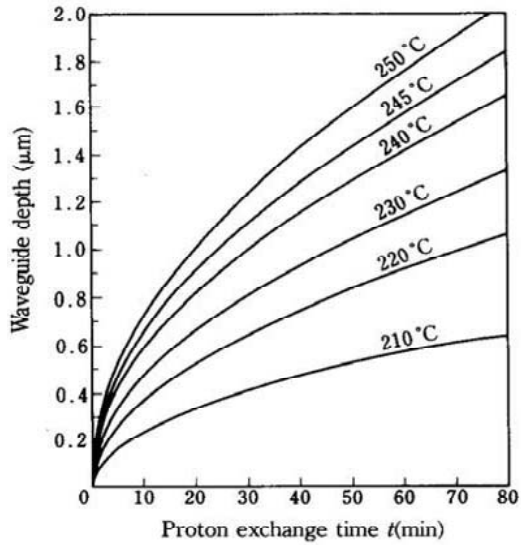

Figure 2.8. *H+:$LiNbO_3$ (z-cut) thickness variation versus protonic exchange duration for different temperature values [Nis 1989]*

The analysis of the protonic exchange shows two important effects: on the one hand, the transformation of a rhomboedric structure into a cubic peroveskit structure; and on the other hand, the instability of the index profile due, in particular, to the migration of the H^+ protons within the substrate over time.

For better control of the exchange process, we can refer to the works of De Micheli *et al.* [Mic 1995] and Korkishko *et al.* [Kor 1999].

The work of De Micheli concerned the effects of the annealing and the concentration of the acid on the waveguide properties. They showed that an annealing in an atmosphere of oxygen at T = 400°C and for t = 4 H makes it possible to transform a step index guide into a graded index guide with variation $\Delta n_e \sim 0.01$. Moreover, the use of a diluted acid and enhanced lithium (lithium benzoate (C_6H_5COOLi)) make it possible to control the surface index which decreases with the increase of Li ion concentration in the bath.

Korkishko *et al.* [Kor 1999] concentrated on the study of the $Li_{1-x}H_xNbO_3$ structure. They highlighted the existence of 7 different phases depending on the conditions of fabrication as indicated in Figure 2.9, below.

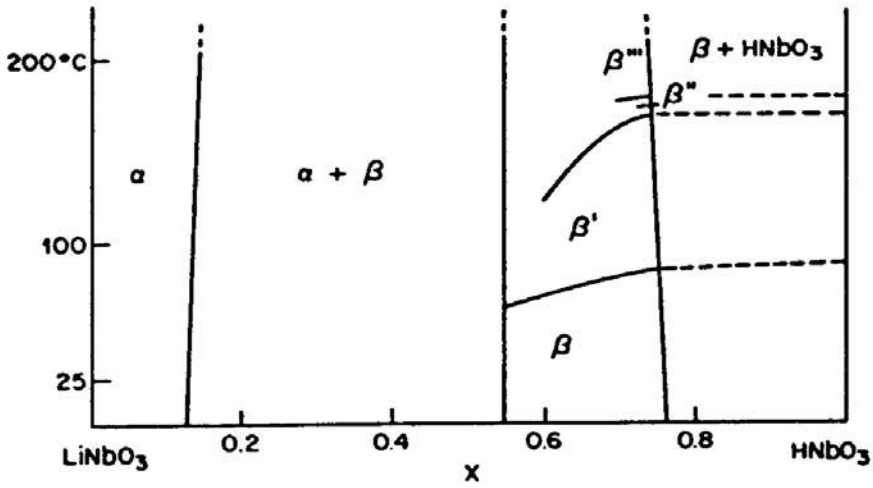

Figure 2.9. *The 7 phases of protonic exchanges in lithium niobate [Kor 1999]*

2.1.2.4. *Implantation technique*

Nowadays, the most common techniques used for waveguide fabrication are incontestably ionic exchange and diffusion, previously mentioned. These two techniques are well controlled in the case of well-known crystals such as $LiNbO_3$, $LiTaO_3$ and KTP. However, their relationship to other potentially interesting materials is far from obvious. This excludes new non-linear materials. For example, in the case of GdCOB, the use of these two techniques seems completely excluded because of the crystalline structure of this material. Moreover, these two techniques can be prejudicial for the non-linear optical properties of the guide, for example, inducing important differences between the experimental and theoretical values of the conversion rates in the case of the exchanged guides [Bor 1993].

The ionic implantation is an alternative technique which appears less detrimental for the crystalline matrix and which can be led at ambient temperature. The remarkable potentialities of this method when used with pure or doped crystalline materials are now widely demonstrated. Ionic implantation was developed more than twenty years ago by P.D. Townsend [Tow 1994] of the University of Sussex (UK) and is now well established.

Several research studies have been devoted to the use of this technique with a broad range of crystalline materials, doped or not [Tow 1990, Tow 1992, Flu 1993, Oul 1995, Mor 1991, Bin 1998]. In particular, the work of P.D. Townsend *et al.* on the He^+ ion implantation and its effects in several non-linear materials ($LiNbO_3$, BNN, BGO ($Bi_4Ge_3O_{12}$), etc.) largely contributed to the success of this method. Other authors were interested in using this technique with other materials, by implanting ions of various natures. Thus, P. Günter *et al.* described a detailed study on the effects of the He^+ implantation in $KNbO_3$ [Flu 1993]. P. Moretti, University of Lyon, contributed thereafter to the development of this technique not only by using other types of materials but also by implanting other types of ions, such as H^+, etc. [Tow 1990, Tow 1992, Flu 1993, Oul 1995, Mor 1991, Bin 1998]. This work shows that the implantation of light ions (H^+, He^+) makes it possible to obtain waveguides with good guiding properties.

Light ion beam implantation has been used to form optical waveguides in numerous non-linear pure or doped crystals. This technique saw some 20 years of development during which it was used to modify the optical properties of materials. It is now reaching its maturity and is subject to valuable application phases. The reason this technique falls behind those previously mentioned is that it requires more complex and expensive equipment. However, commercial applications of implantation to produce optical devices may pull benefits from developments of ion implantation in the field of semiconductor technology [Fav 1993].

2.1.2.4.1. Ionic implantation principle

Details of the implantation process have been the subject of several publications. The principle of implantation consists of mounting the sample onto a special temperature controlled stage in the beam line of a 2 MeV Van De Graaf accelerator. The largest face is bombarded by He^+ (or H+). The ionic implantation induces a refractive index change in the material by two actions. Firstly, at high velocity the ions may induce electronic defects, which may create a slight refractive index variation. Secondly, at the end of their track, ions produce a nuclear damage yielding to the creation of an optical barrier with a substantial refractive index, which is responsible for light confinement by internal total reflection.

Commonly, the sample temperature has to be carefully kept close to 300 K to prevent thermal beam effects which may frustrate the barrier formation. A homogenous radiation at low flux (0.1 μA/ cm^2) is guaranteed by a beam scanning over an area of 10 cm^2 to minimize the charge effects on the radiated surface. To further reduce the optical losses occurring due to tunneling effects through the optical barrier, the beam can be enlarged by performing multiple-energy implants.

Moreover, the flexibility of the implantation technique lies in its ability to control the implantation parameters precisely. This allows us to accurately define the waveguide thickness, which is related to the penetration depth of the ions within the crystal: as with the influence of ions which determine the resulting refractive index variation at the optical barrier. Finally the nature of the implanted ions is a further degree of freedom in terms of the possibility of controlling the induced damages at the optical barrier and thus the related refractive index changes. Note that several routines have been developed to shape the track; and the interaction of the implanted ions with materials applies to the TRIM (Transport of Ions in Matter) code, which in general gives very reliable results of the distribution of ions within the crystal. Ionic implantation uses a Van de Graaff accelerator composed of a source of ions, an accelerator and several arms ending with rooms of controlled temperature (Figure 2.10).

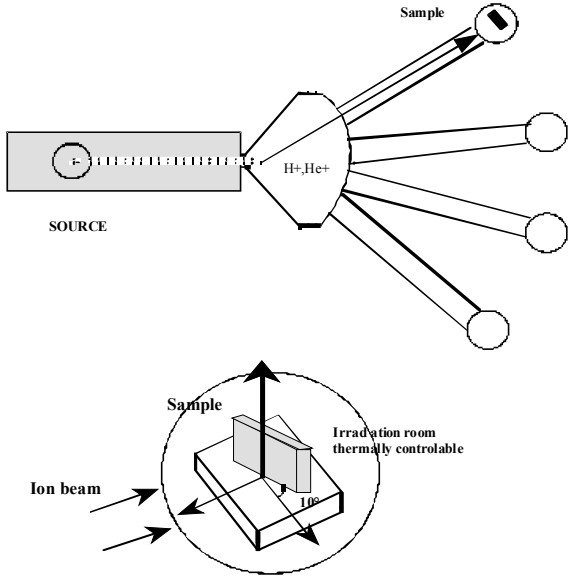

Figure 2.10. *Scheme of the Van de Graaff accelerator (600 KeV – 2MeV)*

The generated beam can have an energy ranging between 600 KeV and 2 MeV. The sample to be implanted is mounted on a plate, inside the room. Its large face is then exposed to an ion beam (H^+, He^+), while the temperature is maintained around 300 K to avoid the heating effects which can deteriorate the fabrication process, in particular, of ferroelectric materials. To avoid the effects of channeling, the sample is turned to 10° from the ion beam line.

Before examining the details of this technique, let us recall its advantages. We can summarize the previous description with the following points:

– the quantity of implanted ions can be easily controlled by measuring the ion beam as a current;

– the energy of the beam makes it possible to control the implantation depth and thus to control in a precise way the thickness of the waveguide;

– the ions of any nature can, theoretically, be implanted;

– the implanted depth of ions can be adjusted on the same target material.

2.1.2.4.2. Implantation effects

The origin of refractive index modification by ionic implantation can be found in the interaction of ion-matter. This interaction is carried out according to two distinct mechanisms: interactions with the electrons of the target (by elastic collisions) and

nuclear collisions (of Coulomb type) with the cores of material atoms. During these processes, the ions undergo a loss of energy for finally being implanted in the substrate.

Electronic defects are explained in the following way: at the time of their penetration in the crystal, the ions yield a part of their energy to the electrons of the crystal lattice atoms which pass in an excited or ionized state. At the end of their path, the ions, slowed down by the interaction with the electrons, collide with the atoms of the target, causing a displacement of the target atoms. These collisions allow the formation of various types of nuclear defects such as the Frenkel defects, gaps and/or interstitial defects.

The implanted ions distribution in the crystal has been the subject of many works. For instance, numerical approach to simulate the ion trajectory often gives interesting results. Currently, TRIM (Transport of Ion in Matter) code, designed by Biersack and Ziegler [Bie 1985], is one of the most frequently used computer codes. TRIM calculation is based on the Monte Carlo algorithm and provides:

– the electronic and nuclear losses profile;

– the moved atoms profile (by ionization or retreat);

– the implanted ions profile;

– the efficiency of pulverization relating to atoms ejection, during ionic implantation.

An example of TRIM simulation is given in Figure 2.11.

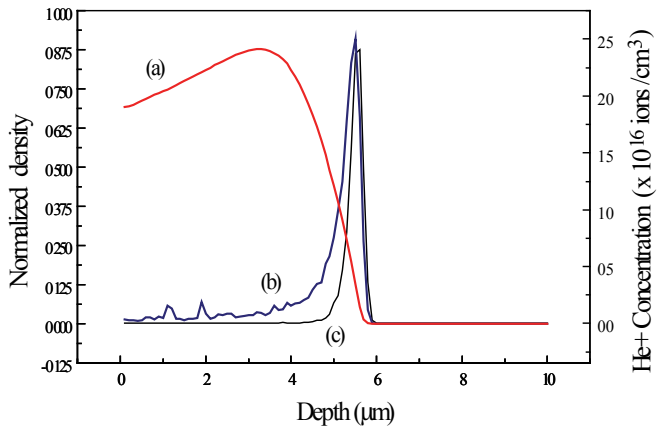

Figure 2.11. *Example of TRIM simulations (a) electronic excitations, (b) nuclear damage, (c) He^+ concentration*

2.1.2.4.3. Ionic implantation effect on the material refractive index

The ionic implantation and the related damages can induce material density and polarizability changes. Knowing that the refractive index of a material is largely dependent on these parameters, a variation of the latter can induce a modification of the index value. Indeed, for a given material, the refractive index is related to the polarizability of its components by the Lorenz-Lorentz relation, given by:

$$\frac{n^2-1}{n^2+1}=\frac{\sum_i \alpha_i}{3\varepsilon_0 V} \qquad [2.1]$$

where α_i is the polarizability of the i components, and V is the volume of the elementary cell.

Thus, the refractive index variation is:

$$\frac{\Delta n}{n}=\frac{\left(n^2-1\right)\left(n^2+2\right)}{6n^2}\left(-\frac{\Delta V}{V}+\frac{\Delta\alpha}{\alpha}\right) \qquad [2.2]$$

The structural changes that may give rise to index effects are predominantly caused by nuclear collision induced damage. However, the lattice restructuring generally results in chemical bond changes, and subsequent polarizability effects. These and other contributions such as stress and piezoelectricity in the material lead to the possibility of index changes, as well as the non-linear susceptibility modifications, even in the guiding region.

In general, refractive index variation induced by ionic implantation can be represented by the following scheme of Figure 2.12.

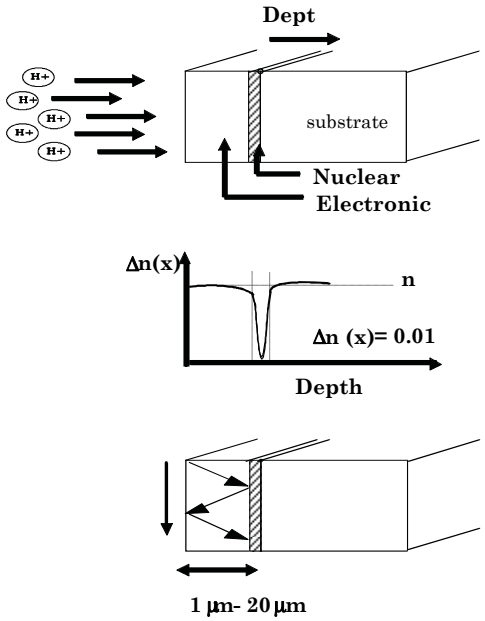

Figure 2.12. *Effects of implantation on the material refractive index*

The general shape shows a decrease in the refractive index from the surface to the optical barrier, which corresponds to the area where ions are deposited. Thus, we find the index of the substrate in the non-affected area. The use of light ions allows us to obtain index profiles with a mild decrease which corresponds to that of a step index waveguide.

It is important to note that the ionic implantation technique makes it possible to produce waveguides with a well defined thickness, which can be selected between 1 µm and 20 µm simply by varying the energy of the beam used. In the same way, the width of the optical barrier can be adjusted by modifying the energy of the implanted ions. In this manner it is possible to improve light confinement. A TRIM calculation makes it possible to determine with precision the thickness of the guiding layer, actually corresponding to the depth of the implanted ions. This is of great importance for the characterization of the waveguide because the only parameter remaining to be determined is the index profile (see Figure 2.13). To determine this it is necessary to study the guiding properties of the guides obtained, in other words, to excite the guided modes of the structure. How to achieve this will be the focus of Chapter 3.

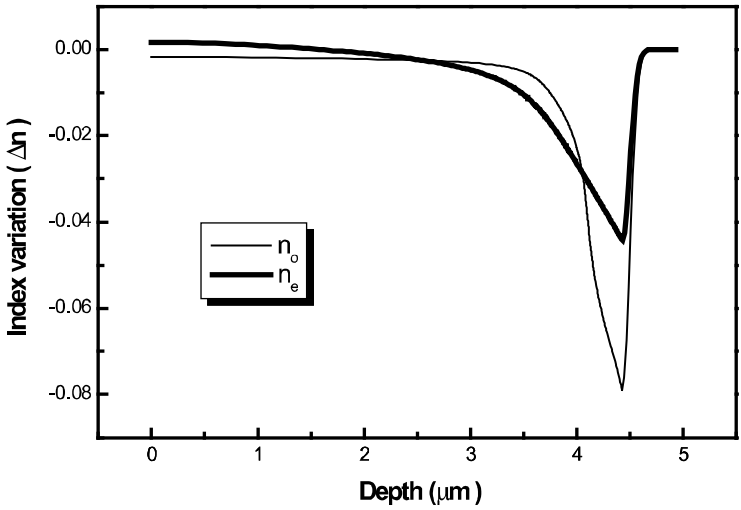

Figure 2.13. *Ordinary and extraordinary index profiles of LiNbO$_3$ waveguide fabricated by He^+ implantation (dose = 2 10^{16} ions/cm^2 and energy = 2 MeV)*

2.1.2.4.4. Channel waveguide fabrication

The channel waveguide fabrication can be considered according to two approaches: one uses successive implantations to build two side optical barriers and the other uses the positive index variation induced by He^+ implantation under certain specific conditions.

The first approach consists of producing a planar guide. This guide is fabricated under the usual conditions, by producing an optical barrier parallel to the surface of the guide. Then, using a mask made up of an adjustable slit, two vertical optical barriers are produced by multiple implantations by varying the energy of the ions beam. These two vertical "walls" ensure lateral light confinement (see Figure 2.14).

The second approach is based on a discovery in recent studies which showed that He^+ implantation could create a positive index variation instead of the expected index decrease [Mus 2003, Che 2006]. Under these conditions, the channel guide is directly obtained by implantation through a mask. This last process makes the implantation technique flexible and simple to perform.

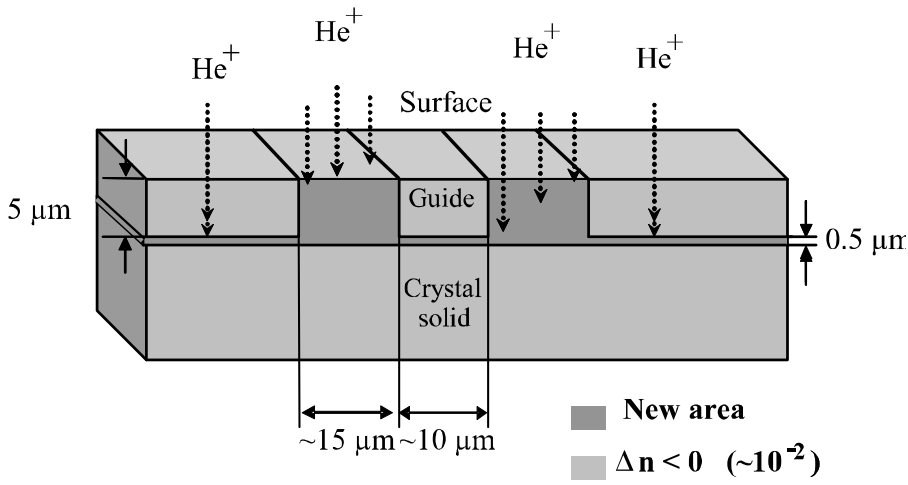

Figure 2.14. *Channel waveguide fabrication by ionic implantation to create vertical "walls"*

Another approach consists of carrying out multiple implantation on the whole sample surface using a mask (which can be a tungsten filament of ten micrometers of diameter), in order to protect the part of the crystal which will be used as a channel guide (see Figure 2.15) [Flu 1996]. It should be indicated that the ionic implantation produces guides which support TE and TM polarizations.

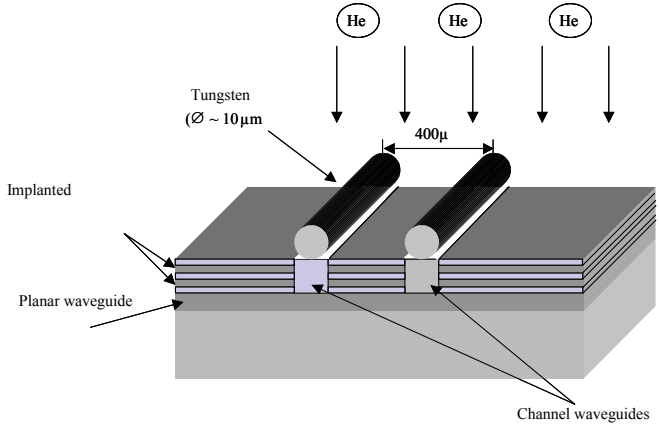

Figure 2.15. *Creation of a channel optical waveguide using multiple implantation through a tungsten micro wire mask*

2.2. Integrated optic materials

Five families of optical materials are commonly used in integrated optics (see Figure 2.16):

– glass;

– organic materials;

– dielectrics;

– semiconductors;

– silica-based materials.

Silica (Si) is the strong link between electronics and photonics. As a matter of fact, photonic components benefit from the development of micro-electronics based on Si. Semiconductor materials such as III-V or II-VI materials in particular find many applications in light emission and detection. Dielectrics generally have non-linear optical properties which confer to them potential applications for optical signal processing through refractive index manipulation. For instance, $LiNbO_3$ is the most well known dielectric material. It has been used for many years for optoelectronic component fabrication. Organic materials or polymers have substantial interest for electro-optic modulation applications and non-linear optics. Finally, integrated optics on glass offer potential benefits to the performance of low cost optoelectronics components, such as optical sensors, etc.

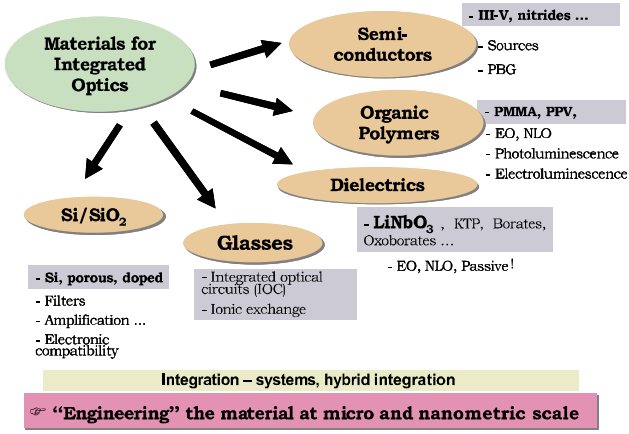

Figure 2.16. *Schematic presentation of different types of optical materials*

Generally, the material must present a good compromise between its optical properties, its homogenity, its structure and its transparency. Moreover, the facility of growth (synthesis) of the material is also a selection criterion.

The first generations of optoelectronic components simply exploited existing materials for their specific properties: direct forbidden band for the emission or effective electro-optical effect for light modulation. In particular, III-V semiconductors and oxides (lithium niobate) allowed the realization of pioneer components which were the foundation of optical telecommunication systems. The versatility of these types of materials continues to hold the interest of researchers, in particular those trying to push the limits of the materials functionalities in terms of band-width, tenability and dimension.

In this section, we will show the principal materials used in the field of integrated optics. The list is certainly far from exhaustive and the reader can consult an already abundant literature on this subject.

2.2.1. *Glass*

The various forms of glass are optically isotropic, and are commonly used in optics. Optical waveguides can be obtained in these materials using a very simple process. Glass is often composed of SiO_2 and B_2O_3 with a small proportion of oxides, such as, Na_2O, K_2O and CaO. In addition, the glass refractive index is related to its density and the electronic polarizability of its components. Consequently, a high index area can be produced by introducing the suitable ions into the substrate [Ram 1988]. Thus, the ionic exchange technique is often employed and consists of using ions of Na^+, Ag^+, K^+ and Tl^+ [Bre 2002]. The CVD method can produce waveguides with small losses [Hua 2004]. It uses carrying gases, such as, O_2, $SiCL_4$, Bbr_3 and GeC_{l4}. The principal advantage of integrated optics on glasses comes from the low cost of the material used and the fabrication process.

2.2.2. *Organic materials*

Organic materials occupy a special place in photonic technologies. Indeed, the requirements for optical materials to satisfy varied requirements of optoelectronics encouraged, in recent years, substantial research activities which consist of connecting the macroscopic properties to the structure on an atomic and molecular scale. In this prospect, physicists and chemists joined their effort in order to develop new materials with the required features. These materials have a strong non-linear susceptibility which can be used in the optical parametric phenomena [Mol 2004,

Kaj 1996]. One of the major advantages of using integrated optical components based on organic materials is their use in the biological field as sensors. In fact, the organic materials can be worked out to react to a specific medium.

Many polymers were developed to fulfill optical waveguide requirements: polyurethane, epoxy, PMMA (polymethyl methacrylate), etc. The technique most frequently used with these polymers is the spin coating method. Consequently, the thickness of the thin layer obtained can be controlled by the deposition conditions (number of rotations, polymer quantity, etc.). Although these materials pose some problems due to their dependence on the temperature, they are waveguides of interest because of their fabrication facility and beneficial characteristics.

2.2.3. *Dielectric materials*

2.2.3.1. *$LiTaO_3$*

$LiTaO_3$ is a positive uniaxial non-linear crystal ($n_e > n_o$ with low birefringence) and belongs to the trigonal system. Its attributes are its low susceptibility to the optical damage and its Curie temperature of 890°C. Optical waveguides were obtained by using the ionic diffusion techniques (Cu) [Tie 1974], protonic exchange [Ahl 1994] and ionic implantation [Lu 1999]. This material is very promising for the development of optical functional systems.

2.2.3.2. *Ceramics (PLZT, PLT, etc.)*

Perovskite type ceramic materials are well known for their ferroelectric, piezoelectric, pyrolectric and electro-optical properties. However the applications of these materials in bulk form in the field of electronics did not experience the expected development (intrinsic limitations with bulk materials). The fabrication of these materials in the form of thin layers makes it possible to open the way with new applications in optoelectronics. Among these materials (Pb, La)TiO_3, still called PLT, presents interesting electro-optical properties [Bou 1999, Kaw 1984]. Thus, PLT thin films were deposited by radio frequency magnetron sputtering on silicon substrates. The optical properties of these layers were studied using a prism coupling technique. The EO coefficient r_{13} measured in the studied thin layers was equal to 55 pm. V^{-1} [Bou 1999]. This result shows the advantage of using this type of material for applications. Other materials such as PZT and PLZT thin films [Kaw 1984, Teo 1995] can also be beneficial for integrated optics.

2.2.3.3. *$KTiOPO_4$ (KTP)*

Potassium titanyl phosphate (KTP) is a ferroelectric material presenting extremely interesting linear and non-linear optical properties [Bie 1988, Ris 1996]. Due to a high optical damage threshold and a good second harmonic generation

coefficient (SHG) d_{33} = 10.7 pm/V, the KTP is usually employed in the frequency doubling devices of infra-red laser beams (1,064 nm). A high coefficient r_{33} (35 pm/V) makes it a good candidate for electro-optical applications. Its use in integrated optics represents strong potentiality because of the ease of waveguide development in this material [Bie 1988, Ris 1996, Sav 1998]. Indeed, several techniques of optical waveguide fabrication have been studied and developed: ionic exchange, ionic diffusion and ionic implantation. Among these, only ionic implantation makes it possible to produce waveguides in samples cut according to principal axes: X, Y and Z. The exchange techniques and ionic diffusion do not allow this because the ionic conductivity of material is variable according to the direction of the principal axes [Bin 1999, Zha 1992]. Moreover, this technique preserves the linear optical properties of the KTP. Undoubtedly this material is a potential candidate for integrated optics.

2.2.3.4. *$LiNbO_3$*

Lithium niobate deserves detailed attention because it constitutes the most important non-linear crystal. This material was extensively studied for a long time and its properties are very well known, initially as a bulk crystal and, recently, as a thin layer or a waveguide. It is still of great interest for integrated optics. The benefits of $LiNbO_3$ lies mainly in its excellent non-linear optical properties and owing to the fact that monocrystals of very good optical qualities, at lower cost, are available. $LiNbO_3$ is transparent in the visible and the infra-red ranges [Räu 1978], and is synthesized in the laboratory in the form of monocrystals. In addition to its very important non-linear coefficients (electro-optics, pyrolectric, piezoelectric), $LiNbO_3$ is also characterized by very good acoustic properties. Thus, lithium niobate, is one of the most frequently used materials in technological applications, such as acoustic and modulating transducers electro-optic modulation, second harmonic generators, optical memory, holographic devices, waveguides, etc. Lithium niobate is a negative uniaxial material ($n_e < n_o$) and belongs to ABO3 grating with oxygen octahedrals (see Figure 2.17). Below its Curie temperature Tc, the crystal is ferroelectric and belongs to the trigonal system (group of C3v space). At higher temperatures > Tc, $LiNbO_3$ is in its para-electric phase [Räu 1978, Mou 2002, Che 2003]. The basic cell of lithium niobate can be represented as follows:

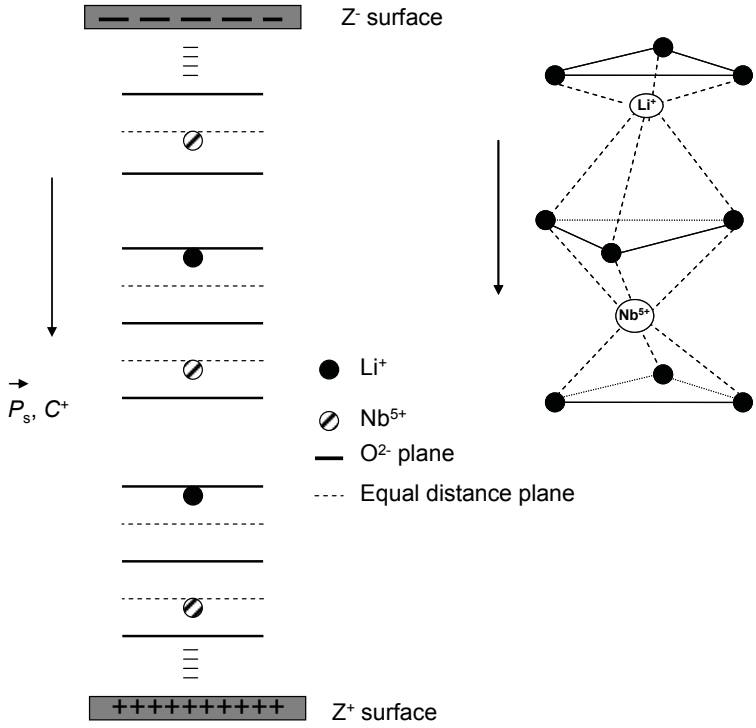

Figure 2.17. *Elementary cell of* $LiNbO_3$

Several growth techniques of $LiNbO_3$ are theoretically possible. In particular, one developed by Bridgman [Che 2003]. However, the most adapted and most frequently used method is that of Czochralski pulling. It was developed by Ballman in 1964 [Ball 1965] where it carried out broad crystals of $LiNbO_3$ starting from a solution of Li_2O-Nb_2O_5. This method consists of using a germ introduced into a crucible containing the mixture to draw the crystal. The temperature of the mixture determines the shape of the crystal. Several orientations of $LiNbO_3$ were developed. Plates of lithium niobate of very good optical quality are thus available on the market. These plates are generally Y-cut, with the optical axis parallel in surface, or Z-Cut, where the optical axis is perpendicular to the surface of the sample (see Figure 2.18).

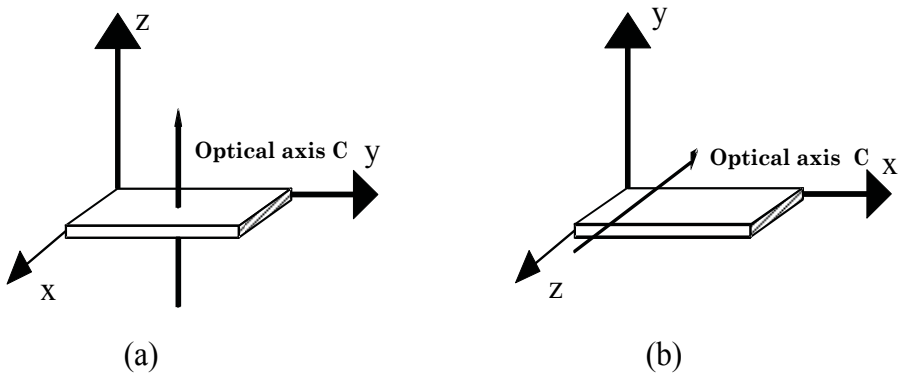

Figure 2.18. *Orientation of $LiNbO_3$: (a) Z-cut; (b) Y-cut*

The various properties of $LiNbO_3$ described above make this material a principal element in the development of optical functional systems. Its Curie temperature, which is relatively high (1210°C), allowed the use of many techniques for optical waveguide fabrication (as previously indicated).

The first waveguides formed by titanium (Ti) doping were performed by Schmidt and Kaminow (see Figure 2.16). These came after attempts to fabricate the waveguide by Li_2O exo-diffusion which allowed only a weak index increase n_e and high losses.

More recently, $LiNbO_3$ waveguides were achieved by ion exchange, in particular, Ag ions using a solution of $AgNO_3$. Proton exchange was also recently developed (see Figure 2.16). Many research activities are currently dealing with this technique in order to understand and control all the mechanisms governing the fabrication process. In recent years, the ionic implantation, in particular by using light ions, has been successfully employed for the development of waveguides with very good optical qualities in this material. Nowadays, many optoelectronic components are commercially available based on $LiNbO_3$ waveguides [Ari 2004].

2.2.4. *Semiconductor materials*

After $LiNbO_3$, III-V semiconductors are materials which have a very important impact on integrated optics. Their importance for photonic technologies comes owing to the fact that they offer the possibility of a true monolithic integration of optoelectronic components. In the case of semiconductor materials, a suitable binary material assembly makes it possible to adjust the wavelength of emission. For

example, the ternary semiconductor $Al_xGa_{1-x}As$ is obtained starting from the substitution of a fraction x of Ga atoms in the binary semiconductor GaAs by Al atoms [Car 1987].

Generally speaking, it is possible to cover the entire optical spectrum by adjusting the energy of the forbidden band and thus the laser emission: the visible field (ZnS, ZnSe, GaN, GaP, etc.), the close infra-red (GaAlAs/GaAs, GaInAs/GaAlAs, InP, GanAsP), the average infra-red (GaSb, InAs, InAsSb, etc.) or the infra-red (PbSe, PbS, HgCdTe, etc.) [Dub 1995, Nel 1985, DER 1991]. For this last window, intra-banded transitions in the quantum wells structures of III-V compounds and the quantum engineering developed with these materials can authorize the observation of a laser emission. In addition, we should not forget II-VI semiconductors [Bou 2004] which in particular allow many applications in the field of optical telecommunications.

2.2.5. *SiO_2/Si materials*

Silicon is transparent for $\lambda \geq 1.2$ μm. In addition, silicon film forms an optical waveguide with a great index contrast between silicon and silica. Moreover, OIS (optical integrated on silicon) substrates are commercially available. From the technological point of view, silica on silicon (SiO_2/Si) integrated optics constitutes a paramount technology in particular to develop passive components for optical telecommunications [Val 1991]. This pull benefits from the development of silicon micro-electronics. In fact the planar components, in integrated optics SiO_2/Si have the most important potential [Maz 1995].

It will also be important to develop other passive functions for optical transmission systems. Finally, it is important to indicate that the hybridization technology of optoelectronic components on a motherboard made of SiO_2/Si and the MEMS development are rupture technologies able to upset the industry of the components.

2.2.6. *New non-linear crystals*

Since 1992 a new series of oxoborate crystals has been synthesized. Ca4GdO(BO3)3 (GdCOB) and Ca4YO(BO3)3 (YCOB) form part of these. They were discovered and patented in 1995 by the Applied Chemistry Laboratory of the State Solid ENSCP (LCAES – Paris) with Crismatec [Aka 1995, Aka 1997]. These new non-linear crystals, GdCOB and YCOB, probably have the best possible ingredients to be potential candidates for applications in non-linear optics. Indeed,

in addition to their mechanical stability and their broad range of transparency, they have sites of substitution favorable to doping by rare earths (Yd3+ and Nd3+). Under these conditions the IR laser emissions of the active ions can be combined with the harmonic generation properties to obtain self frequency conversions [Mou 1999, Cha 1999].

At present, the ionic implantation is the only technique applicable using these crystals [Bou 1998, Wan 2002, Bou 2005, Bou 1999]. The other techniques require the development of a physicochemical process which currently does not exist.

Borates (LTB, β-BBO and LBO) are also crystals with interesting non-linear optical properties [Kes 1996]. They have a broad range of transparency which extends from IR with UV, a threshold of high damage and good non-linear optical coefficients. Making waveguides from these materials makes it possible to extend the use of their performances in integrated optical systems.

The ionic implantation seems to be the only possible technique to produce waveguides in these crystals [Bou 2001, Bou 2000, Bak 2002]. However, the borates present serious disadvantages which constitute a true handicap for their practical use. Indeed, they are generally hygroscopic and have low non-linear coefficients. The latter is not very critical considering the density of energy obtained by light confinement in the guide. However, overcoming problems related to hygroscopic properties of these crystals will undoubtedly be a true technological challenge. Under these conditions it will be possible to consider the study of frequency conversions in the guides obtained.

Tech.	Fabrication				Guide								IO devices	
	Processes	T°	t(h)	Cost	$LiNbO_3$	Parameters	Δn_o	Δn_e	e	Losses	EO	ONL	Flux	EO	ONL
Ti diffusion	Physico-chemical	1000	+ 4	K	z-cut	T°, time, thickness of Ti, post-annealing	**+0.02 TE**	**+0.03 TM**	~µm	0.1 dB/cm	K	J	K	J	K
H+ exchange	Physico-chemical	<250	~2	J	x-cut z-cut	T°, time, concentration, post-annealing	**-0.04**	**+0.12 TM**	~µm	0.1 dB/cm	L	J	J	J	K
H+, He+ implantation	Physical	Amb.	+	L	x-cut y-cut z-cut	Dose, energy post-annealing	**-0.02 TE**	**-0.01 TM**	~µm	0.5-1 dB/cm	J	J	?	?	?

Table 2.1. *Summary of the principal characteristics of LiNbO3 waveguides*

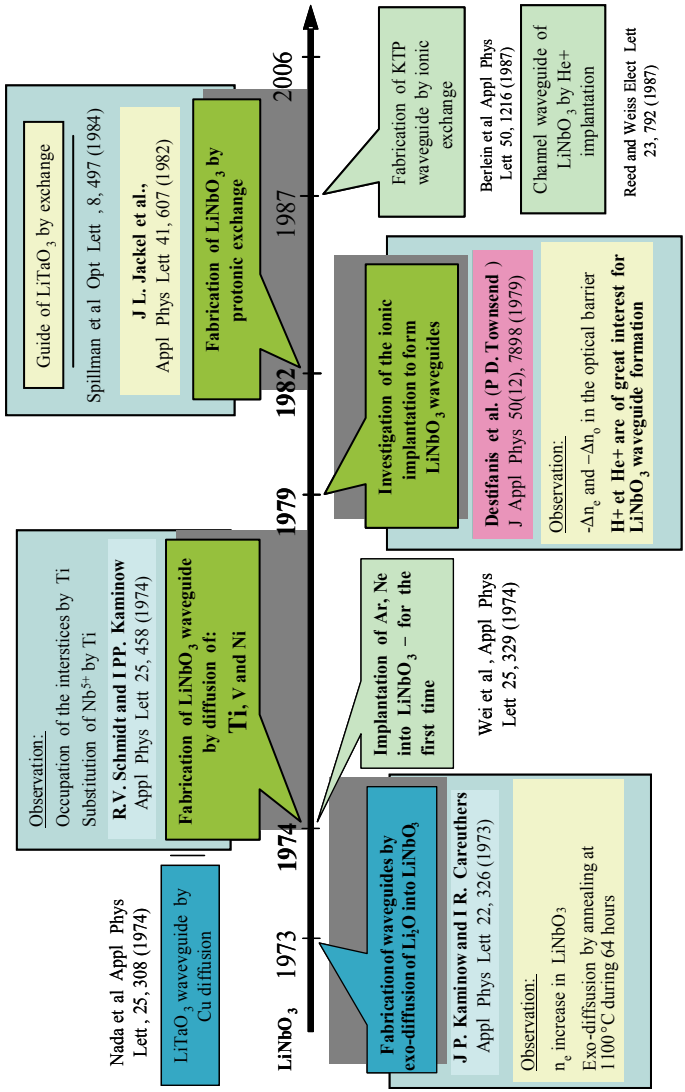

Figure 2.20. *Timeline of waveguide fabrication by substitution*

2.3. Bibliography

[Abo 1993] Abouelleil M.M., "Ion exchange in glasses and crystals", *Annual Review of Materials Science*, 23, 255-268 (1993).

[Aha 1991] Aharoni H., Swart P. L., "Experimental study of the optical properties of LTCVD SiO_2", *Proc. SPIE 1441 (1991) 13th Mtg in Israel on Optical Engineering*, (1991).

[Ahl 1994] Åhlfeldt H., "Nonlinear optical properties of proton-exchanged waveguides in z-cut $LiTaO_3$", *J Appl. Phys.*, 76(6), 3255-3260 (1994).

[Aka 1995] Aka G., Bloch L., Godard J., Kahn-Harari A., Vivien D., Salin F. and CRISMATEC company French Patent no. FR 95/01963, European Patent extension no. 96904152. 4-2205, International patent extension pending (1995).

[Aka 1997] Aka G., Kahn-Harari A., Mougel F., Vivien D., Salin F., Colin P., Pelenc D. and Damelet J.L., "Linear and nonlinear-optical properties of a new gadolinium calcium crystal $Ca_4GdO(BO_3)_3$", *J Opt. Soc. Am.*, B14, 2238-2247 (1997).

[Ari 2004] Arizmendi L., "Photonic applications of lithium niobate crystals", *Phys. Stat. Sol. (a)*, 201(2), 253-283 (2004).

[Bah 1998] Bahtat A., Bouderbala M., Bouazaoui M., Mugnier J., and Druetta M., "Structural characterization of Er^3 doped sol-gel TiO_2 planar optical waveguides", *Thin Solid Films*, 323, 59-62 (1998).

[Bak 2002] Bakhouya C.H., Boudrioua A., Loulergue J.C., Moretti P. and Polgar K., "Implanted waveguides in borate materials for frequency conversion", *Optical Materials*, 18, 73-76 (2002).

[Bal 1965] Ballman A.A., "Growth of piezoelectric and ferroelectric materials by the Czochralski technique", *J Am. Ceram. Soc.*, 48, 112 (1965).

[Bie 1985] Biersach J.P, Ziegler J.F. and Littmark U., *Stopping and Range of Ions in Solids*, Pergamon, New York (1985).

[Bie 1988] Bierlein J.D, Ferretti A. and. Roelofs M.G, "SPIE Optoelectronic Mat. Dev.", *Packaging Interconnects II*, 994, 160 (1988).

[Bin 1998] Bindner P., Boudrioua A, Moretti P. and Loulergue J.C., "Refractive index behavior of He+ implanted waveguides in $LiNbO_3$, LTB and KTP materials", *Nucl. Inst. and Meth. in Phys. Res. B.*, 142, 329-337 (1998).

[Bin 1999] Bindner P., Etude et caractérisation optique linéaire et non linéaire de guides d'ondes plans réalisés par implantation ionique dans $KTiOPO_4$, PhD Thesis, University of Metz (1999).

[Bor 1993] Bortz M.L., Fyres L.A. and Fejer M.M., "Depth profiling of the d_{33} nonlinear coefficient in annealed proton exchanged $LiNbO_3$ waveguides", *Appl. Phys. Lett.*, 62(17), 2012-2014 (1993).

[Bou 1998] Boudrioua A., Moretti P., Loulergue J.C. and Aka G., "Formation of planar optical waveguides in new nonlinear gadolinium calcium oxoborate, $Ca_4GdO(BO_3)_3$ (GdCOB), crystals by 2 MeV He+ implantation", *Optics Letters*, 23(21), 1680-1682 (1998).

[Bou 1999] Boudrioua A., Loulergue J.C., Moretti P., Jacquier B., Aka G. and Vivien D., "Second-harmonic generation in He+- implanted gadolinium calcium oxoborate, $Ca_4GdO(BO_3)_3$ (GdCOB), planar waveguides", *Optics Letters*, 24(18), 1299-1301 (1999).

[Bou 1999] Boudrioua A., Dogheche E., Rémiens D. and Loulergue J.C., "Electro-optic characterization of (Pb, La) TiO_3 thin films using prism-coupling technique", *J Appl. Phys.*, 85(3), 1780-783 (1999).

[Bou 2000] Boudrioua A., Moretti P., Loulergue J.C. and Polgar K., "Helium ion implanted planar waveguides in y-cut and z-cut β-BBO (BaB_2O_4)", *Optical Mat.*, 14(1), 31 (2000).

[Bou 2001] Boudrioua A., Bakhouya ChLoulergue, J.C., Moretti P. and Polgar K., "Low-loss opticla planar waveguides in $Li_2B_4O_7$ (LTB) crystal formed by He^+-implantation", *J Appl. Phys.*, 89(12), 7716-7722 (2001).

[Bou 2004] Boudine B., Sebais M., Halimi O., Mouras R., Boudrioua A. and Bourson P., "Characterization of CdS nanocrystals embedded in KCl single crystal matrix grown by Czochralski method", *Optical Materials*, 25(4), 373-377 (2004).

[Bou 2005] Boudrioua A., Vincent B., Kremer R., Moretti P., Jacquier B. and Aka G., "Linear and non linear optical properties of $Ca_4GdO(BO_3)_3$ (GdCOB): planar implanted waveguides", *JOSA B*, 22(10), 2192-2199 (2005).

[Bre 2002] Brennend A.L.R., Thermal poling of mutioxide silicate glasses and ion exchanged waveguides, Ph D Thesis, ORC Southampton, UK (2002).

[Car 1987] Carenco A., "Semiconductor waveguides in III-V materials for integrated optics", *Proceedings of the Fourth European Conference on integrated Optics (ECIO'87)*, 1-7, Glasgow (1987).

[Cha 1999] Chai B.H.T., "Advances in bulk inorganic nonlinear optical materials", *Optics & Photonics News*, 10(1), 31-38 (1999).

[Che 2001] Chety R., Million E., Boudrioua A., Loulergue J. C., Dahoun A. and Perrière J., "Growth of GdCa4O$(BO_3)_3$ thin films by pulsed-laser deposition for non-linear optical applications", *Journal of Material Chemistry*, 11, 657-659 (2001).

[Che 2003] Chen H., Xia H., Wang J., Zhang J., Xu J. and Fan S., "Growth of $LiNbO_3$ crystals by the Bridgman method", *Journal of Crystal Growth*, 256(3), 219-222; (4) (2003).

[Che 2006] Chen F., Wang L., Jiang Y., Wang X-L., Wang K-M., Fu G., Lu Q-M., Rüter C.H.E. and Kip D., "Optical channel waveguides in Nd:YVO_4 crystal produced by O^+ ion implantation", *Appl. Phys. Lett*., 88, 071123-071126 (2006)

[Der 1991] Deri R.J. and Kapon E., "Low-loss III-V semiconductor optical waveguides", *IEEE Journal of Quantum Electronics*, 27(3), 626-640 (1991).

[Dog 1999] Dogheche E., Boudrioua A., Rémiens D. and Loulergue J.C., "Growth and optical characterization of aluminium nitride thin films deposited on silicon by radio-frequency sputtering"*, J. Appl. Phys. Lett*., 74(9), 1209-1211 (1999).

[Dub 1995] Duboz J-Y., *Matériaux semi-conducteurs à grand gap III-V à base de GaN*, Techniques de l'Ingénieur, Traité Electronique E (1995).

[Dub 1995] Duboz J. Y., *Matériaux semi-conducteurs à grand gap III-V à base de GaN*, Technique de l'Ingénieur, Traité Electronique, E, 1-24 (1995).

[Ely 2001] El-Yadouni A., Soltani A., Boudrioua A., Thevenin P., Bath A. and Loulergue J. C., "Investigation of the optical and electro-optical properties of hexagonal boron nitride thin films deposited by PECVD technique", *Optical Materials*, 17, 319-322 (2001).

[Fav 1993] Favennec P-N, *L'implantation ionique pour la microélectronique et l'optique*, CNET, Masson (1993).

[Fei 1996] Feigelson R. S., "Epitaxial growth of lithium niobate thin films by the solid source MOCVD method", *Journal of Crystal Growth*, 166(1-4), 11-16 (1996).

[Flu 1996] Fluck D., Pliska T., Günter P., Bauer S.T., Beckers L. and Buchal C.H., "Blue-light second-harmonic generation in ion-implanted $KNbO_3$ channel waveguides of new design", *Appl. Phys. Lett*., 69(27), 4133-4135 (1996).

[Flu 1993] Fluck D., Jundt D.H., Günter P., Fleuster M. and Buchal C.H., "Modeling of refractive index profiles of He+ ion-implanted $KNbO_3$ waveguides based on the irradiation parameters", *J. Appl. Phys*., 74(10), 6023-6030 (1993).

[Fuk 1974]. Fukunishi S, Uchinda N., Miyasawa S. and Noda J, "Electro-optic modulation of optical guided wave in $LiNbO_3$ thin film fabricated by EGM method", *Appl. Phys. Lett*., 24(9), 424-426 (1974).

[Hua 2004] Huang C.C., Hewak D.W. and Badding J.V., "Deposition and characterization of germanium sulphide glass planar waveguides", *Optics Express*, 12(11), 2501-2506 (2004).

[Jac 1980] Jackel J.L., "High-Delta n optical waveguides in $LiNbO_3$: thallium-lithium ion exchange", *Appl. Phys. Lett*., 37, 739-741 (1980).

[Hua 2004] Huang C.C., Hewak D.W. and Badding J.V., "Deposition and charaterization of germanium sulphide galss planar waveguides", *Optics epress*, 12(11), 2501-2506 (2004)

[Kad 1989] Kadad I., Réalisation et etude de guides d'ondes optiques plans en nitrure d'aluminium par pulverisation magnetron réactive, PhD Thesis, University of St-Etienne (1989).

[Jac 1982] Jackel J.L., "Suppression of outdiffusion in titanium diffused. $LiNbO_3$.: a review", *J Opt. Commun*., 3, 82-85 (1982).

[Kaj 1996] Kajzar F. and Swalen J.D., *Organic Thin Films for Waveguiding Nonlinear Optics*, series: advances in nonlinear optics, CRC (1996).

[Kam 1973] Kaminow J.P. and Caunthers J.R., "Optical waveguiding layers in $LiNbO_3$ on $LiTaO_3$", *Appl. Phys. Lett*., 22, 326-328 (1973).

[Kaw 1984] Kawaguchi T., Adachi H., Setsune K., Yamazaki O., and Wasa K., "PLZT thin-film waveguides", *Appl. Opt*., 23, 2187- 2190 (1984).

[Kes 1996] Keszler D.A., "Borates for optical frequency conversion", *Current Opinion in Solid State & Materials Science*, 1(1), 204-211 (1996).

[Kon 1996] Kondina O., Hallin C., Ellison A., Borkin A.S., Ivanov G., Henry A., Yakimova R., Touminen M., Vehanen A. and Janzèn E., "High temperature chemical vapor deposition of SiC", *Appl. Phys. Letters*, 69(10), 1456-1458 (1996).

[Kor 1996] Korkishko, Y.N., Fedorov and V.A., "Structural phase diagram of $H_xLi_{1-x}NbO_3$ waveguides: the correlation between optical and structural properties", *IEEE Journal Selected Topics in Quantum Electronics*, 2(2), 187-196 (1996).

[Kor 1999] Korkishko Y.N. and Fedorov V.A., *Ion Exchange in Single Crystals for Integrated Optics and Optoelectronics*, Cambridge International Science Publishing, Cambridge, (1999).

[Lau 1992] Laurell F., Roelofs M.G and Hsiung H., "Loss of optical nonlinearity in proton-exchanged $LiNbO_3$ waveguides", *Appl. Phys. Lett*. 60 (3), 301-303 (1992).

[Lee 1986] Lee D.L., *Electromagnetic Principles of Integrated Optics*, John Wiley & Sons, (1986).

[Lee 1998] Lee S.Y. and Feigelson R.S., "Reduced optical losses in MOCVD grown lithium niobate thin films on sapphire by controlling nucleation density", *J of Crystal Growth*, 186, 594-606 (1998).

[Lu 1999] Lu F., Wang F. X., Li W., Zhang J. H., and Wang K. M., "Annealing behavior of barriers in ion-implanted $LiNbO_3$ and $LiTaO_3$ planar waveguides", *Appl. Opt*., 38, 5122-5126 (1999).

[Maz 1995] Mazzoldi P. anad Righini G.C., "Glasses for optoelectronic devices", in F. Agullo-Lopez's (Ed.) *Insulating Materials for Optoelectronics: New Developments* , World Scientific Publishing Co. Pte. Ltd., (1995).

[Mic 1995] De Micheli M., Ostrowsky D.B., Korkishko Y.N. And Baldi P., "Proton exchanged waveguides in $LiNbO_3$ and $LiTaO_3$ structural and optical properties", in F. Agullo-Lopez's (Ed.) *Insulating Materials for Optoelectronics: New Developments* , World Scientific Publishing Co. Pte. Ltd., (1995).

[Mol 2004] Moliton A., Antony R., Lucas B., Ratier B. and Hiorns R.C., "Progress in organic optoelectronics", *Recent Res. Devel. Applied Phys*., 7, 197-245 (2004).

[Mor 1991] Moretti P., Thevenard P., Sommerfeld F.R. and Godefroy G., "Ion implantation effects in $BaTiO_3$ single crystals", *Nucl. Inst. And Meth. In Phys. Res*., B59/60, 1228-1232 (1991).

[Mou 1999] Mougel F., Les oxoborates de calcium et de terres rares (TR) $Ca_4TRO(BO_3)_3$. Une nouvelle famille de matériaux à fonction multiples pour l'optique : croissance cristalline, propriétés non linéaires et laser, Ph D Thesis, University of Paris VI (France) (1999).

[Mou 2002] Mouras R., Etude par spectroscopie Raman de l'effet des défauts sur les propriétés phtotoréfractifs et electro-optiques des cristaux de niobate de lithium purs et dopes, PhD Thesis, University of Metz (2002).

[Mus 2003] Mussi V., Somma F., Moretti P., Mugnier J., Jacquier B., Montereali R.M. and Nichelatti E., "Mode analysis in He^+-implanted lithium fluoride planar waveguides", *Applied Physics Letters* , 2(82)22, 3886-3888 (2003).

[Nag 1997] Nagy S.C., Robinson B.J., Thompson D.A., Simmons J.G., Nuban M.F., Krawczyk S.K., Buchheit M. and Blanchet R.C., "Growth of InGaAs/InP structures by gas source molecular beam epitaxy on SiO_2-patterned substrates for optoelectronic applications", *Journal of Crystal Growth* , 177(1-2), 1-5 (1997).

[Nel 1985] Nelson J.R., and Dutta N.K., "Review of InGaAsP/InP laser structures and comparison of their performances", in W.T. Tsang (Ed.) *Semiconductor and Semimetals*, Academic Press (1985).

[Nis 1989] Nishihara H., Haruna M. and Suhara T., *Optical Integrated Circuits* , McGraw-Hill, (1989).

[Oul 1995] Ould-Salem S., Etudes des effets d'implantation de protons dans le Niobate de Lithium. Application à la réalisation de guides d'ondes optiques, PhD Thesis, University of Lyon I (1995).

[Pas 2002] Passaro V.M.N., Armenise M.N., Nesheva D., Savatinova I.T. and Pun E.Y.B., "$LiNbO_3$ optical waveguides formed in anew proton source", *J of Lightwave Technology* , 20(1), 71-77 (2002).

[Pau 1986] Paul S., Halle O., Einsiedel H., Menges B., Müllen K., Knoll W.and Mittler-Neher S., "An anthracene-containing PMMA derivative for photoresist and channel waveguide applications", *Thin Solid Films*, 288(1-2), 150-154 (1996).

[Ram 1988] Ramaswamy R.V. and Srivastava R., "Ion exchange galss waveguide : a review", *Journal of Lightwave Technology*, 6(6), 984-1002 (1988).

[Räu 1978] Räuber A., "Chemistry and physics of lithium niobate", *Current Topics in Materials Science I*, 481-601, Amsterdam (1978).

[Ris 1996] Risk W.P. and Loiacono G.M. "Fabrication and characterization of ion-exchanged waveguides in potassium titanyl arsenate", 69(27), 4157-4158 (1996).

[Ris 1991] Risk W.P., "Fabrication and characterization of planar ion-exchanged $KTiOPO_4$ waveguides for frequency doubling", *Appl. Phys. Lett.*, 58(1), 19-21 (1991).

[Roe 1993] Roelofs M.G, Ferretti A., and Berlein J.D, "Proton- and ammonium-exchanged optical waveguides in $KTiOPO_4$", *J.Appl. Phys.*, 73(8), 3608-3613 (1993).

[Sav 1998] Savatinova I., Savova I., Liarokapis E., Ziling C.C., Atuchin V.V., Armenise M.N. and Passaro V.M.N., "A comparative analysis of Rb:KTP and Cs:KTP optical waveguides", *J.Phys. D:Appl. Phys.*, 31, 1667-1672 (1998).

[Sch 1974] Schmidt R.V. and. Kaminow J.P, "Metal-diffused optical waveguide in $LiNbO_3$", *Appl. Phys. Lett.*, 25, 458- 460 (1974).

[Shi 1980] Shiosaki T., Fukuda S., Sakasi K., Kurada H. and Kawabata A., "Second harmonic generation in as-sputtered ZnO optical waveguide", *J.Appl. Phys.*, 19, 2391, (1980).

[Spi 1983] Spillman W.B., Sanford Jr., N.A., and Soref R.A., "Optical waveguides in $LiTaO_3$ formed by proton exchange", *Optics Lett.*, 8(9), 497-498 (1983).

[Swa 1992] Swartz S.L., Wood V.E., "Ferrroelectric thin films", *Cond. Mat. News*, 1(5), 4-13 (1992).

[Teo 1995] Teowee G., Simpson J.T., Zhao T., Mansuripur M., Boulton J.M. and Uhlmann D.R., "Electro-optic properties of sol-gel derived PZT and PLZT thin films", *Microelectronic Engineering*, 29(1)4, 327-330 (1995).

[Tie 1974] Tien P.K., Riva-Sanseverino S., Martin R.J., Ballman A.A. and Brown H., "Optical waveguide modes in single-crystalline LiNbO3-$LiTaO_3$", *Appl. Phys. Lett.*, 24, 503-506 (1974).

[Tow 1990] Townsend P.D., "An overview of ion-implanted optical waveguide profiles", *Nucl. Instrum. Methods Phys. Res.*, B 46, 18–25 (1990).

[Tow 1992] Townsend P.D., "Ion implanted waveguides and waveguide lasers", *Nucl. Inst. and Meth. in Phys. Res.*, B65, 243 (1992).

[Tow 1994] Townsend P.D., Chandler P.J. and Zhang L., *Optical Effects of Ion Implantation*, Cambridge University Press (1994).

[Val 1991] Valette S., "Les composants actifs dans les technologies optiques intégrées sur substrat silicium", *Procedings of OPTO*, Paris (1991).

[Wan 2002] Wang K-M., Hu H., Chen F., Lu F., Shi B-R., Shen D-Y,, Liu Y-G., Wang J-Y. and Lu Q-M., "Refractive index profiles in $YCa_4O(BO_3)_3$ and $Nd:YCa_4O(BO_3)_3$ waveguides created by MeV He ions", *Nucl. Inst. and Methods in Phys. Res.*, B 191, 789-793 (2002).

[Will 2000] Willmott P.R. and Huber J.R., "Pulsed laser vaporization and deposition", *Review of Modern Physics*, 72(1), 315-328 (2000).

[Yan 1994] Yang L., Scott Saavedra S., Armstrong N.R., and Hayes J., "Fabrication and characterization of low-loss, sol-gel planar waveguides", *Analytical Chemistry*, 66(8), 1254-1263 (1994).

[Zha 1992] Zhang L., Chandler P.J., Townsend P.D. and Thomas P.A., "Helium ion implanted optical waveguide in $KTiOPO_4$", *Electronics Lett.*, 28(7), 650-653 (1992).

This page intentionally left blank

Chapter 3

Optical Waveguide Characterization Techniques

Waveguide characterization requires excitation of the guide modes of the structure being studied. The characterization is of major interest, not only to determine the physical properties of the waveguide, but also for the practical use of this component in integrated optical circuits (IOC).

In this chapter, we will point out the various experimental techniques which make it possible to couple light into a waveguide and to determine its optical properties. These techniques can be divided into two families: transversal coupling techniques and longitudinal coupling techniques.

The essential criteria of good coupling can be summarized by three points:

– efficiency;

– selectivity; and

– simplicity.

3.1. Coupling techniques

3.1.1. *Transversal coupling*

The principle of these techniques consists of coupling incident light into waveguides through its cross-section. We can distinguish two main techniques: end-fire coupling and taper coupling

3.1.1.1. *End-fire coupling*

This is a simple and direct technique in that it does not need any additional components. It consists of focusing the incident light beam onto a right cross-section of the waveguide, as shown in Figure 3.1.

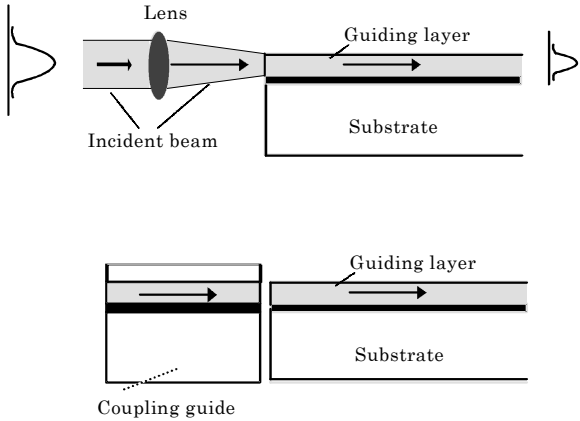

Figure 3.1. *End-fire coupling principle*

The coupling efficiency η particularly depends on the numerical aperture of the incident beam and that of the guided modes to be excited. Thus, it depends on the waveguides features [Hun 1985, Nis 1989]. We can write:

$$\eta = \frac{\left[\int E(x)E_g^{*}(x)dx\right]^2}{\int E(x)E^{*}(x)dx \int E_g(x)E_g^{*}(x)dx} \qquad [3.1]$$

– $E(x)$: incident beam amplitude
– $E_g(x)$: excited mode amplitude

Light coupling can be performed using a laser source, optical fiber or even another waveguide. This method is more appropriate for practical use in integrated optical circuits. However, it is necessary to perform a very high optical polishing of the guide cross-section to avoid optical diffusion losses. Moreover, a very accurate alignment is also needed. Besides, this configuration does not allow selective guided mode excitation.

To summarize, the major drawbacks of these techniques are:

– difficulties related to optical polishing and alignment;

– excitation of all guided modes in the same time due to the use of a convergent light beam;

– instability due to alignment problems;

– the coupling efficiencies, dependence on the experimental conditions.

For instance, by using this technique, a coupling efficiency of 15% in $LiNbO_3$ waveguides excited by a GaAlAs laser has been reported [Hal 1980, Wan 1996]. The best coupling efficiency was found to be of 80%.

3.1.1.2. *Taper coupling*

This method was developed for the first time by P.K. Tien *et al.* [Tie 1971], and uses the cut-off thickness concept. For this, we need to create a tapered structure on the waveguide surface (see Figure 3.2) over a distance of 10 to 100 times the wavelength λ used. Thus, the incident light can be progressively coupled or out-coupled to the waveguide throughout the tapered structure while the cut-off thickness of the guided mode is reached. In other words, the taper allows a continuous variation of the reflection angle around the critical angle already mentioned in Chapter 1.

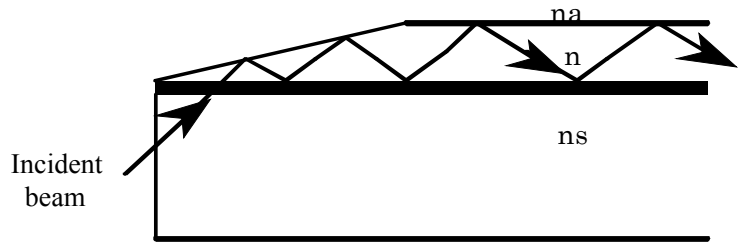

Figure 3.2. *Coupling by taper*

This technique could be of great interest with high index thin films such as GaAs, where it is difficult to find a high index transparent prism [Wan 1996]. Its major drawbacks are:

– it is a destructive method because we need to create a tapered structure on the surface of the guide;

– it is difficult to selectively excite guided modes;

– the best coupling efficiency was found to be 40%.

For instance, P.K. Tien *et al.* [Tie 1971] reported a coupling efficiency of 25% with ZnS thin films and of 40% with organic films deposited on a glass substrate.

3.1.2. *Longitudinal coupling*

In this configuration, guided modes are excited by using light coupling through the surface of the guide. On the one hand, the incident light beam coupling requires that the longitudinal component of the wave vector should be equal to the guided mode propagation constant β. On the other hand, energy transfer from the incident wave to the guide is performed using a coupling device which could be a grating or a coupling prism.

3.1.2.1. *Grating coupler*

This technique was developed by M.L. Dakss *et al.* [Dak 1970] and studied by P.K. Tien *et al.* [Tie 1971] as well. It consists of a surface grating writing onto the waveguide (see Figure 3.3). Incident light diffraction by the grating gives rise to several diffracted components that could be coupled with the guided modes of the structure.

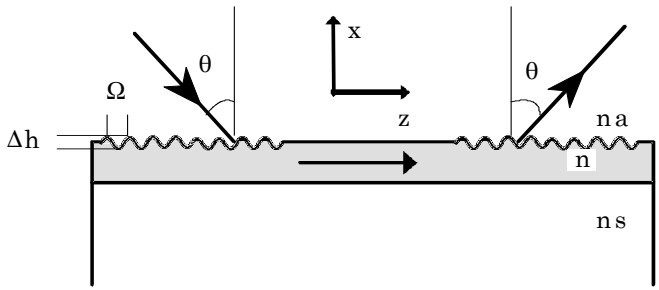

Figure 3.3. *Coupling by network*

When an incident light of a wave vector k_0 is diffracted by a grating of period Ω then the components of a period $2\pi/\Omega$ appear in the longitudinal (parallel to the surface) component of the wave vector. Thus, light can be coupled to guided modes m that fulfill the phase matching condition [Pet 1980]:

$$\beta = kN_m$$
$$N_m = n_0 \sin\theta + \gamma\frac{\lambda}{\Omega} \qquad [3.2]$$

γ: diffraction order (integer:0,±1,±2,±3,...)

λ: wavelength in the medium.

The coupling efficiency is optimal for specific values of θ that are solutions of the previous phase matching equation. It particularly depends on the grating period Ω and Δh, the grating depth. Experimentally, coupling coefficients of 75% have already been reported [Pet 1980, Tie 1972]. However, the efficiency of grating couplers particularly relies on three parameters: the form of the incidental beam, the zone of coupling and the grating structure. The latter requires the control of micro-technology processes such as photolithography, etching, etc., which makes this technique difficult to implement. Also, the losses by transmission can be considerable due to the fact that the grating does not use total reflection.

Nevertheless, grating is one of the most important components for integrated optics as it constitutes a permanent, stable and reproducible coupler. It is used in many functional devices, in particular:

– I/O couplers for optical waveguides;

– optical filters, waveguide to waveguide couplers, etc.

3.1.2.2. *Prism coupling*

This method has been the most frequently used technique since the advent of integrated optics. It was discussed in many published works and it still attracts much interest for optical waveguide characterization. Light confinement within a waveguiding structure obeys the following relation:

$$\begin{aligned} \beta_m &\geq kn_s \geq kn_a \\ \beta_m &= kn\sin\theta \end{aligned} \qquad [3.3]$$

where β_m: horizontal component of the wave vector.

As a matter of fact, an incident beam on the surface of the waveguide cannot excite guided modes. For that, it is necessary to use a high index incidence medium in order to fulfill the previous relation. Prism coupling (Figure 3.4) consists of phase matching between the longitudinal component of the wave vector of the incident wave and the excited guided mode. This can be assured by the utilization of a high index rutile prism (TiO_2).

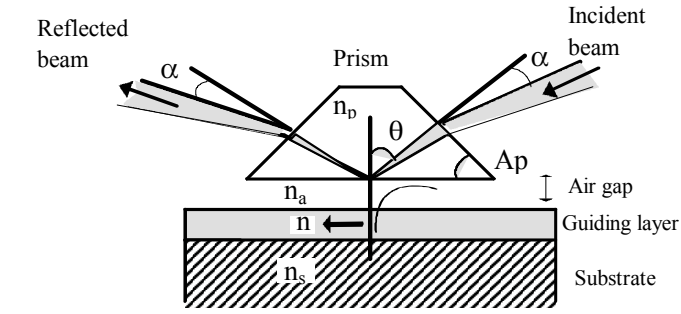

(a) Symmetric prism

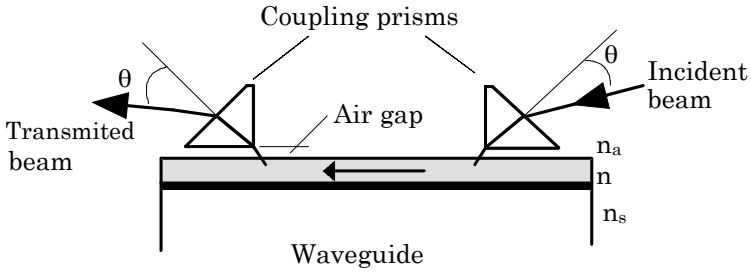

(b) Right angle prism

Figure 3.4. *Prism coupling principal*

In this configuration, the waveguide is pressed against the base of the prism (at a distance of *g*). The incident beam at the prism base is totally reflected and for a certain angle called resonance angles, the incident energy can be launched into the guided modes by a "tunneling effect" (this is similar to the tunneling effect in quantum mechanics) [Pet 1977, Per 1988, Tie 1969, Tie 1970, Tie 1971.a, Tie 1971.b, Ulr 1970,].

The excitation of guided modes is realized throughout the evanescent waves created in the air gap between the prism and the guiding layer (Figure 3.5). From relation [3.3], we can note that this technique allows a selective excitation of guided modes by choosing the appropriate incidence angle. The coupling efficiency mainly depends on:

– the air gap thickness;

– the incident beam profile;

– the incident beam section at the base of the prism.

The last two parameters are related to the laser source and the optical setup used in the experiment. However the first, air gap thickness, depends on the pressure applied upon the coupling prism.

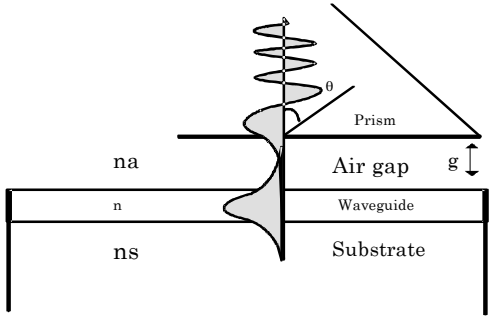

Figure 3.5. *Prism coupling mechanism*

3.1.2.2.1. The prism effect

So that the prism coupling is effective, it is necessary for the thickness of the air gap to be lower than the length of the evanescent wave attenuation (1/8-1/4 of λ) [Ulr 1973]. However, it is clear that as the thickness of the gap decreases, the presence of the prism increasingly disturbs the modes of the guiding structure, in particular, due to total reflection of the guided mode on the interface guide-air which creates evanescent waves which can be out-coupled into the prism.

Indeed, the presence of the prism on top of the superstrate modifies the guiding structure and instead of considering the problem with three layers, it is necessary to deal with the problem of four mediums (prism, air, guiding layer and substrate), as indicated in Figure 3.6.

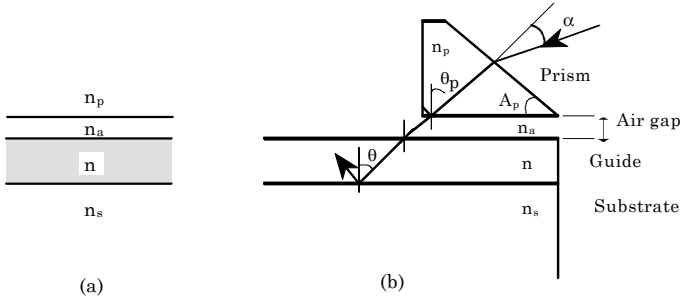

Figure 3.6. *Effect of the prism presence*

We can show that the phase mismatch at the guide-air interface is:

$$\Phi^{(p)}_{(n,n_a)} = \Phi_{(n,n_a)} + \sin\Phi_{(n,n_a)} \cos\Phi_{(n_p,n_a)} \exp(-2gkb) \quad [3.4]$$

with:

$$b = \sqrt{N_m{}^2 - n_a{}^2}$$

$$\Phi_{(j,na)} = arctg\left[\left(\frac{j}{n_a}\right)^{2\rho}\left(\frac{N_m{}^2 - n_a{}^2}{j^2 - N_m{}^2}\right)^{1/2}\right] \quad [3.5]$$

$$\rho = \begin{cases} 0 & \text{for TE} \\ 1 & \text{for TM} \end{cases} \quad [3.6]$$

g: the gap thickness

n_p: prism refractive index

$bj = n, n_p$.

The presence of the prism makes the modes broader and modifies the synchronous angles. In other words, a strong pressure (therefore a weak thickness of the air gap) causes an angular displacement of the guided modes of the free structure. The variation of the effective index of the guided mode m can be given by the following relation [Ulr 1973]:

$$N_m{}^{(p)} - N_m = -K_m \cot g 2\Phi_{(p,na)} \quad [3.7]$$

with:

$$K_m = \frac{\lambda}{2w_\Omega} \quad [3.8]$$

N_m: effective index of the free structure

$N_m^{(p)}$: effective index with the presence of the prism

$\Phi_{(p,na)}$: phase mismatch at the interface (n_p, n_a) (relation [1.2] and [1.3])

λ: wavelength

W_Ω: coupling angular aperture.

From the previous relations [3.4] and [3.7], it is possible to study the influence of the prism on the guided modes of the free structure. For instance, the curves in Figure 3.7 report results obtained for a $LiNbO_3$ waveguide (indices n_o=2.284 and n_e=2.22) showing the variation of N_m as a function of the air gap thickness.

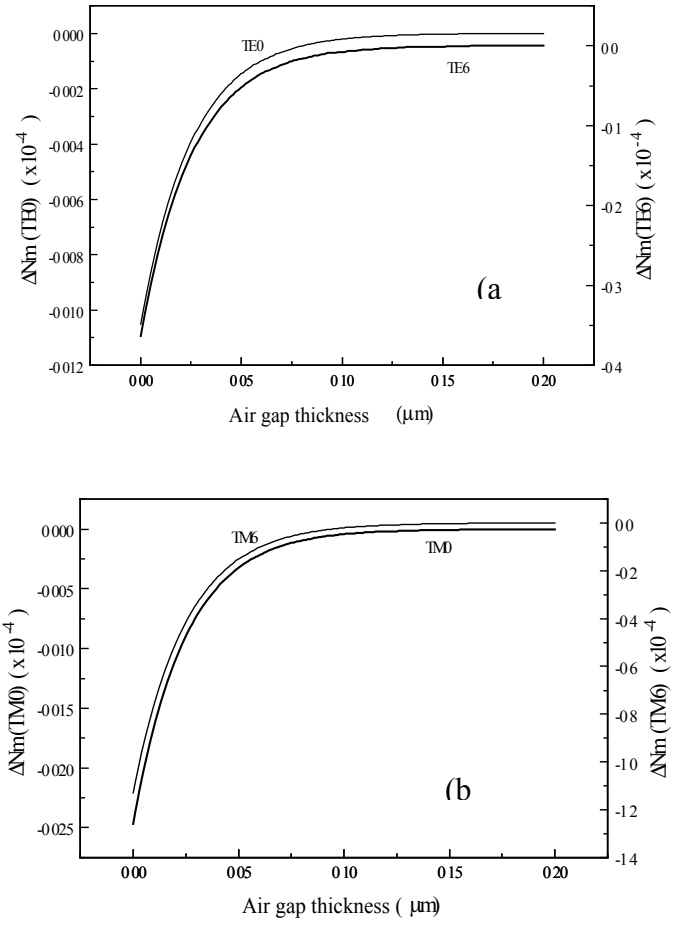

Figure 3.7. *Variation of Nm vs air gap for $LiNbO_3$ waveguide (λ=632 nm):*
(a) TE_0 and TE_6 modes: n=2.22,n_s=2.18 and e=5 μm
(b) TM_0 and TM_6 modes: n=2.284,n_s=2.24 and e=5 μm

Note that a low thickness of the air gap, in other words a rather strong coupling pressure, introduces a variation of the effective index and thus an angular shift of

the guided modes. To avoid this effect, it is necessary to have a working air gap higher than 50 nm.

Beyond this thickness, the variation ΔN_m tends towards zero. However, the coupling efficiency also depends on the depth of the evanescent wave in the air gap. Consequently, an optimal air gap could be located between 0.05 μm and 0.15 μm (λ/8, λ/4). However this variation remains rather weak and could be neglected, in particular for low order modes. Curves in Figure 3.8 give the variation of the effective index produced by an air gap of about 0.02 μm according to the guided modes order *m*.

Note also that high order modes are much more sensitive to the presence of the prism than low order modes. High order modes undergo a large number of total reflections. This sensitivity is more important TM guided modes.

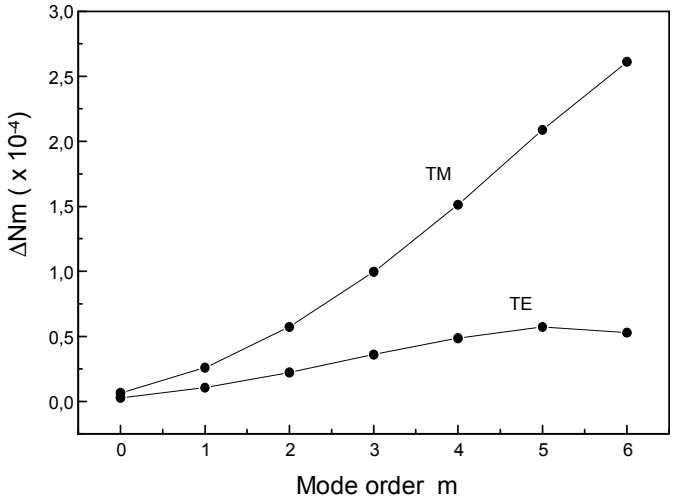

Figure 3.8. *Variation of N_m vs m (guided mode order)*

3.1.2.2.2. Coupling efficiency

The prism coupling efficiency especially depends on the incident beam distribution and the optogeometric parameters of the structure [Tie 1977]. The interaction between the prism and the waveguide is carried out over a length *L* (see Figure 3.9).

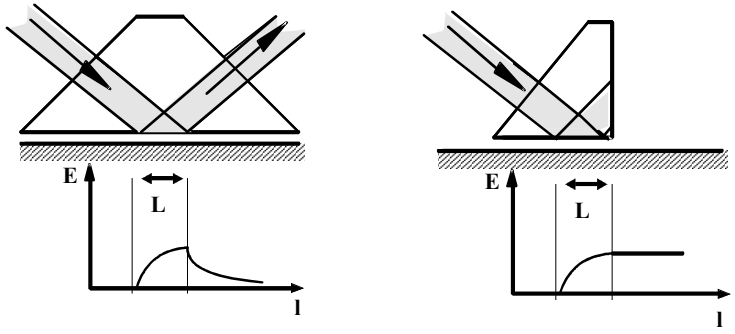

Figure 3.9. *Distribution of the optical field in the prism*

For an ideal guiding structure, the coupling efficiency can be written as [Tie 1977]:

$$\eta = \frac{2}{qL\left[1 - \exp(-qL)\right]^2} \qquad [3.9]$$

with:

$$q = \frac{\sin 2\Phi_{(n,na)} \sin 2\Phi_{(np,na)} \exp(-2kbg)}{d_{eff} \tan \theta_m} \qquad [3.10]$$

Factor q determines the coupling features. This can be calculated using the optogeometric characteristics of the structure studied and the prism index. It can also be experimentally measured.

Note that the coupling efficiency is related to the interaction length between the incident beam and the guide (the diameter of the coupling spot). Thus, in practice, it is more convenient to use a very small diameter.

The utilization of the effective thickness is due to the Goos-Hänchen shift that can be neglected when using a Gaussian beam.

By taking the maximum of expression [3.9], we define the optimum coupling length by the following relation:

$$L = \frac{\pi}{2\eta} \qquad [3.11]$$

and deduce a maximum coupling efficiency of 80%.

Moreover, a simple expression of the coupling efficiency η can be deduced by taking into account the fact that length L can be given by the following relation (see Figure 3.9):

$$L = \frac{W}{\cos\theta_m} \qquad [3.10]$$

with W the beam diameter.

We find: $\eta = \frac{\pi \cos\theta_m}{2W}$ [3.11]

The electric field amplitude E is uniform throughout length L.

To summarize, prism coupling is a very convenient technique to separately excite the guided modes of planar structures. It allows guide characteristic determination, from the measurement of the synchronous angles that correspond to the angular positions of the guided modes. The benefits of this technique are:

– it is selective since it makes it possible to excite separately the guided modes by changing the coupling angle;

– it is easy to set up;

– the coupling uses total reflection (TR), therefore transmission losses can be neglected;

– it is an efficient technique with coupling efficiencies of 80% already reported.

This method is the base of the well-known m-lines spectroscopy [Bou 1996], which will be treated in the following section.

3.2. "*m*-lines" spectroscopy

3.2.1. *The experimental setup*

This setup makes it possible to characterize the linear and non-linear optical properties of planar waveguides and thin films. The incident beam at the base of the coupling-prism is totally reflected. For angular positions corresponding to synchronous angles, the incident energy is thus transferred to the guided modes of the structure (see Figure 3.10).

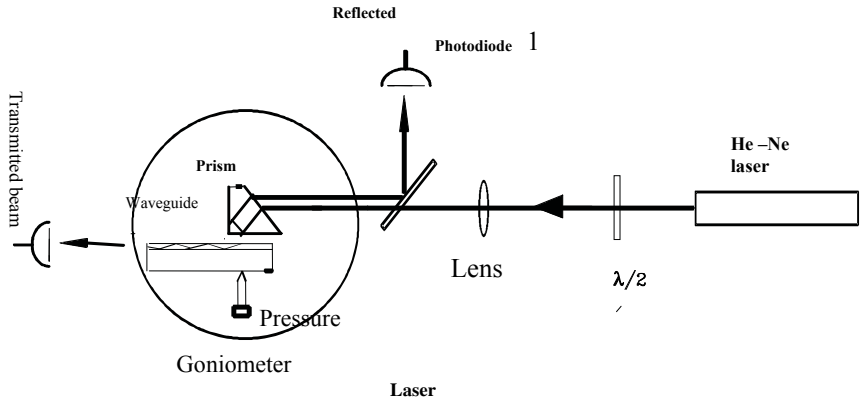

Figure 3.10. *The "m-lines" setup*

Two configurations can be used.

3.2.1.1. *Transmission measurement*

In this case determination of the synchronous angles is obtained by measuring the transmitted light into the guide as a function of the incident angle. This configuration requires the use of a right angle prism. The transmitted (guided) light can be measured in two ways:

– The first consists of measuring the out-coupled light intensity directly from the end section of the guide (Photodiode 2). Therefore, it is very important to use a highly polished end-section of the guide in order to avoid diffusion losses.

– The second uses an extra prism that out-couples the guided light using the same process as the in-coupling (principle of optical reciprocity).

For instance, Figure 3.11 reports the *m*-lines spectrum of proton-exchange $LiNbO_3$ waveguide. The synchronous angles are related to the peak intensity positions.

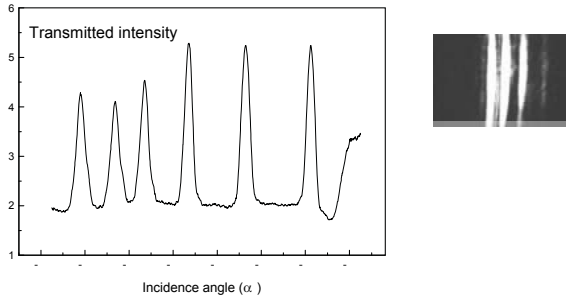

Figure 3.11. *TE guided modes measured by transmission: guide of $LiNbO_3$ fabricated by proton exchange*

3.2.1.2. *Reflection measurement*

In contrast to the previous situation, determination of the synchronous angles is performed by measuring the reflected intensity at the prism base (Photodiode 1). In this case, we can use a right angle prism as well as a symmetric prism. Thus, reflectivity dips in the *m*-lines spectrum give the angular positions of the structure guided modes (see Figure 3.12).

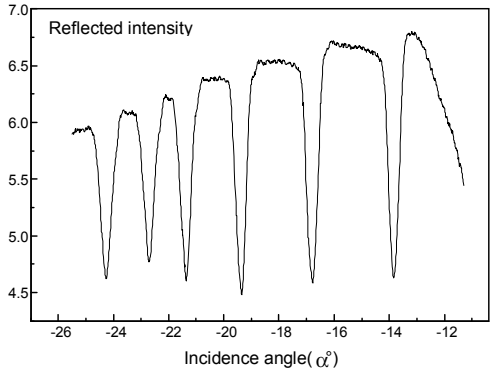

Figure 3.12. *TE guided modes spectrum measured by reflection: guide of $LiNbO_3$ fabricated by proton exchange*

Note that before measuring the guided mode spectrum, it is important to determine the zero angle. For this, we can use the so-called auto-collimation method. In the experimental conditions reported above, we perform an auto-

collimation of the incident beam on the external face of the prism. A beam splitter and a slot can give precise control of the auto-collimation and thus the zero angle determination. A photodiode located in the beam line of the beam-splitter allows the auto-collimated intensity to be measured. The zero angle corresponds to a maximum reflected intensity.

As an example, Table 3.1 reports results obtained by deflection for a $LiNbO_3$ proton-exchanged waveguide. The determination of the synchronous angles (see Figure 3.11 or 3.12) gives the effective indices.

m	α (°)	N_m
0	-24.27	2.2893
1	-22.72	2.2741
2	-21.36	2.2606
3	-19.35	2.2401
4	-16.77	2.2130
5	-13.84	2.1812

Table 3.1. *Effective value indices of a $LiNbO_3$ proton exchanged waveguide*

The flexibility and practical simplicity of the reflection measurement has ensured its use by many researchers for waveguides characterization.

3.2.2. *Experimental arrangement*

3.2.2.1. *The laser beam*

Since guided modes are polarized (TE or TM), the laser beam must have the same polarization as that of the guided mode to be excited. Consequently, a precise knowledge of the incident beam polarization is required in order to efficiently excite all modes. This is carried out by using a polarizer combined with a $\lambda/2$ plate. In addition, the plane of incidence must be strictly parallel to the surface of the rotary table (perpendicular to the large face of the prism). For this the simplest method consists of measuring the height of two points of the beam chosen at a sufficiently adequate distance and carrying out the adjustment by autocollimation.

Note that two configurations are possible: on the one hand we can utilize a convergent beam to simultaneously excite all guided modes, and on the other hand, we can use a parallel incident beam. The latter is more convenient as it allows a selective excitation of guided modes.

3.2.2.2. *Light coupling*

To carry out a good coupling, it is necessary to press the waveguide against the base of the prism to obtain a rather weak air-gap, theoretically about $\lambda/4$. In the case of $LiNbO_3$ waveguides, a dark spot (the coupling point) appears on the base of the prism indicating a good optimization of the air-gap. It must be in the middle of the base of the symmetric prism, and in the vicinity of the right angle if a 90° prism is used.

The opto-geometric parameters of the guide are measured precisely at this point. The adjustment of the position of the coupling system, compared with the device rotation axis (point M in Figure 3.13) using the xyz translators, makes it possible to maintain the invariable coupling point during rotation. According to the position of the angular range to be explored (higher or lower than 0), the position of the prism must be adjusted as indicated in Figure 3.13 [Bou 1996, Ulr 1970]. The incidence point of the laser beam on the face of the prism must be adjusted with l_p/n_p of the system rotation axis (as indicated in Figure 3.13), downwards for $\alpha > 0$ and upwards for $\alpha < 0$ (l_p is the optical length of the beam inside the prism, measured close to $\alpha = 0$).

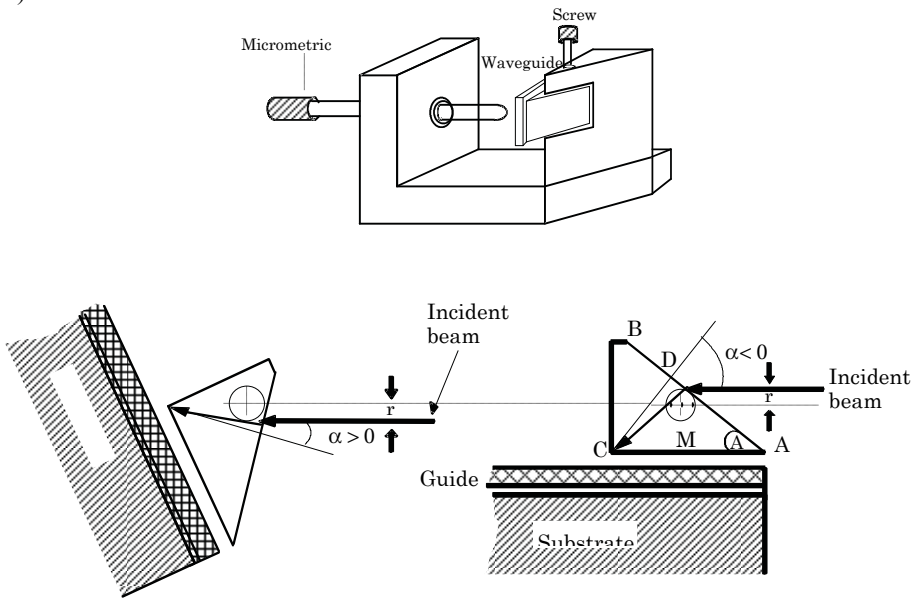

Figure 3.13. *Experimental arrangements required to maintain an invariable coupling point*

Finally, the use of prisms with small dimensions ($l_p < 5$mm) and a high refractive index [Tie 1971, Wan 1996] allows us to obtain an invariable coupling point.

3.2.3. *Measurement accuracy*

In case of planar waveguide characterization, the main parameter to be measured is the effective index N_m given by the following relation:

$$N_m = n_p \sin\theta_m$$
$$= n_p \sin\left[A_p - \arcsin\left(\frac{\sin\alpha}{n_p}\right)\right] \quad [3.12]$$

The precision of the N_m determination was a particular focus of T. Kersten's studies [Ker 1973, Ker 1975] and can be written as:

$$\Delta N_m = \left|\frac{\partial N_m}{\partial n_p}\right| \Delta n_p + \left|\frac{\partial N_m}{\partial A_p}\right| \Delta A_p + \left|\frac{\partial N_m}{\partial \alpha}\right| \Delta\alpha \quad [3.13]$$

This relation indicates that the absolute uncertainty ΔN_m is mainly determined by the uncertainties Δn_p, ΔA_p and $\Delta\alpha$. n_p and A_p (refractive index and the angle of the prism) are known with high precision. Under these conditions, the precision of N_m determination particularly depends on the accuracy of the α angle measurement.

We must also point out that other factors may also be at the origin of measurement errors. For instance the prism effect and the beam divergence could introduce additional errors. However, the beam divergence can be neglected by assuming that the uncertainty of the incident angle measurement, $\Delta\alpha$, takes into account all additional errors. For more details, a discussion on this parameter was reported by R. Ulrich *et al.* [Ulr 1973]. Finally, relation [3.13] can be written:

$$\Delta N_m = (\Delta N_m)_{np} + (\Delta N_m)_{ap} + (\Delta N_m)_{\alpha} \quad [3.14]$$

By using relation [3.12]:

$$(\Delta N_m)_{np} = \frac{n_p \sin(A_p)}{\sqrt{n_p{}^2 - \sin^2(\alpha)}} \Delta n_p \quad [3.15]$$

$$\left(\Delta N_m\right)_{Ap} = \left[\sin(A_p)\sin(\alpha) + \cos(A_p)\sqrt{{n_p}^2 - \sin^2(\alpha)}\right]\Delta A_p \qquad [3.16]$$

$$\left(\Delta N_m\right)_{\alpha} = \cos(\alpha)\left[\cos(A_p) + \frac{\sin(A_p)\sin(\alpha)}{\sqrt{{n_p}^2 - \sin^2(\alpha)}}\right]\Delta\alpha \qquad [3.17]$$

In the experimental conditions previously reported and for a rotation device with a resolution of 10^{-2} (°) (1.74 x 10^{-4} rd), we can easily calculate the absolute values of ΔN_m for different guided modes (by using relation [3.13]).

Using parameters of Table 3.2, we find the following results.

m	α (°)	N_m x10^{-4}	$(\Delta N_m)_{\alpha}$x10^{-5}	$(\Delta N_m)_{np}$x10^{-4}	$(\Delta N_m)_{Ap}$x10^{-4}	ΔN_m
0	-24.27	2.2893	0.97	2.85	0.34	1.60
1	-22.72	2.2742	0.99	2.84	0.34	1.62
2	-21.36	2.2606	1.01	2.84	0.35	1.64
3	-19.35	2.2401	1.03	2.84	0.35	1.67
4	-16.77	2.2130	1.07	2.83	0.36	1.71
5	-13.84	2.1812	1.10	2.83	0.37	1.76

Table 3.2. *Calculation of ΔN_m ($\Delta\alpha$= 1.74x10^{-4} rd, Δn_p= 4x10^{-5}, ΔAp=2x10^{-5})*

In addition, the curve of Figure 3.14a shows the variation of ΔN_m as a function of $\Delta\alpha$ for different guided modes order m = 0, 2 and 5. That of Figure 3.14b provides the ΔNm variation according to the mode order for a given $\Delta\alpha$.

It should be noted that ΔN_m proportionally varies according to $\Delta\alpha$ (Figure 3.14.a), which especially depends on the resolution of the rotation device. To increase the accuracy of Nm it is necessary to use a high-resolution rotation device.

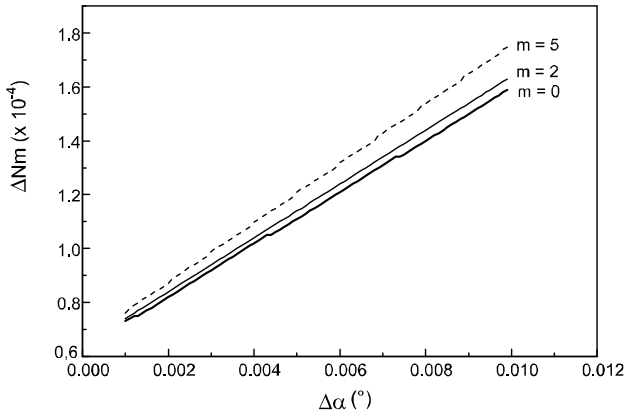

(a)

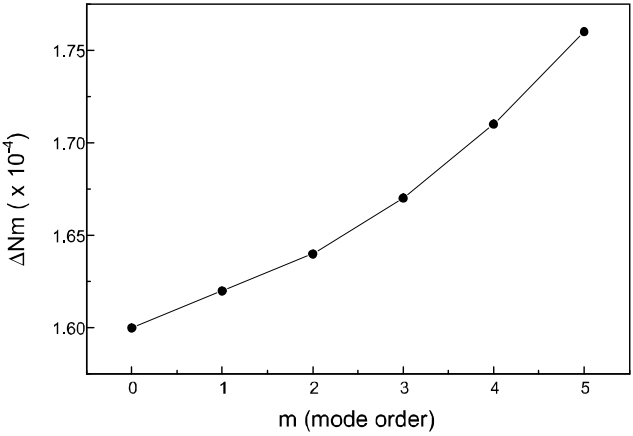

(b)

Figure 3.14. *(a) Variation of ΔNm according to Δα; and (b) variation of ΔNm according to m (Δα=1.74 x 10⁻⁴ rd)*

According to the curve (Figure 3.14b), it is clear that the precision of the low order modes is better than that of high order modes. This is due in particular to the sensitivity of high order modes to the prism presence. As a whole, an angular precision of 10^{-2} (i.e. 0.02) degrees allows a determination of N_m with an accuracy of 1.6 x10^{-4}, which is very satisfactory.

3.2.4. *Theoretical study of the effective index N_m*

It is essential to note that before any experimental characterization, it is necessary to know the angular range of the guided modes, and thus their angular positions for the structure to be studied. In order to do this, it is possible to develop a simulation code which allows us, for a given guiding structure, to calculate N_m and α_m. We will give the basic principles of this procedure.

The problem is as follows: for a given guiding structure with the known parameters, *n*, *n*s, *n*a and *d*, how do we determine how the effective indices of the guided modes are likely to propagate? As the analytical solution of the dispersion equation is almost impossible, a numerical solution can thus be used to determine the values of *N*m. For that, we use calculation by iteration [Hal 1980]. The dispersion equation can be put in the following form:

$$d(N_m) = \frac{\Psi_m(n, N_m)}{\left(n^2 - {N_m}^2\right)^{1/2}} \tag{3.18}$$

$$\text{With } \Psi_m(n, N_m) = m\pi + \Phi_{(n,n_a)}(n, N_m) + \Phi_{(n,n_s)}(n, N_m)$$

and

$$\Phi_{(n,j)}(n, N_m) = arctg\left[\left(\frac{n}{n_j}\right)^{2\rho}\left(\frac{{N_m}^2 - {n_j}^2}{n^2 - {N_m}^2}\right)\right]^{1/2}$$

$$\rho = \begin{cases} 0 & \text{TE} \\ 1 & \text{TM} \end{cases}$$

where j = s, a indicates the substrate or the superstrate.

The function $d(N_m)$ is strictly monotone, $\frac{\partial d(N_m)}{\partial N_m} > 0$. The calculation of N_m is performed within the interval $[n_s, n]$ (see Figure 3.15).

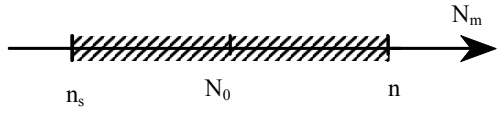

Figure 3.15. *Calculation of N_m*

Firstly we calculate the value of $d(N_0)$ in the middle of the interval; then the obtained value is compared with the normalized thickness, kd:

– if $d(N_0) = kd$, the value to be determined is N_0;

– if $d(N_0) > kd$, the value of N_m is situated in the right part of the interval;

– if $d(N_0) < kd$, the value of N_m belongs to the left part of the interval.

We perform the same calculation by considering the deduced interval part. The limit of the calculation is given when an interval of $N_{mmax} - N_{mmin} \leq 10^{-4}$ $(n - n_s)$ is reached. Thus, N_m is determined by a linear interpolation of $d(N_{mmax})$ and $d(N_{mmin})$. The variation of the guided mode order, m, in equation [3.18] allows the calculation of the values N_m of all guided modes.

Moreover, the effective index N_m is determined by the optogeometric parameters of the structure. In practice, it is often difficult to know all those parameters: n, n_s, n_a and d at the same time. We generally only have access to the two indices n_s and n_a. Under these conditions, it is useful to analyze the variation of the effective index N_m according to each parameter considered separately (others being constant).

The variation of the effective index according to the thickness was already discussed in the first chapter. It is just useful to point out the existence of a cut-off thickness, d_m, beyond that value the mode of order m cannot exist. Generally speaking, the effective index is very sensitive to the thickness variations.

In the same way, starting from the dispersion equation, we can analyze the influence of n and n_s. Note that, the effective index proportionally varies according to the index of the guiding layer and the index for all the guided modes (see Figure 3.16a). Moreover, low order modes are more sensitive to the variation of the guide index than those of a high order.

With regard to the influence of the substrate index, one notes that high order modes are much more sensitive to the variation of n_s than those of low order. In addition, the variation ΔN_m of low order modes, m= 1 for example, is due to the measuring accuracy 10^{-4}; this can be neglected.

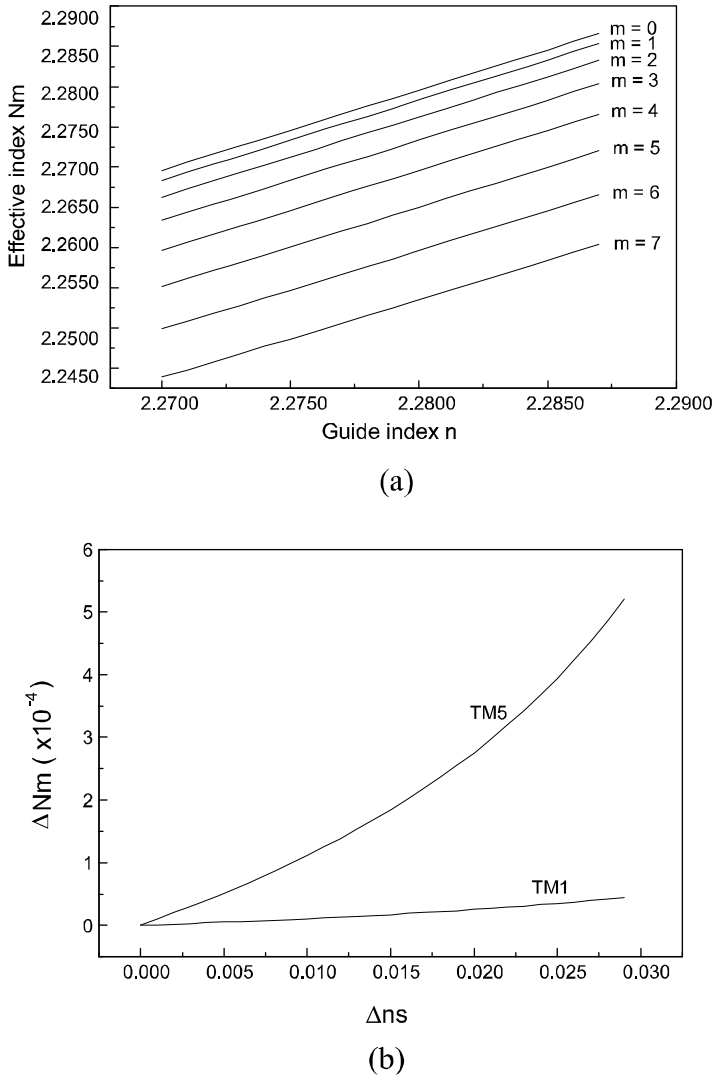

Figure 3.16. *(a) Variation of the effective index N_m as a function of the guide index; (b) variation of N_m as a function of the substrate index; for TM modes (n_s=2.25, d=7μm and 2.270<n<2.288)*

To summarize, the effective index particularly depends on the index and the thickness of the guiding layer, and is not very sensitive to the variation of the substrate index (in particular for low order modes).

3.2.5. *Waveguide parameter determination*

As a matter of fact, the measurement goal of the effective indices is to determine the refractive indices and the thickness of the guiding layer. This is possible by using the dispersion equation, discussed in Chapter 1, which can be put in the following form:

$$F\left(N_m, n, n_s, n_a, d, m, \rho\right) = 0 \qquad [3.19]$$

where m is the mode order and ρ is related to the polarization used (TE or TM).

In this section we present the theoretical tools necessary for the extraction of the optogeometric parameters of the guiding structure, starting from the measured effective indices.

3.2.5.1. *Step index waveguides*

For step index waveguides (constant index), two procedures can be used. The first is based on the adjustment of the experimental guided modes spectrum by calculating the reflection coefficient of a multi-layer structure, R=R(n, ns, na, d) [Bou 2000, Den 1989, Ker 1973, Ker 1975]. In this case, the couple (n, d) is determined to be fitting parameters of theoretical and experimental guided modes spectra. This procedure is sometimes delicate to implement because it can be necessary to introduce other parameters, such as the attenuation coefficient, to optimize the fitting process. In turn, it could be of interest to estimate the losses in the considered layer.

The second approach consists of directly using the effective indices of the guided modes measured by "m-lines" spectroscopy. This uses the principle of iterative calculation starting from the dispersion equation. It constitutes a simple, effective and precise method. This method was reported and discussed by R. Ulrich *et al.* [Ulr 1973].

3.2.5.1.1. Monomode waveguides

In this case, only one effective index is known and determination of the guide refractive index requires the value of the waveguide thickness d and vice versa.

3.2.5.1.2. Two guided modes

Usually, these guided mode orders are 0 and 1. However, in order to generalize the study let us consider two guided modes μ and ν. The corresponding effective indices are N_μ and N_ν. They are related to the refractive index and the thickness of the guide by the dispersion equation which can be written as:

$$kd\left(n^2 - {N_m}^2\right)^{1/2} = \Psi_m\left(n, N_m\right) \qquad [3.20]$$

$$\Psi_m\left(n, N_m\right) = m\pi + \Phi_{(n,na)}\left(n, N_m\right) + \Phi_{(n,ns)}\left(n, N_m\right) \qquad [3.21]$$

$$\text{and} \quad \Phi_{(n,j)}\left(n, N_m\right) = arctg\left[\left(\frac{n}{n_j}\right)^{2\rho}\left(\frac{{N_m}^2 - {n_j}^2}{n^2 - {N_m}^2}\right)\right]^{1/2} \qquad [3.22]$$

$$\rho = \begin{cases} 0 & \text{TE} \\ 1 & \text{TM} \end{cases} \qquad [3.23]$$

where j = s, a indicates the substrate or the superstrate. This can be solved in two ways [Bou 1996, Bou 1996a].

Equation [3.20] contains two unknown factors: n and Nm. Thus we need two equations to determine an exact solution. This system of two equations can be easily obtained using the two measured effective indices $N\nu$ and $N\mu$. Although this solution represents a rigorous mathematical solution, its calculation is somehow difficult to carry out. For this reason, it is possible to use another method based on iterative calculation.

By replacing the two effective indices $N\nu$ and $N\mu$ in equation [3.20], we obtain two equations from which it is possible to eliminate the factor kd. This results in only one equation of n, as follows:

$$n^2 = F\left(n^2\right) \qquad [3.24]$$

with:

$$F\left(n^2\right) = \frac{\left({N_\mu}^2{\Psi_\nu}^2 - {N_\nu}^2{\Psi_\mu}^2\right)}{\left({\Psi_\nu}^2 - {\Psi_\mu}^2\right)} \qquad [3.25]$$

Equation [3.24] cannot be solved explicitly, but a simple iterative calculation allows for the determination of n. The calculation steps are as follows:

– Determination of a starting index n_d. The experiment shows that the value of the guiding layer index is close to the value obtained starting from the measured effective indices, and is given by:

$$n_d = N_\mu + 3(N_\mu - N_\nu) \qquad [3.26]$$

This value allows the iterative calculation to begin.

– Calculation of F(n) to be compared with n; if $F(n_d) - n_d$ is of the order of 10^{-6}, n is the expected value, otherwise the calculation procedure should be performed by using the new value of $n=\sqrt{F(n^2)}$. Numerical calculation indicates that the function *F(n)* always converges to the value of *n.* Subsequently, we can obtain the thickness value d in a straightforward manner using equation [3.20].

In certain cases, when the divergence between the two values of *d* obtained by using N_μ and N_ν values is important, an optimization is essential. This is also the case for multimode waveguides which we will discuss in the next section.

3.2.5.1.3. Multimode waveguides

In this case, it is necessary, as it was highlighted above, to carry out a numerical optimization to determine the best couple (*n*, *d*). Determination of the starting value of the refractive index n_d is carried out in the same manner as the preceding case. The use of iterative calculation, developed above, with all the possible couples (N_μ, N_ν) makes it possible to determine a series of values $n_{\nu\mu}$. The couples of effective indices are chosen so that $N_\nu = 0$ and $N_\mu = [1, (M-1)]$ with M the number of modes.

Thus, the average value of $n_{\mu\nu}$ represents the index value to be determined, in other words:

$$n = \frac{\sum_{\mu\nu} n_{\mu\nu}}{M-1} \qquad [3.27]$$

The experiment showed that this value is generally found with high precision.

Determination of the guiding layer thickness is carried out in the following way: starting from an initial value of *d*, generally given by the waveguide fabrication technique used and the value of *n*, we calculate the expected theoretical effective indices. We then minimize the sum of the squares variations σ defined by:

$$\sigma = \sum_{i=0}^{m} {}^{1}\left(N_{m_{th}} - N_{m_{\exp}}\right)^2 \qquad [3.28]$$

The couple (n, d) thus obtained represents the best values of the index and thickness of the guiding layer which makes it possible to obtain theoretical effective indices that are in close agreement with the measured ones.

It should be noted that the variations (N_{mth} - N_{mexp}) allow a better knowledge of the guide. In particular, if they are lower than measurement uncertainties, we can consider the structure as a step index waveguide. However, if they are definitely higher than uncertainties, the structure is very likely to be a graded index waveguide.

In addition, the curve giving N_{m}^2 according to $(m+1)^2$ can also bring useful knowledge of the guiding structure. Indeed, starting from the dispersion equation [1.17] and if the two interfaces guide-substrate and guide-superstrate are delimited (abrupt variation of the refractive index), we can write:

$$\Phi_{(n,n_a)} = \Phi_{(n,n_s)} = \frac{\pi}{2} \qquad [3.29]$$

and deduce the following relation:

$$N_m{}^2 = n^2 - \frac{\lambda^2}{4d^2}(m+1)^2 \qquad [3.30]$$

This relation is a line equation whose slope determines the waveguide thickness. Its variation compared with the origin gives a value of n that can be used as an initial value in the iterative calculation previously mentioned.

It should be noted that another calculation approach using the measured effective indices was reported by R. Th. Kersten [Ker 1973] and G. Zhang *et al.* [Zha 1988]. It consists of calculating the index and thickness, by optimizing the two functions $R(n)$ and $U(d)$ respectively, given by:

$$R(n) = \sum_{m=0}^{M} {}^{1}\left[\frac{m\pi + \Phi^m_{(n,na)} + \Phi^m_{(n,ns)}}{(m+1)\pi + \Phi^{m+1}_{(n,na)} + \Phi^{m+1}_{(n,ns)}} - \frac{b(m)}{b(m+1)}\right]^2 \qquad [3.31]$$

$$U(d) = \sum_{m=0}^{M-1} \left[m\pi + \Phi^{m}_{(n,na)} + \Phi^{m}_{(n,ns)} - db(m) \right] \quad [3.32]$$

$$b(m) = k\left(n^2 - Nm^2\right)^{1/2} \quad [3.33]$$

where n and d are obtained when $R(n) \rightarrow 0$ and $U(d) \rightarrow 0$ respectively.

Note that in all the calculations developed above, we neglected the influence of the presence of the coupling prism on light phase variation at the interface guide-superstrate. This effect can be disregarded if the air gap is higher than 0.15 μm (λ/4).

3.2.5.2. *Graded index waveguides*

A graded index waveguide is characterized by a refractive index variation along its thickness given by n (x).

In this case the effective index values are solutions of the following dispersion equation (see Chapter 1):

$$k \int_0^{x_l} \sqrt{n^2(x) - {N_m}^2(m)}.dx = \psi(N_m) \quad [3.34]$$

$$\psi(N_m) = m\pi + \frac{\pi}{4} + arctg\left\{ c_p \left[\frac{{N_m}^2 - {n_a}^2}{{n_0}^2 - {N_m}^2} \right]^{1/2} \right\} \quad [3.35]$$

$$c_p = \begin{cases} 1 & \text{for TE} \\ \left(\dfrac{n_0}{n_a} \right)^2 & \text{for TM} \end{cases} \quad [3.36]$$

where x_t is given by $n(x_t) = N_m$, and n_a and n_0 are superstrate (air) and the guide refractive indices for $x = 0$, respectively (surface index).

Two different approaches are also distinguished. The first consists of approaching the index profile using an analytical function. Indeed, the index profile is often determined by the fabrication parameters. For example, the index profile of diffused waveguides can be given by linear functions, exponential or Gaussian [Nai 1977]. Similar functions were used with ionic exchange waveguides. P.K. Tien *et al.* [Tie 1974] also reported the use of the Fermi function to determine the index profile of $LiNbO_3$ and $LiTaO_3$ thin film waveguides obtained using an epitaxial technique. This function was also used with PMMA He^+-implanted waveguides [Kul 1992], and is given by:

$$n(x) = n_s + \frac{\Delta n}{1 + \exp\left(\frac{x - d}{a}\right)} \qquad [3.37]$$

d: the waveguide thickness

a: the width of the index barrier

Δn: the index variation.

The use of this function with equation [3.34] enables the calculation of the theoretical effective indices. The three preceding parameters are then determined by fitting these values to the measured values.

The second approach to solving this problem consists of carrying out an inverse WKB calculation and thus directly using the effective indices for the index profile reconstruction. Generally speaking, the treatment of graded index waveguides using Maxwell's equations reveals a great similarity between the optical wave propagation equation and Schrôdinger's equation of quantum mechanics. In this case, the guided modes of the considered structure represent the stationary solutions of the problem, with the quantum well potential given by V(x) = - n2(x). This approach can even be applied to the step index waveguide. In this case one considers a quantum well with a square potential.

3.2.5.2.1. Summary of the iWKB method

Several versions of the iWKB method have already been reported [Chi 1985, Mat 1995, Whi 1976]. In this section, we will only focus on one version that offers a very good compromise between simple programming and an excellent result precision.

The first calculation step consists of finding out a continuous function $N_m(m)$ by interpolating the measured values N_m. For this a Lagrange interpolation could be efficiently used.

From equation [3.34], the maximum value of N_m is obtained for $x_t = 0$ and $\psi = \pi/2$. Under these conditions m = -3/4. Thus, the iWKB solution consists of calculating x_m. This is carried out step by step according to the following recursive algorithm:

Initial conditions: $m_0 = -3/4$; $\psi = 0$; $x_1 = 0$.

$$x_k = x_{k-1} - \frac{\psi_k - \psi_{k-1}}{k\sqrt{n_{moy}^2 - n^2(m_k)}}$$

$$n_{moy} = \frac{n(m_k) + n(m_{k-1})}{2}$$

$$\psi_k = \int_0^{x_k} \sqrt{n^2(x) - N_m{}^2(m_{k+1})}.dx \qquad [3.38]$$

$$\psi_k = \sum_{j=0}^{k} (x_k - x_{k-1}) \sqrt{\left(\frac{n(m_k) + n(m_{k-1})}{2}\right)^2 - N_m{}^2(m_{k+1})}$$

The first parameter of the calculation, x_1 is given by calculating integral [3.34]:

$$x_1 = x_0 - \frac{\psi_1}{k\sqrt{n_{moy}^2 - n^2(m_1)}}$$

with:

$$\psi_1 = \sqrt{n_{moy}^2 - n^2(m_1)}.(x_1 - x_0) \qquad [3.39]$$

and:

$$n_{moy} = \frac{n(0) + n(m_1)}{2}$$

In this case, the thickness is given by the depth of the index variation n.

The treatment of the example previously reported in Table 3.1 by this method makes it possible to obtain the index profile $n(x)$ displayed in Figure 3.17.

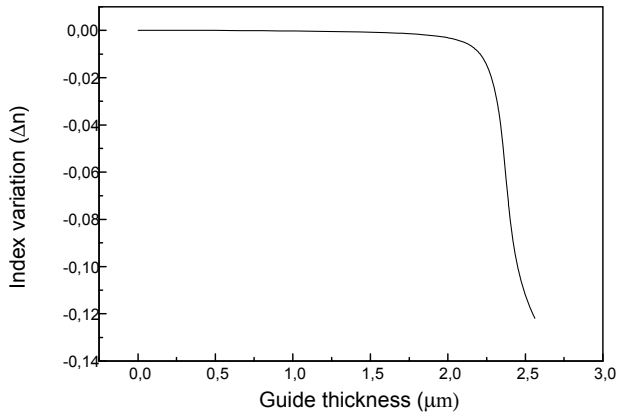

Figure 3.17. *Index profile obtained by iWKB*

We can reasonably estimate the index variation of about 10% and the thickness d=2.52 μm.

The index profile reconstruction stops at the limit of the guiding layer; but it is essentially established this beyond that Δn tends towards zero (we recover the index of the new crystal).

3.2.5.2.2. Note

In both the cases of waveguides discussed above, the knowledge of n_0, the starting index value, is essential for the complete determination of the waveguide parameters. Actually, this value corresponds to the waveguide surface refractive index. Consequently, this value can be measured using the cut-off angle method which gives the angle from which there is transfer of the incident energy into the guide through the interface air-waveguide. In this case, the transmitted beam is parallel to the interface and we can write:

$$N_m = n_p \sin\theta = n_{surf} = n_0 \qquad [3.40]$$

3.3. Optical losses

As indicated in the previous sections, the characterization of optical waveguides requires the determination of two essential parameters: the index profile and the thickness of the guiding layer. These two parameters can inform us about the guiding properties of the structure under investigation. Thus, the thickness of the guide directly influences the number of modes, whereas the index profile determines the light confinement performances of the waveguide. However, the development of optical systems requires the development of integrated optical components able to carry on information, from one point to another, with reliability. Therefore, the optical losses within the structure are a vital parameter to completely characterize the waveguide.

In the following section, we will tackle this problem in two essential parts. In the first part we recall the various physical origins of losses in the waveguides. The second part will be devoted to the measurement techniques of this parameter.

3.3.1. *Optical losses origin*

Whatever the fabrication process, optical losses within waveguides can be attributed to four mechanisms [Kad 1989]:

– absorption losses;

– radiation losses;

– conversion losses;

– diffusion losses.

3.3.1.1. *Absorption losses*

Generally speaking absorption losses within dielectric and ferroelectric waveguides, such as $LiNbO_3$ or $LiTaO_3$, can be neglected. However, they might be important in case of semiconductor materials. These absorptions can be related to: interband transitions, free carriers and impurities.

3.3.1.1.1. Interband absorption

In this configuration, photons with energy higher than the material gap can be strongly absorbed, thus producing electronic transitions from the valence band to the conduction band. This phenomenon is more important in semiconductor materials.

3.3.1.1.2. Free carrier absorption

Also called intraband absorption; this occurs when the photons transmit their energy to electrons of the conduction band or to holes of the valence band.

The absorption coefficient, α_{pl}, due to free carriers can be given by the following relation [Che 1987, Kad 1989]:

$$\alpha_{pl} = \frac{k}{n}\Lambda$$

where [3.41]

$$\Lambda = \frac{Ne^3}{m^2 \varepsilon_0 \omega^3 \mu}$$

n: material refractive index
ω, k: pulsation and wavevector, respectively
N: free carriers concentration
e and m: charge and mass of free carriers, respectively
ε_0: the vacuum permittivity
μ: mobility of the free carriers.

3.3.1.1.3. Impurity absorption

In certain cases, during waveguide fabrication, impurities come to contaminate the guiding layer. These impurities could be a source of absorption for certain wavelengths. However, this situation is very rare because waveguide fabrication processes require total control of all the fabrication parameters.

3.3.1.2. *Radiation losses*

In this case, the energy of the guided modes can be dissipated in the substrate or the superstrate. This applies to leaky modes where the value of the effective indices is very close to that of the cut-off index (substrate or superstrate indices). Note however that this only relates to high order modes. It should be noted that by optimizing the fabrication parameters, we can minimize radiation losses which are generally negligible compared with the other losses.

3.3.1.3. *Conversion losses*

In an ideal guiding structure, guided modes are orthogonal and thus energy transfer between modes cannot occur.

However, in certain non-homogenous waveguides, such energy transfers can take place [Mar 1969]. In this case, low order well confined modes can undergo

losses by coupling with other modes of a high order. However, this problem is less frequent in optical waveguides of very good quality and can be omitted.

3.3.1.4. *Diffusion losses*

Diffusion losses are most important and most frequent in waveguides. We can distinguish two types of diffusion losses: volume diffusion losses and surface diffusion losses [Goe 1969, Tie 1971]. The first are caused by the crystalline imperfections and defects in the material. They depend on the concentration of the impurities (diffusion centers) in the crystal. Consequently, these losses are less important than surface diffusion losses, which we will discuss in greater detail. Also, we particularly treat the case of surface diffusion losses.

3.3.1.4.1. Surface diffusion losses

These losses arise from the roughness of the guide-substrate and guide superstrate interfaces. Correction of this problem can be carried out using the optical rays approach: where an optical ray, being propagated in a guiding structure of a thickness d, undergoes multiple reflections on the two interfaces. The number of these reflections over a length L, is given by the following relation [Kad 1989]:

$$N_r = \frac{L}{2d \tan\left(\frac{\pi}{2} - \theta_m\right)} \qquad [3.42]$$

where θ_m is the reflection angle of the guided mode m.

Diffusion losses appear for each reflection and are important for high order modes because the number of reflection increases according to the order of the modes (θ_m decreases).

For a qualitative description of these losses, we use the attenuation coefficient α_d, which shows that the intensity of the guided mode at a distance z can be put into the following form:

$$I(z) = I_0 \exp(-\alpha z) \qquad [3.43]$$

where I_0 is the initial intensity at $z = 0$.

Coefficient α can be calculated using several methods [Kad 1989, Che 1987, Mar 1969, Goe 1969, Tie 1971]. The simplest one, developed by P.K. Tien [Tie 1971], is based on the Rayleigh's criterion, according to which for an incident

optical power Pi on a surface, the reflected power in a specular direction can be given by the following relation:

$$P_r = P_i \exp\left[-\left(\frac{4\pi\sigma\cos\theta_m}{\lambda}\right)^2\right] \qquad [3.44]$$

where σ is the standard deviation of the amplitudes of thickness fluctuations.

Under these conditions, P. K. Tien showed that the attenuation coefficient could be written:

$$\alpha = A^2\left(\frac{\cos^3\theta_m}{2\sin\theta_m}\right)\left(\frac{1}{d_{eff}}\right) \text{ cm}^{-1} \qquad [3.45]$$

$$\text{where } A = \frac{4\pi}{\lambda}\sqrt{\sigma^2_{(n,n_a)} + \sigma^2_{(n,n_s)}} \qquad [3.46]$$

and d_{eff} is the effective thickness.

Note that coefficient α_d, given by formula [3.45], is proportional to the square of the ratio of material roughness to the wavelength. We can also show that optical losses in dB.cm^{-1} can be calculated using the following relation:

$$a = 4.3\alpha \quad (\text{dB.cm}^{-1}) \qquad [3.47]$$

As a whole, surface diffusion optical losses are generally dominant in dielectric waveguides, such as glasses and oxides. They are of 0.5 to 5 dB.cm^{-1} for low order modes, which increases for high order modes [Tie 1971]. In semiconductors, these losses are less important due to the very minor roughness of the guiding layer (less than 0.01 μm).

3.3.2. *Optical loss measurements*

The basic principle of these measurements consists of comparing the power of the light which is propagated in the guide with the power of the light at launching. However, in practice, many problems emerge, in particular those due to the coupling

and the decoupling, which introduce extra losses that are generally difficult to manage. In addition, a rigorous study of the problem requires the knowledge of the origin of losses which makes it more complicated.

The developed measurement techniques depend, particularly, on the coupling method used according to the guide considered, the nature of the losses, and their importance in the measured losses.

In this section, we will point out the principles of these techniques which generally consist of measuring the attenuation coefficient according to the waveguide length.

3.3.2.1. *End-fire coupling technique*

This simple technique uses end-coupling, as indicated in Figure 3.18. The principle compares the transmittance of several samples of different lengths in order to determine the attenuation coefficient α.

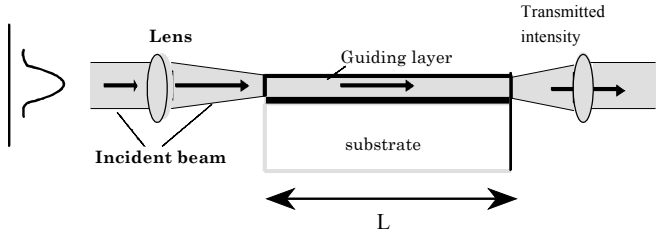

Figure 3.18. *Loss measurements by the end-coupling method*

In practice, it is very difficult to obtain a series of waveguides of the same optical quality and thus the comparison is not compatible. Consequently, it is necessary to cut the same guide for each measurement. Generally, we start with a rather important length L_0. The light is injected into the guide using an objective microscope, or even an optical fiber, as indicated in Figure 3.18. The attenuation coefficient can be written in the following way:

$$\alpha = \frac{\ln\left(\frac{p_0}{p_1}\right)}{L_0 - L_1} \qquad [3.48]$$

where L_0, L_1 and P_0, P_1 are lengths and transmitted powers, respectively, before and after the sample cut.

As an example, F. P. Strohkendl *et al.* [Str 1991] reported optical losses of 3 $dB.cm^{-1}$ in $KNbO_3$ He^+-implanted waveguides using this technique. D. Kip *et al.* [Kip 1995] also reported the optical losses investigation of SBN proton-implanted waveguides using the same principle [Brü 1995]

Nevertheless, the utilization of this technique is somehow limited due to many disadvantages. These arise from the coupling method employed as previously mentioned, and can be summarized as follows:

– it is a destructive method (the guide should be cut for each measurement);

– it is a non-selective method (all the guided modes are simultaneously excited);

– it is difficult to carry out because it needs precise alignment of the experimental set-up, as well as high optical polishing of the guide sections.

3.3.2.2. *Prism coupling method*

This method has been extensively applied to different configurations and is a good alternative to the end-fire coupling technique. As indicated in Figure 3.19, a first prism is used to inject light into the guide, while the second is used to out-couple this light, allowing for the transmitted intensity (guided) measurement. Generally speaking, the first prism is fixed, whereas the second is moved along the guide. Several measurements at different waveguide lengths make it possible to determine the attenuation coefficient according to length L.

The displacement, however, of the out-coupling prism may introduce additional experimental errors. To avoid this situation, we use a third prism [Aru 1986, Web 1973, Won 1980], as shown in Figure 3.19.

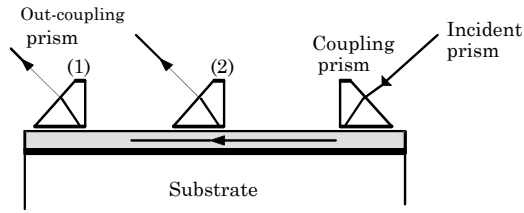

Figure 3.19. *Prism coupling method of optical loss measurement*

Y.H. Won *et al.* [Won 1980] showed that the out-coupled intensity from the third prism is independent of the coupling coefficients and can be written as:

$$I(z) = \frac{P_2 P_3^0}{\Delta P} \qquad [3.49]$$

with:

$$\Delta P = P_3^0 - P_2 \qquad [3.50]$$

P_2^0: light power out-coupled from the second prism without the third prism

P_3: light power out-coupled from the third prism.

This method allows selective measurements, in the sense that we can selectively excite the waveguide guided modes. It is also a non-destructive method (the sample does not need to be cut). However, it is difficult to exactly reproduce the same coupling and out-coupling conditions for the three prisms. Thus, the accuracy of the measurements can be affected.

It is worth noting that a matching liquid of low index (n = 1.33, glycerin n = 1.47) can be used to improve the method performances.

3.3.2.3. *Prism coupling and end-fire out-coupling method*

In this configuration, the prism coupling is used to launch light into the waveguide, and the end-fire out-coupling is used to measure the transmitted light (see Figure 3.20). The latter is performed versus the guide length by moving the coupling prism upon the surface of the waveguide [Bou 1997]. At the same time, the reflected intensity on the prism base is measured in order to determine the coupling coefficient. Under these conditions, we can escape from the coupling coefficient influence.

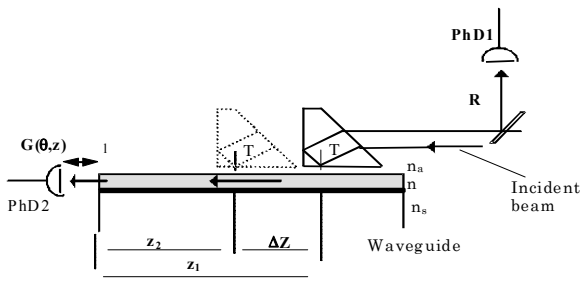

Figure 3.20. *Loss measurement by prism-coupling and end-fire out-coupling*

Two photo-detectors (PhD1) and (PhD2) are used to simultaneously measure the reflected and transmitted intensities. For instance, for waveguide length z, we can write:

$$P_m(z) = \eta_m T_m \exp(-\alpha_m z) \quad [3.51]$$

where η_m is the coupling coefficient; α_m is the attenuation coefficient for the m^{th} mode; $P_m(z)$ is the guided intensity of the m^{th} mode; and T_m is the injected intensity into the prism.

Thus, we can write for z_1 and z_2:

$$P_m(z_1) = \eta_m T_m \exp(-\alpha_m z_1) \quad [3.52]$$

$$P_m(z_2) = \eta'_m T_m \exp(-\alpha_m z_2) \quad [3.53]$$

Generally, $\eta(m)$ and $\eta'(m)$ are different because the coupling conditions are different. However, this method makes it possible to be completely released from this parameter using the two measurement systems (reflection (PhD1) and transmission (PhD2)) simultaneously [Bou 1997].

We start by measuring the transmitted and the reflected intensities for length z_1. Then, before taking a second measurement of the transmitted intensity for length z_2, we adjust the coupling conditions, in particular the air-gap in order to maintain the same initial coupling conditions as for position z_1. For this, we measure the guided modes spectrum by reflection, which can be compared with the spectrum obtained for position z_1. As an example, Figure 3.21 shows the TM guided modes spectra obtained by reflection in a $LiNbO_3$ He+-implanted waveguide.

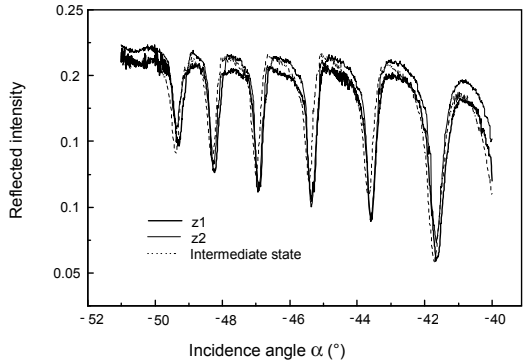

Figure 3.21. *Prism coupling conditions controlled using the reflected intensity measurements*

The superposition of the two guided modes spectra allows us to call the coupling coefficients identical at positions z_1 and z_2. Therefore, η (m) = η'(m). In addition to this, it is important to maintain as constant the distance between the photo-detector (PhD2) and the waveguide end, Figure 3.20, as well as to highly polish the waveguide sections. Under these conditions, light diffusion at the sample extremities can be disregarded. Finally, from relations [3.51] and [3.52], the attenuation coefficient is given by:

$$\alpha_m = \frac{1}{(z_1 - z_2)} \ln\left[\frac{P_m(z_2)}{P_m(z_1)}\right] \quad (\text{cm}^{-1}) \qquad [3.54]$$

This relation is independent of the coupling coefficient. It also allows us to obtain the absolute error $\Delta\alpha$:

$$\Delta\alpha = \frac{2\Delta z}{(z_1 - z_2)^2} \ln\left[\frac{P_m(z_2)}{P_m(z_1)}\right] (\text{cm}^{-1}) \qquad [3.55]$$

where Δz is the absolute error of the guide length z measurements.

This technique was used to measure optical losses in $LiNbO_3$ (He^+, H^+)-implanted waveguides [Bou 1997] and $Li_2B_4O_7$ He^+-implanted waveguides [Bou 2001]. Results indicated optical losses of the order of dB.cm^{-1}.

From relation [3.55], it appears that the measurement accuracy depends in particular on the absolute error of the waveguide length measurement. Therefore, longer samples produce high accuracy results. As a matter of fact, this technique allows us to measure optical losses of 0.1 dB.cm^{-1}.

3.3.2.4 *Surface analysis method*

The techniques previously discussed determine the total losses in the guide, without distinction between the origins of these losses: absorption, radiation, diffusion or conversion. For dielectric waveguides, where the losses by diffusion are dominant, the analysis of the surface of the guide makes it possible to determine the attenuation coefficient. For a uniform guide, the scattered light from the surface can be considered proportional to the guided intensity.

Measurement of the scattered light can be carried out using an optical fiber, (Figure 3.22). A surface waveguide analysis gives the diffused intensity according to the guide length [Oka 1983, Oka 1985, Roe 2004, Ros 1995]. The slope of the obtained curve determines the attenuation coefficient.

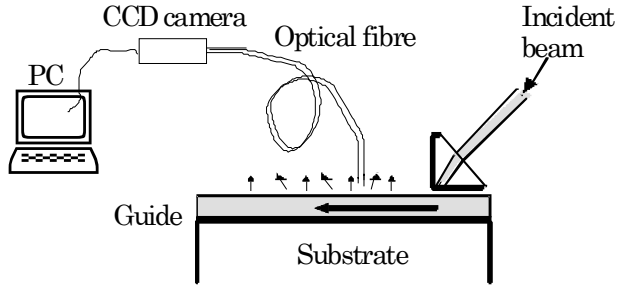

Figure 3.22. *Surface analysis method for determining optical losses*

Note that, we can also use a CCD camera in order to directly collect the scattered light from the waveguide surface [Ros 1995].

For instance, Figure 3.23 displays a photograph of the propagated light into a planar (a) and a channel (b) optical waveguide of $Ca_4YO(BO_3)_3$ (YCOB) He^+-implanted waveguide [Vin 2004].

Figure 3.23. *Photograph of light propagation of (a) planar and (b) channel YCOB He+-implanted waveguide([Vin 2004])*

The analysis of the intensity variation according to the propagation distance (Figure 3.24) makes it possible to obtain diffusion optical losses. For instance, Vincent *et al.* reported losses of 2 $dB.cm^{-1}$ and 1.8 $dB.cm^{-1}$ in planar and channel waveguides, respectively.

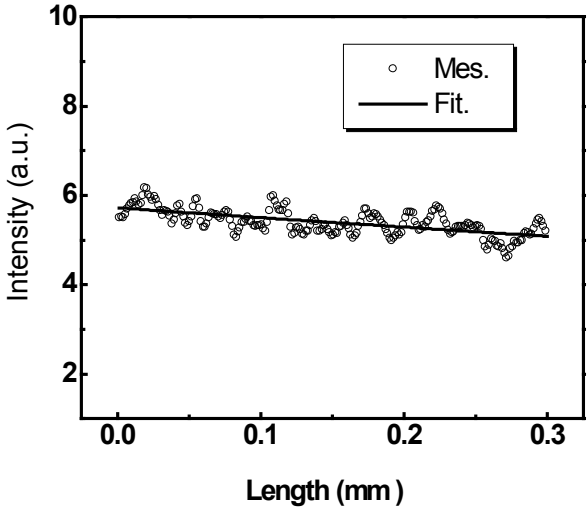

Figure 3.24. *Evolution of the intensity of the guided light according to the propagation length: guide plan YCOB:He+ ([Vin 2004])*

This technique is a non-destructive method as no contact is needed in order to perform measurements. However, its utilization is limited to waveguides where the losses by diffusion are more important than losses by absorption or radiation.

3.3.3. *Characterization in near-field microscopy of optical waveguides*

Scanning near-field optical microscopy (SNOM) makes it possible to observe small details of physical objects, as well as to determine of the electromagnetic field distribution on the sample surfaces, with a sub-wavelength resolution. This technique has been used extensively recently in different configurations. Its application to the study of sub-micron dimensions is of great interest from the fundamental point of view as well as for the characterization and the study of optical compounds. The use of this technique (SNOM) for the study of light confinement in various optoelectronics structures has already been the subject of several publications [Bor 2000, Bou 1992, For 1998, Tas 2002].

The SNOM configuration used is that of near-field collection mode, with a tapered and metallized optical fiber. The evanescent field collected on the surface of the guide is sent towards a photo-detector. The experimental setup is displayed in Figure 3.25.

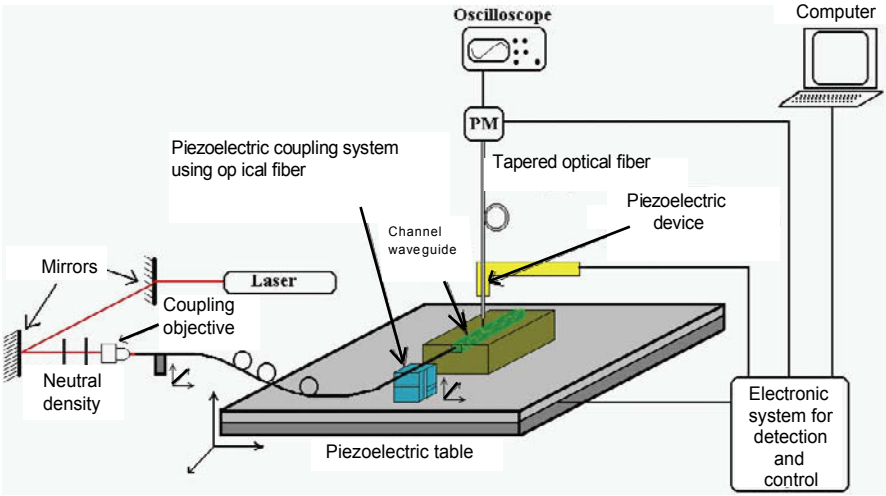

Figure 3.25. *SNOM setup for optical waveguide characterization*

Figure 3.26 reports the topographic and optical images of the exchanged $LiTaO_3$ waveguide. Several images were taken and assembled in order to obtain a total image of the guide over a length of a millimeter. We can note that this study shows that the protonic exchange process produces a dilatation of the crystal in the exchanged zone. Moreover, we observe a light topography of approximately 5 nm on each side of the exchanged zone.

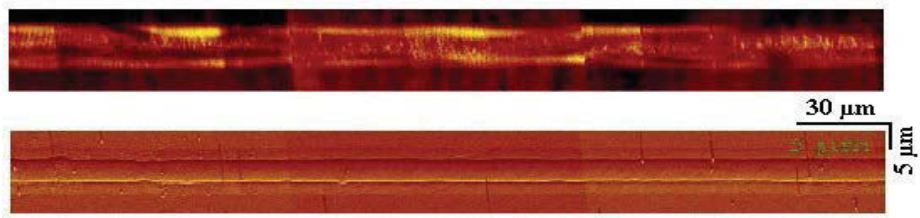

Figure 3.26. *SNOM optical image (top) and topographic image (bottom) of a channel guide of $LiTaO_3$*

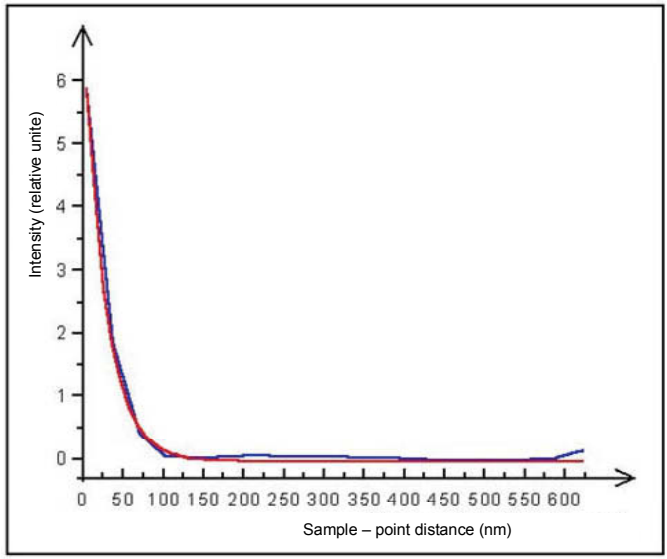

Figure 3.27. *Variation of the evanescent field according to the length of the sample*

Figure 3.27 shows the exponential decay of the evanescent field intensity along the waveguide surface. From this curve, it is possible to deduce the effective index n_{eff} of the guide using the following relation (λ is the working wavelength and I the evanescent field intensity) [Bor 2000, Cam 2002].

$$I(z) = I_0 \exp\left(-4\pi z\sqrt{n_{eff}^2 - 1}/\lambda\right) \qquad [3.56]$$

The curve analysis gives n_{eff} of 2.14. This value is in close agreement with the theoretical value of the extraordinary index of $LiTaO_3$ at $\lambda = 632.8$ nm ($n_{eo} = 2.19$).

3.4. Bibliography

[Aru 1986] Arutunyan E.A. and. Galoyan S.K, "New method for loss measurements in optical waveguides", *Optic. Com.*, 57(6), 391-393 (1986).

[Bor 2000] Borrisé X., Jiménez D., Barniol N., Pérez-Murano F., Aymerich X., "Scanning near field optical microscope for the characterization of optical integrated waveguides", *Journal of Lightwave Technology*, 18(3), 370-374 (2000).

[Bou 1992] Bourillot E., De Fornel F., Salomon L., Adam P., Goudonnet J. P., "Observations des structures guidantes en microscopie à effet tunnel photonique", *J. Optics*, 23(2), 57-62 (1992).

[Bou 1996] Boudrioua A., Réalisation de banc de mesure des coefficients electro-optiques de guides d'ondes planaires par lignes noires. Applications à un guide de $LiNbO_3$ implantés par des prootons, PhD Thesis, University of Metz (1996).

[Bou 1996a] Boudrioua A., Moretti P., Loulergue J.C. and Polgar K., "Waveguides in LTB ($Li_2B_4O_7$) by He+ implantation", *Phys. Stat. Sol. (a)*, 153, 553-557 (1996).

[Bou 1997] Boudrioua A. and Loulergue J.C., "New approach for losses measurements in optical waveguides", *Optics Communications*, 137, 37-40 (1997).

[Bou 2000] Boudrioua A., Moretti P., Loulergue J.C. and Polgar K., "Helium ion implanted planar waveguides in y-cut and z-cut β-BBO (BaB_2O_4)", *Optical Materials*, 14(1), 31-39 (2000).

[Bou 2001] Boudrioua A., Bakhouya C.H., Loulergue J.C., Moretti P.and Polgar K., "Low-loss optical planar waveguides in $Li_2B_4O_7$ (LTB) crystal formed by He^+-implantation", *J. Appl. Phys*., 89(12), 7716-7721 (2001).

[Brü 1995] Brüelisauer S., Fluck D.; Solcia C., Pliska T. and Günter P., "Non-destructive waveguide loss-measurement method using self-pumped phase conjugation for optimum end-fire coupling", *Optics Lett*., 20, 1773-1775 (1995).

[Cam 2002] Campillo A. L., Hsu J. W. P., White C. A., Jones C. D. W., "Direct measurement of the guided modes in $LiNbO_3$ waveguides", *Applied Physics Letters*, 80(13), 2239-2241 (2002).

[Che 1987] Chen B. and Findakly T., "Design and applications", in L.D. Hutcheson (Ed.) *Integrated Optical Circuits and Components*, John Wiley & Sons, New York, (1987).

[Chi 1985] Chiang K.S., "Construction of refractive-index profiles of planar waveguides", *J. Lightwave Tech*., LT-3, 385-391 (1985).

[Dak 1970] Dakss M.L., Kuhn L., Heidrich P.F. and Scott B.A., "Grating couplers for efficient excitation of optical guided waves in thin films", *Appl. Phys. Lett*., 16, 523-525 (1970).

[Den 1989] Dentan V., Lévy Y., Dumont M., Robin P. and Chastaing E., "Electrooptic properties of a ferroelectric polymer studied by attenuated total reflection", *Optics Com*., 69(5-6), 379-383 (1989).

[For 1998] De Fornel F., *Les ondes évanescentes en optique et en optoélectronique*, Eyrolles (1998).

[Goe 1969] Goell J.E., Standley R.D., "Sputtered glass waveguides for integrated optical circuits", *Bell Syst. Tech. J*., 48, 3445-3448 (1969).

[Hal 1980] Hall D.G., Spear-Zino J.D., Koenig H.G., Rice R.R., Powers J.K., Burkhart G.H. and Bear P.D., "Edge coupling of a GaAlAs DH laser diode to a planar Ti:$LiNbO_3$ waveguide", *Appl. Opt*., 19(11), 1847-1852 (1980).

[Hun 1985] Hunsperger R.G., *Integrated Optics Theory and Technologie*, 2nd Edition, Springer-Verlag (1985).

[Kad 1989] Kadad I., Réalisation et étude de guides d'ondes optiques plans en nitrure d'aluminium par pulvérisation magnétron réactive, PhD Thesis, University of St.-Etienne (1989).

[Ker 1973] Kersten R.T., "Numerical solution of the mode-equation of planar dielectric waveguides to determine their refractive index and thickness by means of a prism-film", *Optics Communications*, 9(4), 427-431 (1973).

[Ker 1975] Kersten R.T., "The prism-film coupler as a precision instrument, part 1: accuracy and capabilities of prisms as instruments", *Optica Acta*, 22(6), 503-513 (1975).

[Kip 1995] Kip D., Aulkemeyer S. and Moretti P., "Low-loss planar optical waveguides in strontium barium niobate crystals formed by ion-beam implantation", *Optic. Lett*., 20(11), 1256-1258 (1995).

[Kul 1992] Kulisch J.R., Franke H., Irmscher R. and Buchal C., "Opto-optical switching in ion-implanted poly(methyl methacrylate)-waveguides", *J. Appl. Phys*., 71(7), 3123-3126 (1992).

[Mar 1969] Marcuse D., "Mode conversion by surface imperfection of a dielectric slab waveguide", *Bell Syst. Tech. J*., 48, 3187-3216 (1969).

[Mat 1995] Mathey P., Jullien P. and Bolzinger J.L., "Refractive-index profile econstructions in planar waveguides by the WKB inverse method and reflectivity calculations", *J. Opt. Soc. Am. B*, 12, 1663-1669 (1995).

[Nai 1977] Naitoh H., Nuroshito M. and Nokayama T., "Mode control of Ti-diffused $LiNbO_3$ slab optical waveguide", *Appl. Optics*, 16, 2546-2549 (1977).

[Nis 1989] Nishihara H., Haruma M., and Suhara T., *Optical Integrated Circuits*, McGraw-Hill (1989).

[Oka 1983] Okamura Y., Yoshinaka S.and Yamamoto S., "Measuring mode propagation losses of integrated optical waveguides: a simple method", *Appl. Optics*, 22, 3892-3894 (1983).

[Oka 1985] Okamura Y., Sato S. and Yamamoto S., "Simple method of measuring propagation properties of integrated optical waveguides: an improvement", *Appl. Optics*, 24, 57-60 (1985).

[Per 1988] Persegol D., Réalisation d'un modulateur electro-optique utilisant l'excitation réonnante des modes guides, PhD Thesis, Grenoble Institute of Technology (1988).

[Pet 1977] Petit R., Cadilhac M., "Electromagnetic theory of prism coupler", *J. Optics* 8, 41-49 (1977).

[Pet 1980] Petit R., *Electromagnetic Theory of Gratings*, Springer-Verlag (1980).

[Roe 2004] Roemer A., Millon E., Vincent B., Boudrioua A., Pons-Y-Moll O., Defourneau R.M. and Seiler W., "Epitaxial $PbTiO_3$ thin films grown on (100) MgO by pulsed-laser deposition for optical waveguiding properties", *J. Appl. Phys*., 95, 3041-3047 (2004).

[Ros 1995] Rosso C., Elaboration et caractérisation de l'iodate de lithium ($LiIO_3$) pour l'optique guidée, PhD Thesis, University of Savoie (1995).

[Str 1991] Strohkendl F.P., Fluck D., Günter P., Irmsher R. and Buchal C.H., "Nonleaky optical waveguides in $KNbO_3$ by ultralow dose MeV He ion implantation", *Appl. Phys. Lett.*, 59(26), 3354-3356 (1991).

[Tas 2002] Tascu S., Moretti P., Kostriski S., Martin M. et Jacquier B., "Caractérisation par microscopie en champ proche optique de guides d'onde optique de $LiNbO_3$ et $LiTaO_3$", *Conférence JNOG 2002*, Dijon (2002).

[Tie 1969] Tien P.K., R. Ulrich, and R.J. Martin, "Modes of propagating. light waves in thin deposited semiconductor films", *Appl. Phys. Lett*., 14, 291-294 (1969).

[Tie 1970] Tien P.K. and Ulrich R., "Theory of the prism coupler and thin film light guides", *J. Opt. Soc. of America*, 60(10), 1325-1337 (1970).

[Tie 1971] Tien P.K. and Martin R.J., "Experiments in light waves in a thin, tapered film and a new light wave coupler", *Appl. Phys. Lett*., 18, 398-401 (1971).

[Tie 1971a] Tien P.K., "Light waves in thin films and integrated optics", *Appl. Opt*., 10, 2395-2398 (1971).

[Tie 1971b] Tien P.K., "Light waves in thin films and integrated optics", *Appl. Opt*., 10, 2395-2413 (1971).

[Tie 1972] Tien P.K., Smolinsky G., and Martin R.J., "Thin organosilicon films for integrated optics", *Appl. Opt*., 11, 637-642 (1972).

[Tie 1974] Tien P.K., Riva-Sanseverino S., Martin R.J., Ballman A.A. and Brown H., "Optical waveguide modes in single crystalline $LiNbO_3$-$LiTaO_3$ solid solution films", *Appl. Phys. Lett*., 24(10), 503-505 (1974).

[Tie 1977] Tien P.K., "Integrated optics and new wave phenomena in optical waveguides", *Rev. Mod. Phys*., 49(2), 361-420 (1977).

[Ulr 1970] Ulrich R., "Theory of the prism film coupler by plane wave analysis", *J. Opt. Soc. Amer*., 60(10), 1325-1336 (1970).

[Ulr 1973] Ulrich R. and Torge R., "Measurement of thin film parameters with a prism coupler", *Applied Optics*, 12, 2901-2908 (1973).

[Vin 2004] Vincent B., Boudrioua A., Tascu S., Moretti P. and Aka G., "Optical planar waveguides in the new non linear crystal $Ca_4YO(BO_3)_3$ (YCOB) fabricated by He+ implantation", *Applied Optics*, 43(2), 491-496 (2004).

[Wan 1996] Wang G. Y. and Garmire E., "Efficient coupling into tapered proton-exchanged $LiNbO_3$ waveguides fabricated by vertically controlled immersion", *Opt. Lett*., 21, 42-45 (1996).

[Web 1973] Weber H.P., Dunn F.A. and Leibolt W.N., "Loss measurement in thin film optical waveguides", *Appl. Optics*, 12, 755-758 (1973).

[Whi 1976] White J.M. and Heidrich F.P., "Optical waveguide refractive index profiles determined from measurement of mode indices: a simple analysis", *Appl. Optics*, 15(1), 151-155 (1976).

[Won 1980] Won Y.H., Janssand P.C. and Chartier G.H., "Three-prism loss measurements of optical waveguides", *Appl. Phys. Lett*., 37(3), 269-271 (1980).

[Zha 1988] Zhang G.and Sasaki K., "Measuring anisotropic refractive indices and film thicknesses of thin organic crystals using the prism coupling method", *Appl. Opt*., 27(7), 1358-1361 (1988).

This page intentionally left blank

Chapter 4

Non-linear Effects in Integrated Optics

In physics, it is often a question of studying the relation between a cause and the effects in a given system: such as, for example, the propagation of an electromagnetic wave (cause) in a dielectric medium (place of the produced effects). A phenomenon is described as linear if the effects are proportional to the cause. In the contrary case, the effects are not proportional to the cause, and it is then a non-linear phenomenon, which we will consider in this chapter.

The interaction of an electric field $\vec{E}$ with an optical medium is currently the subject of many publications and books already available [ARM 1962, Blo 1962, Cou 2002, Gün 2000, Lau 1990, Nis 1989, San 1999, Sal 1991, Yar 1984]. This interaction is controlled by the material polarization $\vec{P}$ which represents the density of electric dipole momentums per unit of volume, and indicates the displacement of charges bound to the medium under the influence of the electric field.

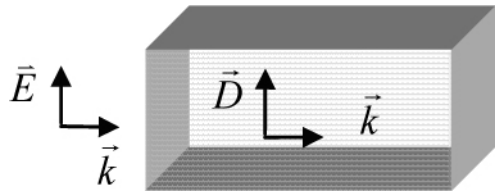

Figure 4.1. *Electromagnetic wave propagation in a dielectric medium*

4.1. General considerations

Generally speaking, the electric displacement vector is written as:

$$\vec{D} = \varepsilon\vec{E} = \varepsilon_0\vec{E} + \vec{P} \qquad [4.1]$$

where $\vec{P}$ is the material polarization, given by:

$$\vec{P} = \varepsilon_0\chi\vec{E} \qquad [4.2]$$

$\varepsilon = \varepsilon_0\varepsilon_r = \varepsilon_0(1+\chi)$, ε_0 is the vacuum dielectric permittivity (8.8542×10^{-12}), and ε_r is the relative dielectric permittivity and χ is the medium dielectric susceptibility.

The electric dipoles oscillating at the frequency of the electromagnetic wave will radiate a field of the same frequency in the medium, and thus will modify the propagation of the optical wave. However, when this field is sufficiently intense around the interatomic field, the medium response (thus the polarization) is a non-linear function of the excitation. The total polarization of the medium can then be written in the form of a Taylor series:

$$\vec{P} = \vec{P}_0 + \varepsilon_0\chi^{(1)}\vec{E} + \varepsilon_0\chi^{(2)}\vec{E}\vec{E} + \varepsilon_0\chi^{(3)}\vec{E}\vec{E}\vec{E} + \ldots.. \qquad [4.3]$$

$\vec{P}_0$ is the spontaneous polarization of the medium (it exists in certain materials), and $\varepsilon_0\chi^{(1)}\vec{E}$ represents the linear polarization of the material.

By considering:

$$\vec{P}^{nl} = \varepsilon_0\chi^{(2)}\vec{E}\vec{E} + \varepsilon_0\chi^{(3)}\vec{E}\vec{E}\vec{E} + \ldots.. \qquad [4.4]$$

this term is the non-linear polarization. $\chi^{(n)}$ are the macroscopic susceptibilities of the medium, also called the non-linear susceptibilities of the order (n). They are given by tensors of rank (n+1). The non-linear polarization [4.4] includes tensorial terms given as [Yar 1984, San 1999]:

$$P_i^{nl} = \varepsilon_0 \sum_{j,k} \chi_{ijk}^{(2)} E_j(\omega_1) E_k(\omega_2) + \varepsilon_0 \sum_{j,k,l} \chi_{ijkl}^{(3)} E_j(\omega_1) E_k(\omega_2) E_l(\omega_3) + \ldots \qquad [4.5]$$

with:

$$1 \le i, j, k \le 3$$

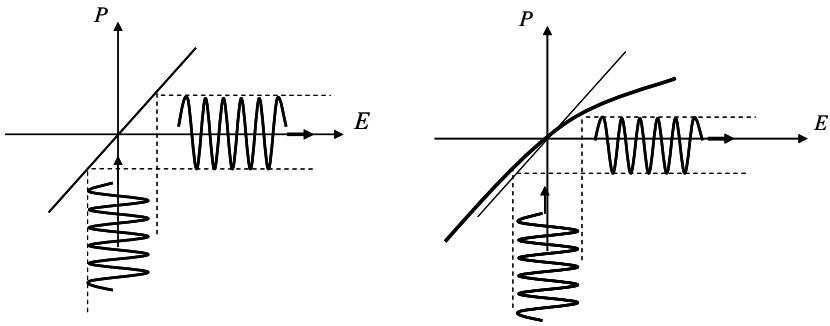

Figure 4.2. *Schematic evolution of the polarization versus the electric field of the optical field: (a) linear medium, (b) non-linear medium*

In the continuation of this chapter, we will be interested more particularly in the non-linear effects of second order which find applications in the generation of laser beams starting from a pump beam. Generally, the term quadratic non-linear optics more particularly refers to the phenomena related to the interaction of two electric fields of pulsations ω_1 and ω_2 with a non-linear material.

In these conditions, the non-linear polarization is:

$$\vec{p}^{\,nl} = \varepsilon_0 \chi^{(2)} \left[\vec{E}_1 \cos\left(\vec{k}_1 \vec{r} - \omega_1 t\right) + \vec{E}_2 \cos\left(\vec{k}_2 \vec{r} - \omega_2 t\right) \right]^2 \qquad [4.6]$$

$$\begin{aligned} \vec{p}^{\,nl} = {} & \varepsilon_0 \chi^{(2)} \vec{E}_1^2 \cos^2\left(\vec{k}_1 \vec{r} - \omega_1 t\right) + \varepsilon_0 \chi^{(2)} \vec{E}_2^2 \cos^2\left(\vec{k}_2 \vec{r} - \omega_2 t\right) \\ & + 2\varepsilon_0 \chi^{(2)} \vec{E}_1 \vec{E}_2 \cos\left(\vec{k}_1 \vec{r} - \omega_1 t\right) \cos\left(\vec{k}_2 \vec{r} - \omega_2 t\right) \end{aligned} \qquad [4.7]$$

also:

$$\begin{aligned} \vec{p}^{\,nl} = {} & \frac{1}{2} \varepsilon_0 \chi^{(2)} \vec{E}_1^2 \left[1 + \cos\left(2\vec{k}_1 \vec{r} - 2\omega_1 t\right) \right] + \frac{1}{2} \varepsilon_0 \chi^{(2)} \vec{E}_2^2 \left[1 + \cos\left(2\vec{k}_2 \vec{r} - 2\omega_2 t\right) \right] \\ & + \varepsilon_0 \chi^{(2)} \vec{E}_1 \vec{E}_2 \left[\cos\left(\left(\vec{k}_1 - \vec{k}_2\right) \vec{r} - \left(\omega_1 - \omega_2\right) t \right) + \cos\left(\left(\vec{k}_1 + \vec{k}_2\right) \vec{r} - \left(\omega_1 + \omega_2\right) t \right) \right] \end{aligned}$$

[4.8]

This induced polarization has components which oscillate at multiple frequencies which are actually only combinations of frequencies (sums, differences) of the incident waves. It thus acts like a source of new oscillating electric fields at new frequencies.

The principal quadratic non-linear phenomena are [San 1999]: optical correction, the generation of second harmonic, parametric amplification and the Pockels effect:

– Optical correction: non-linear polarization has a component of zero pulsation which induces a static electric field in the material. A permanent polarization then appears in the medium, which is due to the accumulation of the electric charges on the faces of the material perpendicular to the polarization of the incident wave (pump). This results in a potential difference which can be measured in experiments.

– The second harmonic generation: non-linear polarization has a double component of pulsation ($\omega+\omega = 2\omega$) which generates a double frequency wave. This is also true if we take $\omega 1 = \omega_2 = \omega$.

– Parametric amplification: a signal of low intensity, of pulsation ω ω_1, is coupled with a very intense beam (pump beam) of pulsation $\omega 3$ ($\omega_1 + \omega_2 = \omega_3$) called the idler. This wave is coupled then with the pump beam to amplify the signal of frequency $\omega_1 = \omega_2 - \omega_3$.

– The Pockels effect: if $\omega_1=\omega >> \omega_2$, the application of an electric field of weak pulsation (static field) compared to the pulsation of the other electric field (optical field) modifies the properties of the material and in particular its refractive indices (linear electro-optic effect), which makes it possible to change the phase, the amplitude or the trajectory of a light wave which crosses it. This phenomenon will be covered in the following chapter.

As a matter of fact, the second order non-linear susceptibility (or quadratic susceptibility) is at the foundation of quadratic optics. It should be mentioned that only non-centrosymmetric materials have a non-zero quadratic susceptibility ($\chi(2) \neq 0$) and are thus likely to present quadratic effects.

In what follows, we particularly focus on the study of second harmonic generation. Initially we will make a general presentation of frequency doubling phenomenon in bulk materials, before concentrating on the realization of this phenomenon in the optical waveguides.

4.2. Second harmonic generation

Quadratic non-linear polarization can be written as:

$$p_i^{nl} = \varepsilon_0 \sum_{j,k} \chi_{ijk}^{(2)} E_j(\omega_1) E_k(\omega_2) \qquad [4.9]$$

with: $1 \le i, j, k \le 3$.

If we want to simplify the expression of the induced polarization, it is more convenient to avoid the use of the tensorial nature of susceptibility. For that we notice that in the case of the second harmonic generation (SHG) the permutation of the indices *k* and *l* does not change anything about the induced polarization. We can thus simplify the expression by using the contracted notation in the form of a 3x6 matrix.

$$d_{il}(-2\omega;\omega,\omega) = \frac{1}{2}\chi_{ijk}^{(2)}(-2\omega;\omega,\omega) \qquad [4.10]$$

Table 4.1 gives the correspondence between the indices (*l* is the couple (j, k)) [4].

l	1	2	3	4	5	6
j, k	xx	yy	zz	zy	zx	xy
	xx	yy	zz	yz	xz	yx

Table 4.1. *Non-linear tensor contracted notations*

By using this contracted notation we can thus write the components of quadratic non-linear polarization in the form of matrix product:

$$\begin{vmatrix} P_x^{(2)}(2\omega) \\ P_y^{(2)}(2\omega) \\ P_z^{(2)}(2\omega) \end{vmatrix} = \begin{bmatrix} d_{11} & d_{12} & d_{13} & d_{14} & d_{15} & d_{16} \\ d_{21} & d_{22} & d_{23} & d_{24} & d_{25} & d_{26} \\ d_{31} & d_{32} & d_{33} & d_{34} & d_{35} & d_{36} \end{bmatrix} \cdot \begin{vmatrix} (E_x(\omega))^2 \\ (E_y(\omega))^2 \\ (E_z(\omega))^2 \\ 2(E_y(\omega))(E_z(\omega)) \\ 2(E_z(\omega))(E_x(\omega)) \\ 2(E_x(\omega))(E_y(\omega)) \end{vmatrix} \quad [4.11]$$

However, the coefficients d_{il} of equation [4.11] are not all independent. Indeed, according to the permutation relations of Kleinman [Kle 1962] and according to the group of symmetry of the crystal, we can reduce the number of independent coefficients the matrix by choosing the system of axis suitably.

A description of these energy transfers can be deduced starting from the Maxwell's equations [ARM 1962, Blo 1962].

If the medium considered is insulating (density of current is zero: $\vec{J} = \vec{0}$), non-magnetic ($\mu = \mu_0$) and if it does not have free charges ($\vec{\nabla} \cdot \vec{D}_{2\omega} = 0$) the Maxwell's equations are written:

$$\begin{cases} \vec{\nabla}\vec{D} & 0 \\ \vec{\nabla}\vec{H} & 0 \\ \vec{\nabla} \wedge \vec{E} & \mu_0 \dfrac{\partial \vec{H}}{\partial t} \\ \vec{\nabla} \wedge \vec{H} & \dfrac{\partial \vec{D}}{\partial t} \end{cases} \quad [4.12]$$

where $\vec{E}$ and $\vec{H}$ are respectively the electric and magnetic fields, and $\vec{D}$ is the electric displacement field given by:

$$\vec{D} = \varepsilon_0 \varepsilon_r \vec{E} + \vec{P}^{nl} \quad [4.13]$$

($\vec{P}^{nl}$ the induced non-linear polarization, ε_0, vacuum permittivity and ε_r non-linear medium relative dielectric permittivity) for these conditions the wave equation can be written:

$$\Delta\vec{E} \quad -\frac{\varepsilon_r}{c^2}\frac{\partial^2\vec{E}}{\partial t^2} = \frac{1}{\varepsilon_0 c^2}\frac{\partial^2\vec{P}^{nl}}{\partial t^2} \qquad [4.14]$$

This equation characterizes the propagation of an electromagnetic wave in a non-linear medium. Its solution makes it possible to calculate the expressions of the electric fields of the harmonic waves generated by the fundamental wave and consequently the power of these waves.

4.2.1. *Second harmonic generation in the volume*

To solve the equation of propagation [4.14], it is more convenient to use complex notations of fields and non-linear polarization. Indeed, an optical field can be given by:

$$\vec{E} = \mathrm{Re}\left\{\vec{E}e^{i\left(\omega t \quad \vec{k}\vec{r}\right)}\right\} = \frac{1}{2}\left(\vec{E}e^{i\left(\omega t \quad \vec{k}\vec{r}\right)} + \vec{E}^{*}e^{\quad i\left(\omega t \quad \vec{k}\vec{r}\right)}\right) = \frac{1}{2}\left(\vec{E}e^{i\left(\omega t \quad \vec{k}\vec{r}\right)} + c.c.\right) \qquad [4.15]$$

For simplicity, we consider the case of a field resulting from three plane waves propagating according to oz axis [Yar 1984] with pulsations ω_1, ω_2 and ω_3:

$$\begin{aligned}
\vec{E}^{\omega_1} &= \frac{1}{2}\left(\vec{E}_1 e^{i(\omega_1 t \quad k_1 z)} + c.c.\right)\\
\vec{E}^{\omega_2} &= \frac{1}{2}\left(\vec{E}_2 e^{i(\omega_2 t _ k_2 z)} + c.c.\right)\\
\vec{E}^{\omega 3} &= \frac{1}{2}\left(\vec{E}_3 e^{i(\omega_3 t \quad k_3 z)} + c.c.\right)
\end{aligned} \qquad [4.16]$$

The quadratic non-linear polarization is:

$$\vec{p}^{\,nl} = \varepsilon_0 \chi^{(2)}\left[\vec{E}^{\omega_1} + \vec{E}^{\omega_1} + \vec{E}^{\omega_3}\right]^2 \qquad [4.17]$$

This relation contains the following term:

$$\vec{p}^{\,nl} = \varepsilon_0 \chi^{(2)}\left[\vec{E}_1\vec{E}_2 e^{i[(\omega_1+\omega_2)t \quad (k_1+k_2)z]}\right] \qquad [4.18]$$

Where $\omega_3 = \omega_1 + \omega_2$, this term constitutes a source for the wave ω_3. This also applies for the three pulsations considered. In this case, for the wave of pulsation ω_1, equation [4.14] becomes:

$$\Delta\vec{E}^{\omega_1} - \frac{\varepsilon_r}{c^2}\frac{\partial^2 \vec{E}^{\omega_1}}{\partial t^2} = \frac{\chi^{(2)}}{2c^2}\frac{\partial^2}{\partial t^2}\left[E_3 E_2^* e^{i[(\omega_3 \quad \omega_2)t \quad (k_3 \quad k_2)z]} + c.c.\right] \qquad [4.19]$$

In addition, from the expression of $\vec{E}^{\omega_1}$, we can write:

$$\begin{aligned}\Delta\vec{E}^{\omega_1} &= \frac{1}{2}\frac{\partial^2}{\partial z^2}\left(\vec{E}_1 e^{i(\omega_1 t \quad k_1 z)} + c.c.\right) \\ &= -\frac{1}{2}\left[k_1^2 E_1 + 2ik_1\frac{dE_1}{dz}\right]e^{i(\omega_1 t \quad k_1 z)} + c.c\end{aligned} \qquad [4.20]$$

In the previous relation, the term $\frac{d^2 E_1}{dz^2}$ has been neglected.

In these conditions, the non-linear propagation equation becomes (by taking $\frac{\partial}{\partial t} = i\omega$):

$$\begin{aligned}&-\frac{1}{2}\left[k_1^2 E_1 + 2ik_1\frac{dE_1}{dz}\right]e^{i(\omega_1 t \quad k_1 z)} + c.c \\ &= -\frac{\omega_1^2 \varepsilon_{r1}}{c^2}e^{i(\omega_1 t \quad k_1 z)} + c.c - \frac{\omega_1^2 \chi^{(2)}}{2c^2}E_3 E_2^* e^{i[(\omega_1 t \quad (k_3 \quad k_2)z)]} + c.c\end{aligned} \qquad [4.21]$$

By multiplying this equation by $\frac{i}{k_1}e^{\ i(\omega_1 t \quad k_{1z})}$, we obtain:

$$\frac{dE_1}{dz} = -\frac{i\omega_1}{2}\sqrt{\frac{\mu_0 \varepsilon_o}{\varepsilon_{1r}}}\chi^{(2)} E_3 E_2^* e^{\ i(k_3 \quad k_2 \quad k_1)z} \qquad [4.22]$$

It should be noted that similar expressions can be obtained for the two remaining fields. The generation of the second harmonic appears as a particular case for which two of the waves considered have the same pulsation ω. If we consider $\omega=\omega_1=\omega_2$, then, if we neglect the depletion of the fundamental wave, the electric field of the harmonic wave has as an expression [Lau 1990, Sal 1991]:

$$\frac{d\vec{E}_{SH}}{dz} = -i\omega_F \sqrt{\frac{\mu_0 \varepsilon_o}{\varepsilon_r^{2\omega}}} d_{eff} \vec{E}_F \vec{E}_F e^{i(k_{SH} \quad 2k_F)z} \qquad [4.23]$$

where $\varepsilon_r^{2\omega}$ is the relative permittivity of the non-linear medium at the harmonic frequency, E_F is the electric field of the fundamental wave and d_{eff} is the non-linear coefficient of the medium.

Let us consider:

$$\Delta k = k_{SH} - 2k_F \qquad [4.24]$$

Δk representing the phase mismatch between the fundamental and harmonic waves. By integrating equation [4.23] over a length of interaction L, inside the non-linear medium with an initial condition $E_{SH}(0) = 0$, we obtain the expression of the electric field of the harmonic wave:

$$\vec{E}_{SH}(L) = -i\omega_F \sqrt{\frac{\mu_0 \varepsilon_0}{\varepsilon_r}} d_{eff} E_F^2 \frac{e^{i\Delta kL} - 1}{i\Delta k} \qquad [4.25]$$

The intensity of the harmonic wave is given by the Poynting vector:

$$I_{SH} = \frac{P_{SH}}{A} = \frac{1}{2} \sqrt{\frac{\varepsilon_0 \varepsilon_r}{\mu_0}} \left| \vec{E}_{SH} \right|^2 \qquad [4.26]$$

I_{SH} and P_{SH} are respectively the intensity and the power of the harmonic beam and A the interaction surface between the fundamental wave and the non-linear medium. We could imagine that a low value of A and thus a strong focusing of the pump beam could increase the intensity of the harmonic wave considerably. That is not completely exact because a strong focusing causes a strong divergence of the beam as soon as we move away from the focal point which, in turn, creates a decrease of the pump power. In practice, the optimal surface section of the beam is considered about λ0L [San 1999, Cou 2002] (λ0: wavelength of the beam pumps in the vacuum).

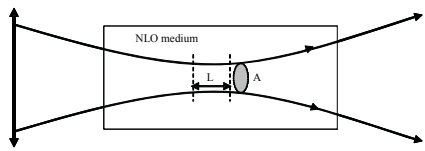

Figure 4.3. *Beam interaction with non-linear medium: compromise between the beam waist and the interaction length*

Finally, by replacing relation [4.25] with relation [4.26], we obtain:

$$I_{SH} = \frac{P_{SH}}{A} = 8\frac{\mu_0^{\frac{3}{2}}\sqrt{\varepsilon_0}\omega_F^2}{\varepsilon_F\sqrt{\varepsilon_{SH}}} d_{eff}^2 L^2 \frac{P_F^2}{A^2} \frac{\sin^2\left(\frac{1}{2}\Delta kL\right)}{\left(\frac{1}{2}\Delta kL\right)^2} \quad [4.27]$$

The conversion efficiency can therefore be given as:

$$\eta = \frac{P_{SH}}{P_F} = \left[\frac{2\omega_F^2}{n_F^2 n_{SH} c^3 \varepsilon_0}\right]\left(d_{eff}^2 L^2\right)\frac{P_F}{A} \frac{\sin^2\left(\frac{1}{2}\Delta kL\right)}{\left(\frac{1}{2}\Delta kL\right)^2} \quad [4.28]$$

with: $c = \frac{1}{\sqrt{\mu_0\varepsilon_0}}$ and $n = \sqrt{\varepsilon_r\mu_r}$.

Note that the conversion efficiency depends on the non-linear medium features (indices, length of propagation), on the coefficient deff and especially on phase mismatch Δk.

4.2.1.1. *Birefringence phase matching*

Any technique employing the process of frequency conversions must solve a main issue: the realization of phase matching between the pump beam (the input beam) and the harmonic beam (the output beam), to eliminate any destructive interference [Blo 1965, Lau 1990, Sal 1991]. Harmonic power and thus the conversion efficiency are maximum when the phase matching is carried out, i.e.:

$$\Delta k = k_{SH} - 2k_F = 0 \quad [4.29]$$

Under these conditions the cardinal sine of expression [4.20] is equal to 1. In all the other cases, this term has a lower value and consequently the harmonic power is of less importance. We define a working length of the non-linear medium necessary to create a harmonic wave. This length *l*c is called the coherence length (see Figure 4.4). It is deduced from the argument of the cardinal sine function when this function is equal to the unit:

$$l_c = \frac{2\pi}{\Delta k} = \frac{\lambda}{4\left(n_{2\omega} - n_{\omega}\right)} \qquad [4.30]$$

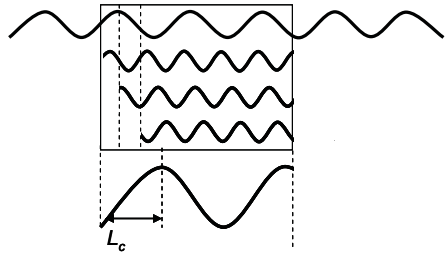

Figure 4.4. *Illustration of the coherence length effect on SHG*

In practice, the phase matching condition is difficult to create in crystals [Ito 1975, Eck 1990]. The primary reason of this difficulty is related to the dispersion of the materials, which generally does not have the same refractive indices for the two wavelengths. The most frequently employed method for achieving phase matching, uses natural birefringence existing in the uniaxial or biaxal crystals to compensate for the difference of refractive indices due to dispersion. This method consists of finding directions of propagation inside the crystal, such as the ordinary index at a given frequency which is equal to the extraordinary index corresponding to the other frequency. This strongly limits the harmonic wavelengths obtained.

Let us consider for example a negative, dispersive uniaxial medium in an area of weak absorption, so that the ordinary n_o and extraordinary n_e indices of the crystal increase when the wavelength λ of light radiation decreases. It is thus not possible to reach the phase matching between two waves of the same polarization and of different wavelength. The most direct approach to reach the phase matching is to use two waves of different polarizations to obtain the phase matching by birefringence.

The ellipsoid of the indices gives the value of the index of the extraordinary wave according to the angle of propagation θ:

$$\frac{1}{n_e^2(\theta)} = \frac{\cos^2\theta}{n_0^2} + \frac{\sin^2\theta}{n_e^2} \qquad [4.31]$$

If $n_e^{2\omega} < n_o^{\omega}$ is satisfied for a given value of λ, we can therefore find an angle θ for which:

$$n_e^{2\omega}(\theta_m) = n_0^{\omega} \qquad [4.32]$$

As an example, in Figure 4.5 the refraction indices of lithium niobate with 20°C are plotted according to the wavelength. We see in Figure 4.5b that the intersection of the two curves indicates a possible phase matching at 1,077 nm if the fundamental wave is polarized according to the ordinary index (in the xy plane) and the harmonic wave according to the extraordinary index (according to axis z).

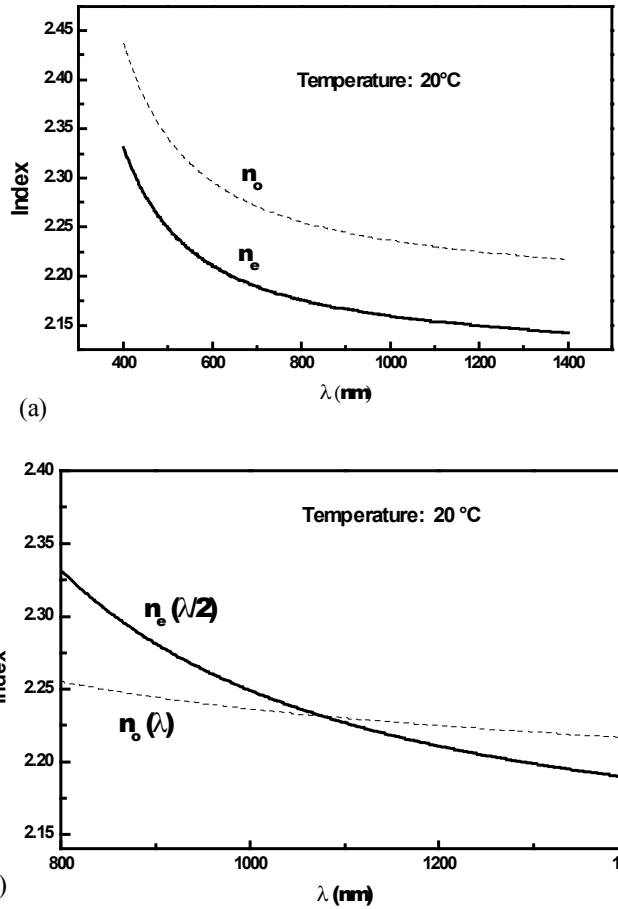

Figure 4.5. *Illustration of the birefringence phase matching in the case of $LiNbO_3$*

Phase matching can be carried out in various ways: by varying the wavelength of the fundamental wave or by varying the temperature of the crystal. The main advantage of the birefringence phase matching is that it uses the intrinsic properties

of the crystal, and does not require any additional technological process after the crystal growth (a part from its cut).

The principal disadvantages of this technique come from the impossibility of carrying out the SGH with any wavelength in particular to short λ (in blue for example) because of a too low birefringence. This is the case of the lithium niobate ($LiNbO_3$) (see Figure 4.5b). Also, the useful non-linear coefficient is always the diagonal element of the tensor which is seldom most important, in the case of $LiNbO_3$. The coefficient d_{31} used in the example above is approximately 5 pm/V, while the highest coefficient of $LiNbO_3$ is the d_{33} of 30 pm/V.

4.2.2. *Quasi-phase matching (QPM)*

This technique has enabled, over these last years, new laser sources based on frequency conversions of low power lasers to become available on the market [Web 1993, Lau 1999]. In this configuration, we reach quasi-phase matching between the fundamental and the harmonic waves by a periodic variation of the polarization of the material [Mye 1995, Pru 1996].

Armstrong *et al.* [ARM 1962] proposed for the first time in 1962 a technique known as quasi-phase matching, to compensate for phase mismatch introduced by chromatic dispersion. This technique consists of modulating the non-linear coefficient of the material in a periodic way, forcing the fundamental and harmonic waves to remain in phase.

Fejer *et al.* [Fej 1992] reported an approach of the quasi-phase matching phenomenon based on the treatment of the coupled-equations by means of Fourier Transforms. The work of the Fejer group allows us to understand how the inversion of the material polarization compensates for the phase mismatch.

Let us consider now a fundamental wave which is propagated according to the ox direction, and which gives rise to a harmonic wave of double pulsation. We also assume a non depletion of the pump and a weak variation of the amplitude at a distance similar to the wavelength. Assuming that we change the sign of the non-linear coefficient along the axis of the crystal (see Figure 4.6), for each change of sign, phase mismatch between the fundamental wave and the harmonic wave are increment of π. Thus, if we choose the period Λ of twice the coherence length, the sign change of the non-linear coefficient will make it possible to compensate for the phase mismatch of each interface. We can thus write:

$$2k_{\omega} - k_{2\omega} - m\frac{2\pi}{\Lambda} = 0 \qquad [4.33]$$

m: an integer, which gives the QPM order.

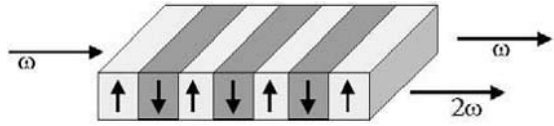

Figure 4.6. *Frequency doubling by QPM*

In the continuation of this part, we will show the main steps of calculation which make it possible to understand this mechanism of artificial phase matching. The reader can find an abundance of literature on this subject, both articles of scientific journals and specialized books.

In the case of QPM, the non-linear coefficient d_{eff} is no longer a constant, and is modulated along the propagation direction. This is given as:

$$d(x) = g(x)d_{eff} \qquad [4.34]$$

where $g(x)$ is the modulation function ($-1<g(x)<1$) along the *ox axis*.

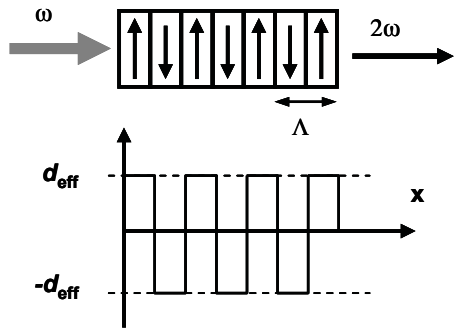

Figure 4.7. *Modulation of the non-linear coefficient*

Thus, the integration of relation [4.15] gives:

$$E_{SH}(L) = \Gamma \int_0^L d(x) e^{\ i\Delta kx} dx \qquad [4.35]$$

where $\Gamma = -i\omega_F \sqrt{\frac{\mu_0 \varepsilon_0}{\varepsilon_r}} E_F^2$.

Note that for phase matching, if $d(x)=d_{\text{eff}}$ and $\Delta k=0$, then the integration equation [4.35] can be easily obtained as:

$$E_{SH}(L) = \Gamma d_{eff} L \qquad [4.36]$$

To return to the case of QPM, by replacing equation [4.26] with equation [4.27], we obtain:

$$E_{SH} = \Gamma d_{eff} L G(\Delta k) \qquad [4.37]$$

$$\text{with } G(\Delta k) = \frac{1}{L} \int_0^L g(x) e^{\ i\Delta kx} dx \qquad [4.38]$$

We can see by comparing equations [4.37] and [4.36] that the G(Δk) is a factor of reduction of the second harmonic amplitude compared to the ideal phase matching.

If $g(x)$ is a periodic function of Λ, then it can be written as:

$$g(x) = \sum_{m=\ -\infty}^{\infty} G_m . e^{iK_m x} \qquad [4.39]$$

where $K_m = \frac{2\pi\ m}{\Lambda}$ is the QPM grating period, and m is an integer giving the QPM order.

It is understood that for a certain value of m, K_{m} is close or equal to Δk and the integral of equation [4.38] is dominated by this term (all others being affected by an exponentially decreasing term). Equation [4.27] can then be written:

$$E_{SH} \approx ie^{\ \frac{\Delta k' L}{2}} \Gamma d_Q L \sin c\left(\frac{\Delta k L}{2}\right) \qquad [4.40]$$

where $d_Q = d_{eff} G_m$ is the amplitude of the m^{th} harmonic of d(x) and $\Delta k' = k_{sh} - 2k_F - K_m$.

It is thus noted that two things differentiate the QPM process from perfect phase matching: first of all phase mismatch includes an additional term K_m, introduced by the periodic modulation of the non-linear coefficient and then the effective non-linear coefficient is reduced by a factor of G_m.

Generally speaking, the modulation of the non-linear coefficient consists of a periodic inversion of its sign. In this case the function $G(x)$ is a rectangular function of value ± 1 (see Figure 4.7).

With the positive sections of length l, the duty cycle is defined as the ratio:

$$\alpha = \frac{l}{\Lambda} \qquad [4.41]$$

By considering that the m^{th} term of the Fourier series fulfills the phase matching condition, i.e. $K_m=\Delta k$, therefore the Fourier coefficient can be written as:

$$G_m = \frac{2}{m\pi}\sin(m\pi\alpha) \qquad [4.42]$$

Note that from equation [4.42], for an optimal duty cycle, i.e. the sin function is equal to unit ($m\pi\alpha=\pi/2[2\pi]$ with $0<\alpha<1$), we obtain a non-linear coefficient d_Q as:

$$d_Q = \frac{2d_{eff}}{m\pi} \qquad [4.43]$$

Nevertheless, from equation [4.19] the second harmonic intensity is proportional to d_{eff}^2. Thus, for the QPM case, the conversion efficiency is reduced by a factor of $(2/m\pi)^2$. For instance, Table 4.2 summarizes duty cycles corresponding to first order QPM and the reduction ratio of the conversion efficiency (η_{QAP}/η_{APB}) compared to birefringence phase matching based on the same non-linear coefficient.

QPM order (m)	η_{QAP}/η_{APB}	Duty cycle (α)%
1	$(2/\pi)^2$	50
2	$1/4(2/\pi)^2$	25/75
3	$1/9(2/\pi)^2$	17/50/83
4	$1/16(2/\pi)^2$	12/38/62/88

Table 4.2. *Comparison of QPM and BPM*

In the case of m=2 and for all the even m, a duty cycle of 50% cannot compensate for the phase mismatch. Indeed, in this case at the end of a distance *ml*c, all the energy of the second harmonic is reconverted into fundamental energy. It is clear according to the table above that the benefit of QPM over BPM is its use of a more significant non-linear coefficient. In BPM the waves which interact have different polarizations and the non-linear coefficients are those which are not diagonal; whereas in QPM the coefficients used can be diagonal because the waves can have the same polarization, but the diagonal coefficients are generally highest (in $LiNbO_3$, d_{31}~5 pm/V whereas the d_{33}~30 pm/V).

By taking into account the factor $(2/\pi)2$, we can increase the output conversion efficiency while passing from the BPM to the QPM. Under these conditions, the interaction between the harmonic waves generated over the coherence length is constructive. It should be noted that the first order QPM which consists of reversing polarization with each length of coherence, is most effective, and approaches the conditions of perfect phase matching.

The applications of the QPM strongly depend on the period Λ of the periodically polarized structure (PP). We can distinguish three categories of possible applications, as given in Table 4.3.

Period Λ	Applications
Λ< 15 μm	SHG, SFG of IR lasers OPO pumped by visible lasers
15 μm < Λ < 25 μm	DFG of IR lasers SHG of telecom lasers
Λ> 25 μm	OPO pumped by IR lasers

Table 4.3. *Applications of QPM as a function of the PPLN grating period*

If the sign of the non-linear coefficient is changed for half of the coherence lengths, and when the duty cycle is 50%, the conversion efficiency can be written as [Con 1973, Fej 1992, Mag 1990, Yar 1973]:

$$\eta = \frac{P_{SH}}{P_F} = \left[\frac{2\omega_F^2}{n_F^2 n_{SH} c^3 \varepsilon_0}\right]\left(\frac{2d_{eff}L^2}{\pi m}\right)^2 \frac{P_F}{A} \qquad [4.44]$$

The maximum of conversion efficiency is obtained for the first order (m = 1).

Finally, in periodically polarized crystals, phase matching is not dependent on the inherent characteristics of the material: on the contrary, it makes it possible to eliminate the problems involved in the conventional phase matching techniques such as the "walkoff" and the angular tolerance.

However, the fabrication of these periodically polarized structures requires the utilization of delicate technological processes. The following section will be devoted to the basic principles of these experimental techniques of polarization inversion in $LiNbO_3$, the most used crystal in this case.

4.2.3. *Fabrication of periodically poled structures*

4.2.3.1. *General considerations*

In order to illustrate the polarization reversal concept, let us take the case of $LiNbO_3$ (see Figure 4.8). The structure of niobate of lithium belongs to the group of R3c space. Its structure depends on both its composition and the temperature. For temperatures lower than its Curie temperature (1120°), $LiNbO_3$ consists of a stacking of planes made up of 3 oxygen atoms, and two planes forming a hexagon. The sequence of atomic connections is Nb-Li□-Nb-Li… (□ indicate a vacant site). The hexagons are filled one third by atoms of lithium, one third by atoms of niobium with the remainder being a vacuum [Mou 2002, Pro 1990, Rid 1997, Xue 2002]. The axis is defined as being the axis at the same time parallel with the alignment of the niobium and lithium atoms, and perpendicular to the oxygen planes.

In the para-electric phase the lithium atoms are exactly in an oxygen plane and the niobium atoms are in the medium graft of two oxygen planes. However, in its ferroelectric phase, (T < the temperature of Curie) the ion Li+ shifts to the bottom of the oxygen plane, whereas the ion Nb^{5+} moves upwards compared with its initial site. These shifts generate local charges inside the material, inducing a spontaneous polarization of the crystal. The face c+ (z+) of the material is defined as the face on the side of the ions Li+ and Nb^{5+} (see Figure 4.8).

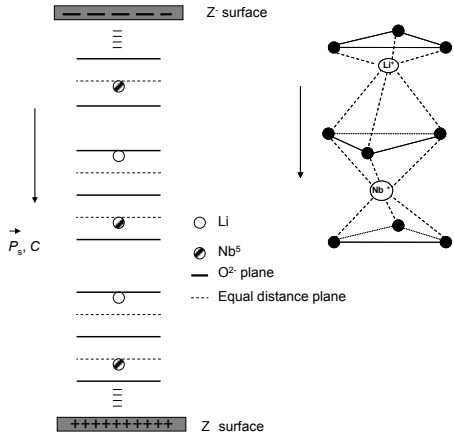

Figure 4.8. *$LiNbO_3$ elementary cell*

Fabrication of the periodically polarized structures of $LiNbO_3$ (PPLN) consists of carrying a structure made up of ferroelectric fields of opposite spontaneous polarization from one zone to another.

4.2.3.2. *Experimental techniques of polarization reversal*

Generally, the techniques which allow the inversion of spontaneous polarization can be electric, physicochemical or electron beam radiation [ARM 1992]. The use of these techniques strongly depends on the material. However, the process used must allow the realization of a homogenous periodic structure over a large length without deteriorating the transparency and linear optical properties of the crystal. To achieve this, electric poling (by application of an electric field) gives the best results, and is the most promising by far.

Before developing this technique, we will initially point out the basic principles of the other techniques.

4.2.3.2.1. Ionic diffusion

This developed for the first time in $LiNbO_3$ by titanium diffusion [Hou 1995]. The inversion of polarization is possible only if the diffusion is carried out on the positive z-face of the sample. Moreover, the temperature of diffusion must be close to the Curie temperature, the duration of the diffusion is generally short ~10 mn and the thickness of titanium must be suitably selected. From the experimental point of view, we initially carries out a photolithography mask by depositing a photosensitive layer of resin on the z+ face of the sample; then a layer of titanium (a few tens of nm) is deposited. After the chemical rinsing of the photoresist layer, the remaining titanium is then diffused in a furnace, under oxygen flow.

As the diffusion takes place at temperatures close to the Curie temperature of the material, the weak electric field created by the concentration gradient of titanium is sufficient to reverse the material spontaneous polarization [Nas 1965].

This technique presents major disadvantages in particular relating to the phenomenon of lateral diffusion, which decreases the height of modulation and thus reduces the conversion efficiency. Moreover, the domain shape obtained is of triangular form that also deteriorates the output conversion efficiency.

Note also that the exo-diffusion of lithium in the case of $LiNbO_3$ can cause an increase in the extraordinary index, additional to the polarization reversal.

4.2.3.2.2. Ionic exchange

This technique has already been presented in Chapter 2. It is usually used for the fabrication of waveguides in many materials. In the case of $LiNbO_3$ and $LiTaO_3$, it consists of exchanging on the surface the Li+ ions of the crystal with the H+ ions of an acid bath. The exchange is done at temperatures ranging between 200°C and 300°C, over a period ranging from a few minutes to a few hours.

However, an inversion of polarization can occur while the sample is under a heat treatment for a few minutes even a few hours of being close to its Curie temperature [Miy 1979]. This inversion occurs only on the negative z face of the crystal. The depth of the reversed zone can reach hundreds of microns when times of exchange or annealing are important. Under these conditions, to carry out a PPLN structure for example, the same operation is performed through a mask carried out beforehand by photolithography [Miy 1979, Nak 1990, Miz 1996]. The mask can be a metallic layer of Ta of 60 nm, deposited by sputtering on z face of the sample. This metal is not attacked by the benzoic acids and pyrophosphoric. The tantalum is then removed by reactive ionic etching (RIE) using a gas of SF6.

Note the same difficulties arise as with the diffusion technique, in particular when obtaining a square shape of the reversed domains. Indeed, the domains obtained present a circular form. Moreover, it is necessary to reach a sufficient annealing temperature so that the polarization reversal is carried out. So an additional annealing is generally necessary before carrying out a guiding structure, because of the high variation of the refractive index due to the presence of the protons. These operations might, finally, cause a reduction of the non-linear coefficient of the crystal [Bor 1993, Lau 1992].

4.2.3.2.3. Electron beam radiation

This technique was used in particular with $LiNbO_3$ on its negative z face [Nut 1992, Res 2000]). The dose of the electron beam is about 10^7-10^{10} e/μm^2. The

polarization reversal was observed at room temperature, without application of electric field, and on the entire thickness of the sample (1 mm) [Die 2004, Ito 1991]. As an indication, the following table gives some examples of the experimental conditions used.

E-beam-	Nutt *et al.*	He *et al.*	Restoin *et al.*
Tension (kV)	20 -30 (30)	25	25
Current (nA)	7	0.5	1.5-14
Scanning speed (µm/s)	200- 800		4.2-16.7
Beam diameter (nm)	500	70-400	
Charge density (µC/cm^2)		50-500	
Metallization	+Z by Au	+Z by Au	+Z by u/Pd

Table 4.5. *Experimental conditions of E-beam radiation for PPLN fabrication*

Bombardment by an electron beam creates a local electric field which causes a displacement of the ions Nb5+ and Li+ [Went 1992]. If the local field is around the coercive field of the crystal, it causes an inversion of polarization. Xue *et al.* report that the Nb5+ ions move in first because nothing prevents this movement from its site in the unit cell. The displacement of Nb5+ reduces its distance with the ion Li+ and thus increases the electrostatic force of repulsion between the two ions. Consequently, the Li+ ions are driven in their turn. It should be noted that Li+ moves more quickly than Nb5+. PPLN structures are obtained either by periodic scanning or by periodically insulating the crystal with a mask. This technique in particular makes it possible to carry out relatively low periods that are difficult to obtain using the other techniques.

4.2.3.3. *Fabrication of PPLN structures by eclectic field poling*

4.2.3.3.1. Principle

Two approaches can be used. The first consists of applying an electric field parallel to the axis of the spontaneous polarization of the material at a temperature close to the material's Curie temperature. In this case an electric field of a few volts per centimeter would move the Niobium and Lithium ions, which causes a reversal of polarization [Vin 2003]. By cooling the crystal, we preserve this new orientation imposed on the crystal.

The second approach is undertaken at room temperature. In this case the field to be applied is high. For example, the polarization reversal of $LiNbO_3$ is carried out

with electric fields close to the breakdown field of the material [Mil 1998, Gri 1997]. This technique was used with several materials in particular $LiNbO_3$ [Gri 1997], $LiTaO_3$ [Hay 1986] and the KTP [Ege 1993]. The main issue encountered in these experiments is the conductivity of the material, which can generate the destruction of a material like the KTP. In addition, the use of this method at high temperatures is relatively difficult because the integrity of the electrodes cannot be preserved.

Nevertheless, this technique showed its effectiveness for the fabrication of periodically polarized crystals for frequency conversion by QPM. Moreover, enormous progress was made in comprehending and developing a reproducible and reliable industrial process. PP crystals are nowadays commercially available. However, the realization of PP structures requires the use of periodic electrodes whose fabrication is a real technological challenge. Indeed tremendous conditions of cleanliness must be maintained, with the permanent concern of carrying out a periodically polarized structure of rectangular form. The process used followed the procedure for PP structures fabrication, and will be developed further: the development of periodic electrodes with the desired step, fabrication of the PP structure by application of the electric field and the control and the testing of the structure obtained.

4.2.3.3.2. Experimental process

During this process, it is necessary to answer certain questions relative to the practical use of the structure. These questions are as follows:

– What is the period of the QPM necessary for the required application?

– How can we control the temperature of the PP crystal precisely, the wavelength of the laser pumps and the angle of the PP crystal to maintain a good conversion efficiency?

– What will be the expected conversion efficiency?

Preparation

During each experiment, two tasks must be rigorously accomplished:

– Orientation and polishing of the sample: the sign of z faces of the sample (1 mm) can be given by X-ray diffraction, or by chemical etching.

– Cleaning the sample: a coarse cleaning using chemicals such as acetone or alcohol must be followed by a fine cleaning preferably using oxygen plasma.

Electrode fabrication

The development of grating electrodes on the first face of the sample (z+) constitutes the crucial step of this process. The second face being covered with a plane and uniform electrode, and will constitute the mass. It is necessary to use electrodes which resist the temperature and which do not oxidize. For example, a layer of gold of 250 nm could be appropriate. To allow the fixing of this layer of gold, a layer of nickel/chrome can initially be deposited [Fej 1992].

We can distinguish three processes.

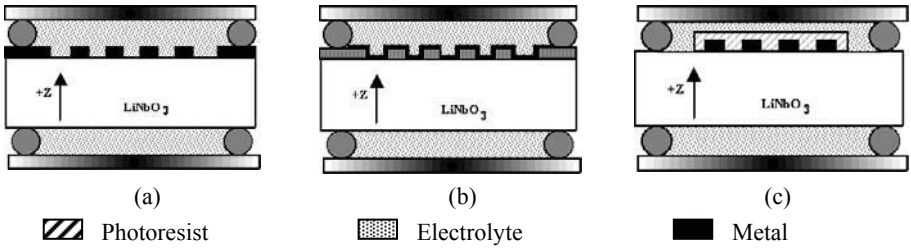

Figure 4.9. *PPLN structure fabrication processes*

Process (A):

– deposition of a photosensitive layer of positive resin (not very thick), decomposition conditions are, spinner 5,000 turns/min, time = 30 s, thickness = 500 nm;

– insolation of the resin through a mask;

– lift-off, acetone is used to remove the unexposed area of resin;

– deposition of a metallic layer of Au or Al of 2 μm;

– incorporation of the sample into an electrolyte cell of LiCl.

Process (B):

– deposition of a layer of photosensitive positive resin (not very thick), decomposition conditions are, spinner 5,000 turns/min, time = 30 s, thickness = 500 nm;

– insolation of the resin through a mask;

– lift-off, acetone is used to remove the unexposed area of resin;

– incorporation of the sample into an electrolyte cell of LiCl.

Process (C):

– deposition of a metallic layer (Au or Al) of 2 μm;

– deposition of a photosensitive positive resin (not very thick), decomposition conditions are, spinner 5,000 turns/min, time = 30 s, thickness = 500 nm;

– insolation of the resin through a mask;

– lift-off, acetone is used to remove the unexposed area of resin;

– etching of the uncovered part of the metallic layer;

– deposition of a photoresist layer of 2 μm over the metallic grating;

– incorporation of the sample into an electrolyte cell of LiCl.

The last method (C) (insulating on driver) produced better results probably because of the best definition of the metal edges. However, it requires two steps of photolithography. The other methods are easier because they require only one step of photolithography. It should be noted that the presence of a metal layer supports the process of polarization reversal.

The use of electrolyte cells allows the application of an electric field exceeding 25 kV/mm without destruction of the sample. The choice of metal, the resin and the electrolyte still causes many research tasks aimed at optimizing the fabrication process.

Electric field application

The defects which can appear at the time of the photolithography (dust, irregularities in the photoresist deposition, etc.) can generate many short-circuits during the application of the electric field. A control by optical microscope is generally necessary before the application of the electric field. The application of an electric field close to the coercive field of the material (21 kV/mm for $LiNbO_3$) at room temperature allows the reverse polarization of the crystal. This reversal is effective at the end of 50 ms. The poling electrical circuit can be represented in the following way (see Figure 4.10).

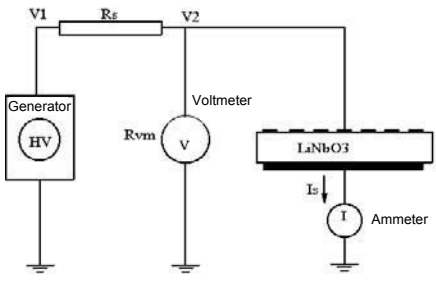

Figure 4.10. *The electrical circuit for PPLN structure development (left); and a photograph of an electrical cell (right)*

Polarization reversal realization and control

During the fabrication of PP structures, two types of control can be considered: *in situ* and *ex situ* controls.

In situ control:

This control is carried out either by optical or electrical methods. The sight check is based on the fact that the non-linear coefficient d_{33} and the electro-optical coefficient r_{33} have the same physical origin, namely the second order non-linearity of the material. Consequently, a change of the sign of d_{33}, while reversing the polarization also involves a change of the sign of r_{33}. To determine if the sign of the polarization of a crystal (guide) was reversed, we can compare the interference figure between a reference beam and the beam which crosses the PP structure, with the interference figure obtained with a beam which crosses the virgin substrate with a known orientation.

Ex situ control:

Several methods are possible, including local methods such as the chemical etching and volume methods based on the pyrolectric effect.

Chemical etching: for example, in the case of $LiNbO_3$, a solution of hydrofluoric and nitric acid (1 HF vol. with 50% + 2 vol. of HNO_3 with 65%) makes it possible to reveal its polarization [Nas 1965]. Indeed the etching speed depends on the face of the crystal. It is faster on the -z faces than on those of +z and +y (for face x, there is no difference for symmetry reasons). Consequently, the -z face presents hillocks revealing defects in the crystalline structure of the material, whereas the +z face remains intact. The prolongation of the chemical etching over several hours generally causes a frosted -z face. Under these conditions, a chemical etching carried out on a PP crystal causes periodic deteriorations of the PP surface.

Chemical etching is generally initiated by protonization, which explains why the –z face is etched more quickly; because it easily absorbs the positive charges contained in the HF solution [Col 2002, Son 2002]. Although this technique can in certain cases induce an error because it is sensitive to the defects existing in the crystal, it remains the most direct, simplest and reliable method. It should be noted that this method can also be used to determine the -z face of the $LiNbO_3$ sample.

Pyro-electric effect: is related to the variation of the crystal polarization versus the variation of its temperature [Hob 1966]. This polarization variation induces an electric current which circulates if one connects the two faces of the sample by an external circuit. The observation of the potential difference sign at the boundaries of the sample which also gives the direction of the current, makes it possible to determine the sign of the z face. Under these conditions, with an adequate

deposition of electrodes, we connect one of the two faces of a PP sample to the mass and use a micro-point on the other face, in order to collect and analyze the electrical signal. To heat the sample locally, Argon or a focused CO2 laser beam is generally used. If the +z face is related to the micro-point, then the tension obtained is negative.

For example, Figure 4.11 shows three photographs of PPLN structures revealed by chemical etching. We must emphasize that the homogenity of the PPLN grating for short periods remains a very important issue.

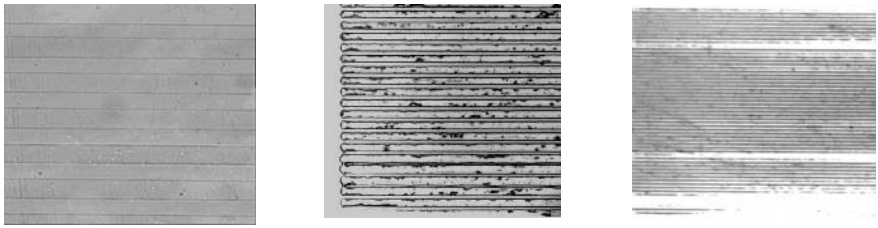

(a) (b) (c)

Figure 4.11. *Example of PPLN structures revealed by chemical etching: (a) 20 µm, (b) 10 µm and (c) 4.8 µm*

To test the optical effectiveness of these PP gratings, it is important to experimentally investigate SHG in these structures preferably associated with waveguides, to increase the effects of electromagnetic confinement. This aspect will be the subject of the following part of this chapter.

Electric poling mechanism

Undoubtedly, the work reported by Miller *et al.* [Mil 1998] constitutes a reference of first choice to promote understanding of the polarization inversion process of $LiNbO_3$ by electric poling. Moreover, in this work, the authors carried out a systematic study of the experimental conditions of PPLN structure development. This study includes in particular the evaluation of the influence of various parameters such as the value of the tension applied, the number of nucleation centers per area unit, the size of the reversed fields (in depth and in diameter), the influence of the electrolyte used or the nature of the electrodes, etc. They also developed an ideal model and a calculation algorithm to determine the distribution of the field applied in the crystal according to the geometry of the electrodes. Miller *et al.* thus studied three essential phenomena: the steps of the mechanism, the working electric field values and the electrodes to be used:

– Mechanism by steps

From the calculation of the electric field distribution and determination of its optimal value, Miller *et al.* established their model on the basis of five assumptions:

1. the fields are perpendicular to ox;

2. the transverse movement of the domains walls is controlled by the E_z component of the electric field applied;

3. the transversal propagation velocity of the domains walls and the electric field are the same everywhere in the crystal;

4. nucleation appears only on the electrodes edges;

5. ionic conductivity is neglected in the entire volume of the crystal.

Thus, Miller *et al.*, could describe the kinetics of domain creation and propagation. They present a mechanism made up of several phases during the formation of a domain grating (see Figure 4.12).

The beginning of the polarization inversion starts under the electrodes edges (see Figure 4.12). This step is also called domains nucleation. The domains of reversed polarization thus created have a conical form with a hexagonal base. They propagate in this form to the opposite face of the crystal where their tip takes a hexagonal form which very quickly reaches the size of the base of the opposite face (see Figure 4.12, step B). The domain then has a tubular form with a hexagonal section (see Figure 4.12, step C). The domains are then propagated in the direction perpendicular to that of the application of the electric field in priority under the electrodes (see Figure 4.12, step D) then on both sides of the electrodes (see Figure 4.12, step E).

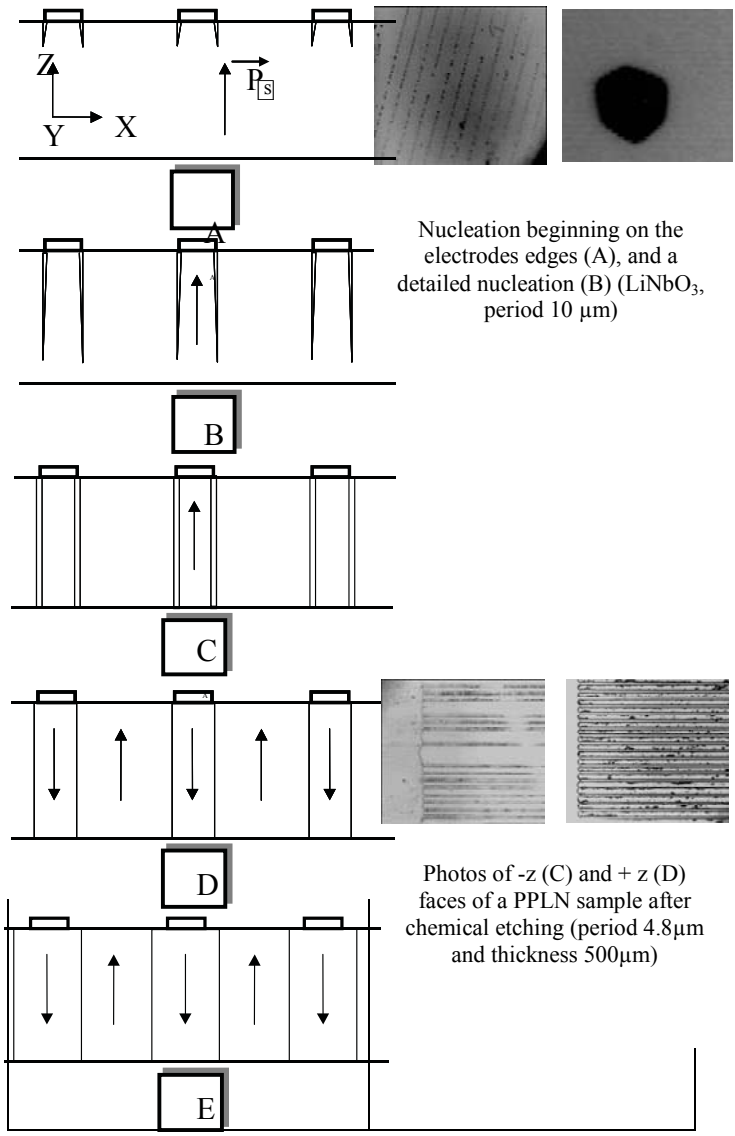

Figure 4.12. *Polarization reversal by electric poling: a mechanism by steps [Mil 1998 and Vin 2003]*

– The applied electric field value

Miller *et al.* [Mil 1998] established the domain wall propagation velocity according to the poling field amplitude, while varying the value of the electric field from 10 kV/mm to 30kV/mm (see Figure 4.13).

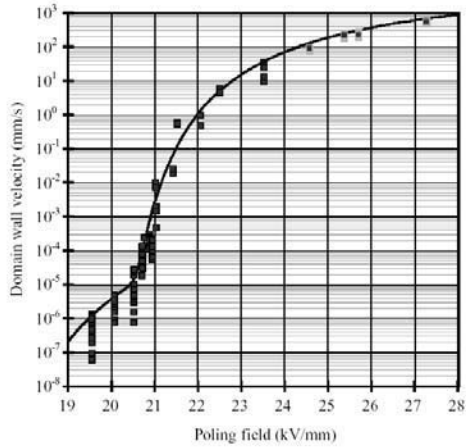

Figure 4.13. *Domain wall propagation velocity as a function of the applied electric field (figure extracted from [Mil 1998])*

The experimental measurements were fitted using the function given by the following equation [Mil 1998]:

$$v(E) = \Phi(E - E_1)v_1 \exp\left(-\frac{\delta_1 E_1}{E - E_1}\right) + \Phi(E - E_2)v_2 \exp\left(-\frac{\delta_2 E_2}{E - E_2}\right) \quad [4.45]$$

where Φ is the Heaviside function and the fitting parameters related to the curve of Figure 4.13 are reported in Table 4.6.

E_1=19.4 kV/mm	E_2=15.0 kV/mm
v_1=16.3 m/sec	v_2=362 µm/sec
δ_1=1.29	δ_2=13.83

Table 4.6. *Fitting parameters of the curve in Figure 4.13 using relation [4.45]*

We note on the curve of Figure 4.13 the appearance of an inflection point at the value of 20.75 kV/mm. At this value of the field, the domains propagation is most

sensitive to the variations of the applied field. The idea is to work with a value of the field which allows self-termination of the periodic inversion of polarization. When the domains grow beyond the electrodes, a charge deposition can occur on the sample surface. These charges decrease the value of the electric field in the material. Then, the mechanism of polarization inversion stops. With the value of 20.75 kV/mm we thus obtain a periodically polarized structure without domain lateral propagation until coalescence.

– Electrodes and their period

Finally, one of the most useful results of the model developed by Miller *et al.* [Mil 1998] is the relation determining the electrodes geometry (more precisely their duty cycle) according to the grating period of the PPLN structure with a duty cycle of 50%. This relation provides the curve in Figure 4.14.

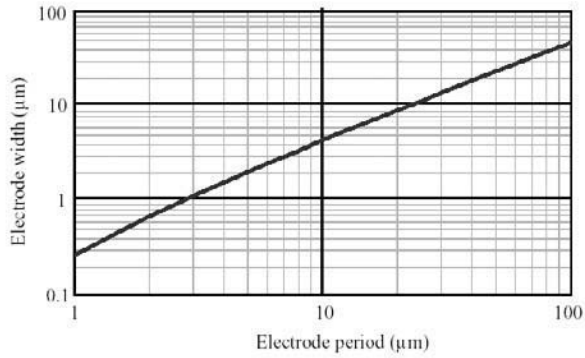

Figure 4.14. *Duty cycle of electrodes in order to obtain a PPLN structure with a duty cycle of 50%, as a function of the grating period (figure extracted from [Mil 1998])*

Figure 4.14 states, for example, that to obtain a PPLN with a 4.8 µm period, it is necessary to use electrode grating with a 4.8 µm period but with electrodes approximately 2 µm in width.

4.3. Second harmonic generation within waveguides

As we saw in Chapter 1, in an optical waveguide, various modes can be propagated at various velocities and are characterized by their effective indices N_m (m: the order of the guided mode). Under these conditions, a new degree of freedom exists using phase matching by modal dispersion [Bab 1991, Bou 1999, Flu 1996, Pli 1998, Zha 1992].

By considering that the incident power does not undergo a depletion we can easily show that the conversion efficiency is in the following form:

$$\eta = \frac{P_{SH}}{P_F} = \left[\frac{2\omega_F^2}{N_{mF}^2 N_{mSH} c^3 \varepsilon_0}\right]\left(d_{eff}^2 L^2\right)\frac{P_F}{A_{OVL}}\frac{\sin^2\left(\frac{1}{2}\Delta kL\right)}{\left(\frac{1}{2}\Delta kL\right)^2} \quad [4.46]$$

N_{mF} and N_{mSH} being effective indices of fundamental and harmonic modes, respectively with:

$$A_{OVL} = \frac{1}{I_{OVL}^2} \quad [4.47]$$

where I_{OVL} is the overlap integral between the fundamental and the harmonic modes:

$$I_{OVL} = \iint E(2\omega)E(\omega)E^*(\omega)dxdy \quad [4.48]$$

This factor is a concept specific to waveguides. It can be described as being a space integral of the product of the fundamental power normalized by the distribution of the electric field through the non-linear area of the guide. An important value of this integral is its high conversion efficiency.

We will initially discuss how the overlap integral is important in the conversion efficiency. This term is indeed dominating if we want to obtain high ratio of an output second harmonic generation. After this, and starting with the expressions of the fields profiles for TE and TM polarizations, we will give the expression of this overlap integral.

We consider a fundamental field polarized according to z being propagated in direction ox, not presenting variation according to y.

$$\vec{E}_F(x,y,z,t) = \vec{E}_F(x,y,z)e^{i\omega t} = \begin{bmatrix} 0 \\ 0 \\ A_{0F}F_F(z)e^{i(\omega_F t \quad \beta_F x)} \end{bmatrix} \quad [4.49]$$

If we project equation [4.49] on the z axis, a solution for the harmonic wave will be in the form:

$$\vec{E}_{SH}(x,y,z,t) = \vec{E}_{SH}(x,y,z)e^{i\omega t} = \begin{bmatrix} 0 \\ 0 \\ A_{SH}(x)F_{SH}(z)e^{i(\omega_{SH}t \quad \beta_{SH}x)} \end{bmatrix} \quad [4.50]$$

where β_F and β_{SH} are projections of the wave vectors on the propagation axis; and A_{0F} and $A_{SH}(x)$ are the amplitudes of the fundamental and harmonic fields. Note that the fundamental field does not depend on x. As a matter of fact, assuming the pump signal is without depletion, we assume a lossless medium with a weak conversion ratio.

$F_F(z)$ and $F_{SH}(z)$ are the normalized field profiles, such that:

$$\begin{aligned} &\int_{\infty}^{+\infty} F_F(z)\,F_F^*(z)dz = 1 \\ &\int_{\infty}^{+\infty} F_{SH}(z)\,F_{SH}^*(z)dz = 1 \end{aligned} \quad [4.51]$$

In the case of $LiNbO_3$, x, y and z correspond to the crystal axis, thus the second order non-linear tensor is given as:

$$\frac{\chi^{(2)}}{\varepsilon_0} = \begin{bmatrix} 0 & 0 & 0 & 0 & d_{31} & -d_{22} \\ -d_{22} & d_{22} & 0 & d_{31} & 0 & 0 \\ d_{31} & d_{31} & d_{33} & 0 & 0 & 0 \end{bmatrix} \quad [4.52]$$

The non-linear polarization is then written:

$$\vec{P}_{SH}^{nl}(x,y,z,t) = \vec{P}_{SH}^{nl}(x,y,z)e^{i2\omega t} \quad [4.53]$$

$$P_{SH}^{nl}(x,y,z) = \varepsilon_0 \left[d_{ij}\right] \begin{bmatrix} 0 \\ 0 \\ E_F^2(x,y,z) \\ 0 \\ 0 \\ 0 \end{bmatrix} = \varepsilon_0 d_{33} E_F^2(x,y,z) \quad [4.54]$$

From non-linear wave equation [4.23] previously mentioned, we can show that for a weak interaction and for a guided mode:

$$F_{SH}\frac{\partial^2 A_{SH}}{\partial x^2}+A_{SH}\frac{\partial^2 F_{SH}}{\partial z^2}-\beta_{SH}^2 A_{SH}F_{SH}-2i\beta_{SH}F_{SH}\frac{\partial A_{SH}}{\partial x} \\ =-4\omega^2\mu_0\varepsilon A_{SH}F_{SH}-4\omega^2\mu_0\varepsilon_0 d_{33}(A_{0F}F_F)^2 e^{i\Delta\beta x} \quad [4.55]$$

with: $\Delta\beta=\beta_{SH}-2\beta_F$

We assume that $\frac{\partial A_{SH}}{\partial x}\beta_{SH} >> \frac{\partial^2 A_{SH}}{\partial^2 x}$ (weak interaction approximation), thus we obtain:

$$\left[\nabla_{yz}^2 F_{SH}+\left[4\omega^2\mu_0\varepsilon-\beta_{SH}^2\right]F_{SH}\right]A_{SH}(x)-2i\beta_{SH}F_{SH}\frac{\partial A_{SH}}{\partial x} \\ =-4\omega^2\mu_0\varepsilon_0 d_{33}(A_{0F}F_F)^2 e^{i\Delta\beta x} \quad [4.56]$$

In addition, within the waveguide, we have: $\nabla_z^2 F_{SH}+\left(4\omega^2\mu_0\varepsilon-\beta_{SH}^2\right)F_{SH}=0$, thus the propagation equation becomes:

$$2i\beta_{SH}\frac{\partial A_{SH}}{\partial x}F_{SH}(z)=4\omega^2\mu_0\,\varepsilon_0\,d_{33}\,A_{0F}^2\,F_F^2\,e^{i\Delta\beta x} \quad [4.57]$$

By multiplying by the complex conjugate profile of the mode, we obtain:

$$2i\beta_{SH}\frac{\partial A_{SH}}{\partial x}F_{SH}(z)F_{SH}^*(z)=4\omega^2\mu_0\,\varepsilon_0\,d_{33}\,A_{0F}^2\,F_{SH}^*(z)F_F^2\,e^{i\Delta\beta x} \quad [4.58]$$

Thereafter, by integrating over the right section of the waveguide using equation [4.50] we obtain:

$$2i\beta_{SH}\frac{\partial A_{SH}}{\partial x}=4\omega^2\mu_0\,\varepsilon_0\,d_{33}\,A_{0F}^2\int_{\infty}^{+\infty}F_{SH}^*(z)F_F^2\,e^{i\Delta\beta x}dz \quad [4.59]$$

$$\frac{\partial A_{SH}}{\partial x}=-\frac{2\omega^2\mu_0\,\varepsilon_0\,i}{\beta_{SH}}d_{33}\,A_{0,F}^2\int_{\infty}^{+\infty}F_{SH}^*(z)F_F^2\,e^{i\Delta\beta x}dz \quad [4.60]$$

also:

$$\frac{\partial A_{SH}(x)}{\partial x} = -ie^{i\Delta\beta x} Bd_{33} S_{eff} \qquad [4.61]$$

with:

$$B = \sqrt{\mu_0\, \varepsilon_0}\left(\frac{\omega}{N_{m\,SH}}\right) A_{0F}^2 = \frac{1}{c}\left(\frac{\omega}{N_{mSH}}\right) A_{0F}^2 \qquad [4.62]$$

and:

$$S_{eff} = \int_{\infty}^{+\infty} F_{2\omega}^{*}(z) F_{\omega}^{2}(z)\, dz \qquad [4.63]$$

By integrating over an interaction length L, we obtain:

$$A_{SH}(x) = -i \int_0^L e^{i\Delta\beta x} Bd_{33} S_{eff}\, dx \qquad [4.64]$$

$$A_{SH}(x) = -id_{33} BS_{eff} \int_0^L e^{i\Delta\beta x} dx \qquad [4.65]$$

$$A_{SH}(L) = -id_{33} B \frac{\left(e^{i\Delta\beta L} - 1\right)}{i\Delta\beta} S_{eff} \qquad [4.66]$$

$$A_{SH}(L) A_{SH}^{*}(L) = d_{33}^2 B^2 L^2 \sin c^2\left(\frac{\Delta\beta L}{2}\right) S_{eff}^2 \qquad [4.67]$$

The harmonic power is then given:

$$P_{SH}(L) = \frac{1}{2}\sqrt{\frac{\varepsilon_0}{\mu_0}} N_{mSH} \int_{\infty}^{+\infty} \left|E_{SH}(L, z)\right|^2 dz \qquad [4.68]$$

$$P_{SH}(L) = \frac{1}{2}\sqrt{\frac{\varepsilon_0}{\mu_0}} N_{mSH} \left|A_{SH}(L)\right|^2 \int_{\infty}^{+\infty} \left|F_{SH}(z)\right|^2 dz \qquad [4.69]$$

$$P_{SH}(L) = \frac{1}{2} d_{33}^2 L^2 S_{eff}^2 \sin c^2\left(\frac{\Delta\beta L}{2}\right)\sqrt{\frac{\varepsilon_0}{\mu_0}}\frac{\omega^2}{c^2 N_{mSH}}\left|A_{0F}(L)\right|^4 \qquad [4.70]$$

also:

$$P_F = \frac{1}{2}\sqrt{\frac{\varepsilon_0}{\mu_0}} N_{mF}\left|A_{0F}\right|^2 \int_{\infty}^{+\infty}\left|F_F(z)\right|^2 dz = \frac{1}{2}\sqrt{\frac{\varepsilon_0}{\mu_0}} N_{mF}\left|A_{0F}\right|^2 \qquad [4.71]$$

$$P_{SH}(L) = 2\frac{\mu_0}{c} P_F^2 S_{eff}^2 \frac{\omega^2 d_{33}^2 L^2}{N_{mSH} N_{mF}{}^2} \sin c^2\left(\frac{\Delta\beta L}{2}\right) \qquad [4.72]$$

This equation is identical to [4.46] using $S_{eff} = I_{OVL}$.

Finally, in the case of QPM and from equation [4.43] we can write equation [4.72] as follows:

$$P_{SH}(L) = 2\frac{\mu_0}{c} P_F^2 S_{eff}^2 \frac{\omega^2 L^2}{N_{mSH} N_{mF}{}^2}\left(\frac{2d_{33}}{\pi m}\right)^2 \sin c^2(\pi m\alpha) \qquad [4.73]$$

By considering:

$$A_{OVL} = \frac{1}{S_{eff}^2}$$

$$P_{SH}(L) = 2\frac{\mu_0}{c} P_F^2 \frac{\omega^2 L^2}{A_{OVL} N_{mSH} N_{mF}{}^2}\left(\frac{2d_{33}}{\pi m}\right)^2 \sin c^2(\pi m\alpha) \qquad [4.74]$$

where A_{OVL} is the interaction effective thickness for a planar waveguide (effective surface for a channel waveguide). If we compare equation [4.74] with equation [4.28], we realize (a part from the term introduced by the QPM) that only the term of the interaction surface changes. In the first case, it is about the surface of the beam in the massive crystal (the waist), while in the second case, it is about a surface which is typically of about the waveguide size (if we consider a channel waveguide). This second value being much weaker, typically an order of magnitude,

we understand well that the harmonic power (and thus conversion efficiency) can also gain an order of magnitude thanks to the use of the waveguide.

4.3.1. *Overlap integral calculation*

Calculation of the overlap integral is important to determine the efficiency of the second harmonic generation process. For this we use the expressions of the normalized electric fields for the TE and TM modes [Yar 1984]. We will present here the case of a TM → TE interaction. However, calculation can be easily extended to TM → TM, TE → TE and TE → TM interactions.

The expression of the overlap integral for the TM → TE interaction is:

$$S_{eff}^{(m,m,n)} \equiv \int_{\infty}^{+\infty} H_y^{(m,\omega/2)} H_y^{(m,\omega/2)} E_y^{(n,\omega)} dz \qquad [4.75]$$

where *H*y is the fundamental field profile and *E*y is the harmonic profile (their expressions were given in Chapter 1).

We previously reported the expression of the electric field amplitude for a step-index asymmetric waveguide. The normalization condition imposes:

$$\int_{\infty}^{\infty} [E_y^{(m)}(z)]^2 dz = \frac{2\omega\mu}{\beta_m} \qquad [4.76]$$

For TM modes, we can also write:

$$\int_{\infty}^{\infty} [H_y^{(m)}(z)]^2 dz = \frac{2\omega\varepsilon_0 n^2(z)}{\beta_m} \qquad [4.77]$$

The overlap integral ($m^{-1/2}$) can then be written as:

$$S_{eff}^{(m,m,n)} \equiv \frac{1}{\left(\frac{2\omega_m\varepsilon_0 n^2(z)}{\beta_m}\right)\left(\frac{2\omega_n\mu}{\beta_n}\right)^{1/2}} \int_{\infty}^{+\infty} H_y^{(m,\omega/2)} H_y^{(m,\omega/2)} E_y^{(n,\omega)} dz \qquad [4.78]$$

The overlap integral must be at its maximum in order to obtain the best conversion rate. We must thus use a waveguide with a minimal thickness,

emphasizing the interest of the monomode waveguide. However, the value of the overlap integral strongly depends on the guide characteristics.

As an indication, Figure 4.15 gives the variation of this integral according to the variation of the index and thickness of the guiding layer, respectively. These calculations were carried out for a waveguide of GdCOB, fabricated by He^+-implantation [Bou 2005]. Note that the overlap integral increases with the variation of the index, and tends towards a constant after a variation Δn estimated at 10^{-2}. Regarding the influence of the variation, it shows the existence of an optimal value of the guide thickness, which makes it possible to have the maximum value of the overlap integral regardless of the interaction process.

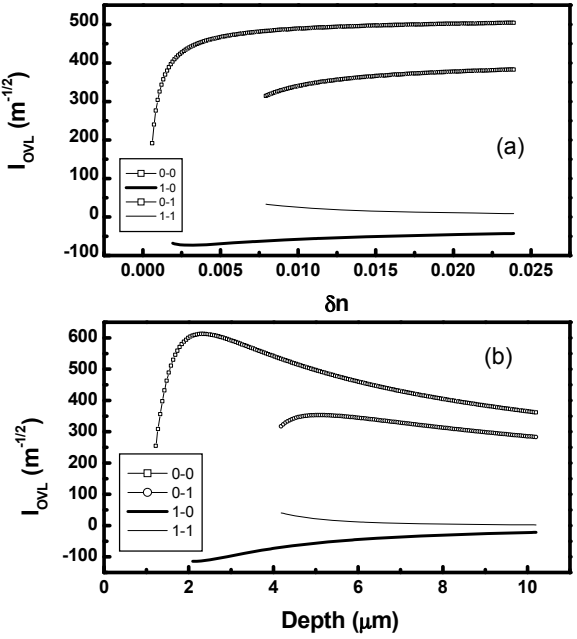

Figure 4.15. *Overlap integral variation as a function of (a) the index variation, (b) the waveguide thickness variation. These curves correspond to a GdCOB: He+ planar waveguide [Bou 2005]*

We saw in section 4.2 that the fundamental and harmonic waves must fulfill the phase matching condition, i.e. that the index seen by one or the other should be the same. Otherwise, we have to compensate for phase mismatch by using a periodically polarized structure. However, we also saw in Chapter 1 that the index seen by a guided mode is different from that of the guiding layer. The conditions of QPM or BPM are, therefore, somehow disturbed. As a matter of fact, it is necessary to have

equality between the fundamental and harmonic effective indices. We speak then about phase matching by modal dispersion [Bou 2005].

From the variation of the effective indices according to the wavelength, we note that there are numerous possibilities of phase matching as shown in Figure 4.15. However, it is worth noting that the conversion efficiency is very different according to the interaction considered because of the value of the overlap integral (see equation [4.78]) which varies greatly. For example, the interactions between even modes and odd modes are to be strongly avoided. Moreover, the losses strongly increase according to the guided mode order and one can make the assumption that the privileged interaction in the guides is almost always the interaction between the zero order modes. As an example, Figure 4.16 displays the $TM_0(\omega)$ and $TM_0(2\omega)$ interaction (point A on the figure).

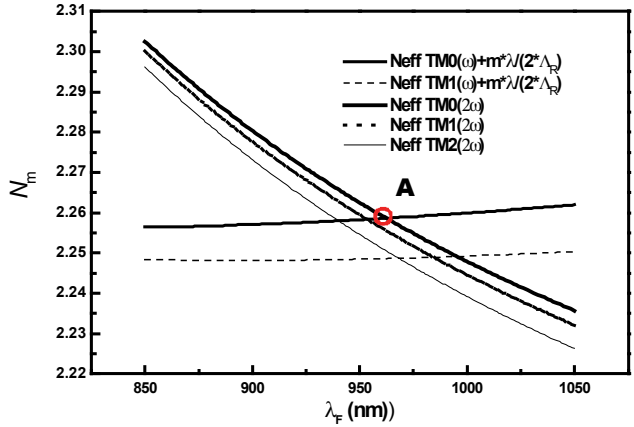

Figure 4.16. *Phase matching by modal dispersion in case of $LiNbO_3$:He+ planar waveguide*

The curves of Figure 4.16 were plotted for a waveguide of PPLN: He+, Λ_R = 4.8 µm, thickness = 3.4 µm and $\Delta n=3.10^{-2}$. From this figure, we can understand the interest in using waveguides, as it is possible to obtain phase matching at various wavelengths even if this phase matching does not have all the same efficiency for the reasons previously, reported.

Finally, we must also point out the possibility of using the Cerenkov configuration [Bos 1991, Mic 1992, Tie 1971] based on the phase matching between the fundamental guided mode and the second harmonic radiation mode. This mechanism appears when the phase velocity of the guided mode is higher than that of the free wave in the substrate. Although the conversion efficiency can be important under certain conditions, which depend especially on the guide

parameters, the quality of the doubled beam thus remains poor and not very advantageous compared with that obtained in a simple guide.

4.4. Non-linear optical characterization of waveguides

4.4.1. *SHG setup*

This setup (see Figure 4.17) allows the qualification and the test of second harmonic generation of waveguides, using a YAG:Nd laser at 1.06 μm as well as a Ti-sapphire tunable laser. Measurements consist of collecting the variation of the harmonic power according to the fundamental wavelength and the pump power. These measurements make it possible to determine the waveguide conversion efficiency.

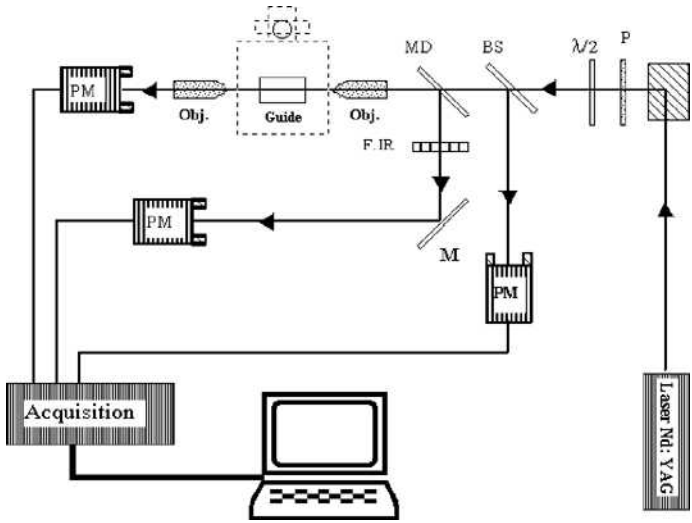

Figure 4.17. *SHG setup by transmission in order to control the non-linear performance of the waveguide (P: polarizer, BS:beam splitter, PM: photomultiplier, F. IR: IR filter, Obj: objective microscope)*

In the study of the non-linear response of the guiding area compared to the virgin substrate [Åhl 1993, Bou 2001, Had 1996], we use the generation of the second harmonic signal by reflection (GSHR) (see Figure 4.18). We can thus determine the effects of the fabrication process on the non-linear properties of the guide. In this configuration, we measure the fundamental (ω) and harmonic (2ω) signals reflected by the waveguide section, according to the depth. The comparison

of the response of the guiding layer and the optical barrier (for implanted waveguides, for instance) related to that of the virgin substrate allows us to evaluate the effects of the fabrication process on the waveguide's non-linear properties.

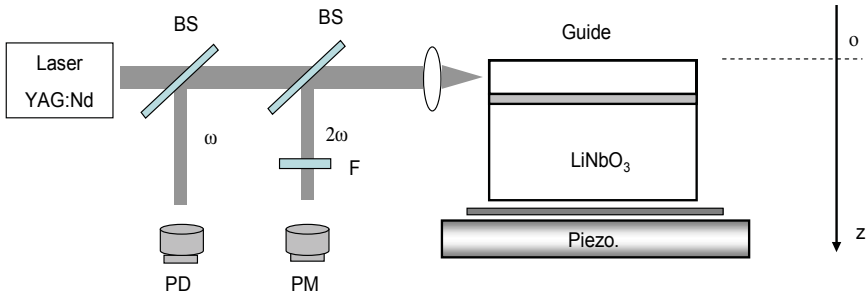

Figure 4.18. *SHG setup by reflection in order to control the non-linear performance of the waveguide (P: polarizer, BS: beam splitter, PM: photomultiplier, PD: photodiode, F: filter, Obj: objective microscope)*

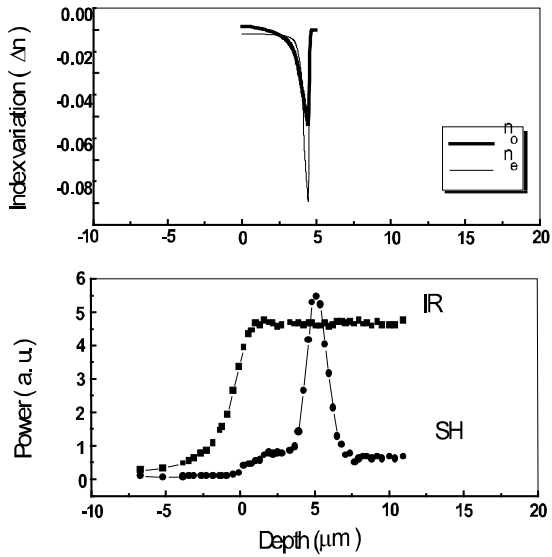

Figure 4.19. *Example of results obtained using the experimental setup of Figure 4.18: He+-implanted $LiNbO_3$ waveguide [Bou 2001]*

The example in Figure 4.19 shows the non-linear response He+-implanted $LiNbO_3$ waveguide [Bou 2001]. These results are compared with the index profiles of the guiding area. Note that at the optical barrier position, we observe strong

increase in the SH signal. However, it has been shown that this effect is not due to an increase of the non-linear coefficient in this part of the material [Bou 2001].

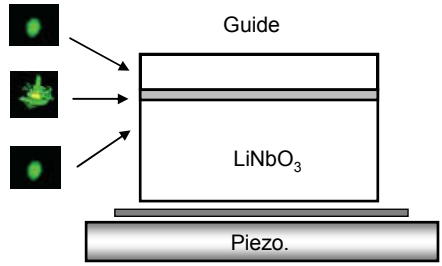

Figure 4.20. *Illustration of the SH beam reflected from the end section of the $LiNbO_3$ He+-implanted waveguide [Bou 2001]*

As shown in Figure 4.20, the spatial quality of the SH beam is very poor, indicating an important alteration of the crystal lattice located at the optical barrier position. Moreover, it is also noted that the non-linear response of the waveguide body is similar to that of the virgin substrate. It indicates the fact that the ionic implantation almost does not disturb the non-linear optical properties of the waveguide.

4.4.2. *Second harmonic generation by reflection*

In 1962, Bloembergen and Pershan [Blo 1962] described and explained, for the first time, the phenomenon of second harmonic generation appearing at the interface separating a linear medium from a non-linear medium.

By solving Maxwell's equations in the particular case of the interaction of two light waves with a non-linear medium, Bloembergen and Pershan pointed out the creation, at the mediums interface of two harmonic waves of pulsation 2ω, One of the harmonic beams is propagated in the non-linear medium and is called the transmitted harmonic beam. The second is emitted in the linear medium as a reflected harmonic beam.

Electric and magnetic fields of transmitted harmonic waves in the non-linear medium are given by [Blo 1962, Kre 1999]:

$$\begin{cases} \vec{E}_T^{2\omega} = \vec{e}_T \mathrm{E}_T^{2\omega} \exp i(2\omega t - \vec{k}_T^{2\omega}\vec{r}) - \dfrac{P^{NL}\varepsilon_0{}^1}{\left(n_{NL}^{2\omega}\right)^2 - \left(n_{NL}^{\omega}\right)^2}\left[\vec{p} - \dfrac{\vec{k}_s\left(\vec{k}_s\vec{p}\right)}{\left|k_T^{2\omega}\right|^2}\right]\exp i(2\omega t - \vec{k}_s\vec{r}) \\ \vec{H}_T^{2\omega} = \dfrac{c}{2\omega}\left(\vec{k}_T^{2\omega} \wedge \vec{e}_T\right)\mathrm{E}_T^{2\omega} \exp i(2\omega t - \vec{k}_T^{2\omega}\vec{r}) - \dfrac{P^{NL}\varepsilon_0{}^1}{\left(n_{NL}^{2\omega}\right)^2 - \left(n_{NL}^{\omega}\right)^2}\left(\vec{k}_s \wedge \vec{p}\right)\exp i(2\omega t - \vec{k}_s\vec{r}) \end{cases} \quad [4.79]$$

It is important to note that the presence of the harmonic wave in the linear medium is imposed by the continuity relations at the interface. The expressions of the harmonic fields in this medium are:

$$\begin{cases} \vec{E}_R^{2\omega} = \vec{e}_R \mathrm{E}_R^{2\omega} \exp i(2\omega t - \vec{k}_R^{2\omega}\vec{r}) \\ \vec{H}_R^{2\omega} = \dfrac{c}{2\omega}\left(\vec{k}_R^{2\omega} \wedge \vec{e}_R\right)\mathrm{E}_R^{2\omega} \exp i(2\omega t - \vec{k}_R^{2\omega}\vec{r}) \end{cases} \quad [4.80]$$

The wave vector directions $\vec{k}_R^{2\omega}$ and $\vec{k}_T^{2\omega}$, of the reflected and transmitted harmonic waves, the unit vectors direction $\vec{e}_R$ and $\vec{e}_T$ and the amplitudes of reflected $\mathrm{E}_R^{2\omega}$ and transmitted $\mathrm{E}_T^{2\omega}$ waves are determined from the limit conditions at the interface separating the two mediums.

4.4.2.1. *Reflected second harmonic beam power*

In this section, we consider the linear medium as a hemicylindrical prism (see Figure 4.21). The second harmonic wave can have two states of polarization: its electric field can be either parallel to the plane of incidence (TM polarization) or perpendicular to this plane (TE polarization). These two states of polarization depend on the medium symmetry. In the case of a TE polarized fundamental wave, the harmonic wave is also TE polarized. When the considered harmonic wave is polarized perpendicular to the plane of incidence, the amplitude of the electric field of this wave is given by the following relation [Kre 1999, Kre 2003]:

$$E^{2\omega} = -P^{NL}\varepsilon_0{}^1 \frac{1}{\left(n_s^{2\omega}\cos\theta_T + n_s^{\omega}\cos\theta_S\right)\left(n_s^{2\omega}\cos\theta_T + n_p^{2\omega}\cos\theta_m\right)} \quad [4.81]$$

The amplitude of this field is a function of the fundamental electric field amplitude $\left|\vec{E}_{in}^{\omega}\right|$ and is written as:

$$\left|\vec{E}^{\omega}\right| = \frac{2n_p^{\omega}\cos\theta_{in}}{n_p^{\omega}\cos\theta_{in} + n_S^{\omega}\cos\theta_S}\left|\vec{E}_{in}^{\omega}\right| \qquad [4.82]$$

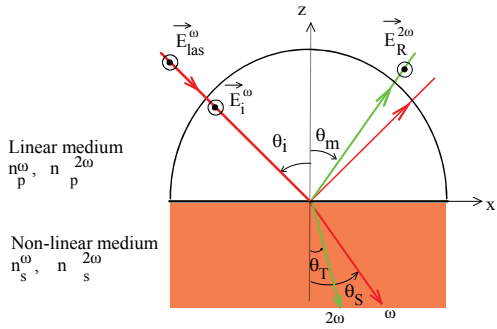

Figure 4.21. *TE polarized fundamental incident wave induces a TE harmonic wave at the interface between the linear and the non-linear mediums*

In these conditions the harmonic power $P^{2\omega}$ can be written as:

$$P^{2\omega} = \frac{c\,n_p^{2\omega}\left(t^{2\omega}\right)^2}{\varepsilon_0}\left|\frac{d_{eff}\left(\frac{2n_p^{\omega}\cos\theta_{in}}{n_p^{\omega}\cos\theta_{in}+n_S^{\omega}\cos\theta_S}\,t^{\omega}\left|\vec{E}_{las}^{\omega}\right|\right)^2}{\left(n_s^{2\omega}\cos\theta_T + n_s^{\omega}\cos\theta_S\right)\left(n_s^{2\omega}\cos\theta_T + n_p^{2\omega}\cos\theta_m\right)}\right|^2 \frac{\cos\theta_m}{\cos\theta_{in}}A \qquad [4.83]$$

Measurements of the harmonic power are relative measurements. The principle of these measurements consists of recording the power of the second harmonic signal and comparing the obtained results with those of a reference material. Consequently, if the experimental conditions remain the same, the parameters A, t^{ω}, $t^{2\omega}$, $\vec{E}_{las}^{\omega}$, independent of the samples, do not vary and thus need not be determined.

This principle is at the foundation of the SHEW (second harmonic wave generated with evanescent wave) technique developed by Kiguchi *et al.* [Kig 1994]. Moreover, this detail is of great importance because it underlines the flexibility of the SHEW technique which does not require the determination of the incident beam features, which is necessary for other methods.

4.4.2.2. *The SHEW setup*

The experimental setup is presented in Figure 4.22. The incident laser beam is divided into two by a beam splitter. One of the beams is directed towards a reference arm in order to control the incident power. The other beam is focused on the plane face of a hemicylindrical prism, while the sample is placed in optical contact against the the planar face of the prism. Measurement consists of recording the power of the harmonic signal according to the angle of incidence. The non-linear coefficients and the refraction indices (at ω and 2ω) of the sample are obtained by fitting the experimental curves [Kre 1999, Kre 2003].

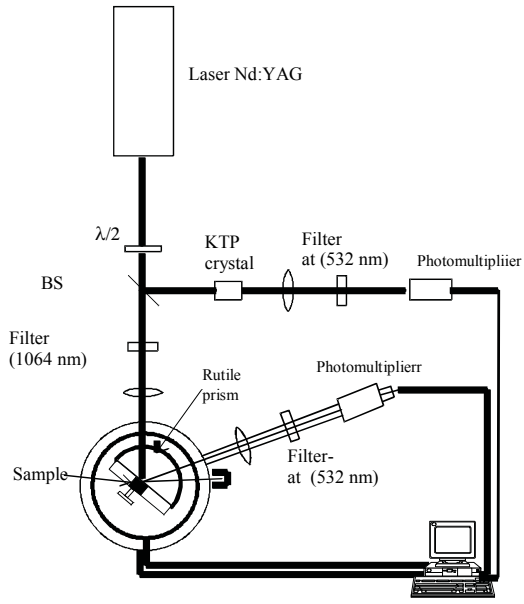

Figure 4.22. *SHEW setup for non-linear optical characterization of materials in powder, thin films and bulk forms*

The SHEW signal, which interests us, is observed at the time of total reflection. Under these conditions the fundamental wave is not propagated in the non-linear medium and thus the SHEW technique is not sensitive to phase matching conditions.

This technique has been developed mainly to study materials in the form of powders; it was also adapted to investigate thin layers and waveguides [Kre 1999].

As an example, results obtained for the $LiNbO_3$ sample are presented in Figures 4.22a and b. The experimental curves are fitted using relation [4.83] by the least squares method. Concerning the refractive indices, the experimental conditions allow us to determine the extraordinary indices $n_s^{e,\omega}$ and $n_s^{e,2\omega}$ at ω and 2ω for a TE fundamental wave and the ordinary index $n_s^{o,\omega}$ at ω and the extraordinary index $n_s^{e,2\omega}$ at 2ω for TM polarization.

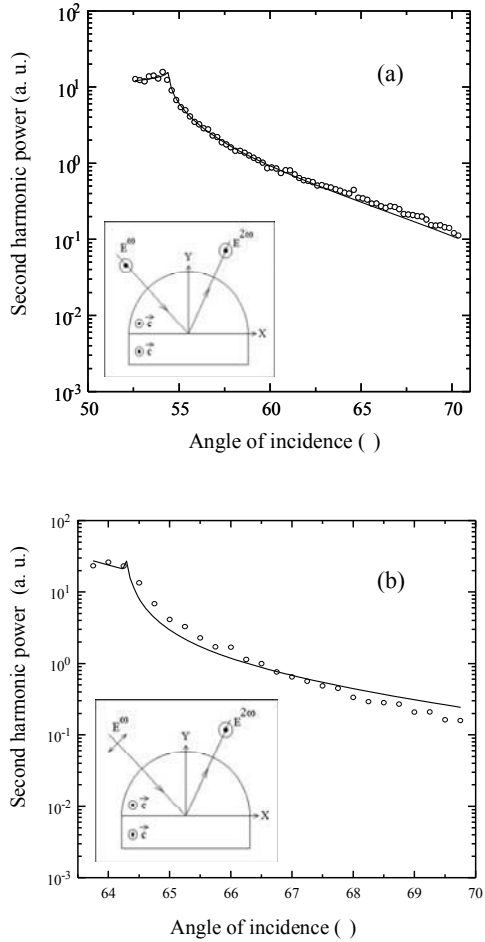

Figure 4.23. *SH signal versus the angle of incidence: (a) $LiNbO_3$ He+ implanted waveguide and (b) $LiNbO_3$ H+ implanted waveguide. The experimental data are fitted using relation [4.83] [Kre 2003]*

The investigation of ionic implantation effect on the surface and volume non-linear optical properties of waveguides was also undertaken by Kremer *et al.* [Kre 1999] using this SHEW technique. Figure 4.23 reports the results obtained in the case of He+ and H+ implanted waveguides in LiNbO3. As indicated in Table 4.7, these measurements revealed a degradation of about 50% of the *d*33 non-linear coefficient of the He+ implanted sample, whereas H+ implantation did not induce any modification of this non-linear coefficient.

However, in this configuration, the effects of ionic implantation are probed to a few hundred nanometers corresponding to the penetration depth of evanescent wave. Consequently, we have to be careful when extending the conclusions of these measurements to the entire volume of the guiding area. Indeed, SH measurements by reflection (already reported in the previous sections) showed that the non-linear properties of the guiding area core are not affected by He+ implantation or by that of H+ (see section 4.4.1).

Sample	d_{33} (± 10%) (pm/V)	$\frac{d_{33}(sample)}{d_{33}(LN\ virgin)}$
LN (virgin)	25	1
LN:He^+	13.25	0.53
LN:H^+	26.75	1.07

Table 4.7. *Measurement of the d_{33} coefficient of $LiNbO_3$ He+ and H+ implanted waveguides using the SHEW technique [Kre 1999]*

4.4.3. *Second harmonic generation in waveguides*

This study is carried out using end-fire coupling and out-coupling setup. The experimental arrangement is presented in Figure 4.24. The phase matching within the waveguide is carried out by modal dispersion.

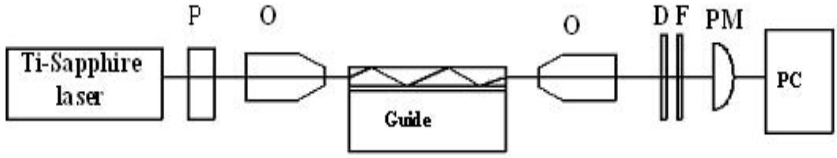

Figure 4.24. *SHG in waveguide setup (P: polarizer, O: microscope objective, D: neutral density, F: filter and PM: detector)*

Measurements consist of collecting the variation of SH power according to the fundamental wavelength and the pump power of a Ti-Sapphire laser. Figure 4.25 shows the harmonic signal evolution according to λ for a PPLN-10µm He+ implanted waveguide [Vin 2005]. The experimental data are fitted by a cardinal sine function which makes it possible to determine the interaction length of about 1 mm.

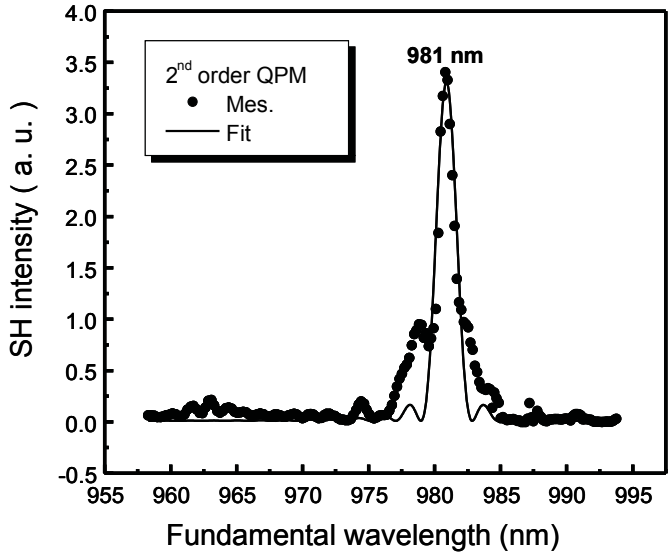

Figure 4.25. *SH intensity as a function of the pump wavelength, waveguide of PPLN: He+. 2nd order QPM [Vin 2005]*

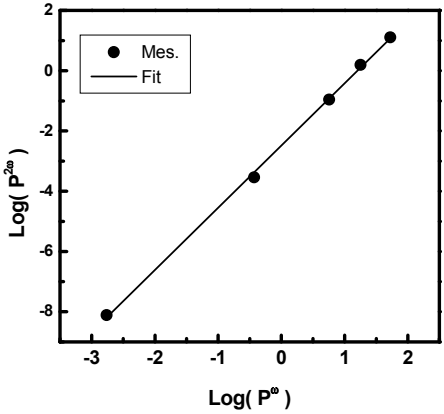

Figure 4.26. *SH power versus pump power, PPLN: He+. 2nd order QPM [Vin 2005]*

Figure 4.26 shows the variation of the harmonic power according to the pump power coupled into the waveguide. The slope of this line in the logarithmic scale is about 2.06; it confirms the quadratic interaction of the studied non-linear process.

QPM order	Bulk PPLN λ_{QPM} (nm)	SHG in PPLN: He+ waveguide			
		Theory			Experiment
		Interaction	λ_{QPM} (nm)	I_{OVL} ($m^{-1/2}$)	λ_{QPM} (nm)
2nd	969	$TM_0^{\omega} \rightarrow TM_0^{2\omega}$	978	1,373	981
		$TM_1^{\omega} \rightarrow TM_0^{2\omega}$	1,007	995	
3rd	800	$TM_0^{\omega} \rightarrow TM_0^{2\omega}$	866	1,430	869
		$TM_1^{\omega} \rightarrow TM_0^{2\omega}$	881	1,064	
4th	794.8	$TM_0^{\omega} \rightarrow TM_0^{2\omega}$	800	1,474	804
		$TM_1^{\omega} \rightarrow TM_0^{2\omega}$	808	1,110	

Table 4.8. *Results of QPM interaction within PPLN: He+ waveguide; comparison with the expected theoretical results [Vin 2005]*

The SHG interaction was found to be a second order $TM_0^{\omega} \rightarrow TM_0^{2\omega}$ type, with a QPM wavelength of 981 nm. This wavelength is in accordance with the theoretical

calculation indicated in Table 4.8. For a pump power of about 100 mW, Vincent *et al.* [Vin 2005] found a conversion efficiency of 3.6×10^{-3}% /W. This value is 40% higher than that of the same massive PPLN sample. Finally, Table 4.7 also indicates the 3rd and the 4th order QPM wavelengths. In these cases, the interactions are also $TM_0^{\omega} \rightarrow TM_0^{2\omega}$ type.

4.5. Parametric non-linear optical effects

4.5.1. *Parametric amplification*

In this section, we will point out the effects of the second order that involves two laser waves. However, the interested reader will be able to find many references treating parametric non-linear optics phenomena – see for example [Yar 1984, San 1999].

Let us consider an incident optical wave of pulsation ω_1 (called the pump wave, see Figure 4.26). Starting from this wave, we are interested in the process which makes it possible to generate two waves of pulsations ω_2 and ω_3, such that:

$$\omega_1 = \omega_2 + \omega_3 \qquad [4.84]$$

In a simplified way, we can say that optical parametric amplification is similar to the SHG phenomenon. The only difference is in the direction that the energy transfers are carried out. Contrary to the SHG where a photon of high frequency (doubled) is created starting from two photons of lower frequencies, in the process of optical parametric amplification energy passes from a photon of high frequency ω_1 towards two photons of lower frequencies ω_2 and ω_3. This effect can start from noise. However, starting from an optical wave of pulsation ω_2, it is amplified and is generally called the signal. The wave of pulsation ω_3 ($\omega_3 = \omega_1 - \omega_2$) is called the idler.

The generation of wave $\vec{E}_3$ makes a parametric combination between the incident wave $\vec{E}_1$ and wave $\vec{E}_3$ possible. In these conditions a polarization with pulsation $\omega_2 = \omega_1 - \omega_3$ can be created, the latter generating an optical wave $\vec{E}_2$.

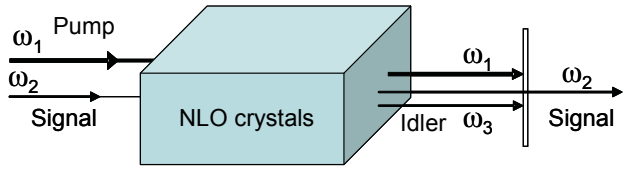

Figure 4.27. *Schematic illustration of the amplification parametric process*

We can show that the electric fields E_2 and E_3 are given by the following relations:

$$\frac{\partial E_2(z)}{\partial z} = \frac{i\omega_2 \chi^{(2)}}{2n_2 c} E_1(z) E_3^*(z) \exp[i\Delta k z] \qquad [4.85]$$

$$\frac{\partial E_3(z)}{\partial z} = \frac{i\omega_3 \chi^{(2)}}{2n_3 c} E_1(z) E_2^*(z) \exp[i\Delta k z] \qquad [4.86]$$

with $\Delta k = k_1 - k_2 - k_3$, and where n_2 and n_3 are the medium indices at pulsations ω_2 and ω_3 respectively.

Note that the fields vary proportionally versus each other's amplitudes. This system of coupled equations describes the parametric amplification. As in the case of the SHG, the process efficiency depends on the realization of phase matching condition given by the following relation:

$$n_1\omega_1 = n_2\omega_2 + n_3\omega_3 \qquad [4.87]$$

4.5.2. *Optical parametric oscillation (OPO)*

As has been mentioned, the optical parametric amplification is a process in which the pump beam is transformed into two beams: the signal and the idler. This process allows the conversion of a laser beam into other frequencies according to the relation:

$$\frac{1}{\lambda_{pump}} = \frac{1}{\lambda_{signal}} + \frac{1}{\lambda_{idler}} \qquad [4.88]$$

By assuming that the phase matching is satisfied, the parametric interaction is weak and the spatial variation of the field amplitude E_1 of the pump wave is negligible, we can show that the preceding system of coupled equations is reduced to [Cou 2002, San 1999]:

$$\begin{aligned} E_2(L) &= E_2(0) + i\eta_2 E_1(0) E_3^*(0) \\ E_3(L) &= E_3(0) + i\eta_3 E_1(0) E_2^*(0) \end{aligned} \qquad [4.89]$$

with: $\eta_i = \dfrac{\omega_i L}{2 n_i c} \chi^{(2)}$.

By placing an optical parametric amplifier in a resonant cavity, it will be possible to increase the process gain (in this case it is possible to generate signal and idler waves starting from the noise) by resonant oscillations [Yar 73, Yar 84, San 99]. The optical parametric oscillator (OPO) is schematized in Figure 4.27; it includes a non-linear crystal of length L inserted into an optical cavity of length L'. The two mirrors of the cavity are considered completely reflective for the pulsations ω_2 and ω_3 (the reflection coefficient R ~ 1). The device is pumped by an intense laser of pulsation ω_1.

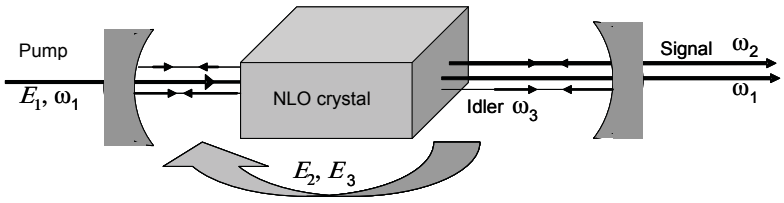

Figure 4.28. *Optical parametric oscillation (OPO) principle*

There are two types of cavities: the cavity with simple resonance where R is large for ω_2 or ω_3, and the cavity with double resonance where R is large for both ω_1 and ω_2. In the case of double resonance, we can show that the resonance condition is given by the following relation:

$$\frac{\omega_1}{2\pi c} = \frac{m_2}{(n_2 - 1)L + L'} + \frac{m_3}{(n_3 - 1)L + L'} \qquad [4.90]$$

This relation emphasizes the fact that the fields E_2 and E_3 are in phase with them selves after one reflection in the cavity. The OPO oscillates only for one of the discrete values of L'.

In addition, the oscillation condition dictates that the field is identical to itself in phase and also in amplitude after reflection in the cavity. In other words, the gain equals the losses. The amplitudes of the signal and idler fields at the input and output of the crystal are given by the following relation:

$$E_i(0) = \sqrt{R}E_i(L) \approx \left(1 - \frac{T}{2}\right)E_i(L) \qquad (\text{i} = 2, 3) \qquad [4.91]$$

The combination of this relation with the previous system [4.78] gives:

$$\begin{cases} TE_2(0) = 2i\eta_2 E_1(0)E_3^*(0) \\ TE_3(0) = 2i\eta_3 E_3(0)E_2^*(0) \end{cases} \qquad [4.92]$$

This system can be solved as:

$$|E_1(0)|^2 = \frac{(1-R)^2}{4\eta_2\eta_3} \qquad [4.93]$$

This relation shows that the optical parametric oscillation can take place at a minimal value of the pump power (threshold power) which corresponds to the equality between the gain and the losses. This value strongly depends on the reflection coefficient R of the cavity.

The previous calculation leads to the *Manley-Rowe* relation:

$$\sqrt{\eta_3}|E_2(0)| = \sqrt{\eta_2}|E_2(0)| \qquad [4.94]$$

This relation can be also written as:

$$\frac{2\varepsilon_0 n_2 c|E_2(0)|^2}{\hbar\omega_2} = \frac{2\varepsilon_0 n_3 c|E_3(0)|^2}{\hbar\omega_3} \qquad [4.95]$$

This equation indicates that numerical flows of the photons in the two waves emitted by the OPO are equal: the photons are created by pairs (ω_2, ω_3).

In the conventional OPO, the generated wavelengths are limited by the availability of non-linear crystals which can simultaneously satisfy the phase matching condition, the energy conservation and the conditions of optical transmission. The output of these OPOs are generally controlled by the angle and

temperature tuning of the refractive indices of the crystal. The angular tuning especially depends on the angular tolerance and the walkoff, which restrict the interaction length and reduces the conversion efficiency. The temperature tuning is generally intended for weak range wavelengths.

For all these reasons, it is preferable to use periodically polarized crystals, thus, avoiding the BPM problems.

4.6. Laser sources based on non-linear optics

In this section, we will try to give an outline of the state-of-the-art research concerning the use of non-linear optics (NLO) to develop laser sources. We will not evoke in an exhaustive way the situation of the NLO and the lasers because the field is in permanent evolution and each day new products are implemented. The principal contribution of the NLO relates obviously to the settling of laser sources in the visible.

Indeed, generally speaking, obtaining a laser radiation in the visible range is currently done either with laser diode containing semiconductor materials, or with cumbersome lasers (laser in Ar+), or by frequency doubling in bulk crystals pumped by an IR diode laser. However, gas lasers are currently disappearing from the market, so the competition remains between the diode laser and the micro-sources laser based on frequency conversions.

The very first diode laser in the visible at 515 nm based on ZnSe was announced by the 3M company, in 1991 [Mol 2001, Tou 1999]. This was a major event which crowned more than 20 years of research and development on a global scale. Less than ten years later, in 1999 Nichia Corporation (Japan) announced the marketing of the first blue-purple diode lasers at 400 nm based on GaInN, with a lifespan higher than 10,000 operating hours uninterrupted at room temperature [Mol 2001].

Although the blue-purple diode laser is today a commercial product, serious limitations still remain. These difficulties are in particular due to the growth problems (doping, defects), to the control of electric conductivity by the doping of these semiconductors, to the ohmic contact and to the instability of the alloy and the problem of the substrate [Mol 2001, Nak 1997, Tou 1999]. Moreover, rather important piezoelectric field effects which appear in the form of a very intense internal electric field (1-7 MV/cm) cause a shift in the wavelength, a reduction in the radiation efficiency and a widening of the emission rays. The consequences of this are a single short operation time and poor laser beam quality.

Another major limitation of the diode laser relates to the difficulty of carrying out wavelengths other than 400 (±10) nm, because the current structures are based on InGaN. For example, the effective diode laser emitting in the green does not exist yet. It is also extremely difficult to increase the power as long as the growth problems are not controlled. The majority of these problems are solved only partially and still constitute today the motivation of many research teams throughout the world.

Therefore, the use of frequency doubling in non-linear crystals could constitute a first choice solution. For example, the use of Nd^{3+} doped YAG crystals emitting at 1,064 μm coupled with a non-linear crystal of KTP, which carries out the frequency conversion in the visible range to 532 nm, is currently and has for many years been used as a reliable device.

Moreover, the use of waveguides allows for the considerable increase of the conversion output of the system, thanks to the light confinement. It also allows the miniaturization of laser device, which would be appropriate for general public applications. This was made possible by the fabulous development of diode lasers emitting in the infra-red (800 nm – 1.6 μm) which are used as pump sources. These laser diodes are usually marketed and their efficiency is well established. We find in particular sources of 100 mW – 1 W largely sufficient to be coupled to a waveguide.

One limiting factor which can influence the efficiency of such a system is related to the coupling system. However, these micro-laser systems benefit from the already existing technology, which was developed for the diode laser systems and laser-fiber optics in telecommunication networks. The requirements of coupling, namely a precise alignment and good stability, are currently well controlled technologies. Under these conditions, the space quality of the visible laser beam obtained by these systems is better than that of the visible diode lasers. It should be noted that this quality strongly depends on the uniformity of the guiding structure.

Moreover, other major advantages of the systems based on the frequency conversion in waveguides comes from the use of quasi-phase matching (QPM). The QPM makes it possible to generate all wavelengths in the transparency range of the non-linear material by the correct choice of the PP structure period.

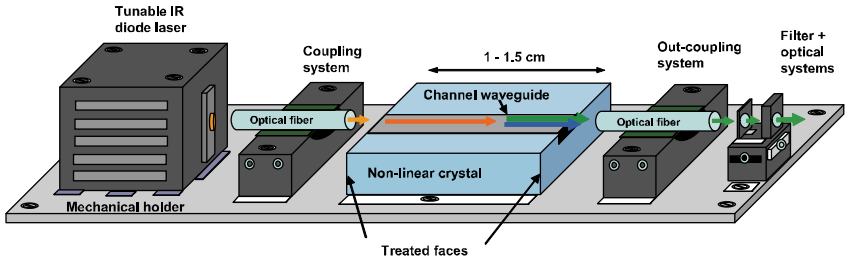

Figure 4.29. *Scheme of all solid laser devices based on NLO*

Another solution emerging over recent years consists of using frequencies self-conversion in crystals, which present at the same time non-linear properties and laser properties [Cha 1999]. These materials have sites of substitution favorable to doping by rare earths (Yd^{3+} and Nd^{3+}). Under these conditions the IR laser emissions of the active ions can be combined with the properties of harmonics generation to obtain a self-conversion of frequency. For instance, as we saw in Chapter 2, the new non-linear crystals GdCOB ($Ca_4GdO(BO_3)_3$) and YCOB belong to this family of crystals and they probably have the best possible ingredients to be potential candidates for applications in integrated non-linear optics. The use of self-conversion makes it possible to considerably simplify the design of the laser cavity. Indeed, in the conventional intra-cavities using the frequency doubling, the two laser and non-linear mediums are placed inside the cavity. Consequently, alignment problems are to be solved, increasing the cost and the complexity of the system. In the case of a self-doubling device, only one crystal is used and it is used at the same time like a laser and a frequency doubling medium.

These technologies will also allow the development of display devices based on the utilization of the three primary colors: blue, green and red. Although several technologies divide the display market, it is not probable; only one technology can dominate the various display types [Cha 1999]. We note, for example, that for the wide display systems (40-100"), the market remains very open and no technology seem to be clearly dominating; whereas LEDs control the market of the giant screens (> 100"). The technology based on the frequency conversion is able to provide laser systems emitting in blue, green and red. Once these systems are developed with a reduced cost, this technology will have a real chance to be competitive on the market of the 40-100" screens.

Laser sources also play a central role in modern communication networks. The traffic of data will continue to increase, with particular thanks to DWDM technology. This revolution was made possible thanks to the development of silica optical fiber with losses less than 0.2 dB km^{-1}. Several telecommunications windows were used in relation to the technology of the available laser sources. Note, for

example, 800 nm, the 1.3 μm window, and more recently the 1.5 μm window thanks to the development of tunable light sources based on semiconductors in that range of wavelengths. Moreover, these technologies are well established and progress unrelentingly.

Recently a new type of optical fiber made its appearance on the market of telecommunications. It concerns plastic optical fiber (POF) of PMMA type [Mar 1994]. These fibers have certain advantages that silica fibers do not present. They are light, flexible and have a broad diameter (0.25-1 mm) that facilitates their installation. All these properties allow their use in the communication networks, in particular in the short distances connections between the customer, the office and the network. Bite rate of about 300 Mbits to 3 Gbits were carried out [Zub 2001].

POF have very high attenuations in the telecommunications windows (1.3 μm and 1.5 μm) and thus cannot be used with the IR sources. However, they have weak and acceptable attenuations for the interurban network in the range of the visible wavelength, in particular the green light. Consequently the laser development of visible sources can accelerate the implementation of the POF in the telecommunication network. In this context, laser sources based on waveguides can play a very important role.

As a whole, each technology seems to offer advantages and attributes. Nevertheless, the NLO technology has a potential whose exploitation still has not been fully undertaken and it may yet become a leading technology, especially as NLO phenomena are numerous and their combination could bring viable solutions.

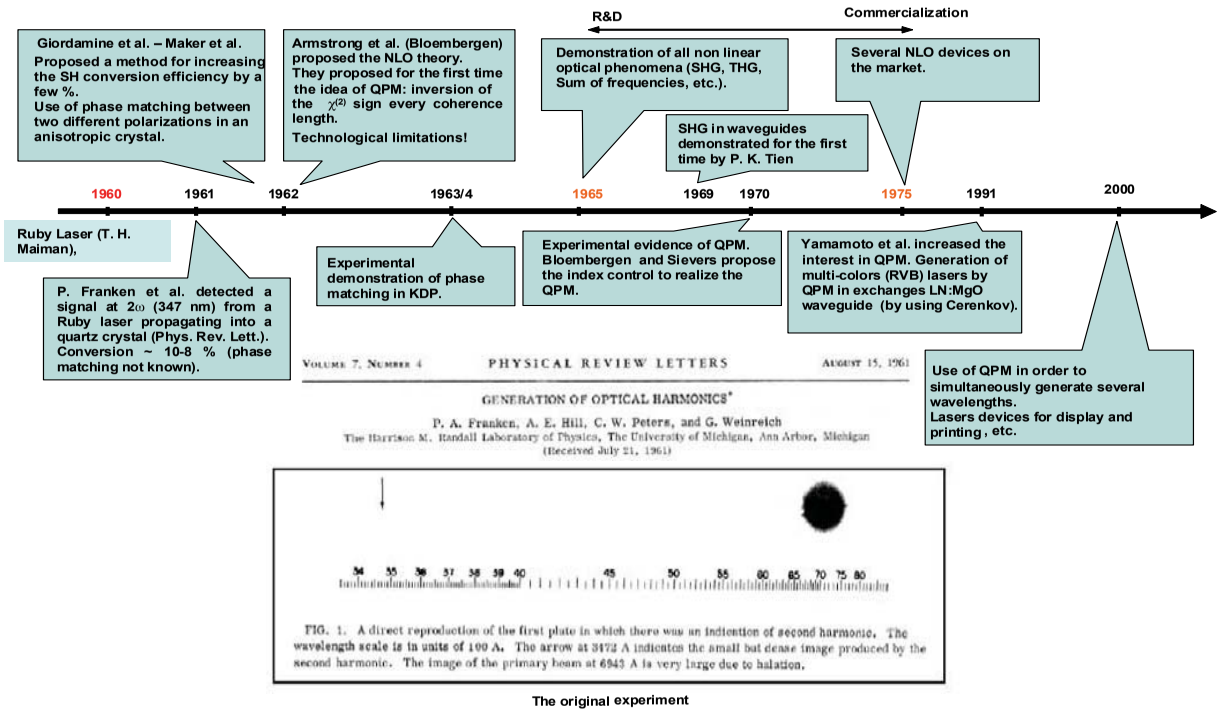

Figure 4.30. *History of non-linear optics development*

4.7. Bibliography

[Åhl 1993] Åhlfeldt H., Laurell F. and Arvidson G., "Strongly reduced optical nonlinearity in lithium tantalate due to proton exchange", *Electron Lett*., 29(9), 819-820 (1993).

[Arm 1962] Armstrong J.A., Bloembergen N., Ducuing J. and Pershan P.S., "Interaction between light waves in a nonlinear dielectric", *Phys; Rev*., 127, 1918- 1939 (1962).

[Arm 1992] Armani F., Génération de seconde harmonique par quasi accord de phase dans les guides d'ondes niobate et tantalite de lithium, PhD Thesis, University of Nice Sophia-Antipolis (1992).

[Bab 1991] Babsail L., Lifante G. and Townsend P.D., "Second-harmonic generation in ion-implanted quartz planar waveguides", *Appl. Phys. Lett*., 59(4), 384-386 (1991).

[Blo 1962] Bloembergen N. and Pershan P.S., "Light waves at the boundary of nonlinear media", *Phys. Rev*., 128, 606-626 (1962).

[Blo 1965] Bloembergen N., *Nonlinear Optics*, The Benjamin/Cummings Publishing Company, Inc. (1965).

[Bor 1993] Bortz M.L., Fyres L.A. and Fejer M.M., "Depth profiling of the d_{33} nonlinear coefficient in annealed proton exchanged $LiNbO_3$ waveguides", *Appl. Phys. Lett*., 62(17), 2012-2014 (1993).

[Bos 1991] Bossard C.H., Flörsheimer M., Küpfer M. and Günter P., "Cerenkov-type phase matched second harmonic generation in DCANP Langmuir-Blodgett film waveguides", *Optics Comm*., 85, 247-51 (1991).

[Bou 1999] Boudrioua A., Loulergue J. C., Moretti P., Jacquier B., Aka G. and Vivien D., "Second-harmonic generation in He+- implanted gadolinium calcium oxoborate, $Ca_4GdO(BO_3)_3$ (GdCOB), planar waveguides", *Optics. Letters*, 24(18), 1299-12101 (1999).

[Bou 2001] Boudrioua A., Laurell F., Moretti P. and Loulergue J. C., "Nonlinear optical properties of (H+, He+)-implanted planar waveguides in Z-cut $LiNbO_3$: annealing effect", *J. Opt. Soc. Am. B*, 18(12), 1832-1840 (2001).

[Bou 2005] Boudrioua A., Vincent B., Kremer R., Moretti P., Jacquier B. and Aka G., "Linear and non linear optical properties of $Ca_4GdO(BO_3)_3$ (GdCOB), planar implanted waveguides", *JOSA B*, 22(10), 2192-2199 (2005).

[Cha 1999] Chai B.H.T., "Advances in bulk inorganic nonlinear optical materials", *Optics & Photonics News*, 31-38 (1999).

[Col 2002] Sones C.L., Mailis S., Brocklesby W.S., Eason R.W. and Owen J.R., "Differential etch rates in z-cut LiNbO3 for variable HF/HNO_3 concentrations", *J. Mater. Chem*., 12, 295-298 (2002).

[Con 1973] Conwell E.M., "Theory of second harmonic generation in optical waveguides", *IEEE J. of Quantum Electronics*, SE-9(9), 867-879 (1973).

[Cou 2002] Courtois J. Y., "Optique non linéaire", in Fabre, C., Pocholle J. P. (eds), *Les lasers et leurs applications scientifiques et médicales*, EDP Sciences (2002).

[Die 2004] Dierolf V. and Sandmann C., "Direct-write method for domain inversion patterns in $LiNbO_3$", *Applied Physics Letters*, 84 (20), 3987-3989 (2004).

[Eck 1990] Eckardt R.C., Masuda H., Fan Y.X. and Byer R.L., "Absolute and relative nonlinear optical coefficients of KDP, KD*P, BaB_2O_4, $LiIO_3$, MgO:$LiNbO_3$ and KTP measured by phase-matched second-harmonic generation", *IEEE J. Quantum Electronic*, 26, 922-933 (1990).

[Ege 1993] Eger D., Oron M. and Katz M., "Optical characterization of $KTiOPO_4$ periodically segmented waveguides for second-harmonic generation of blue light", *J. Appl. Phys*., 74 (7), 4298-4302 (1993).

[Fej 1992] Fejer M.M., Magel G.A., Jundt D.H. and Byer R.L., "Quasi-phase-matched second harmonic generation: tunig and tolerances", *IEEE J. Quantum Electron*., 28, 2631-2654 (1992).

[Flu 1996] Fluck D., Pliska T., Günter P., Bauer St., Beckers L. and Buchal C.H., "Blue light second harmonic generation in ion implanted $KNbO_3$ channel waveguides of new design", *Appl. Phys. Lett*., 69(27), 4133-4135 (1996).

[Gri 1997] Grisard A., Lallier E., Gary G. and Aubert P., "ferroelectric integrated optics: recent developments", *IEEE of Quantum Electronics*, 33(10), 1627-1635 (1997).

[Gün 2000] Günter P. (Ed.), *Nonlinear Optical Effects and Materials*, Springer – Optical Sciences (72) (2000).

[Had 1996] El Hadi K., Interactions paramétriques dans des guides d'ondes réalisés par échange protonique sur niobate de lithium polarisé périodiquement, PhD Thesis, University of Nice Sophia-Antiplois (1996).

[Hay 1986] Haycock P.W. and Townsend P.D., "A method of poling $LiNbO_3$ and $LiTaO_3$ below T_c", *Appl. Phys. Lett*., 48(11), 698-700 (1986).

[He 2003] He J., Tang S. H., Qin Y. Q., Dong P., Zhang H. Z., Kang C. H., Sun W. X. and Shen Z. X., "Two-dimensional structures of ferroelectric domain inversion in $LiNbO_3$ by direct electron beam lithography", *Journal of Applied Physics*, 93(12), 9943-9946 (2003).

[Hob 1966] Hobden M.V. and Warner J., "The temperature dependance of the refractive indices of pure lithium niobate", *Phys. Lett*., 22(3), 243-244 (1966).

[Hou 1995] Houé M. and Townsend P. D., "An introduction to methods of periodic poling for second-harmonic generation", *J. Phys. D: Appl. PHYS*., 28, 1747-1763 (1995).

[Ito 1975] Ito H., Naito H. and Inbo H., "Generalized study on angular dependence of induced second order non linear optical polarizations and phase matching in biaxial crystals", *J. Appl. Phys*., 46(9), 3992-3998 (1975).

[Ito 1991] Ito H. and Takyu C., "Fabrication of periodic domain grating in $LiNbO_3$ by electron beam writing for application of nonlinear optical processes", *Electron. Lett*., 27(14), 1221-1222 (1991).

[Kig 1994] Kigushi M., Kato M., Kumegawa N. and Tanigushi Y., "Technique for evaluating second-order nonlinear optical materials in powder form", *J. Appl. Phys*., 75(9), 4332-4339 (1994).

[Kle 1962] Kleinman D.A., "Nonlinear dielectric polarization in optical media", *Phys. Rev*., 126, 1977-1979 (1962).

[Kre 1999] Kremer R., Réalisation d'un banc automatisé pour la mesure des non linéaires quadratiques par génération de second harmonique en réflexion totale: application à la caractérisation des matériaux sous forme de poudre, de cristaux et de guides d'onde, PhD Thesis, University of Metz (1999).

[Kre 1999] Kremer R., Boudrioua **A.**, Loulergue J.C. and Iltis A., "Effective nonlinear coefficients of organic powders measured by second harmonic generation in total reflection: numerical and experimental analysis", *J. Opt. Soc. Am. B*, 16(1), 83-89 (1999).

[Kre 2003] R. Kremer, A. Boudrioua, P. Moretti and J.C. Loulergue, "Measurements of the non-linear d_{33} coefficients of light-ion implanted lithium niobate by second harmonic generation in total reflection geometry", *Optics Communication*, 219, 389-393 (2003)

[Lau 1990] Laurell F., Second harmonic and sum-frequency generation in lithium niobate waveguides, PhD Thesis (1990).

[Lau 1992] Laurell F., Roelofs M.G. and Hsiung H., "Loss of optical nonlinearity in proton-exchanged $LiNbO_3$ waveguides", *Appl. Phys. Lett*., 60(3), 301-303 (1992).

[Lau 1999] Laurell F., "Periodically poled materials for miniature light sources", *Optical Materials*, 11, 235-244 (1999).

[Mag 1990] Magel G. A.,. Fejer M. M,. Byer R. L, "Quasi-phase-matched second harmonic generation of blue light in periodically poled $LiNbO_3$", *Appl. Phys. Lett*., 56, 108-110 (1990).

[Mar 1994] Marcou J., *Les fibres optiques plastiques: mise en oeuvre et applications*, Clube Fibres optiques plastiques (1994).

[Mic 1992] De Micheli M.P., "Guided wave nonlinear optics", in D.B. Ostrowsky and R. Reinisch (Eds.), *Second Harmonic Generation in Cerenkov Configuration*, Kluwer Academic Publishers (1992).

[Mil 1998] Miller G.D., Periodically poled lithium niobate: modelling, fabrication, and nonlinear-optical performance, PhD Thesis, Stanford University, USA (1998).

[Miy 1979] Miyazawa K., "Ferroelectric domain inversion in titane diffused $LiNbO_3$ optical waveguide", *J. Appl. Phys*., 50(7), 4599-4603 (1979).

[Miz 1996] Mizuuchi K., Yamamoto K., and Kato K., "Harmonic blue light generation in bulk periodically poled MgO:$LiNbO_3$", *Electron. Lett*., 22, 2091-2092 (1996).

[Mol 2001] Molva E., *Une histoire de diode bleue*, Photoniques, 1, 28-35 (2001).

[Mou 2002] Mouras R., Etude par spectroscopie Raman de l'effet des défauts sur les propriétés vibrationnelles, photoréfractives et electro-optiques des cristaux de niobate de lithium purs et dopés, PhD Thesis, University of Metz (2002).

[Mye 1995] Myers L. E., Eckardt R. C., Fejer M., Byer R. L., Bosenberg W. R. and Pierce J. W., "Quasi-phase-matched optical parametric oscillators in bulk periodically poled $LiNbO_3$", *J. Opt. Soc. Am. B*, 11(12), 2102-2116 (1995).

[Nak 1990] Nakamura K., Shimizu H., "Ferroelectric inversion layers formed by heat treatment of proton exchanged $LiTaO_3$", *Appl. Phys. Lett*., 56(16), 1535-1536 (1990).

[Nak 1997] Nakamura S. and Fasol G., *The Blue Laser Diode*, Springer (1997).

[Nas 1965] Nassau K., Levinstein H.J. and Loiacono G.M., "The domain structure and etching of ferroelectric lithium niobate", *Appl. Phys. Lett*., 6(11), 228-229 (1965).

[Nas 1965] Nassau K., Levinstein H.J., "Ferroelectric behavior of lithium niobate", *Appl. Phys. Lett*., 7(3), 69-70 (1965).

[Nis 1989] Nishihara H., Haruna M. and Suhara T., *Optical Integrated Circuits*, McGraw-Hill, (1989).

[Nut 1992] Nutt A.C.G, Gopalan V. and Gupta M.C., "Domain inversion in $LiNbO_3$ using direct electron-beam writing", *Appl. Phys. Lett*., 60(23), 2828-2830 (1992).

[Pli 1998] Pliska T., Fluck D., Günter P., Beckers L. and Buchal C., "Linear and nonlinear optical properties of $KNbO_3$ ridge waveguides", *J. Appl. Phys*., 84(3), 1186-1190 (1998).

[Pro 1990] Prokhorov A.M. and Kuz'minov Y.S., *Physics and Chemistry of Lithium Niobate*, Taylor & Francis (1990).

[Pru 1996] Pruneri V., Electric field periodicallyu inverted $LiNbO_3$ for optical frequency conversion, PhD Thesis, Southampton University, UK (1996).

[Res 2000] Restoin C., Darraud-Taupiac C., Decossasa J.L., Vareille J.C., Hauden J., "Ferroelectric-domain-inverted gratings by electron beam on $LiNbO_3$", *Materials Science in Semiconductor Processing*, 3, 405-407 (2000).

[Rid 1997] Ridah A., Bourson P., Fontana M. D. and Malovichko G. "The composition dependence of the Raman spectrum and new assignment of the phonons in $LiNbO_3$", *J. Phys. Condens. Matter*, 9, 9687-9693 (1997).

[Sal 1991] Saleh Bahaa E.A. and Teich MC., *Fundamentals of Photonics*, Wiley Interscience Publication, (1991).

[San 1999] Sanchez F., *Optique non linéaire*, Ellipse (1999).

[Son 2002] Sones C.L., Mailis S., Brocklesby W.S., Eason R.W. and Owen J.R., "Differential etch rates in z-cut $LiNbO_3$ for variable HF/HNO_3 concentrations", *J. Mater. Chem.*, 12, 295-298 (2002).

[Sut 1995] Sutheland R.L., *Handbook of Nonlinear Optics*, United Press of America (1995).

[Tie 1971] Tien P.K., Ulrich R. and Martin R.J., "Optical second harmonic generation in from of Cerenkov radiation from thin-film waveguide", *Appl. Phys. Lett*., 19, 266-267 (1971).

[Tou 1999] Tournié E., *Les diodes lasers bleu-UV; état de l'art*, Optique et Photonique, 19-25 (1999).

[Vin 2003] Vincent B., Conversion de fréquances dans les guides d'ondes fabriqués par implantation ionique des cristaux périodiquement polarisés, PhD Thesis, University of Metz (2003).

[Vin 2005] Vincent B., Boudrioua A., Kremer R. and Moretti P., "Second harmonic generation in He+- implanted periodically poled $LiNbO_3$ wavegudies", *Optics Communication*, 247(4-6), 461-469 (2005).

[Web 1993] Webjörn J., Siala S., Nam D.W., Waarts R.G. and Lang J., "Visible laser sources based on frequency doubling in nonliear waveguides", *IEEE Journal of Quantum Electronics*, 33(10), 1673-1686 (1993).

[Xue 2002] Xue D., and Kitamura K., "Dielectric characterization of the defect concentration in lithium niobate single crystals", *Solid State Communications*., 122, 537-541 (2002).

[Yar 1973] Yariv A., "Coupled-mode theory for guided wave optics", *IEEE J. of Quantum Electronics*, 9(9), 919-933 (1973).

[Yar 1984] Yariv A. and Yeh P., *Optical Waves in Crystal*, New York (1984).

[Zha 1992] Zhang I., Chandler P. J., Townsend P. D., Alwahabi Z. T. and McCaffery J., "Second harmonic gneneration in ion implanted $KTiOPO_4$ planar waveguides", *Electronics Letters*, 28(16), 1478-1480 (1992).

[Zub 2001] Zubia J. and Arrue J., "Plastic optical fibers: an introduction to their technological processes and applications", *Optical Fiber Technology*, 7, 101-140 (2001).

Chapter 5

The Electro-optic Effect in Waveguides

5.1. Introduction

The development of functional systems for telecommunications and signal processing via optical means requires, amongst other things, the modulation of the signal used. This modulation can be internal in the case of laser diodes, achieved by adjusting current and temperature [Tam 1990]. It can also be external using physical phenomena such as the electro-optic (EO) effect and the acousto-optic effect [Gün 1987, Nis 1989, San 1999, Tur 1966, Yar 1984]. The modulation by electro-optic effect allows an ultrarapid modulation, which provides a wide band of transmission. It also allows the development of integrable structures, functioning with low power command signals.

The electro-optic effect consists of modifying the refractive index of the guiding medium by applying an external electric field. For that reason, numerous electro-optic materials have formed the subject of several important researches. Thus, dielectrics are in current usage due to their outstanding electro-optic properties. The utilization of these materials in integrated optics, where the light wave propagates in a medium of a few micrometers in thickness, requires the knowledge of the electro-optic properties of these materials in thin layer configuration.

In this chapter, we will first mention the theoretical tools necessary for understanding this non-linear optic effect; we will then describe the different techniques for measuring electro-optic coefficients currently in use. We will finish the chapter with a few examples of integrated optic devices using the EO effect.

5.2. The electro-optic effect

In the following, we take a particular interest in the linear electro-optic effect, also called Pockels effect. In this case, the refractive index of the material varies linearly according to the electric field applied. This effect usually exists only in non-centrosymmetric crystals, such as lithium niobate [Nis 1989, Gün 1987, San 1999, Tam 1990, Yar 1984].

The optical properties of an anisotropic medium are generally characterized by its 3x3 symmetric dielectric tensor. In a system formed by the proper axes of the crystal, the tensor can be written as [Sal 1991, Vog 1987]:

$$[\varepsilon] = \begin{bmatrix} \varepsilon_{11} & 0 & 0 \\ 0 & \varepsilon_{22} & 0 \\ 0 & 0 & \varepsilon_{33} \end{bmatrix} \qquad [5.1]$$

In such a crystal, the relation between the electric field vector $\vec{E}$ and the induction vector $\vec{D}$ can be written as:

$$\vec{D} = \varepsilon_0 [\varepsilon] \vec{E} \qquad [5.2]$$

where ε_0 is the dielectric vacuum permittivity, and $[\varepsilon]$ is the tensor of the relative dielectric permittivity of the medium.

The density of the electric energy within the waveguide is written:

$$U = \frac{1}{2} \vec{E}\vec{D} = \frac{\varepsilon_0}{2} \sum_{ij} \varepsilon_{ij} E_i E_j = \frac{1}{2\varepsilon_0} \sum_{ij} \varepsilon_{ij}^{-1} D_i D_j \qquad [5.3]$$

or:

$$\sum_{ij} \left(\frac{1}{n_{ij}^2} \right) D_i D_j = 2\varepsilon_0 U \qquad [5.4]$$

By replacing $\frac{\vec{D}}{\sqrt{2U\varepsilon_0}}$ with $\vec{r}$, we can define the ellipsoid of the indices:

$$\sum_{ij}\left(\frac{1}{n_{ij}^2}\right)x_i x_j = 1 \qquad [5.5]$$

In the principal axes system of the material this relation becomes:

$$\frac{D_x{}^2}{n_x^2}+\frac{D_y{}^2}{n_y^2}+\frac{D_z{}^2}{n_z^2}=2\varepsilon_0 U \qquad [5.6]$$

$$\frac{x^2}{n_x^2}+\frac{y^2}{n_y^2}+\frac{z^2}{n_z^2}=1 \qquad [5.7]$$

where $\varepsilon_{jj}=n_j^2$ and j=x,y,z .

The half axes of this ellipsoid, according to x, y and z, are equivalent to the proper indices of the crystal, n_x, n_y and n_z, respectively. In the presence of an applied electric field, $\vec{E}^a$, the index ellipsoid is modified. It can be expressed using relation [5.5] as [Vog 1987]:

$$\sum_{ij}\Delta\left(\frac{1}{n\left(\vec{E}^a\right)_{ij}^2}\right)x_i x_j = 1 \qquad [5.8]$$

The linear electro-optic effect is described by the variation of the index ellipsoid. Generally, the dimensions of the ellipsoid as well as its orientation in space can also be modified.

$$\sum_{ij}\Delta\left(\frac{1}{n\left(\vec{E}^a\right)_{ij}^2}\right)-\Delta\left(\frac{1}{n(0)_{ij}^2}\right)=r_{ij\,k}E_k^a \qquad [5.9]$$

By combining the two equations [5.7] and [5.9], we can write:

$$\left(\frac{1}{n_x^2}+r_{1k}E_k^a\right)x^2+\left(\frac{1}{n_y^2}+r_{2k}E_k^a\right)y^2+\left(\frac{1}{n_z^2}+r_{3k}E_k^a\right)z^2 + 2r_{4k}E_k^a yz+2r_{5k}E_k^a zx+2r_{6k}E_k^a xy=1 \qquad [5.10]$$

or:

$$\Pi_{11}x^2 + \Pi_{22}y^2 + \Pi_{33}z^2 + 2\Pi_{23}yz + 2\Pi_{31}zx + 2\Pi_{12}xy = 1 \qquad [5.11]$$

with:

$$\Pi_{ij} = \Delta\left(\frac{1}{n^2_{ij}}\right) \qquad [5.12]$$

i,j = x, y, z

The constants Π_{ij} are linked to the applied electric field by the relation:

$$\Pi_{ij} = \Delta\left(\frac{1}{n^2}\right)_i = \sum_{j=1}^{3} r_{ij}E_j^a \qquad [5.13]$$

where: r_{ij} are the electro-optic coefficients of the material, and i = 1, 2, 3, 4, 5, 6 and j = 1, 2, 3 are associated with x, y and z respectively, in the contracted notation of Voigt:

$$11 \rightarrow 1,\ 22 \rightarrow 2,\ 33 \rightarrow 3,\ 23 \rightarrow 4,\ 13 \rightarrow 5,\ 12 \rightarrow 6$$

Finally, the constants Π_{ij} are linked to the applied electric field by the following tensorial relation [Pap 1975, Sal 1991, Vog 1987]:

$$\begin{bmatrix} \Pi_{11} - \dfrac{1}{n_x^2} \\ \Pi_{22} - \dfrac{1}{n_y^2} \\ \Pi_{33} - \dfrac{1}{n_z^2} \\ \Pi_{23} \\ \Pi_{31} \\ \Pi_{12} \end{bmatrix} = \begin{bmatrix} r_{11} & r_{12} & r_{13} \\ r_{21} & r_{22} & r_{23} \\ r_{31} & r_{32} & r_{33} \\ r_{41} & r_{42} & r_{43} \\ r_{51} & r_{52} & r_{53} \\ r_{61} & r_{62} & r_{63} \end{bmatrix} \begin{bmatrix} E_x \\ E_y \\ E_z \end{bmatrix} \qquad [5.14]$$

This relation determines the variation of the refractive index induced by the application of an electric field via the Pockels effect, expressed by the electro-optic coefficients r_{ij}.

Thus, the EO effect modifies the birefringence of a medium with the help of an electric field applied to the sample. This first-order non-linear phenomenon can also be analyzed with the expression of the material polarization developed in Chapter 4. In fact, the polarization of a medium containing the foundation of two fields, one optic the other electric, is written:

$$P_i = \varepsilon_0 \chi_{ij} E_j + \varepsilon_0 \chi^{(2)}_{ijk} \left(E_j E^a_k + E^a_j E_k \right) \qquad [5.15]$$

E is the optic field and E^a the applied electric field, which is often a static field or owns a frequency clearly inferior to the optical frequency. In this case the relation is written [5.2]:

$$D_i = \varepsilon_0 \left(1 + \chi_{ij}\right) E_j + 2\varepsilon_0 \chi^{(2)}_{ijk} E^a_k E_j = \left[\varepsilon_0 \left(1 + \chi_{ij}\right) + 2\varepsilon_0 \chi^{(2)}_{ijk} E^a_k \right] E_j \qquad [5.16]$$

From this equation, we can write the tensor of the dielectric permittivity of the medium:

$$\varepsilon_{ij} = \left(1 + \chi_{ij}\right) + 2\chi^{(2)}_{ijk} E^a_k \qquad [5.17]$$

This equation combined with [5.9] provides a relation between Pockel's electro-optic coefficients and the second order susceptibility in the principal axes system:

$$r_{ijk} = -\frac{2\varepsilon_0}{\varepsilon_{ii}\varepsilon_{jj}} \chi^{(2)}_{ijk} = -\frac{2}{n^4} \chi^{(2)}_{ijk} \qquad [5.18]$$

For this purpose, we write: $\left(\frac{1}{n^2}\right)_{ij} = \varepsilon_0 \eta_{ij}$ and we use the rules for inverted matrices:

$$\begin{aligned} \eta_{ii} &= \left(\varepsilon_{ii}\right)^{1} \\ \eta_{\substack{ij \\ i \neq j}} &= \frac{-\varepsilon_{ij}}{\varepsilon_{ii}\varepsilon_{jj}} \end{aligned} \qquad [5.19]$$

In practice, the choice of the direction of the applied electric field is essential. That is due to the fact that many electro-optic materials, such as $LiNbO_3$, GaAs and $LiTaO_3$, have more important electro-optic coefficients for some orientations rather than for others.

Note: the analysis of the electro-optic effect can also be carried out in a heuristic and simplified way by considering the development of the Taylor series of the refractive index, according to the applied field. In fact, we can write:

$$n(E) = n(0) + c_1 E + c_2 E^2 + ... \qquad [5.20]$$

The coefficients of the series are given by:

$$c_1 = \left.\frac{dn}{dE}\right|_{E=0} \quad \text{et} \quad c_2 = \left.\frac{d^2 n}{dE^2}\right|_{E=0} \qquad [5.21]$$

Besides, we define the inverse permittivity of the medium by:

$$\eta = \frac{\varepsilon_0}{\varepsilon} = \frac{1}{n^2} \qquad [5.22]$$

The latter depends on the electric field applied through the variation of the refractive index. So, we can write:

$$\Delta\eta = \frac{d\eta}{dn}\Delta n = -\frac{2}{n^3}\left(c_1 E + c_2 E^2 + ...\right) \qquad [5.23]$$

It is then possible to introduce two new coefficients:

$$r = -\frac{2c_1}{n^3} \quad \text{and} \quad s = -\frac{2c_2}{n^3} \qquad [5.24]$$

which allow us to write, from [5.23]:

$$\eta(E) = \eta(0) + rE + sE^2 + ... \qquad [5.25]$$

Thus, these linear r and quadratic s electro-optic coefficients exhibit proportionality between the variation $\Delta\eta$ and the E and E^2.

Under these conditions, relation [5.20] becomes:

$$n(E) = n(0) - \frac{1}{2} r n^3 E - \frac{1}{2} s n^3 E^2 + ... \qquad [5.26]$$

This equation allows us to define the Pockels effect using:

$$n(E) = n - \frac{1}{2} r n^3 E \qquad [5.27]$$

Note that the EO coefficients generally depend on the frequency of the applied electric field, on the optic wave and in some cases on the temperature of the crystal. Numerous materials also feature piezoelectric properties which influence their EO characteristics by the inverted piezoelectric effect which induces a variation of the index by photoelastic effect. In this case, we distinguish the EO coefficient at constant strain r^T (low frequencies) and the EO coefficient at constant deformation r^S (for modulation frequencies higher than the acoustic frequencies).

$$r_{ij}^T = r_{ij}^S + [p]\,[d]$$

$[p]$ and $[d]$ are photoelastic and piezoelectric tensors, respectively. However, the EO coefficient r^S due to the authentic EO effect is predominant for modulation frequencies higher than 1 kHz. In this case, the piezoelectric contribution can be neglected.

For the remainder of this chapter, the case of $LiNbO_3$ will be the subject of particular attention, because it represents the most important EO material and many optical integrated components based on this crystal are available on the market.

5.2.1. *The case of $LiNbO_3$*

Lithium niobate is certainly one of the materials featuring the most important Pockels effect. It is very often used in integrated optics to make phasors, commutators or separators of polarization states [Alf 1980, Alf 1982, Alf 1987, Ari 2004, Leo 1980, Woo 2000]. This negative uniaxial crystal owns a trigonal symmetry. In its proper system *oxyz*, with the following optic axis *oz*, its electro-optic tensor is written [Ari 2004, Nis 1989]:

$$[r_{ij}] = \begin{bmatrix} 0 & -r_{22} & r_{13} \\ 0 & r_{22} & r_{13} \\ 0 & 0 & r_{33} \\ 0 & r_{51} & 0 \\ r_{51} & 0 & 0 \\ -r_{22} & 0 & 0 \end{bmatrix} = \begin{bmatrix} 0 & -6.8 & 9.6 \\ 0 & 6.8 & 9.6 \\ 0 & 0 & 30.9 \\ 0 & 32.6 & 0 \\ 32.6 & 0 & 0 \\ -6.8 & 0 & 0 \end{bmatrix} \text{(pm/V)} \qquad [5.28]$$

The most important terms are r_{13} and r_{33}. Under these conditions, equation [5.10] becomes:

$$\left(\frac{1}{n_0^2} - r_{22}E_y + r_{13}E_z\right)x^2 + \left(\frac{1}{n_0^2} + r_{22}E_y + r_{13}E_z\right)y^2 + \left(\frac{1}{n_e^2} + r_{33}E_z\right)z^2 + 2r_{51}E_y yz + 2r_{51}E_x xz - 2r_{22}E_x zx = 1 \quad [5.29]$$

Note that according to the orientation of the electric field, we obtain either singular terms or cross terms, which intervene in the change of the refractive index (which we will discuss later).

5.2.1.1. *The electric field* $\vec{E} \,//\, O\vec{z} \,//\, \vec{c}$

We consider a Y-cut $LiNbO_3$ crystal. The electric field is applied parallel to the optical axis $\vec{C}$ using two electrodes deposited on the surface of the sample (Figure 5.1). In this case, the field $\vec{E}$ has only one component E_z ($E_x = E_y = 0$), and equation [5.29] becomes:

$$\left(\frac{1}{n_0^2} + r_{13}E_z\right)x^2 + \left(\frac{1}{n_0^2} + r_{13}E_z\right)y^2 + \left(\frac{1}{n_e^2} + r_{33}E_z\right)z^2 = 1 \quad [5.30]$$

This equation represents an ellipsoid whose principal axes are associated with the proper indices of the crystal.

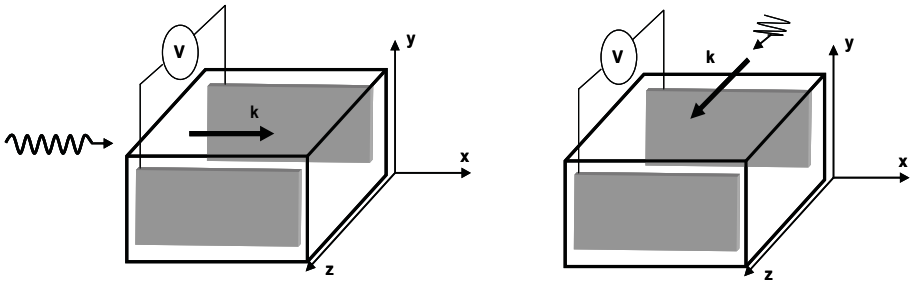

(a) $\vec{k} \perp \vec{E} \,//\, \vec{C}$. (b) $\vec{k} \,//\, \vec{E} \,//\, \vec{C}$.

Figure 5.1. *Pockels effect in a Y-cut $LiNbO_3$ crystal*

In this configuration, only the two coefficients r_{13} and r_{33} intervene, thus creating a deformation of the ellipsoid of the indices. However, the propagation direction of the light wave in the crystal determines which of the two indices comes into play.

5.2.1.1.1. Transversal configuration – wave vector $\vec{k} \perp \vec{E}$ $(\vec{k} \perp \vec{c})$

The propagation of the wave occurs according to the Ox axis (Figure 5.1a). In this case, $x = 0$ ($D_x = 0$) and the plane of polarization of the wave is the ellipse obtained by the intersection with the index ellipsoid, of a plane passing through the origin perpendicular to Ox (see Figure 5.2). It is defined by the following relation:

$$\left(\frac{1}{n_0^2} + r_{13}E_z\right)y^2 + \left(\frac{1}{n_e^2} + r_{33}E_z\right)z^2 = 1 \qquad [5.31]$$

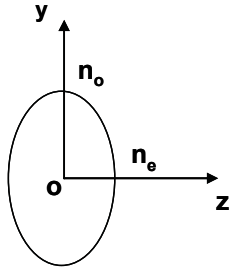

Figure 5.2. *Ellipse of the polarization of the optical wave propagating perpendicularly to the optical axis*

According to the polarization of the wave (*TE* or *TM*), we distinguish two possible situations. In the case of a *TM* polarization, the electric field of the wave is parallel *Oy*, and is thus perpendicular to the optical axis $\vec{c}$ of the crystal.

We find:

$$n_x(E) = n_y(E) = n_o(0) - \Delta n_o \qquad [5.32]$$

So: $$n_o(E) = n_o - \frac{1}{2}n_o^3 r_{13}E_z \qquad [5.33]$$

In the case of a *TE* polarization, the electric field of the wave is parallel to the optical axis $\vec{c}$ of the crystal (// to the Oz axis). By using the same analysis previously developed, we find:

$$n_z(E) = n_e(0) - \Delta n_e \qquad [5.34]$$

$$n_e(E) = n_e - \frac{1}{2} n_e^3 r_{33} E_z \qquad [5.35]$$

In this case, a variation of the extraordinary index occurs, via the electro-optic effect, by means of the electro-optic coefficient r_{33}. It is the most important Pockels effect in $LiNbO_3$.

5.2.1.1.2. Longitudinal configuration – wave vector $\vec{k} \,//\, \vec{E}$ $(\vec{k} \,//\, \vec{c})$

In this case (see Figure 5.1b), $D_z = 0$, thus $z = 0$. The plane of wave polarization is a circle defined by the intersection with the index ellipsoid of a plane perpendicular to *Oz* passing through the origin (see Figure 5.3). It is defined by the following relation:

$$\left(\frac{1}{n_0^2} + r_{13} E_z\right) x^2 + \left(\frac{1}{n_0^2} + r_{13} E_z\right) y^2 = 1 \qquad [5.36]$$

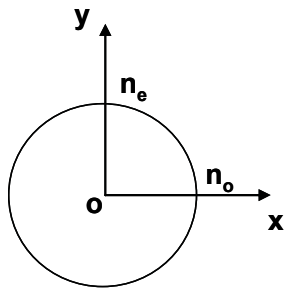

Figure 5.3. *Plane of optical wave polarization propagation parallel to the optical axis*

In this configuration, regardless of the wave polarization (*TE* or *TM*), its electric field remains perpendicular to the axis $\vec{c}$. Consequently, the wave has a new refractive index n_x or n_y ($n_x = n_y$) which depends only on the ordinary index and is written:

$$n_x = n_y = n_o \left(1 + n_o^2 r_{13} E_z\right)^{1/2} \qquad [5.37]$$

As the term $n_o^2 r_{13} E_z$ is very small, we can write:

$$n_x(E) = n_y(E) = n_o(0) - \Delta n_o \qquad [5.38]$$

with:

$$\Delta n_o = \frac{1}{2} n_o^3 r_{13} E_z \qquad [5.39]$$

This equation represents the variation of the index, via the Pockels effect, determined by the electro-optic coefficient r_{13} and the amplitude of the electric field applied.

In short, in both cases the x, y and z axes always coincide with the principal axes of the crystal because no cross term intervenes. In other words, the index ellipsoid only undergoes dilatation (see Figure 5.4), thus creating a variation of the birefringence of the material. It is also interesting to note that the sign of the refractive index variation depends on the polarity of the voltage applied. The maximum value of the index variation is in the order of 1.6 x 10^{-3}. This corresponds to the electric field of the crack in lithium niobate (10V/m) [Nis 1989, Sal 1991].

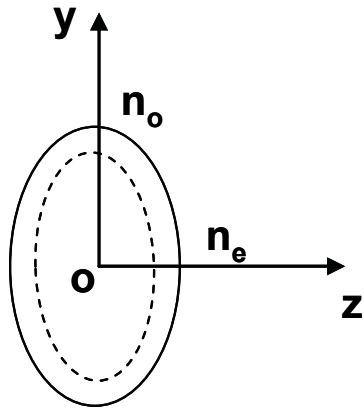

Figure 5.4. *Meridian section of the index ellipsoid with and without the electric field E parallel to the optical axis*

5.2.1.2. *The electric field* $\vec{E} \perp \vec{c}$

This configuration is very rarely used because the electro-optic coefficients involved are low and without any practical interest. However, we will discuss the broad lines. Let us consider the case of a Y-cut crystal where the electric field is

applied according to the *Oy* axis. In this case, the component E_y is not zero and the optical indicator can be written, based on equation [5.30], as follows:

$$\left(\frac{1}{n_0^2} + r_{22}E_y\right)y^2 + +\left(\frac{1}{n_e^2}\right)z^2 + 2r_{51}E_y yz = 1 \qquad [5.40]$$

As coefficient Π_{23} is different from zero, the axes *x, y, z* do not coincide with the eigen axes of the crystal any longer. Consequently, a rotation of the axes *y* and *z* of an angle θ_{eo}, allows us to eliminate the cross term in *yz* from the previous equation. Thus, the system of the eigen axes *Oxyz* is converted into a new system *OxYZ* according to the following relation [Nis 1989, Sal 1991]:

$$\begin{bmatrix} x \\ Y \\ Z \end{bmatrix} = \begin{bmatrix} 1 & 0 & 0 \\ 0 & \cos\theta_{eo} & -\sin\theta_{eo} \\ 0 & \sin\theta_{eo} & \cos\theta_{eo} \end{bmatrix} \begin{bmatrix} x \\ y \\ z \end{bmatrix} \qquad [5.41]$$

Axes *x, Y* and *Z* are now the new principal axes of the index ellipsoid of the crystal, which can be written:

$$\frac{Y^2}{n_y^2} + \frac{Z^2}{n_z^2} = 1 \qquad [5.42]$$

with the angle of rotation given by the following relation:

$$\tan 2\theta_{eo} = \frac{2r_{51}E_y}{\left(n_e{}^2 - n_o{}^2\right)} \qquad [5.43]$$

Finally, we find:

$$\begin{aligned} n_y &= n_o - \frac{1}{2}n_o^3 r_{22}E_y + \frac{1}{2}n_o^3 r_{51}E_y \tan 2\theta_{eo} \\ n_z &= n_e - \frac{1}{2}n_e^3 r_{51}E_y \tan 2\theta_{eo} \end{aligned} \qquad [5.44]$$

In the case of $LiNbO_3$, the electro-optic coefficient r_{22} is low and the factor $tan\theta_{eo}$ is very small. Consequently, the variation of the refractive indices n_y and n_z can be neglected. So, we can write:

$$\begin{aligned} n_y &\approx n_o \\ n_z &\approx n_e \end{aligned} \qquad [5.45]$$

In fact, in this configuration, there is a rotation of the index ellipsoid around the axis *Ox* (see Figure 5.5). The dielectric tensor of the crystal after rotation becomes:

$$[\varepsilon] = \begin{bmatrix} \varepsilon_{11} & 0 & 0 \\ 0 & \varepsilon_{22} & \delta\varepsilon_{23} \\ 0 & \delta\varepsilon_{23} & \varepsilon_{33} \end{bmatrix} \qquad [5.46]$$

Under the previously described conditions, and for $\theta_{eo} << 1$, the components of the dielectric tensor are written:

$$\begin{aligned} \varepsilon_{11} &= \varepsilon_{22} \approx n_o^2 \\ \varepsilon_{33} &\approx n_e^2 \\ \delta\varepsilon_{23} &= -n_o^2 n_e^2 r_{51} E_y \end{aligned} \qquad [5.47]$$

This induces a variation of the polarization of the crystal, according to the axis *Oz* given by the following relation:

$$\delta P_z = \varepsilon_0 \delta\varepsilon_{23} E_y^{op} \qquad [5.48]$$

This equation shows that the variation of the polarization of the extraordinary wave is induced by the electric field of the ordinary wave, E_y. In other words, the rotation of the index ellipsoid produces a coupling between the two polarizations, ordinary and extraordinary. This phenomenon is used for *TE-TM* mode conversion in integrated optics [Sal 1991].

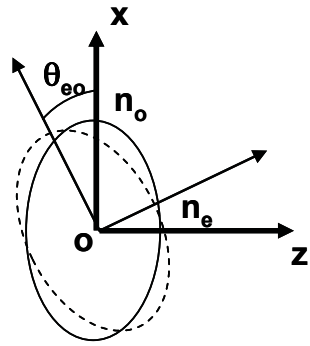

Figure 5.5. *Meridian section of the index ellipsoid with and without the electric field E perpendicular to the optical axis*

Other configurations of the applied electric field and of the optic wave propagation, which involve the coefficients r_{22} and r_{51} can be considered.

Finally, the two most used electro-optic coefficients in lithium niobate are r_{13} and r_{33}. In the following section, we will mention the principal measurement or waveguides EO coefficient measurement techniques.

5.3. The electro-optic effect in waveguides

The whole analysis developed in the previous sections remains valid in the case of a guiding structure. However, two major differences are to be considered. On the one hand, light propagation in the guides occurs according to guided modes and thus as seen in Chapter 1, the dispersion equation allows us to determine the effective indices of the structure as well as the profile of the optical field in the guide. On the other hand and even more importantly, integrated optics uses coplanar electrodes. In fact, the applied electric field is created in the guide by the application of a voltage between the two electrodes deposited on its surface. This is represented in Figure 5.6, which is valid regardless of the configuration of the material used: Y-cut or Z-cut. However, for Z-cut guides, two electrodes in sandwich configuration can be more appropriate because the electric field within the guide is obtained directly by the relation:

$$E_{el} = \frac{V}{d} \qquad [5.49]$$

where d is the thickness of the sample and V the voltage applied.

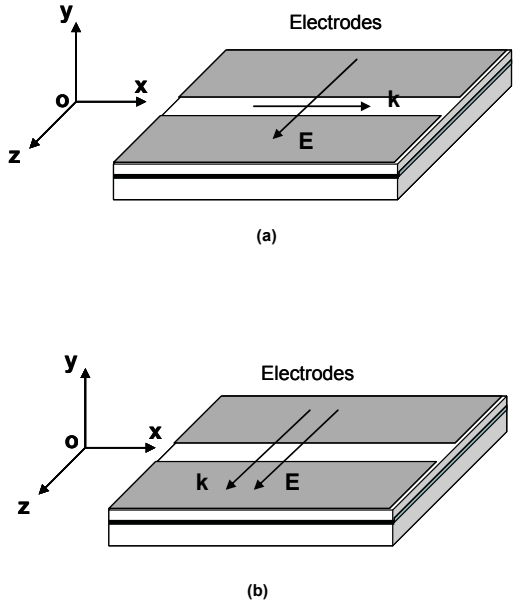

Figure 5.6. *Configurations of coplanar electrodes used with waveguides d: (a) transversal configuration (b) longitudinal configuration*

For the configuration in Figure 5.5, the distribution of the electric field within the guide is not generally uniform. In this case, the index variation produced by the electro-optic effect is written [Nis 1989, Sal 1991]:

$$\Delta n_i = \frac{1}{2} n_i^3 r_{ij} \Gamma_r \frac{V}{g} \qquad [5.50]$$

with: $i = o, e$. $r_{ij} = r_{13}, r_{33}$ according to the polarization used. g is the interelectrodes distance, and V the applied voltage.

Γ_r is a factor which takes into account the overlap between the electric field and the field of the optical wave. It is given by the following relation [Nis 1989]:

$$\Gamma_r = \frac{\iint E_{op}^2(y,z) E_{el}(y,z) dydz}{\iint E_{op}^2(y,z) dydz} \qquad [5.51]$$

In this situation, determination of the index variation passes requires the analysis of the distribution of the elecric field applied.

5.3.1. *Analysis of the electric field distribution*

The electric field induced in the guiding layer by two electrodes deposited on the surface can be obtained by using several methods widely discussed by Durand [Dur 1953]. The simplest method consists of a conform transformation [Cha 1971, Leo 1980, Kim 1989, Mar 1982, Ram 1982, Van 1974] which we will describe below.

Let us consider the idealized configuration of the electrodes represented in Figure 5.6.

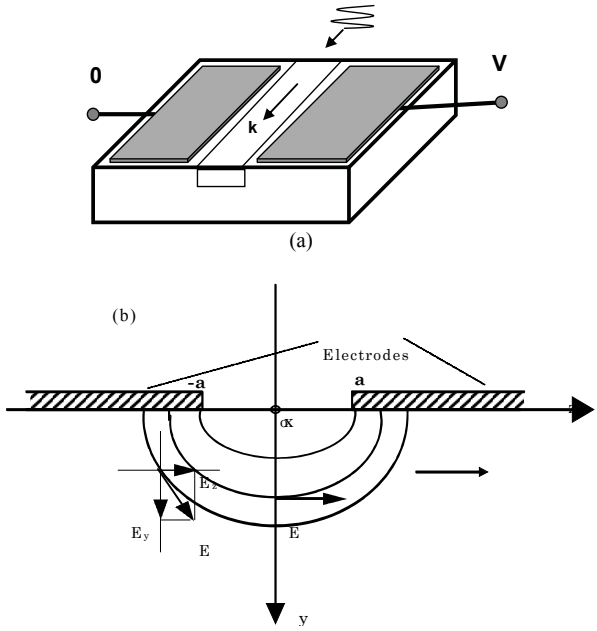

Figure 5.7. *Idealized configuration of the electrodes*

The metallic layers are assumed to be thin and extend from:

$z = -\infty$ to z=-a , and z=a to $z=+\infty$

In the case of a Y-cut $LiNbO_3$ crystal, the dielectric tensor is diagonal and the electrostatic potential V is the solution of Laplace's equation [Dur 1953]:

$$\begin{aligned} &\frac{\partial^2 \mathrm{V}}{\partial \mathrm{z}^2} + \frac{\partial^2 \mathrm{V}}{\partial \mathrm{y}^2} = 0 && \text{for} \quad \mathrm{y} \langle 0 \\ &\varepsilon_z \frac{\partial^2 \mathrm{V}}{\partial \mathrm{z}^2} + \varepsilon_\mathrm{y} \frac{\partial^2 \mathrm{V}}{\partial \mathrm{y}^2} = 0 && \text{for} \quad \mathrm{y} \rangle 0 \end{aligned} \qquad [5.52]$$

Using the following transformation : $y' = \sqrt{\frac{\varepsilon_z}{\varepsilon_\mathrm{y}}}\,\mathrm{y}$, we can write:

$$\frac{\partial^2 \mathrm{V}}{\partial \mathrm{z}^2} + \frac{\partial^2 \mathrm{V}}{\partial \mathrm{y}'^2} = 0 \qquad [5.53]$$

For simplicity, we will keep the notation with y instead of y' ($y = y'$).

In addition to these equations, we have the conditions of continuity through the crystal-air interface, of the normal component of the electric displacement field and the tangential component of the electric field. We also have boundary conditions given by: $V = 0$ and $V = V_\mathrm{a}$ on the two electrodes.

The method of conform recovery consists of transforming the calculation problem of the electrostatic field $E(y, z)$ into a complex plane. For a complex function $W(z)$ given by:

$$W(z) = U(y, z) + iV(y, z) \qquad [5.54]$$

with $z_c = z + iy,$ and according to Cauchy-Riemann's theorem [Dur 1953], we can write:

$$\begin{aligned} &\frac{\partial U}{\partial y} = \frac{\partial V}{\partial z} \\ &\frac{\partial U}{\partial z} = -\frac{\partial V}{\partial \mathrm{y}} \end{aligned} \qquad [5.55]$$

A second derivation of equation [5.54] gives the following relations:

$$\frac{\partial^2 U}{\partial z^2} + \frac{\partial^2 U}{\partial y^2} = 0$$
$$\frac{\partial^2 V}{\partial z^2} + \frac{\partial^2 V}{\partial y^2} = 0 \qquad [5.56]$$

Thus, U and V independently satisfy Laplace's equation. Consequently, the 2D electrostatic field is totally determined by the complex potential function $W(z)$ according to the two following relations:

$$E_z = \frac{V}{\pi} \mathrm{Im} \frac{dW}{dz_c}$$
$$E_y = \frac{V}{\pi} \sqrt{\frac{\varepsilon_z}{\varepsilon_y}} \mathrm{Re} \frac{dW}{dz_c} \qquad [5.57]$$

We can take as a solution the function given by [Mar 1982]:

$$W(z) = \frac{V}{\pi} \arccos\left(\frac{z_c}{a}\right) \qquad [5.58]$$

Finally, the two components of the electric field can be written:

$$E_z = \frac{V}{\pi\sqrt{2}} \frac{\left\{\left(a^2 + y^2 - z^2\right) + \left[a^4 + z^4 + y^4 + 2z^2y^2 + 2a^2\left(y^2 - z^2\right)\right]^{1/2}\right\}^{1/2}}{\left[a^4 + z^4 + y^4 + 2z^2y^2 + 2a^2\left(y^2 - z^2\right)\right]^{1/2}}$$
$$E_y = \frac{V}{\pi\sqrt{2}} \frac{\left\{-\left(a^2 + y^2 - z^2\right) + \left[a^4 + z^4 + y^4 + 2z^2y^2 + 2a^2\left(y^2 - z^2\right)\right]^{1/2}\right\}^{1/2}}{\left[a^4 + z^4 + y^4 + 2z^2y^2 + 2a^2\left(y^2 - z^2\right)\right]^{1/2}} \qquad [5.59]$$

With these two relations, we can study the variation of the two components of the electric fields E_y and E_z according to the depth y (depth of the guide) and the interelectrode distance (z). In fact, the curves (a), (b), (c) and (d) in Figure 5.7 give the results of this study.

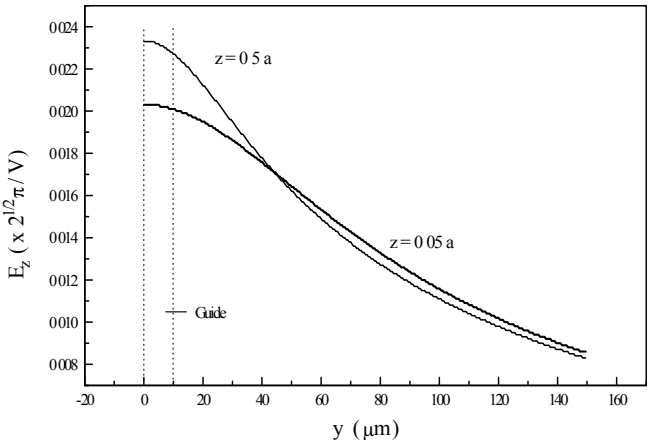
0.024
0.022
0.020
0.018
0.016
0.014
0.012
0.010
0.008
z = 0 5 a
z = 0 05 a
Guide
-20
0
20
40
60
80
100
120
140
160
y (μm)
E_z (x 2^1/2 π / V)

(a)

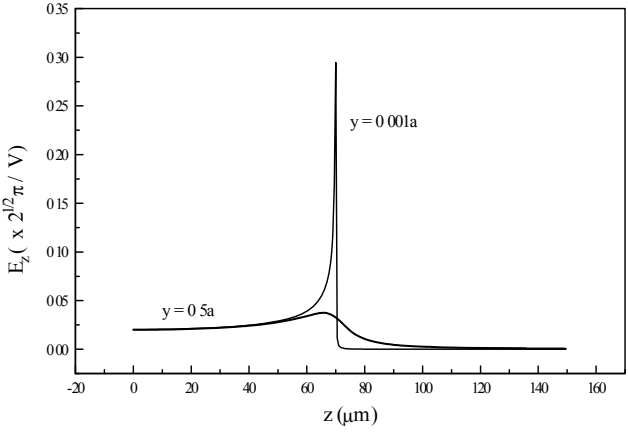
0.35
0.30
0.25
0.20
0.15
0.10
0.05
0.00
y = 0 001a
y = 0 5a
-20
0
20
40
60
80
100
120
140
160
z (μm)
E_z (x 2^1/2 π / V)

(b)

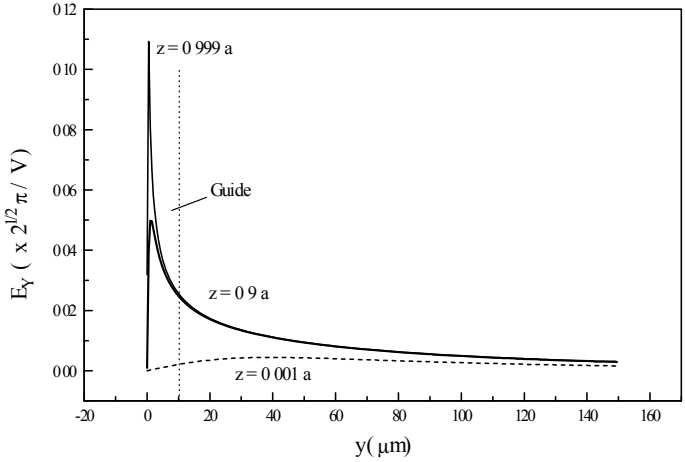

(c)

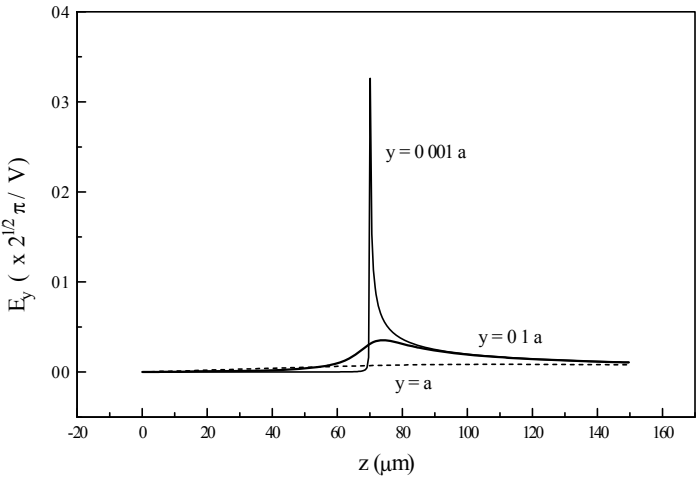

(d)

Figure 5.8. *Variation of the electric field according to the two coordinates y, z: (a) E_z=f(y), (b) E_z = f(z), (c) Ey = f(y), (d) Ey = (z) a = 70 μm*

Note that on the thickness of a guide (<10 μm), component E_z varies very low according to the depth y for any point z between the two electrodes (curve a). Besides, this component does not vary according to z if it is in the middle of the electrodes (curve b).

Regarding component E_y, its variation according to depth is negligible if it is in the middle of the electrodes and it is maximal in their vicinity (point effect) (curve c). In the middle of the electrodes the variation according to z is negligible regardless of the depth y considered.

Moreover, the two expressions [5.59] can be substantially simplified in the planes $y = 0$ and $z = 0$. We obtain for y = 0:

$$\vec{E} \begin{cases} E_z = \dfrac{\mathrm{V}}{\pi\left(\mathrm{a}^2 - z^2\right)^{1/2}} \\ E_y = 0 \end{cases} \qquad [5.60]$$

and in the plane $z = 0$, in the middle of the electrodes, we have:

$$\vec{E} \begin{cases} E_z = \dfrac{\mathrm{V}}{\pi\left(\mathrm{a}^2 + y^2\right)^{1/2}} \\ E_y = 0 \end{cases} \qquad [5.61]$$

These two expressions are in accordance with the curves given above. In other words, we note that component E_z, which intervenes in the EO effect, varies very little in the middle of the electrodes and that component E_y is more significant, especially near the electrodes.

In practice, we can consider that light propagation occurs in the middle of the electrodes (coupling achieved in the middle). Consequently, only the second system of equations [5.61] can be considered. This system of equations obtains the curves in Figure 5.9. They show the variation of component E_z according to the depth (depth of the guide) for different distances between the electrodes.

It is obvious that for interelectrode distances that are relatively more significant compared with the thickness of the guide, this component and consequently the electric field can be considered uniform in the guiding layer.

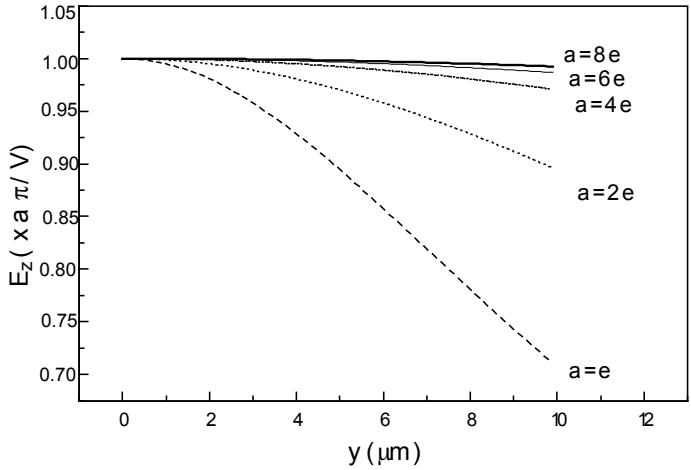

Figure 5.9. *Variation of Ez according to depth y (e: thickness of the guide)*

Equation [5.61] becomes:

$$E_z = \frac{V}{\pi a\left(1+\frac{y^2}{a^2}\right)^{1/2}} \qquad [5.62]$$

As previously indicated, the thickness of the guide is generally low compared with the space between the electrodes ($y << a$). Consequently, we can totally neglect the variation of the electric field in direction Oy and component E_z becomes:

$$E_z = \Gamma V \qquad \text{for} \quad 0 < y \leq e \qquad [5.63]$$

with: $\Gamma = \frac{1}{\pi a}$.

This simple expression allows us to determine the electro-optic coefficients of the guide (of lithium niobate, for example), as we will see later.

In short, with this experimental configuration of electrodes, for guides whose thickness is less that ten micrometers, it is possible to consider the distribution of the

electric field, within the guiding layer, as being uniform and constant according to equation [5.63].

5.4. Electro-optic measurement techniques

The fabrication of integrated electro-optic modulators has led to the development of numerous measurement techniques of electro-optic coefficients in their guiding structures [Bou 1996, Kob 1990]. We can distinguish four principal families:

– the interferometric techniques, particularly those using the Fabry-Perot interferometer [Eld 1991] and the Mach-Zehnder interferometer [Bec 1983];

– the polarimetric techniques, based on the changing of the wave polarization which propagates in the electro-optic medium, also called phase modulation techniques [Iza 1992];

– the angular displacement of guided modes techniques, based on the measurement of the synchronous angle variation during the application of an electric field. It is also the case for the utilization of the attenuated total reflection (ATR) [Den 1989, Her 1991, Mor 1989, Swa 1995];

– the techniques based on directional intermode coupling, which use the fact that the energy transferred from one mode to an adjacent mode depends on the refractive index of the interguide medium [Ten 1988, Kub 1980].

This final technique is seldom used compared to the first three techniques, particularly those based on the Mach-Zehnder interferometer and the angular displacement of guided modes. In the following section, we will describe the principal characteristics of these techniques.

5.4.1. *The Mach-Zehnder interferometer*

This method is the most frequently used [Bec 1983, Kub 1980]. It can be employed with a wide range of materials, polymers or dielectric. It has been widely applied with $LiNbO_3$ waveguides fabricated by diffusion [Won 1982], protonic exchange [Tsa 1988] and lately with He^+ et H^+ implanted guides [Bou 1998, Des 1979, Ree 1987]. This method consists of setting, on the same guiding structure, two paths to guide the light. These two paths work as two arms of an interferometer located between two electrodes deposited on the surface, as shown in Figure 5.10.

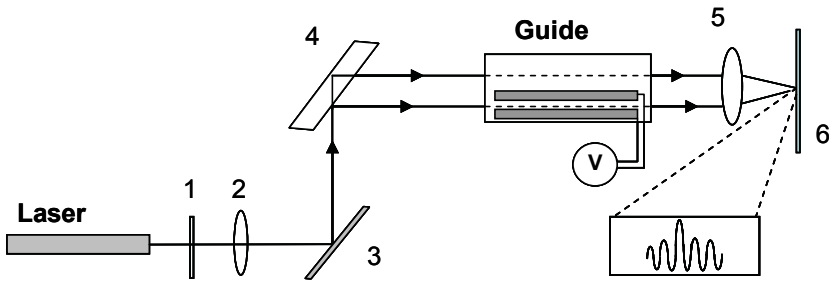

Figure 5.10. *Mach-Zehnder interferometer to measure EO coefficients in guides*

By reducing the diameter of the laser beam, with a setup of lenses, two light waves can be coupled, via a beam splitter, into the two arms of the setup. At the output, we observe the interference phenomenon between the two waves in the focal plane of a converging lens. An enlarging system is used to visualize the interference figure on a screen. A phase mismatch, between the two guided beams, occurs during the application of a voltage via the two electrodes, thus generating a variation of index by the electro-optic effect. This is shown by a displacement of the interference fringes.

By measuring the required voltage for a displacement of a distance equal to an interfringe, one determines V_π, which is linked directly to the electro-optic coefficients of the material. The configuration and the polarization used determine the EO coefficient involved.

In the case of a Y-cut $LiNbO_3$ waveguide, for a *TM* polarization of the light used, the relation between V_π and the electro-optic coefficient r_{13} is given by:

$$V_\pi = \frac{\lambda G}{n_0^3 r_{13} l \Gamma} \qquad [5.64]$$

l: length of the electrodes

G: interval between the electrodes

λ: wavelength used.

where Γ is the factor determining the integral recovery between the optical field and the applied electric field (already discussed in the previous sections).

This technique gives satisfying results and its use is very well known. However, it generally requires a thorough polishing of the edge of the guidewave and a very

accurate alignment of the setup. Besides, it can be used efficiently only with monomode guides.

The first works on the electro-optic $LiNbO_3$ waveguides measured with this technique have shown surprising results. For example, Destefanis et al. [Des 1979] report a reduction r_{13} and r_{33} of 60% in the He^+ and H^+ implanted guides; whereas Reed et al. [Ree 1987] report a degradation of 20% in these guides. In the guides fabricated by diffusion and protonic exchange, the degradation is so large that Becker [Bec 1983] suggest the disappearance of the electro-optic effect in the guiding layer.

However, current improvement brought to fabrication processes of waveguides in $LiNbO_3$ with these three techniques has enabled minimization of the alterations that non-linear optic properties of the guiding region can undergo. This has led to the development and the marketing of integrated electro-optic modulators with a $LiNbO_3$ base, usually used in the optical network.

In addition, this technique is used in the "*m*-line" configuration, that is to say with a prism coupler as shown by Novak et al. [Nov 1995].

5.4.2. *The polarization change technique*

This technique is based on the gap between the two ordinary and extraordinary waves propagating in the waveguide due to the application of an electric field along the optical axis of the crystal which generates a refractive index variation [Iza 1992]. As shown in Figure 5.11, the waveguide is shown between a polarizer and an analyzer crossed at 45° to the optical axis C of the crystal.

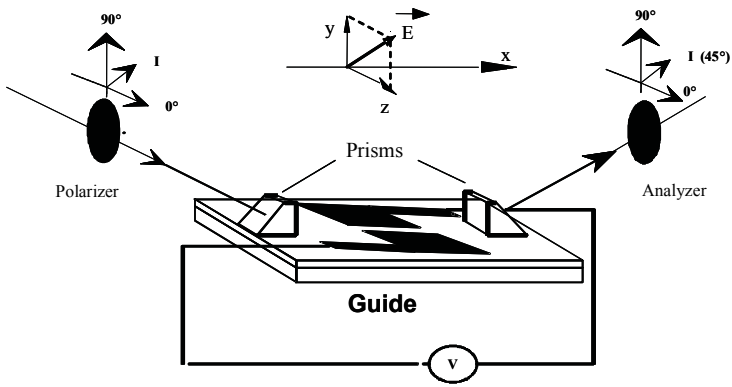

Figure 5.11. *Polarimetric setup*

In the case of a guide of $LiNbO_3$, the light wave polarized at 45° according to the normal splits up into two rays, one ordinary and the other extraordinary, whose optic fields E_y and E_z can, respectively, be written:

$$E_y(t,x) = \frac{E_i}{\sqrt{2}}\cos(\omega t - \varphi_y)$$
$$E_z(t,x) = \frac{E_i}{\sqrt{2}}\cos(\omega t - \varphi_z) \qquad [5.65]$$

where dephasings are given by:

$$\varphi_y = k_0 n_y x = k_0 x\left(n_0 - \frac{1}{2}n_o^3 r_{13} E_{ap}\right)$$
$$\varphi_z = k_0 n_z x = k_0 x\left(n_e - \frac{1}{2}n_e^3 r_{33} E_{ap}\right) \qquad [5.66]$$

Thus, the phase mismatch between the two rays varies according to the distance x by the following formula:

$$\Delta\varphi = \varphi_y - \varphi_z = k_0(n_o - n_e)x + \frac{1}{2}k_0 n_e^3 r_c x E_{ap} \qquad [5.67]$$

with:

$$r_c = r_{33} - \left(\frac{n_o}{n_e}\right)^3 r_{13} \qquad [5.68]$$

(linear combination of r_{ij} coefficients).

Equation [5.65] shows that the electric field vector of the optical wave undergoes a rotation during propagation. As in the previous case, we characterize the setup by V_π voltage, which corresponds, this time, to the voltage which generates a dephasing π between the two ordinary and extraordinary waves. This is given by:

$$V_\pi = \frac{\lambda d}{n_e^3 r_c l} \qquad [5.69]$$

l: guide length

d: distance between electrodes.

The measurement of V_π enables us to deduce the electro-optic coefficient r_c.

For a setup with a prism coupler see (Figure 5.11), the two ordinary and extraordinary waves propagate like two guided *TM* and *TE* modes. This configuration can only be used with a material featuring a very low birefringence. In this case the excitation angles of the *TM* modes can coincide with those of the *TE* modes [Iza 1992, Nov 1995].

In short, this technique does not allow the separate measurement of electro-optic coefficients and its use, with waveguides, is limited to materials with low birefringence.

5.4.3. *Angular displacement of guided modes (AnDiGM) technique*

The principle of this technique has been used in the configuration of attenuated total reflection (ATR) to measure the electro-optic coefficients in thin layers, particularly of polymers [Den 1989, Mor 1989, Swa 1995], of ZnO [Per 1993] and of AlN [Grä 1992]. The same principle has been applied in the *m*-lines configuration (see Figure 5.12) to measure the electro-optic coefficients of protons (H+) implanted $LiNbO_3$ waveguides [Bou 1995, Tsa 1988].

This method is based on the modification of the resonant coupling angles caused by the refractive index variation due to the electro-optic effect. In fact, the angular position of the guided modes depends greatly on the guiding layer refractive index. Consequently, a change in the refractive index introduces a modification of the synchronous angles of the guided modes (and so a variation of their effective indices). Thus, the measurement of the angular displacement of the guided modes enables us to come back to the index variation, which is proportional to the electro-optic coefficients.

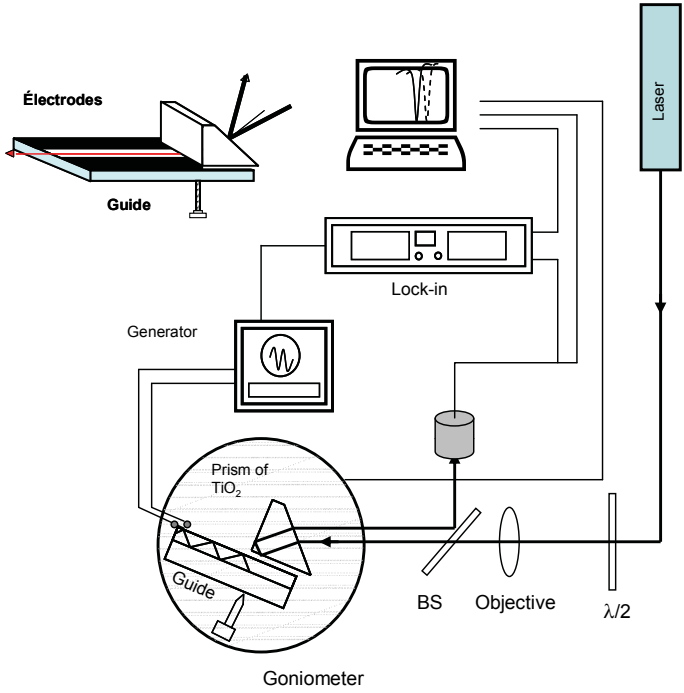

Figure 5.12. *Setup of m-lines for the measure of waveguide EO coefficients*

To apply a voltage on the sample, two very thin and semi-infinite gold electrodes, separated by a gap, 2a = 150 μm, by evaporation of 0.30g of gold (Au) are firstly deposited on the surface of the crystal. To obtain the gap between the electrodes, we use a mask made of a very thin tungsten wire. This choice is purely practical and has no physical consequence.

Firstly, we measure the guided modes spectrum without an electric field. Secondly, we measure again with the application of an electric field. The comparison and the analysis of the two spectra of guided modes obtained enable us to determine the electro-optic coefficients of the guide. This analysis will be presented in the next sections.

The application of the field can be done using a direct or alternative voltage generator. The latter case combined with a Lock-in amplifier gives a better accuracy and does not require the application of high voltage. In fact, the utilization of a static field and the direct measurement of the angular displacement of the guided modes

require the application of high voltage (of the order of 1,000 V). In addition, the sensitivity and therefore the accuracy of this configuration are relatively low.

The following section will be devoted to the calculation of the index variation from the angular displacement of modes.

5.4.3.1. *Relation between the index variation and the angular displacement of modes*

The parameter directly measurable in the *m*-line configuration is the synchronous angle (of coupling) – see Chapter 2. So, the question to ask now is: how can we link the angular displacement with the index modification?

Let Δn and $\Delta\alpha$ be the index and the synchronous angle variations, respectively. We can write:

$$\Delta\alpha_m = \frac{\partial\alpha_m}{dn}\Delta n + \frac{\partial\alpha_m}{de}\Delta e \qquad [5.70]$$

where Δe represents the thickness variation due to the piezoelectric effect, which can intervene during the application of an electric field on a crystal such as $LiNbO_3$.

This relation represents the equation of a straight-line of type $c = ax + by$.

The a and b coefficients are calculated from the mode dispersion equation, developed in Chapter 1, and the geometric optics relations which intervene in prism coupling (see Figure 5.13).

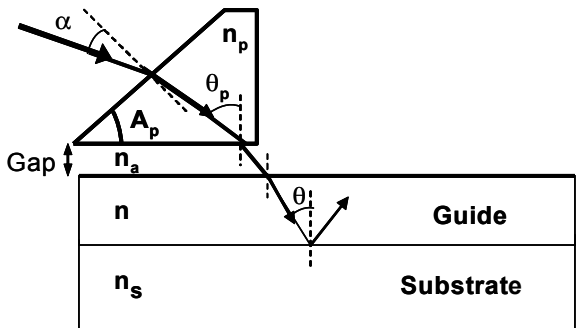

Figure 5.13. *Angular relation in the structure of guide-prism coupling*

From Figure 5.13, we can write:

$$\begin{cases} n_p \sin\phi_m = \sin\alpha_m \\ \theta_p = A_p - \phi_m \\ n\sin\theta_m = n_p \sin\theta_p = N_m \end{cases} \quad [5.71]$$

$$\sin\theta = \frac{n_p}{n}\sin\left[A_p - \arcsin\left(\frac{\sin\alpha}{n_p}\right)\right] \quad [5.72]$$

where θ_m is the synchronous angle in the guide; with, the dispersion equation:

$$kne\cos\theta - \Phi_{(n,,na)} - \Phi_{(n,ns)} = m\pi \quad [5.73]$$

From these considerations we find:

$$\begin{cases} a = \dfrac{\partial\alpha_m}{\partial e} = \dfrac{1}{K_a}\left[\dfrac{k(n\cos\theta)^2}{kne\sin\theta + B}\right] \\ b = \dfrac{\partial\alpha_m}{\partial n} = \dfrac{1}{K_a K_b} \end{cases} \quad [5.74]$$

with:

$$K_a = -\cos\alpha.\left[\cos A_p + \frac{\sin A_p.\sin\alpha}{\sqrt{n_p^2 - \sin^2\alpha}}\right] \quad [5.75]$$

$$K_b = \frac{kne\sin\theta + B}{kne + B\sin\theta - An\cos\theta} \quad [5.76]$$

$$\begin{aligned} A &= \frac{\partial\phi_{(n,na)}}{\partial n} + \frac{\partial\phi_{(n,ns)}}{\partial n} \\ B &= \frac{\partial\phi_{(n,na)}}{\partial\theta} + \frac{\partial\phi_{(n,ns)}}{\partial\theta} \end{aligned} \quad [5.77]$$

$$\Phi_{(n,j)} = 2\arctan\sqrt{\frac{n^2\sin^2\theta - j^2}{n^2 - n^2\sin^2\theta}} \qquad (TE) \qquad [5.78]$$

$$\Phi_{(n,j)} = 2\arctan\sqrt{\frac{n}{j}\left(\frac{n^2\sin^2\theta - j^2}{n^2 - n^2\sin^2\theta}\right)} \qquad (TM) \qquad [5.79]$$

$j = n_a, n_s$
k: the wave vector
A_P and n_p: the angle and the index of the prism coupling, respectively
θ_m: the internal angle and α_m: the external angle.

5.4.3.2. *Determination of EO coefficients*

The setup illustrated in Figure 5.12 enables us to measure the reflected intensity R according to α (the guided modes spectrum), and its variation when a modulated electric field is applied to the sample, at the same time. On the one hand, the variation of the reflected intensity ΔR_{exp} measured directly through Lock-in amplifier detection, can be written:

$$\Delta R_{exp} = \frac{\partial R}{\partial \alpha}\Delta\alpha \qquad [5.80]$$

On the other hand, the calculation of the angular derivative of the guided modes spectrum gives $\frac{\Delta R_{th}}{\Delta\alpha}$. Consequently, we can determine the angular variation as follows:

$$\Delta\alpha_m \quad \frac{\Delta R_{th}}{\Delta R_{exp}} \qquad [5.81]$$

By assuming that the modulation of the voltage only induces a translation of the guided peak and does not modify its shape, we can evaluate from the experimental curves the variation of the peak position $\Delta\alpha$ introduced by the field.

We then obtain:

$$\frac{\Delta R_{\max} - \Delta R_{\min}}{\Delta \alpha} = \left[\frac{\partial R}{\partial \alpha}\right]_{\max} \qquad [5.82]$$

with: $\Delta R_{\max} - \Delta R_{\min}$, the amplitude of the curve $\Delta R = f(\alpha)$ (see Figure 5.15).

Note that $\frac{\partial R}{\partial \alpha}$ is calculated by working out the average slope $R = f(\alpha)$ at the inflection points.

Under these conditions, we draw the curve $\Delta e = f(\Delta n)$ for all the modes (m=0,1,2) in polarization *TE* (and *TM*). The intersection of these lines gives the experimental values of Δe and Δn (see Figure 5.16).

As an example, this technique has been used to measure the EO coefficients of He^+ implanted $LiNbO_3$ guides (fabricated with a beam: E = 2 MeV, D = 2x10^{16} ions/cm^2 – see Chapter 2). Figure 5.14 shows the TM modes of the $LiNbO_3$ guide: He+, which enables us to determine the optogeometric parameters of the guiding layer:

n_o = 2.2827 ± 0.0002
n_e = 2.2051 ± 0.0004
e = 3.95 ± 0.07 μm

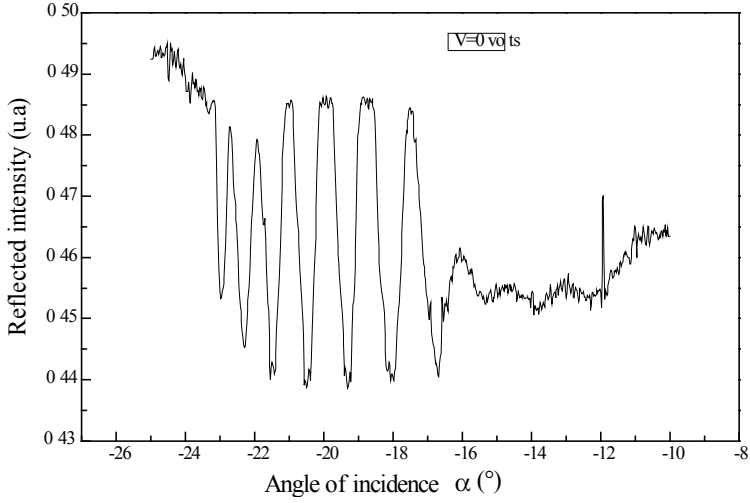

Figure 5.14. *Spectrum of TM guided modes of He+ implanted LiNbO*[3]

Figures 5.15a and b represent the modulation of the reflective intensity according to the incidence angle, calculated and measured for a voltage of the order of 82 V.

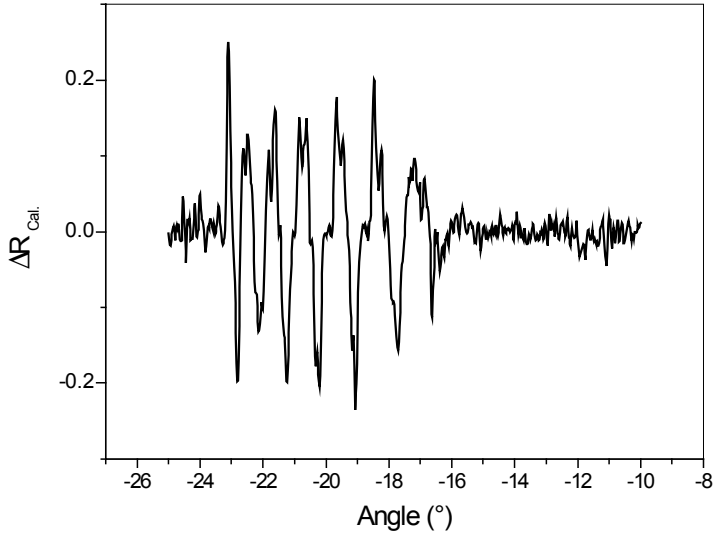

(a) Δ*R* calculated

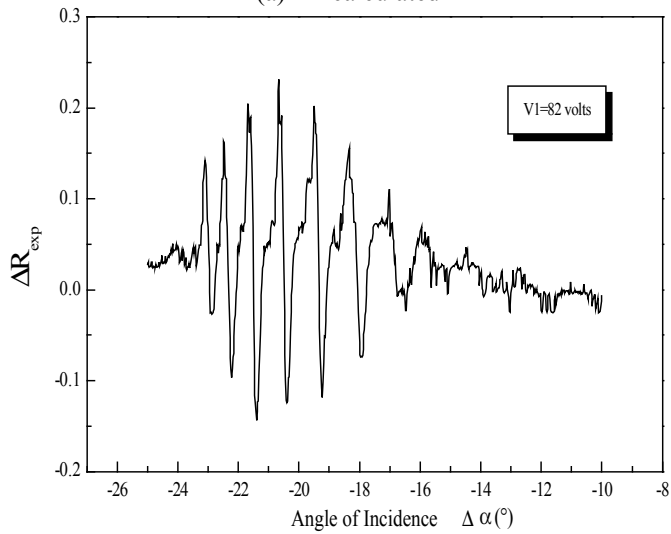

(b) Δ*R* measured

Figure 5.15. *Variation of reflectivity calculated and measured (TM guided modes of He+ implanted $LiNbO_3$ guides)*

Under these conditions, we draw the curve $\Delta e = f(\Delta n)$ for all modes (m=0,1,2) in *TE* polarization and *TM*. The intersection of these lines gives the experimental values of Δe and Δn (see Figure 5.16).

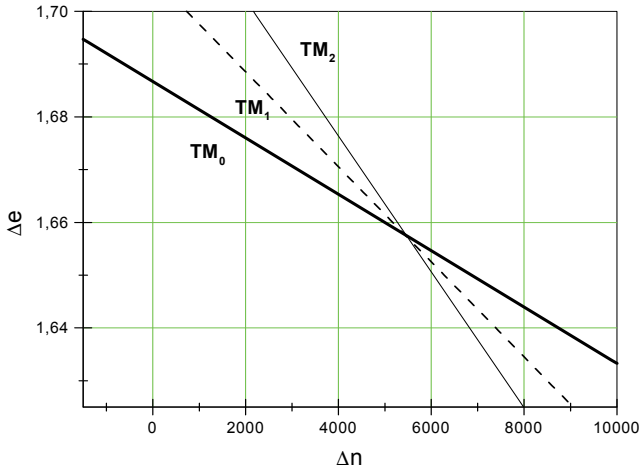

Figure 5.16. *Variation of Δe (X10^{-6}) according to Δn (X10^{-7}) for different guided modes (TM guided modes of He+ implanted LiNbO^3 guides)*

Finally the values of EO coefficients obtained are: r_{13}=11.7 ± 0.2 pm/V and r_{33} = 30.2± 0.7 pm/V. This study has shown that the ionic implantation (as already mentioned) does not affect the non-linear optical properties of the guiding region.

5.4.3.2.1. Case study

If we neglect the contribution of the piezoelectric effect on the angular displacement of guided modes, it is possible to write:

$$\Delta\alpha = \frac{d\alpha}{dn}\Delta n = \frac{d\alpha}{dN_m}\frac{dN_m}{dn}\Delta n \qquad [5.83]$$

with:

$$\Delta n = \frac{1}{2} n^3 r_{ij} E \qquad [5.84]$$

$\Delta n = \Delta n_o, \Delta n_e$; $n = n_o, n_e$

where r_{ij} are the most important terms of the EO tensor of the crystal.

In the case of $LiNbO_3$, $r_{ij} = r_{13}, r_{33}$ according to the polarization used. E is the applied electric field, and α is the synchronous coupling angle.

Afterwards, we can write: $\Delta n = K_a \; K_b \; \Delta\alpha$ [5.85]

with: $K_a = \dfrac{dN_m}{d\alpha}$ and $K_b = \dfrac{dn}{dN_m}$.

From the two previous relations [5.83] and [5.85], we obtain:

$$\Delta\alpha = \frac{n^3 r_{ij} E}{2 K_a \; K_b} = f(V) \qquad [5.86]$$

thus we express the angular displacement according to the applied voltage. These are two directly measurable parameters. In practice (the Pockels effect) we measure the angular displacement according to the applied voltage:

$$\Delta\alpha = C\,V \qquad [5.87]$$

The adjustment of the curve obtained by a line allows the constant C (C_o and C_e in TM and TE polarization respectively) to be determined. Finally, from the two previous relations [5.86] and [5.87], the electro-optic coefficients can be written:

$$r_{ij} = \frac{2 K_a K_b V}{n^3 E} C \qquad [5.88]$$

In the case of a $LiNbO_3$ crystal, the electro-optic coefficients r_{13} and r_{33} can be written:

$$r_{13} = \frac{2 K_{ao} K_{bo} V}{n_o^3 E} C_o \qquad [5.89]$$

$$r_{33} = \frac{2 K_{ae} K_{be} V}{n_e^3 E} C_e \qquad [5.90]$$

5.4.3.3.*The absolute error* Δr_{ij}

Generally, we can write:

$$r_{i3} = 2\pi K\left(\frac{1}{n_i^3}\right)a.c_i \qquad [5.91]$$

with constants $K = K_a K_b$ and i = o, e.

From this relation we can deduce the absolute error Δr_{i3}:

$$\Delta r_{i3} = \frac{2\pi K}{n_i^3}\left(a\Delta c_i + c_i\Delta a + \frac{3ac_i}{n_i}\Delta n_i\right) \qquad [5.92]$$

It is obvious that the greatest uncertainty during determination of the coefficient r_{i3} comes from the two parameters a and c_i, the interelectrode distance and the slope of the line, $\alpha = f(V)$.

Consequently, we can write:

$$\Delta r_{i3} \approx \frac{2\pi K}{n_i^3}\left(a\Delta c_i + c_i\Delta a\right) \qquad [5.93]$$

From this relation, we can estimate the absolute uncertainties of r_{13} and r_{33} values:

$\Delta r_{13} = \pm 0.2$ pm. V^{-1}

$\Delta r_{33} = \pm 1.2$ pm. V^{-1}

5.5. Optical devices using the electro-optic effect

Before concentrating on the guided configuration, let us first examine a few basic EO devices in a bulk crystal.

5.5.1. *Phase modulators*

As discussed in section 5.1, there are two possible configurations: the first is the transversal modulation, with the propagation direction perpendicular to the applied filed (see Figure 5.17a). The second configuration is the longitudinal modulation where the propagation of the optical wave is parallel to the applied electric field (see Figure 5.17b) [Yar 1984].

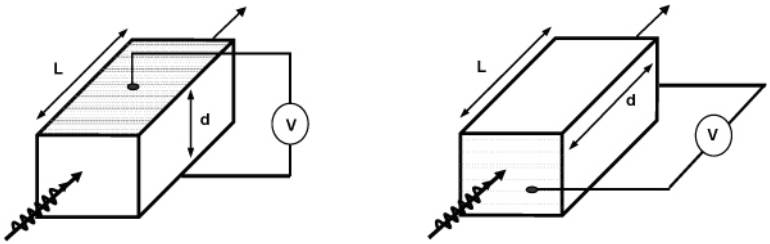

Figure 5.17. *(a) Transversal modulator and (b) longitudinal modulator.*

However in both cases, when the optical wave passes through the EO cell with the length L, its phase undergoes a variation given by:

$$\Delta\varphi = \frac{2\pi}{\lambda_0} n(E)L = \frac{2\pi}{\lambda_0}\left(n(0) - \Delta n\right)L \qquad [5.94]$$

with the variation of index:

$$\Delta n = \frac{1}{2} n_{eff}^3 r_{eff} E = \frac{1}{2} n_{eff}^3 r_{eff} \frac{V}{d} \qquad [5.95]$$

In this equation, the index "*eff*" is related to the index and the EO coefficient involved in the EO effect. These depend on the polarization used. See, for example, equations [5.33] and [5.39].

Then, we can write:

$$\Delta\varphi = \varphi_0 - \pi \frac{r_{eff} n_{eff}^3 L}{\lambda_0 d} V = \varphi_0 - \pi \frac{V}{V_\pi} \qquad [5.96]$$

where:

$$V_\pi = \frac{\lambda_0}{r_{eff} n_{eff}^3} \frac{d}{L} \qquad [5.97]$$

Parameter V_π is called the half-wave voltage and corresponds to a variation of π in the phase of the optical wave. This effect could produce a destructive interference phenomenon. For example, in the case of a transversal $LiNbO_3$ modulator and for a polarized wave following axis z (the optical axis) the paramters to be taken into account are $n_{eff} = n_e$ and $r_{eff} = r_{33}$. For a He-Ne (λ = 632 nm) laser, n_e = 2.2 and r_{33} = 30 pm/V, the half-wave voltage is $V_\pi = 2\,d/L$ kV. If we take L=10d, then voltage V_π = 190 V. If we consider a longitudinal modulator, the parameters under consideration are n_o= 2.28, r_{13} = 9.6 pm/V. In this case knowing that L=d, the half-wave voltage V_π = 5.4 kV. The half-wave voltage is much larger in longitudinal modulation than in the transversal modulation.

Equation [5.96] indicates that the phase mismatch of the wave varies linearly according to the applied voltage. Consequently, it is possible to modulate the phase of the wave by modulating the voltage applied. In fact, if we consider the applied voltage given by:

$$V(t) = V_m \sin \omega_0 t \qquad [5.98]$$

for an optical wave given by:

$$E(t) = E_{op} \cos \omega t \qquad [5.99]$$

at the output of the modulator, the optical wave undergoes a phase modulation and becomes (if we take $\prod_0$ for the origin of equation [5.96]):

$$\begin{aligned} E(t) &= E_{op} \cos(\omega t - \Delta\varphi) = E_{op} \cos\left(\omega t - \pi \frac{V_m}{V_\pi} \sin \omega_0 t\right) \\ &= E_{op} \cos(\omega t - \delta \sin \omega_0 t) \end{aligned} \qquad [5.100]$$

$$\delta = \pi \frac{V_m}{V_\pi}$$

where δ represents the modulation index.

Equation [5.100] can be developed using the Bessel functions, which enable the spectral repartition of the optical beam at the output of the modulator [Yar 1984]. We notice that parameter V_π particularly depends on the ratio d/L. The latter determines the order of magnitude of the applied voltage, which is of the order of a few hundred volts for transversal modulators; and from 1 to several hundred volts in the longitudinal configuration [Sal 1991, Yar 1984].

The interaction time between the electric signal and the optical field must also be adjusted in order to optimize the functioning of the modulator. In fact, if the applied voltage varies in a significant way during the optical wave transit-time, then the phase modulation obtained can be detrimental to the functioning of the modulator.

Thus, we generally tend to control the interaction between the optical wave and the electric signal by changing the way the signal is applied. This phenomenon will be discussed in the following sections.

5.5.2. *Intensity modulators*

Intensity modulation is achieved by modulating the phase of the optical wave. There are two possible configurations: the first consists of using a Mach-Zehnder interferometer, and the second uses the principle of phase or polarimetric delay.

5.5.2.1. *Polarimetric modulator*

The principle of this modulator is based on the use of the variation of light polarization by the EO effect. The setup consists of using a crystal or an EO guide in a cross polarizer configuration.

Where the incident optical wave (coupled) contains the two components of TE and TM polarizations (see Figure 5.18), the EO modulator operates as a dynamic phase delayer.

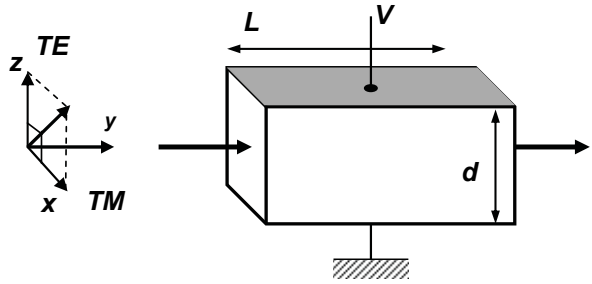

Figure 5.18. *Diagram of the polarimetric phase modulator principle*

For the $LiNbO_3$ crystal, by using both relations [5.33] and [5.35], we can show that TE and TM polarizations undergo a delay when compared, given by:

$$\Gamma = \frac{2\pi}{\lambda_0}\Delta n(E)L = \frac{2\pi}{\lambda_0}(n_o - n_e)L - \frac{\pi}{\lambda_0}\left(r_{13}n_o^3 - r_{33}n_e^3\right)EL \qquad [5.101]$$

This delay is written:

$$\Gamma = \Gamma_0 - \pi\frac{V}{V_\pi} \qquad [5.102]$$

with:

$$V_\pi = \frac{d}{L}\frac{\lambda_0}{\left(r_{13}n_o^3 - r_{33}n_e^3\right)} \qquad [5.103]$$

and:

$$\Gamma_0 = \frac{2\pi}{\lambda_0}(n_o - n_e)L \qquad [5.104]$$

The latest parameter represents the static delay.

As previously mentioned, to obtain an intensity modulator we can use an EO cell in a cross polarizer configuration, crossed as shown in Figure 5.19.

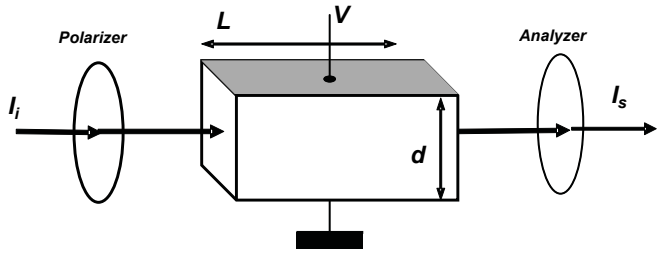

Figure 5.19. *Intensity modulator in a polarimetric configuration*

We can show that the transfer function of this setup can be written [Yar 1984]:

$$T = \sin^2\frac{\Gamma}{2} \qquad [5.105]$$

Γ given by relation [5.99] is written, for a sinusoidal voltage:

$$\Gamma = \Gamma_0 - \pi \frac{V_m \sin \omega_0 t}{V_\pi} \qquad [5.106]$$

By choosing $\Gamma_0 = \frac{\pi}{2}$, we can write:

$$T(V) = \sin^2\left(\frac{\pi}{4} - \pi \frac{V_m \sin \omega_0 t}{2V_\pi}\right) \qquad [5.107]$$

As an example, the transfer function (relation [5.104]) is illustrated in Figure 5.20.

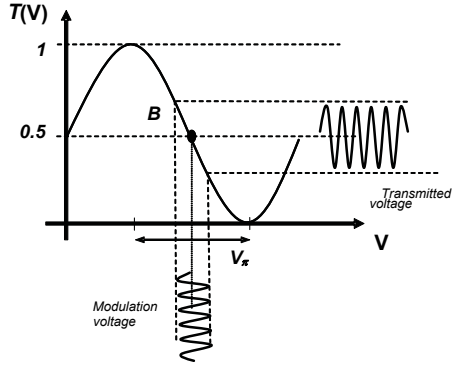

Figure 5.20. *Transfer function of a polarimetric modulator*

For a voltage $V \ll V_\pi$, this relation can be written in the following form:

$$T(V) = \frac{1}{2}\left[1 - \sin(\pi \frac{V_m}{V_\pi} \sin \omega_m t)\right] \approx \frac{1}{2} - \frac{\pi}{2} \frac{V_m}{V_\pi} \sin \omega_m t \qquad [5.108]$$

we use $\sin^2\left(\frac{\pi}{4} - \alpha\right) = \frac{1}{2}[1 - \sin(2\alpha)]$.

Under these conditions, the modulated intensity is a linear reproduction of the modulation voltage.

Finally, it must be noted that static delay Γ_0 can be adjusted optically by adding to the setup a quarter-wave plate, or electrically with an added continuous component of the applied voltage. The static component of this delay causes, by a minor modulation of the voltage, a sinusoidal modulation of the signal transmitted. However, this modulation configuration is not very well adapted to integrated optics. Hence, the use of EO modulators such as the Mach-Zehnder modulator is more important. This we will discuss later.

5.5.2.2. *Mach-Zehnder modulator*

In the case of a Mach-Zehnder interferometer, we apply a phase modulator to one of the two arms, as shown in Figure 5.21. This principle also applies to the integrated modulator (which will be discussed later on) except for the fact that the two arms of the interferometer are obtained on the same optical waveguide using two Y-type junctions. This configuration was presented in section 5.3.1 with the discussion about the measurement techniques of EO coefficients in waveguides.

A simple analysis of the setup shows that during recombination of the two light beams, an interference phenomenon appears because of the phase mismatch undergone by the optical waves on the two arms of the Mach-Zehnder. This phase mismatch is due, on the one hand, to the variation of the refractive index via the EO effect and on the other hand to the difference of the optical path between the two trajectories followed by the light.

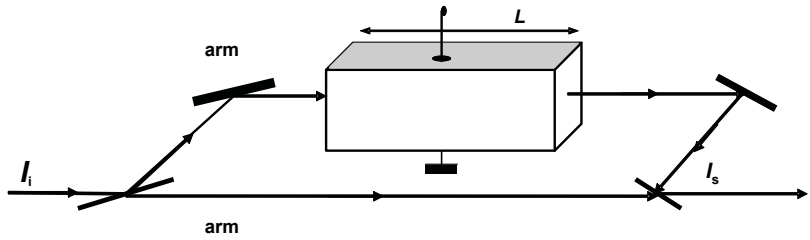

Figure 5.21. *Diagram of the principle of a Mach-Zehnder EO modulator using a massive crystal*

By using relation [5.27], the total dephasing can be written:

$$\Delta\varphi = \frac{2\pi}{\lambda_0}\left(n(E)L + \delta_{21}\right) \qquad [5.109]$$

where δ_{12} represents the difference of the optical path between arms 2 and 1 in the absence of the EO crystal.

We can show that intensity at the output can be written:

$$I_s = I_i \cos^2 \frac{\Delta\varphi}{2} \qquad [5.110]$$

$$\Delta\varphi = \varphi_2 - \varphi_1 \qquad [5.111]$$

where φ_1 and φ_2 represent the variations of the wave phase on both arms, 1 and 2 respectively.

The transfer function of this device is given by:

$$T = \frac{I_s}{I_i} = \cos^2 \frac{\Delta\varphi}{2} \qquad [5.112]$$

From relation [5.112] and using relation [5.96] we can write:

$$T(V) = \cos^2\left(\frac{\varphi_0}{2} - \pi \frac{V}{2V_\pi}\right) \qquad [5.113]$$

$$\varphi_0 = \varphi_{20} - \varphi_1$$

where φ_0 represents the static dephasing.

For a sinusoidal modulating voltage:

$$V = V_m \sin \omega_m t \qquad [5.114]$$

Relation [5.112] is illustrated in Figure 5.22 So the functioning of the modulator can be adjusted by the phase-mismatch due to the difference of the optical path. If this difference is chosen with $\varphi_0 = \pi/2$, the setup works in the linear part of the transfer function (point *B* in Figure 5.22):

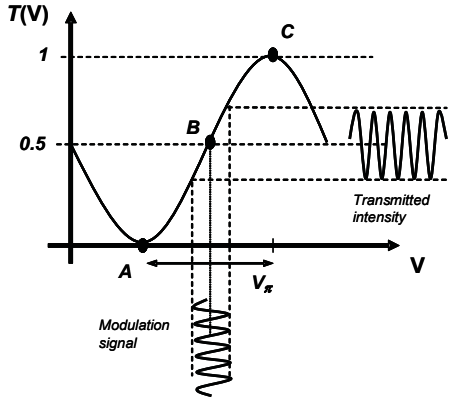

Figure 5.22. *Transfer function of a Mach-Zehnder EO modulator*

$$T(V) = \frac{1}{2}\left[1 + \sin\left(\pi \frac{V_m \sin \omega_m t}{V_\pi}\right)\right] = \frac{1}{2}\left[1 + \sin\left(\Gamma_m \sin \omega_m t\right)\right] \qquad [5.115]$$

$$\Gamma_m = \pi \frac{V_m}{V}$$

$$T(V) = \frac{1}{2}\left[1 + \sin\left(\pi \frac{V_m \sin \omega_m t}{V_\pi}\right)\right] \approx \frac{1}{2} + \pi \frac{V_m \sin \omega_m t}{2V_\pi}$$

$(V << V_\pi)$

Here the output intensity (light intensity) of the modulator varies linearly according to the modulation voltage.

In the case where φ_0 is a multiple of 2π, we will obtain from [5.102]:

$$\begin{aligned} T(0) &= 1 \\ T(V_\pi) &= 0 \end{aligned} \qquad [5.116]$$

In this case, the modulator commutes between the two states “light” and “no light”. This principle is commonly used in integrated optics and it is the foundation of integrated EO modulators use in the field of optical communications.

5.5.2.2.1. Limitations of the EO modulation

Regardless of the configuration and the type of modulation previously mentioned, the performances of the modulator are limited by two main factors: on the one hand, the geometry of the optical beam used; and on the other hand, the transit time. To illustrate this we will consider the case of bulk crystal based modulators. The integrated EO modulators having also other constraints linked to light confinement and the input/output optical components, which will be discussed at the end of this chapter.

Regarding the influence of the geometry of the beam, we can easily observe this phenomenon by taking into account the relation of the half-wave voltage V_π [5.94] or [5.100]. These two relations show that V_π is proportional to d/L. In the case of a Gaussian beam with a *waist* w_0, the radius of the beam is given by [San 1999]:

$$w(y) = w_0\sqrt{1+\left(\frac{\lambda y}{\pi w_0^2}\right)^2} \qquad [5.117]$$

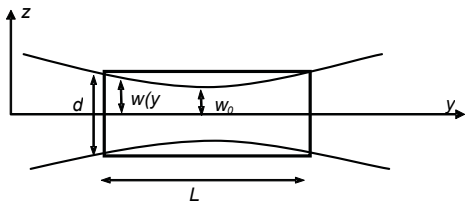

Figure 5.23. *Propagation of a Gaussian beam in an EO crystal*

The minimum value d of the crystal width, to obtain an optimum EO effect, corresponds to a *waist*, which is in the middle of the crystal. This is written:

$$d = 2w\left(\frac{L}{2}\right) \qquad [5.118]$$

$$d_{\min} = 2\sqrt{\frac{\lambda L}{\pi}} \qquad [5.119]$$

In practice, this value is taken at a multiplying factor for safety reasons.

Let us now examine the limitations linked to transit time. In fact in the calculations developed in the previous sections, we have implicitly neglected the variation of the applied electric field over a period corresponding to the wave propagation time through the crystal.

To illustrate this phenomenon, we will consider the phase modulator shown in section 5.4.1.

Generally speaking, the transit time of light in a crystal is given by:

$$\tau = \frac{n}{c} L \qquad [5.120]$$

For a $LiNbO_3$ crystal with a length of 1cm and whose indices are $n_e = 2.20$ and $n_o = 2.28$, the transit times for the two polarizations TE and TM are 70 ps and 90 ps respectively.

The total phase mismatch undergone by the wave at an instant t can be written (from relation [5.96]):

$$\Delta\varphi = \varphi_0 - \pi \frac{r_{eff} n_{eff}^3}{\lambda_0 d} \int_0^{\tau} V(t) \frac{c}{n} dt \qquad [5.121]$$

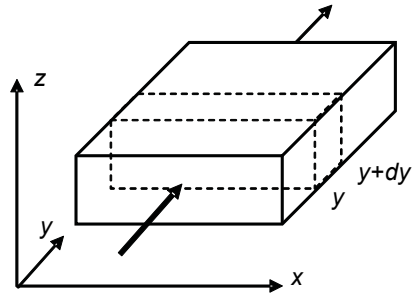

Figure 5.24. *Illustration of transit time in an EO crystal*

If we consider a sinusoidal voltage $V(t) = V_m \cos \omega_0 t$, the previous relation gives after integration:

$$\Delta\varphi = \varphi_0 - \pi \frac{r_{eff} n_{eff}^3 V_m}{\lambda_0 d} \frac{c\tau}{n} \left[\frac{\sin \omega_0 \tau}{\omega_0 \tau} \right] \qquad [5.122]$$

We note that the total phase mismatch is maximum (which is necessary for an efficient modulation) when *sin*c tends to 1, in other words when $\omega_0 \tau << 1$. This relation is written:

$$\frac{\tau}{T_0} << \frac{1}{2\pi} \qquad [5.123]$$

So the transit time must be much lower than the modulation period. In addition, the tolerated limit of the reduction of the total phase mismatch is of the order of l0%, which corresponds to $\omega_0 \tau = \pi/2$. Under these conditions, the maximum modulation frequency is written:

$$f_{\max} = \frac{c}{4nL} \qquad [5.124]$$

As an example, for a lithium niobate crystal of 1 cm in length and for a *TE* polarization (n_e = 2.20), the frequency $f_{\max}$ = 3.4 GHz (this value is more or less the same for a *TM* polarization).

To solve this problem, it is possible to use an electric field which propagates in the same direction as the optical wave. In fact, the applied field becomes a progressive wave and the modulator is called traveling-wave modulator. A schema of the principle of this type of setup is given in Figure 5.24.

The applied voltage takes the shape of a traveling wave:

$$V = V_m \cos(\omega_0 t - k_v y) \qquad [5.125]$$

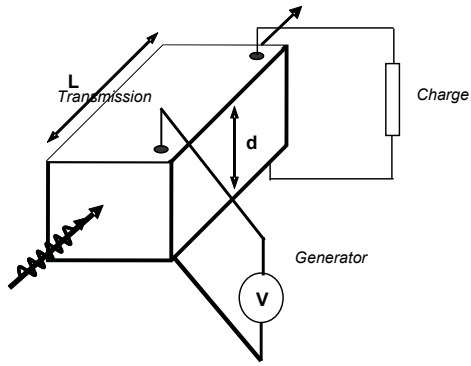

Figure 5.25. *Diagram of the principle of a traveling-wave EO modulator*

With a similar calculation to the one above, we can write:

$$\Delta\varphi = \varphi_0 - \pi \frac{r_{eff} n_{eff}^3 V_m}{\lambda_0 d} \frac{c\tau}{n} \left[\frac{\sin \omega_0 \left(1 - \frac{v_\varphi}{v_m} \right) \tau}{\omega_0 \left(1 - \frac{v_\varphi}{v_m} \right) \tau} \right] \qquad [5.126]$$

$$\Delta\varphi = \varphi_0 - \pi \frac{r_{eff} n_{eff}^3 V_m}{\lambda_0 d} \frac{c\tau}{n} \sin c \left[\omega_0 \left(1 - \frac{v_\varphi}{v_m} \right) \tau \right]$$

where v_φ is the phase velocity of the optical wave and v_m the phase velocity of the electric wave. We can notice that when the two phase velocities are equal, sinc function becomes equal to 1, and a maximum phase mismatch is obtained. In this case the transit time has no effect on the functioning of the modulator regardless of the length of the crystal.

Finally, another important parameter linked to the configuration of the electrodes is the capacity C. In fact, the EO cell behaves like a capacity C which, associated with a charge *R,* determines the bandwidth of the modulator:

$$\Delta f = \frac{1}{2\pi RC} \qquad [5.127]$$

5.6. Integrated optic setups using the electro-optic effect

In optical communication networks, external modulators, in particular those using the electro-optic effect, play a very important role. EO modulators exist in several forms and use different materials. However, EO modulators based on $LiNbO_3$ are particularly interesting because of the performances they offer. Integrated components usually work with low command voltage and offer very high modulation frequencies. Waveguides are obtained by Ti diffusion or by ionic exchange. The coupling is often performed using an optical fiber [Woo 1993, Naz 1993, Bin 2006, Bin 2003, Cou 2002].

The benefits of integrated devices based on waveguides compared with those based on bulk components comes from the fact that limitations linked to the diffraction of the laser beam can be totally eliminated thanks to the light confinement in the guide. Consequently, the propagation of guided waves can be easily controlled and numerous guide configurations can be used offering diverse and varied functions.

Within the framework of this book, we will limit ourselves to the presentation of two examples of integrated EO modulators, namely phase and intensity modulators. Interested readers will find more examples in numerous publications dealing with the subject [Tam 1990].

However, EO components based on waveguides are fabricated, in particular, by using specific and appropriate electrode configurations. To do this, a preliminary study of the distribution of the electric field according to the geometry of the electrodes is often necessary.

5.6.1. *Optimal design of the electrodes for integrated EO modulators*

The electric field in the waveguide is obtained using two co-planar electrodes as shown in Figure 5.17. In this case, the knowledge of the distribution of the electric field and its recovery with the electric field of the optical wave is essential for improved functioning of the modulator. The optimization of the design of the electrodes was, amongst others, reported by Marcuse et al. [Mar 1982]. In integrated optics, modulators use one or two waveguides generally channels and preferably monomodes. The application of an electric field modifies the propagation constant of the guided mode through the variation of the refraction index by the EO effect.

In this section, a few basic notions will be given about the design of electrodes for integrated EO modulators. A detailed analysis of the different possible configurations requires a specific study which goes beyond the framework of this

book. For further details, the reader can refer to numerous references which deal with this subject [Bin 2003, Cou 2002].

For $LiNbO_3$, the variation undergone by the index and also by the propagation constant depends on the direction of the applied electric field compared with the direction of the optical axis. As shown in previous paragraphs, the optimum situation consists of applying an electric field parallel to the optical axis of the crystal. However, two questions are still to be solved. The first deals with the optimum geometry of the electrodes in terms of interelectrodes space and dimensions (widths and thickness). The second question deals with the optimum position of the guide beneath the electrodes to obtain the maximum EO effect [Bin 2003, Bin 2006, Cou 2002, Hui 1998, Lee 2003, Liu 1982, Ran 1992]. This question is important, particularly when the phases of the two TE and TM polarizations must be adjusted by the applied field.

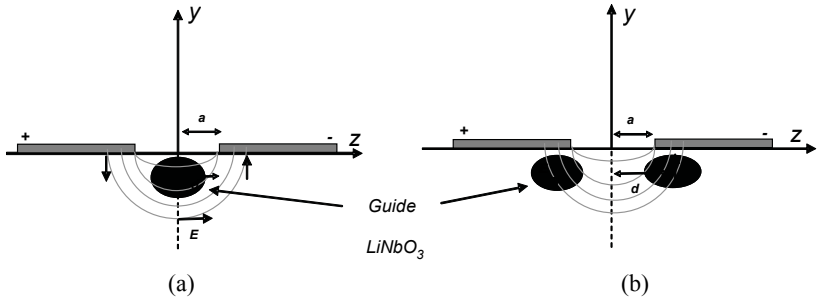

Figure 5.27. *Geometry of the semi-infinite electrodes above: (a) one guide; and (b) two waveguides*

In the case of two semi-infinite electrodes in Figure 5.27a, the position of the channel guide depends on the cut of the crystal and on the interelectrodes space, as well as on the component of the electric field to be used. This issue was the focus of section 5.2.1. The distribution of the electric field is given by relations [5.59] and illustrated by Figure 5.7.

For a z-cut crystal with the optical axis perpendicular to the surface, the optimum position of the guide is near the tip of one of the two electrodes ($d > a$), where the vertical component of the field is maximum. However, if it is a y-cut crystal (the optical axis being parallel to the surface), the waveguide must be placed in the middle of the interelectrode space where the horizontal component E_z of the electric field is maximum (see Figure 5.27a). Nevertheless, in this case, if the interelectrodes space is very big compared to the dimensions of the guide, the

optimum position of the guide is slightly closer to one of the two electrodes with $d<a$.

Figure 5.27b illustrates the possibility of using two guides, each set beneath one of the two electrodes (see Figure 5.27b). Here, the two EO effects are reversed because of the direction of the electric field. This creates a directional coupler via the "push-pull" effect. In this situation, it is important to have a minimum interelectrode space. However, it is not necessary to place the tips of the two electrodes strictly above the center of the two guides.

In practice, the semi-infinite electrodes are not really used and the situation described so far represent an approximation of the issue. The electrodes usually have widths comparable to the interelectrodes space (see Figure 5.28).

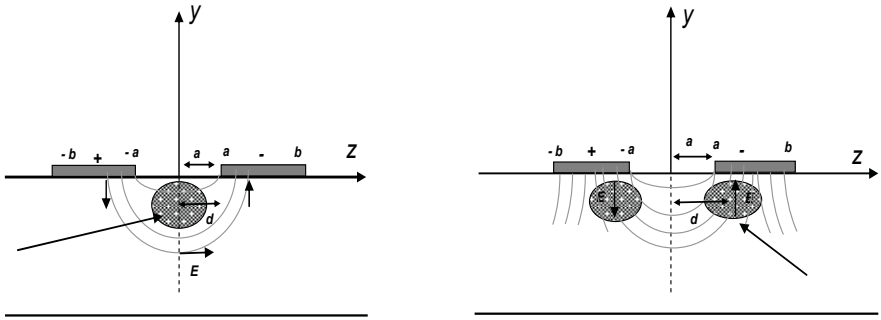

Figure 5.28. *Geometry of finite dimension electrodes: (a) one guide and (b) two waveguides*

For two finite electrodes, we can show that the two components of the electric field are given by [Mar 1982, Ram 1982, Van 1974, Liu 1982]:

$$E_z = -\frac{U}{2aK}\frac{\cos(\Phi)}{\left(A^2+B^2\right)^{\frac{1}{4}}}$$
$$E_y = \frac{U}{2aK}\sqrt{\frac{\varepsilon_z}{\varepsilon_y}}\frac{\sin(\Phi)}{\left(A^2+B^2\right)^{\frac{1}{4}}} \qquad [5.128]$$

with:

$$A \quad \left(1 \quad \frac{k^2}{a^2}(z^2 \quad y^2)\right)\left(1 \quad \frac{1}{a^2}(z^2 \quad y^2)\right) \quad 4\frac{k^2}{a^4}z^2y^2$$

$$B \quad 2\frac{k^2}{a^2}zy\left(1 \quad \frac{1}{a^2}(z^2 \quad y^2)\right) \quad 2\frac{1}{a^2}zy\left(1 \quad \frac{k^2}{a^2}(z^2 \quad y^2)\right) \qquad [5.129]$$

$$\Phi \quad \frac{1}{2}\arctan\left(\frac{B}{A}\right)$$

Figure 5.29 shows the evolution of the electric field vector obtained in this electrodes configuration. Use of the previous equations enables us to calculate the variation of the index in the guide according to its position in comparison with the two electrodes.

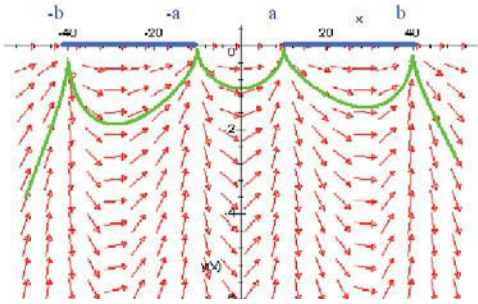

Figure 5.29. *Distribution of the electric field obtained by two finite dimension electrodes*

Note that component E_z varies very little according to depth, and almost does not vary according to z if it in the middle of the electrodes. Moreover, component E_y has a negligible variation according to y or z, if it is in the middle of the electrodes.

It is interesting to note that in most cases, it is necessary to place silica as a buffer layer between the optical guides and the electrodes, in order to minimize the influence of the metallic layer on the optical wave propagation. The drawback of using this layer is related to the command voltage, which must be increased because the electric field seen by the guide is weakened [Chu 1993, Sab 1986].

5.6.2. *Integrated EO phase modulator*

We saw in section 5.5 that in a bulk EO modulator, phase mismatching induced by EO effect is given by:

$$\Delta\varphi = \pi \frac{V}{V_\pi} = \frac{\pi L}{\lambda_0} r_{eff} n_{eff}^3 \frac{V}{d} \qquad [5.130]$$

In the case of an EO modulator based on waveguides, this relation is no longer valid as it is. In fact, on one hand the two coplanar electrodes induce an inhomogenous electric field in the guide which is far different from V/d (see previous section); and on the other hand the guided propagation imposes the existence of proper modes with propagation constants and a distribution of the optical field according to the guided mode. Under these conditions we must think in terms of the effective index of guided modes and of recovery between the electric field and the optical field [Kim 1989].

In an EO modulator based on a waveguide, phase mismatch becomes:

$$\Delta\varphi = \Delta\beta_m L = \frac{2\pi}{\lambda_0} \Delta N_m L \qquad [5.131]$$

where $\Delta\beta_m$ and ΔN_m are the variations induced by the EO effect of the propagation constant and the effective index of the mode m, respectively.

From the dispersion equation of guided modes (explained in Chapter 1), it is possible to write:

$$\Delta N_m = \Gamma \, \Delta n \qquad [5.132]$$

Γ being the factor of proportionality between the index variation by EO effect and the modification of the effective index of the resulting mode. This factor is always < 1 and it is weaker when the mode is near the cut-off [Tam 1990].

In the same way, the variation of the refractive index induced by two coplanar electrodes is written:

$$\Delta n = \frac{1}{2} r_{eff} n_{eff}^3 \frac{V}{a} \Gamma_{ovl} \qquad [5.133]$$

where Γ_{ovl} is a factor of reduction due to the recovery between the electric and optical fields. This is given by the overlap integral:

$$\Gamma_{ovl} = \frac{\iint E_{op}^2(y,z) E_{el}(y,z) dydz}{\iint E_{op}^2(y,z) dydz} \qquad [5.134]$$

This factor is also less than 1, its value depending notably on the width separating the two electrodes.

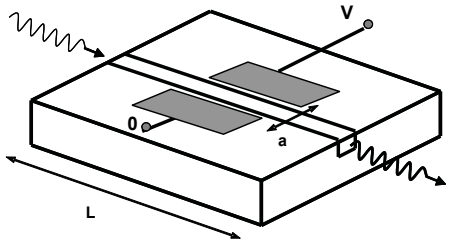

Figure 5.30. *Phase modulator in integrated optics*

If we consider a the interelectrode space and l their length, as a first approximation the half-wave voltage can be written:

$$V_\pi = \frac{\lambda_0}{\Gamma\, \Gamma_{ovl} r_{eff} n_{eff}^3} \frac{a}{l} \qquad [5.135]$$

With the utmost rigor, the analysis of the distribution of the electric field, which was developed in section 5.2.1 should be used. Nevertheless it is possible to realize from equation [5.135] that the ratio $\frac{a}{l}$ is very low, thus the half-wave voltage is within the order of a few volts. The functioning of this type of modulator has been shown for frequencies higher than 100 GHz.

Interestingly, the waveguide must be essentially monomode. The existence of several guided modes reduces the performances of the modulator and complicates its design. The EO coefficient r_{eff} which intervenes depends on the relative positions of the electrodes, on their widths and of the position on the guide (of the guided mode) in comparison with them.

5.6.3. *Integrated EO intensity modulator (Mach-Zehnder)*

This component was described in section 5.3.1, as well as in the presentation of bulk EO intensity modulators (see section 5.4.2). The basic principle consists of using two Y-junctions face to face as shown in the following figures. The two electrodes are placed either on one of the arms of the Mach-Zehnder (see Figure 5.31a) or above both arms (see Figure 5.31b). The position of the two guides in comparison with the electrodes must be carefully analyzed and made according to the performances and the application desired. See, for instance, section 5.5.1.

Let us consider a z-cut $LiNbO_3$ crystal. By applying a voltage to the electrodes in Figure 5.31b and in the case of the TM_{00} guided mode, the mode propagating in the upper arm undergoes a phase mismatch of $+\Delta\varphi$ and interferes with the mode propagating in the lower arm, which undergoes a phase mismatch of $-\Delta\varphi$. The total phase mismatch between the two modes in both arms is $2\Delta\varphi$.

Finally, the phase mismatch is written:

$$\begin{aligned} 2\Delta\varphi &= \pi \frac{V}{V_\pi} \\ V_\pi &= \frac{\lambda_0}{2\Gamma\, \Gamma_{ovl} r_{33} n_e^3} \frac{a}{l} \end{aligned} \qquad [5.136]$$

Through a simple analysis based on the interference phenomenon between two electromagnetic waves, we can show that intensity at the output of the modulator is [Tam 1990]:

$$P_s = \frac{P_e}{2}\left[\frac{\left(1-\sqrt{r}\right)^2}{1+r} + 4\frac{\sqrt{r}}{1+r}\cos^2\left(\frac{\pi}{2}\frac{V}{V_\pi}\right)\right] \qquad [5.137]$$

where r is the ratio of the intensities between the two arms of the Mach-Zehnder ($r = I_1/I_2$). From the previous equation, the extinction ratio is given by:

$$E = 10\log\frac{P_s(\max)}{P_s(\min)} = 10\log\left(\frac{1+\sqrt{r}}{1-\sqrt{r}}\right)^2 \quad (dB) \qquad [5.138]$$

Note that the extinction ratio of the modulator depends particularly on the intensity ratio between the two arms. If the ratio tends towards 1, the extinction ratio tends towards the infinity. For example, if $r = 2$, the extinction ratio $E = 15$ dB. In this particular case (z-cut $LiNbO_3$), the half-wave voltage can be very low, in the order of a few volts according to the dimensions and the space between the electrodes.

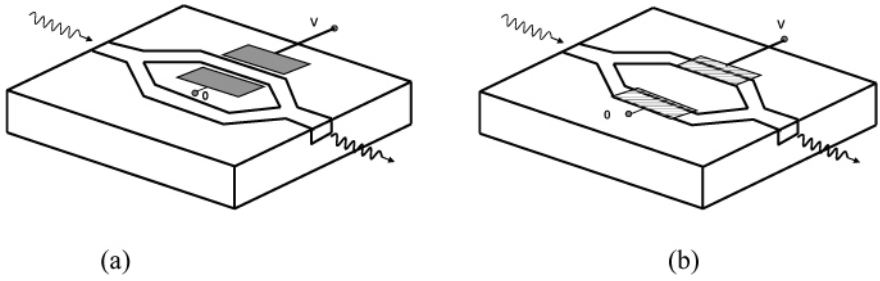

Figure 5.31. *Diagram of the principle of a Mach-Zehnder modulator in integrated EO*

Let us also note that the fabrication of this type of modulator is currently very well developed and that Y-junctions can be obtained precisely. In practice losses in this type of junction can be minimized by adjusting the junction angle. In the same way by choosing a suitable electrode configuration (i.e. by placing two sets of electrodes on both arms), we can make the modulator independent of light polarization.

Finally, high bandwidth can be obtained using this type of EO modulator in the configuration described in section 5.4.2.2.1, that is to say, with a traveling electric wave as shown in Figures 5.32a and b. In this case the bandwidth is determined by the phase matching between the optical wave and the radio frequency wave.

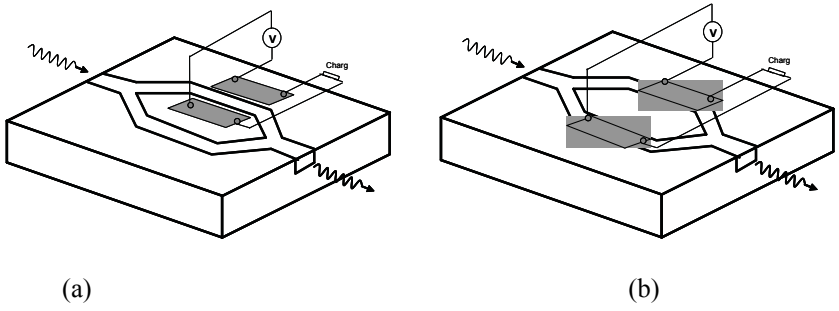

Figure 5.32. *Diagram of the principle of a Mach-Zehnder modulator with an integrated traveling wave*

Our presentation of integrated EO modulators is far from exhaustive and remains obviously simplified. In fact, a detailed analysis requires us to take into account other factors linked notably to the functioning of the EO modulator, such as drift and chirp issues. Modulators need to be maintained in the linear region of their EO characteristics. However, the functioning point can undergo a shift or drift in time due to a slow variation of the phase between the arms of the Mach-Zehnder.

A rigorous study of EO modulators also demands an electrical component approach. In fact, the performances of the EO modulator strongly depend on the structure of the electrodes used. The most frequently used structure is the one based on traveling wave electrodes. For example, if a push-pull configuration is considered, the potential difference is applied between the central electrode and the mass electrodes (see Figure 5.33a). In this case, the electrodes can be represented by a transmission line (see Figure 5.33b) [Cou 2002].

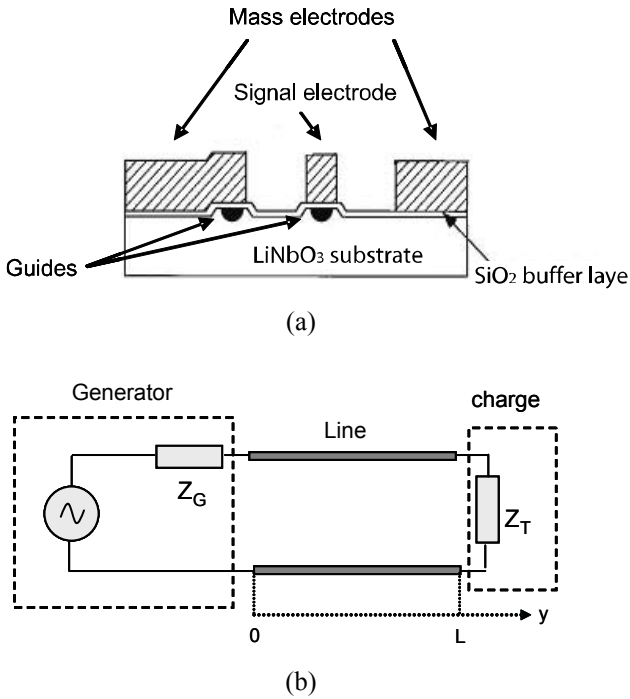

Figure 5.33. *The principle of a Mach-Zehnder modulator and its equivalent diagram in the form of a transmission line*

A transmission line is a structure with two conductors supplied by a voltage generator of intern impedance Z_G, completed by a Z_T (see Figure 5.33b). A simplified study of the transmission line supposes that it is ideal:

– the conductors have an infinite conductivity, in other words the electric and magnetic fields do not penetrate the conductor;

– the line is considered infinite, so length L is greater than the waveguide;

– the line is surrounded by a homogenous and isotropic dielectric.

Under these conditions, the electric and magnetic fields are transversal and the propagation equations of the electromagnetic field are then equivalent to the propagation of the current i and the potential u, in a line composed of elementary and tiny sections (length dy), as illustrated in Figure 5.34.

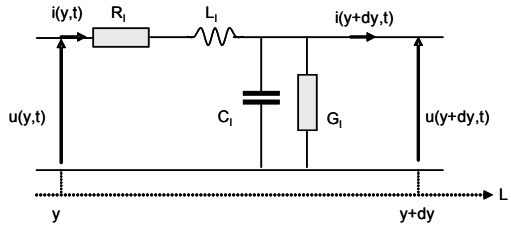

Figure 5.34. *Equivalent electric diagram*

Each elementary section is characterized by the following parameters:

– lineic resistance R_l (Ω/m), which represents losses by conduction;

– lineic inductance L_l (H/m) due to the magnetic field inter and intra conductors;

– lineic capacity C_l (F/m) formed by the dielectric and the two conductors, represents active energy losses in the dielectric;

– lineic conductance G_l (S/m) due to the insulating defects and to the dielectric losses, represents reactive energy losses in the dielectric.

A simplified study of this problem enables us to determine the characteristic parameters of the transmission line and consequently of the EO modulator. We will describe the outline of this investigation.

In a sinusoidal system, we can define a complex voltage and current:

$$\begin{aligned} \underline{u}(y,t) &= \underline{U}(y)\exp(j\omega t) \\ \underline{i}(y,t) &= I(y)\exp(j\omega t) \end{aligned} \qquad [5.139]$$

The equations of the lines are:

$$\begin{aligned} \frac{d^2\underline{U}(y)}{dy^2} - Z_l Y_l \, \underline{U}(y) &= 0 \\ \frac{d^2\underline{I}(y)}{dy^2} - Z_l Y_l \, \underline{I}(y) &= 0 \end{aligned} \qquad [5.140]$$

with $Z_l = R_l + L_l\omega$ and $Y_l = G_l + jC_l\omega$.

The general solution:

$$\begin{aligned}\underline{U}(y) &= \underline{U_I}\exp(-\gamma y) + \underline{U_R}\exp(-\gamma y)\\ \underline{I}(y) &= \underline{I_I}\exp(-\gamma y) + \underline{I_R}\exp(-\gamma y)\end{aligned} \qquad [5.141]$$

where U_I and $\underline{I_I}$ are the amplitudes of the incident wave and $\underline{U_R}$ and $\underline{I_R}$ are the amplitudes of the reflected wave.

We define the complex propagation constant by:

$$\gamma = \sqrt{Z_l Y_l} = \alpha + j\beta \qquad [5.142]$$

with α the attenuation (lineic attenuation coefficient) and β the lineic phase mismatch.

If the line is without losses: $R_l = 0$ and $G_l = 0$, consequently $\alpha = 0$, and we obtain:

$$\beta = \omega\sqrt{C_l L_l} \qquad [5.143]$$

The secondary parameters of the line are characteristic impedance Z_c, the electric effective index n_{eff} and the attenuation coefficient α. These parameters characterize, respectively, the reflection at the end of the line, the propagation velocity of the signal and the diminution of the amplitude propagating. The characteristic impedance $Z_c(\Omega)$ is defined by the following expression:

$$Z_c = \sqrt{\frac{Z_l}{Y_l}} = \sqrt{\frac{R_l + j\omega L_l}{G_l + j\omega C_l}} \qquad [5.144]$$

If the line is without losses, the impedance is purely real:

$$Z_c = \sqrt{\frac{L_l}{C_l}} \qquad [5.145]$$

The effective electric index is given by:

$$n_{eff} = \frac{v_\varphi}{c} = \frac{1}{c\sqrt{C_l\, L_l}} \qquad [5.146]$$

The attenuation coefficient α, which characterizes losses in transmission lines, is related to several phenomena:

– *Conduction losses* (resistive losses or metallic losses) are given by relation:

$$\alpha_c = \frac{R_l\,(f)}{2Z_c} \qquad [5.147]$$

R: resistance of the conductor

Z_C: characteristic impedance

Conduction losses are linked to the skin-effect. Namely, for a high frequency, current is located in a thickness (δ) called skin thickness. A current density appears on a thickness of the metal (δ) given by:

$$\delta = \sqrt{\frac{\rho}{\pi\mu f}} \qquad [5.148]$$

ρ: resistivity of the current or the conductor (Ω.m)

$\mu = \mu_r \mu_o$: magnetic permeability of the conductor

$\mu_o = 4\text{x}\pi\text{x}10^{-7}$ H/m: permeability of the vacuum

μ_r: relative permeability

f: frequency (Hz).

Note that conduction losses (α_c) increase proportionally to the square root of the frequency, and represent the main cause of attenuation of the electric wave.

– *Dielectric losses* (dielectric attenuation) are due to the charge leakage in the dielectric when it is not completely insulated:

$$\alpha_d = \frac{\omega}{2}\sqrt{\mu_d \mu_r}\ \tan\delta_d \qquad [5.149]$$

where $tan\ \delta_d$ is the ratio between $Im(\varepsilon)$ and $Re(\varepsilon)$ which depends on the frequency.

It is interesting to note that dielectric losses cannot be neglected at high frequencies.

As a whole, characteristic parameters of the transmission line (of the electrodes), which are attenuation α, impedance Z_c, and effective index n_{eff}, are determined from in line primary parameters (R_l, L_l, C_l and G_l), which in turn are defined by the structure of the electrodes. These parameters directly influence the functioning of the EO modulator and more specifically the bandwidth and the chirp.

In fact, the amplitude modulation of an optical signal can be accompanied by a parasite frequency modulation called "*chirp*". The modification of the spectrum obtained can modify the signal envelop propagating in the fiber.

The chirp depends in particular on the characteristics of the arms of the Mach-Zehnder, and on the cut of the $LiNbO_3$ used in order to have the same EO interaction on each arm of the Mach-Zehnder [Kaw 2001, Kim 2002, Shi 1994]. Another parameter that can also influence the chirp of a modulator is the extinction ratio, which depends, among other things, on the losses in the two arms of the modulator. The control of these different factors requires much attention both at the level of the waveguide fabrication process and at the level of the management of applied voltages as well as the electronic circuits used.

The chirp parameter, which indicates a variation of the carrying frequency of the optical signal is generally defined from the phase and intensity of the optical wave as follows:

$$\alpha = \frac{\dfrac{d\Phi}{dt}}{\dfrac{1}{E}\dfrac{dE}{dt}} \qquad [5.150]$$

where E is the amplitude of the electric field of the optical wave and Φ is the phase mismatch induced by the modulator.

From this expression we infer:

$$\alpha = -\cos(\Delta\Phi)\left(\frac{A_1 + A_2}{A_1 - A_2}\right) \qquad [5.151]$$

where A_1, A_2 are amplitudes of the optical phase induced by the applied electric field in each arm of the structure Mach-Zehnder structure.

In the case of small amplitude of modulation (A_1, A_2 <<1) and if $\Phi = -\frac{\pi}{2}$, the chirp parameter can be written:

$$\alpha \cong \alpha_0 \equiv \frac{A_1 + A_2}{A_1 - A_2} \qquad [5.152]$$

Under these conditions, if the electrodes are symmetric (A_1 = -A2) we obtain $\alpha_0 = 0$, and if the electric signal is applied to only one optical path (A_2 = 0) then $\alpha_0 = 1$.

Generally speaking, this parameter can affect the performances of optical transmissions because of the dispersion in optical fibers. Consequently, the management of the chirp according to the characteristics of the transmission line can considerably improve the performances and the capacity of the optical transmissions. An analysis of these effects can be found in [Cou 2002].

5.7. Modulation in optical networks: state-of-the-art

The evolution of data transmission using optical fiber has sped up since the appearance of the WDM (*wavelength demultiplexing multiplexing*) technique, which enables data to reach binary speeds of a few Tb/s transported by a single fiber. After having transmitted 2.5 Gb/s, then 10 Gb/s per channel on transmission lengths which reach hundreds of km, the need for high speed transmission (currently higher or equal to 40 Gb/s) on longer transmission lengths keeps growing. Figure 5.35 shows the evolution of the capacity per fiber from the 1980s until today.

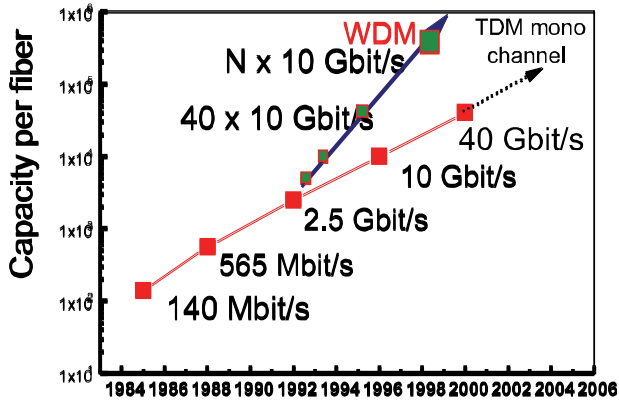

Figure 5.35. *Evolution of the transmission capacity per fiber since 1984*

Sensitivity to propagation defects increases along with the bit rate, both for linear effects due to chromatic dispersion (CD) and to polarization-mode dispersion (PMD) of the fiber, and for non-linear effects mainly induced by the Kerr effect (the refractive index dependence on the light intensity). The total acceptable accumulated CD for a speed of 10 Gb/s is of the order of 100 ps/nm (equivalent to 60 km of G652 fiber). This value decreases to about 60 ps/nm for a speed of 40 Gb/s (i.e. under 4 km of the same fiber!). The level of PMD acceptable makes many fibers installed before 1995 unusable; which explains why most solutions being developed are based on particular management designs for dispersion along the line. CD and PMD cause a temporal broadening of the optical signal, as well as a degradation of the transmission quality [Joi 1996, Noé 2004, Dut 1998, Sun 2002].

In addition to these problems inherent to optical fibers, the spreading of the future high-speed telecommunications network (40 Gb/s and beyond) requires the development of new optoelectronic components fitted for these transmission speeds. This is particularly true for laser sources covering the 1.5 μm window and to some extent the 1.3 μm window [Ben 2004, Suz 2003]. This case poses problems with two aspects: on one hand, the modulation of the laser beam; and on the other hand, the optical amplification. Direct modulation lasers are used for speeds up to 2.5 Gb/s. Beyond 2.5 Gb/s, so 10 Gb/s and later 40 Gb/s, the direct modulation of the laser is no longer possible and the use of an external modulator is necessary. In fact, the modulation of the density of charge carriers modifies at the same time absorption and the refractive index of the active layer of the laser. This induces, for example, a *chirp* of the order of -5 for an InP laser. This *chirp* parameter is one of the main determining factors in the performance of an optical transmission line because the induced modifications of the signal, considerably modify the envelope

of the signal transmitted in the fiber and accentuate the effects of CD and PMD dispersions.

External modulation can be achieved using physical phenomena such as electro-absorption or the electro-optic effect. However, electro-absorbing modulators (EA) are not fitted for high-speed transmissions because of their chirp parameter, which is never zero. As a result, the use of electro-optic modulators seems to be the most promising direction.

From the material point of view, EO modulators are mainly based on polymers, III-V semi-conductors and dielectrics (particularly $LiNbO_3$) [Boo 2002, Don 2000, Jia 2001, Lec 2000, Nag 1997, Mit 1995, Ree 2005]. For example, much research and development has been devoted to the study of the EO effect in PMMA polymers. Spectacular performances have been obtained with EO coefficients over 100 pm/V and command voltages in the order of 1 V. However, the major drawback of these materials remains their lifespans and their stability over time. As long as III-V semi-conductor materials are concerned, their low EO coefficients (of the order of 3 pm/V) are compensated by their high refractive indices (e.g. 40 Gb/s modulators based on GaAs are commercialized). Nevertheless, although those modulators feature a zero chirp, command voltages in the order of 5 V and an optical bandwidth of 30 GHz, their use is limited to the C optical band. Consequently their exploitation for WDM or TDM applications is very limited. However, technological efforts have been made over recent years to improve the performances of these modulators.

For all these reasons, $LiNbO_3$-based electro-optic modulators seem to be the most viable solution for Nx10 Gb/s systems. These modulators take more than half of the world market. However, the technology and the control of $LiNbO_3$ modulators remains delicate and the "ideal" commercial product does not exist yet. One of the major problems of $LiNbO_3$ is the command voltage, which for modulators of 40 Gb/s are in the range of 6 to 8 V. Also EO modulators based on $LiNbO_3$ feature low losses which can reach 0.1 $dB.cm^{-1}$ according to the fabrication process implemented (for example protonic exchange). The command voltages are of a few volts according to the configuration used and their functioning covers *C* and *L* telecommunication bands because they are independent of the wavelength. Moreover, the chirp of those modulators adds to their success at optical long-distance transmissions; for further details refer to [Cou 2002].

$LiNbO_3$ EO modulators are x-cut modulators and z-cut modulators. In the x-cut configuration (see Figure 5.35), the modulator is symmetric; that is to say that the two guides are placed in the middle of the interelectrode gaps and undergo the same EO effect but of opposite signs. The polarization of the wave is generally TE (parallel to the optical axis). In this case the phase of the optical wave from the first

guide compensates that of the signal from the second arm of the Mach-Zehnder. Consequently, the total field coming out of the modulator does not undergo any residual modulation and the *chirp* of this type of modulator is zero.

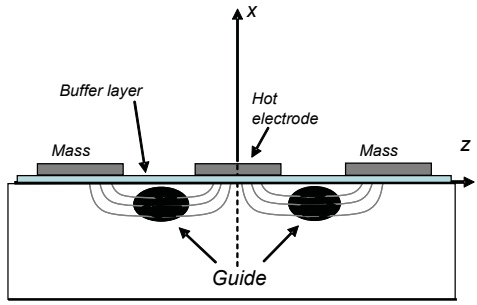

Figure 5.36. *Diagram of the principle of an EO Mach-Zehnder modulator x-cut in $LiNbO_3$*

Although these modulators can be used for very high-speed transmissions (40 Gb/s), they exhibit a major drawback linked to the command voltage which remains high (about 15 V). For this reason, the z-cut configuration seems to be more interesting because it allows the use of a command voltage lower than 10 V. In this configuration, the two guides are placed below the electrodes in order to use the vertical component of the electric field which implies the EO coefficient r_{33} ($\vec{E}$ parallel to the optical axis). Moreover the polarization of the guided wave is TM, in order to have the optical field in the same direction as the optical axis. This type of modulator offers many advantages, most notably in terms of bandwidth and command voltage. In fact, bandwidths of 40 GHz to 100 GHz and command voltages ranging from 2 to 6 V have been reported [Hag 1986, Bur 1999]. These performances are obtained in particular by using a "ridge" structure, which enables control of the phase matching between the electrical and optical waves. However, the chirp parameter is not zero (about 0.7) in this configuration. This factor comes from the asymmetry between the two arms of the Mach-Zehnder, which do not see the same electrical field because it is more intense below the hot electrode than below the mass. To solve this problem, alternative structures have recently been proposed [Kim 1989, Kim 2002, Sab 1986]. Note, for example, those that use the recovery between the optical field and the electrical field in the two arms in order to balance the modulator.

Another method frequently used in telecommunication networks, consists of placing the two guides below two hot central electrodes (see Figure 5.37). Each is driven by a synchronized voltage whose amplitude is independent [Kor 1991]. Under these conditions, the chirp can be cancelled by applying two identical

voltages of opposite signs. The command voltage of these modulators with dual structures can reach a few volts for transmissions of only 10 Gb/s.

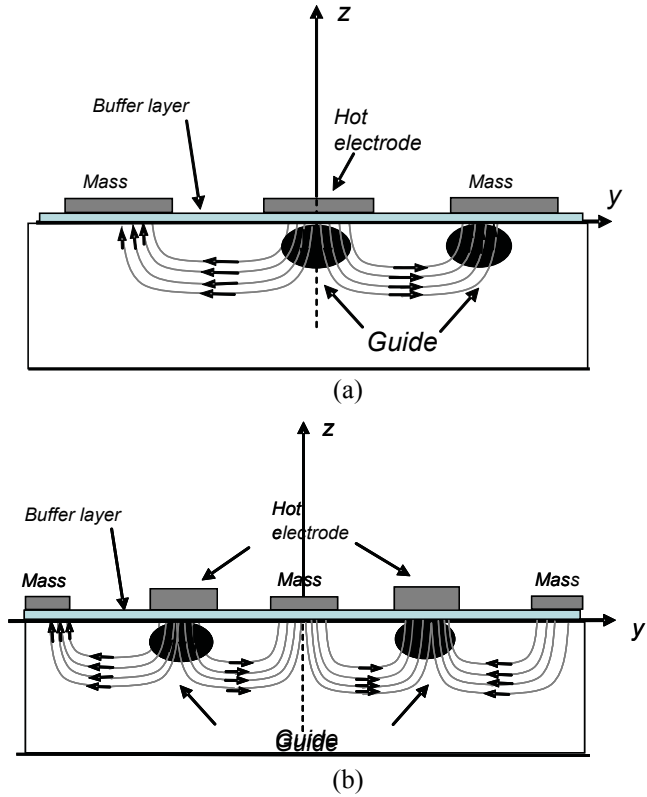

Figure 5.37. *Diagram of the principle of an EO Mach-Zehnder modulator based on z-cut $LiNbO_3$: (a) configuration with only one driver and (b) dual configuration.*

Finally, another structure has been proposed by Porte et al. [Por 2000, Cou 2002, Cou 2002b, Cou 2004]. This consists of using the inversion of ferroelectric domains to change the sign of the index variation induced by EO effect (see Figure 5.38). This principle has been used to develop several bulk or integrated optical components [Cab 2004, Cab 2004b]. In the solution proposed by Porte et al., it is necessary to make the EO modulator have a zero chirp or controllable. To do so, a shift of the electrodes is used, combined with an inversion of the ferroelectric domains of the material, to control the chirp of a z-cut type modulator. It has been shown that the control of the chirp increases along with the number of inverted zones. This control is achieved by adjusting length L_1 of the inverted zones to those of the non-inverted zones L_2. A diagram of the principle of this type of modulator is presented in Figure 3.38.

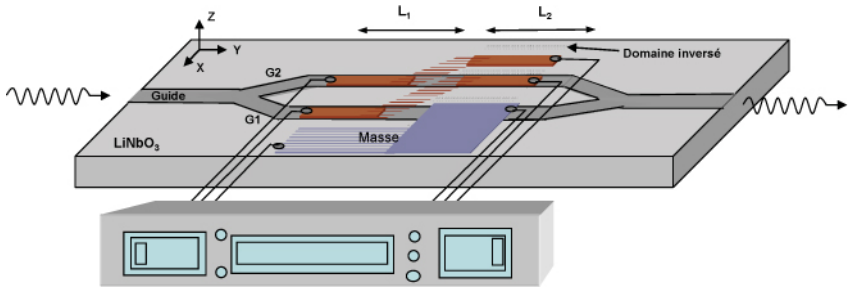

Figure 5.38. *Diagram of the principle of an EO Mach-Zehnder modulator based on a z-cut $LiNbO_3$ with inversion ferroelectric domains*

Finally, an interesting lead to explore is that of $LiNbO_3$ thin layers (or other materials featuring interesting electro-optic properties), which would use electrodes in a "sandwich" configuration instead of the current coplanar configuration. In the same way, electroabsorption modulators remain an important domain to develop either for long-distance transmissions or for short-distance applications. A detailed analysis of the market of EO modulators and their functioning principles can be found in references [Cab 2004, Cab 2004b] from which Table 5.1 is taken. This table compares the performances of the EO modulators currently available on the market.

External Mach-Zehnder $LiNbO_3$ modulator commercially available

Company	Electric bandwidth (GHz)	V_π DC/AC (V)	Insertion losses (dB)	Return optical losses (dB)	S_{11} (dB)	Impedance (Ω)	Optical band (nm)	Maximum optical power (mW)	Functioning temperature (°C)
Lucent	30	6/–	6	– 40	– 15	50	1,525 and 1,565	30	0 to 70
JDS Uniphase	20(to – 6 dB)	12/6	5	– 50	– 10	50	1,550 and 1,320	200	0 to + 70
AMS	20	10	6	– 40	– 10	50	1,550 and 1,320	–	–
GEC	18	15	5	– 40	– 10	50	1,550 and 1,300	100	+10 to + 40
EOSPACE	20	–	–	–	–	–	–	–	–

Optical source with 10 Gb/s Mach-Zehnder modulator commercially available

Company	Wavelength range	Number of channels	Polarization current (mA)	SMSR (dB)	Electrical bandwidth (GHz)	Polarization tension (V)	Optical power (mW)	S_{11} (dB)	Optical isolation (dB)	Functioning temperature (°C)
NORTEL	ITU 200 GHz	21	275	37	8 (TBC)	5	0.9	10	30 (TBC)	0 to 70

Table 5.1. *Performances of EO modulators commercially available according to [Cab 2004]*

5.8. Bibliography

[Alf 1980] Alferness R.C. and Buhl L.L., "Electro-optic waveguide TE – TM mode converter with low drive voltage", *Optics Letters*, 5(11), 473-475 (1980).

[Alf 1982] Alferness R.C. and Buhl L.L., "High speed waveguide electro-optic polarization modulator", *Optics Letters*, 7(10), 500-502 (1982).

[Alf 1987] Alferness R.C. and Buhl L.L., "Ti:$LiNbO_3$ waveguide electro-optic beam combiner", *Optics Letters*, 12(10), 778-780 (1987).

[Ari 2004] Arizmendi L., "Photonic applications of lithium niobate crystals", *Phys. Stat. Sol.(a)*, 201 (2), 253-283 (2004).

[Bec 1983] R.A.Becker, "Comparison of guided wave interferometric modulators fabricated on LiNbO3 via Ti indiffusion and proton exchange", *Appl. Phys. Lett.* 43(2), 131-133 (1983).

[Ben 2004] Bensoussan M., "Les nouvelles technologies photoniques", www rd francetelecom.com, (2004).

[Bin 2003] Binh L.N., "A finite differential analysis of symmetric and asymmetric travelling wave electrodes for ultra-broadband modulators", Technical report, MECSE, Monash University (2003).

[Bin 2003b] Binh L.N."A finite difference analysis of symmetric and asymmetric travelling wave electrodes for unltra-broadand modulators", Technical reports, MECSE, Monash University (2003).

[Bin 2006] Binh L.N., "Lithium niobate optical modulators: devices and applications", *Journal of Crystal Growth*, 288, 180-187 (2006).

[Boo 2002] "40Gbps NRZ integrated transmitter", www.Bookham.com , (2002).

[Bou 1996] Boudrioua A., Réalisation d"un banc de mesure de…, PhD Thesis, University of Metz (1996).

[Bou 1995] Boudrioua A., Moretti P.and Loulergue J.C., "Fabrication, characterization and electro-optic performances of proton-implanted waveguides in $LiNbO_3$", *J. Non-Cryst. Sold.*, 187, 443-447 (1995).

[Bou 1998] Boudrioua A., Ould Salem S., Moretti P., Kremer R.and Loulergue J.C., "Electro-optic coefficients in H+-ion implanted $LiNbO_3$ planar waveguide", *Nucl. Inst. and Meth. in Phys. Res. B*., 147, 393-398 (1998).

[Bur 1999] Burns W.K., Howerton M.M., Moeller R.P., Krähenbühl R., McElhanon R.W.and Greenblatt A.S., "Low drive voltage, broad-band LiNbO3 modulators with and without etched ridges", *IEEE Journal of Lightwave Tech.*, 17(12), 2551-2555 (1999).

[Cab 2004] Cabon B., Chazelas J. and Dolfi D., "Optoélectronique hyperfréquence : Composants et fonctions", *Techniques de l'Ingénieur*, Comp. E *3 333*, 1-10 (2004).

[Cab 2004b] Cabon B., Chazelas J. and Dolfi D., "Optoélectronique hyperfréquence : Modulation, liaisons et commutation", *Techniques de l"Ingénieur*, Comp.E 3 331, 1-15 (2004).

[Cha 1971] Channin D.J., "Voltage induced optical waveguide", *Appl. Phys. Lett*., 19, 128-130 (1971).

[Chu 1993] Chuang W-C., Chang W-C., Lee W-Y., Leu J-H.and Wang W-S., "A comparison of the performance of $LiNbO_3$ traveling wave phase modulators with various dielectric buffer layers", *Journal of Optical Communications*, 14(4), 142-148 (1993).

[Cou 2002] Courjal N., Modulateur $LiNbO_3$ à faible chirp par inversion de domaine ferroélectrique, PhD Thesis, University of Besançon (2002).

[Cou 2002b] Courjal N., Porte H., Martinez A.and Goedgebur J.P., "$LiNbO_3$ Mach-Zefnder modulator with chirp adjusted ferroelectric domain inversion", *IEEE Photonics Tech.Letters*, 14(11), 1509-1511 (2002).

[Cou 2004] N.Courjal, J.M.Dudley and H.Porte, "Extinction-ratio-independent method for chirp measurements of Mach-Zehnder modulators", *Optics Express*, 12(3), 442-448 (2004).

[Den 1989] Dentan V., Lévy Y., Dumont M., Robin P.and Chastaing E., "Electrooptic properties of a ferroelectric polymer studied by attenuated total reflection", *Optics Com*., 69(5), 379-383 (1989).

[Des 1979] Destefanis G.L., Gaillard J.P., Ligeon E.L., Valette S., Farmery B.W. and Townsend P.D. "The formation of waveguide and modulation in $LiNbO_3$ by ion implantation", *J. Phys*., 50 (12), 7898 (1979).

[Don 2000] Donval A., Toussaere E.Hierle R.and Zyss J., "Polymer based polarization insensitive amplitude modulator: conception, technology and demonstration", *Synthetic Metals*, 115, 21-27 (2000).

[Dur 1953] Durand E., "*Electrostatique et Magnétostatique*", Masson and Cie, Ed. (1953).

[Dut 1998] Dutton H.J.R., "Understanding optical communications", IBM, International Technical Support Organization, (www redbooks.ibm.com) (1998).

[Eld 1991] Elderin C.A., Knoesen A. and Kowel S.T., "Use of Fabry-Perot devices for the characterization of polymeric electro-optic films", *J. Appl. Phys*., 69(6), 3676 (1991).

[Grä 1992] Gräupner P., Pommier J.C., Cachard A. and Coutaz J.L., "Electro-optical effect in aluminum nitride waveguides", *J. Appl. Phys*., 71(9), 4136-4139 (1992).

[Gün 1987] Günter P. (Ed.), *Electro-optic and Photorefractive Materials*, Springer, Berlin (1987).

[Hag 1986] Haga H., Izutsu M. and Sueta T., "$LiNbO_3$ traveling-wave light modulator/switch with an etched groove", *IEEE J. of Quant. Elect*., QE-22(6), 902-906 (1986).

[Her 1991] Herminghaus S., Smith B.A. and Swalen J.D., "Electro-optic coefficients in electric field poled polymer waveguides", *J. Opt. Soc; Am. B*, 8(11), 2311-2317 (1991).

[Hui 1998] Hui K.W., Chiang K.S., Wu B.and Zhang Z.H., "Electrode optimization for high-speed travelling wave integrated optic modulators", *Journal of Lightwave Tech*., 16(2), 232-238 (1998).

[Hui 2004] Hui R., Zhang S., Zhu B., Huang R., Allen C. and Demarest D., "Advanced optical modulation formats and their comparison in fiber optic systems", Technical report, Information and Telecommunication Technology Center, University of Kansas (2004).

[Iza 1992] Izawa K. and Okamoto N., "Optical modulation using a poled polymer waveguide doped with mixed organic nonlinear materials MNA and p-NA", *N-L. Optics*, 3, 247 (1992).

[Jia 2001] Jiang Y., Cao Z., Chen G., Dou X. and Chen Y., "Low voltage electro-optic polymer light modulator using attenuated total internal reflection", *Optics & Laser Technology*, 33, 417-420 (2001).

[Jin 1991] Jin H., Bèlanger M. and Jakubczyk Z., "General analysis of electrodes in integrated optics electrooptic devices", *IEEE J. of Quant. Elect*., QE-27(2), 243-251 (1991).

[Joi 1996] Joindot I. and Joindot M., "Les télécommunications par fibre optique", *Techniques et sciences des télécommunications*, Dunod (1996).

[Kaw 2001] Kawanishi T., Kogo K., Oikawa S. and Izutsu M., "Direct measurement of chirp parameters of high-speed Mach-Zehnder-type optical modulators", *Optics Communications*, 195, 399-404 (2001).

[Kim 1989] Kim C.M. and Ramaswamy R.V., "Overlap integral factors in integrated optics modulators and switches", *Journal of Lightwave Tech*., 7(7), 1063-1069 (1989).

[Kim 1989b] Kim C.M. and Ramaswamy R.V., "Overlap integral factors in integrated optics modulators and switches", *Journal of Lightwave Tech*., 7(7), 1063-1070 (1989).

[Kim 2002] Kim H. and Gnauck A.H., "Chirp characteristics of dual-drive Mach-Zehnder modulator with a finite DC extinction ratio", *IEEE Photonics Tech. Letters*, 14(3), 298-300 (2002).

[Kob 1990] Kobayashi T., "A method for measuring electrooptical constants", *Non-Linear Optics*, 1, 239-252 (1990).

[Kor 1991] Korotky S.K., Veselka J.J., Kemmerer C.T., Minford W.J., Moser D.T., Watson J.E., Mattoe C. and Stoddard P.L., "High speed low power optical modulator with adjustable chirp parameters", *Top.Meeting Integrated Photonic Res. P.TuG2* (1991).

[Kub 1980] Kubota K., Noda J. and Mikami O., "Traveling wave optical modulator using a directional coupler $LiNbO_3$ waveguide", *IEEE J. of Quantum Electronics QE*, 16(7), 754-760 (1980).

[Lee 2003] Lee B., Byun J. and Kim B-K., "Analysis of coplanar $LiNbO_3$ waveguide structures applicable to electrooptic modulator with FDTD method", *Microwave and Optical Tech. Letters*, 39(3), 234-237 (2003).

[Lec 2000] Leclercq J-L.**,** Garrigues M.**,** Letartre X.**,** Seassal CH.and Viktorovitch P., **"**InP-based MOEMS and related topics", *J. Micromech. Microeng*., 10, 287-292 (2000).

[Leo 1980] Leonberger F.J., "High speed operation of $LiNbO_3$ electro-optic interferometric waveguide modulators"*, Optics Letters*, 5(7), 312-314 (1980).

[Liu 1996] Liu P-L., "Bandwidth, field distribution, and optimal electrode design for waveguide modulators", *J. Appl. Phys*., 53(10), 6681-6686 (1982).

[Mar 1982] Marcuse D., "Optimal electrode design for integrated optics modulators"*, IEEE J. Quant. Elect*., QE-18 (3), 393-398 (1982).

[Mit 1995] Mitomi O., Noguchi K. and Miyazawa H., "Design of ultra-broad-band LiNbO3 optical modulators with ridge structure", *IEEE Trans. on Microwave Theory and Tech*., 43(9), 2203-2207 (1995).

[Mor 1989] Morichère D., Dentan V., Kjzar F., Robin P., Lévy Y.and Dumont M., "Kerr effect and electrostriction in thin polymeric films: application to polysilane films", *Optics Com*., 74(1), 69-74 (1989).

[Nag 1997] Nagata H., Mitsugi N., Ichikawa J.and Minowa J., "Materials reliability for high speed lithium niobate modulators", Invited paper, *Proceedings of the SPIE Optoelectronic Integrated Circuits*, 3006, 301-313 (1997).

[Naz 1993] Nazarathy M., Berger J., Ley A.J., Levi I.M. and Kagan Y., "Progress in externally modulated AM CATV transmission systems", *Journal of Lightwave Technology*, 11, 82-85 (1993).

[Nis 1989] Nishihara H., Haruna M. and Suhara T., *Optical Integrated Circuits*, McGraw-Hill, (1989).

[Noé 2004] Noé R., "PMD in high bit rate transmission and means for its mitigation", Invited paper, *IEEE Journal of Selected Topics in Quant.Electronics*, 10(2), 341-355 (2004).

[Nov 1995] Novak P., Kolarova P., Schröfel J., Hradilova J. and Ctyroky J., "APE waveguides in LiNbO3 and their application in electrooptic devices", *EOS meeting, Photonics* (1995)

[Pap 1975] Papuchon M., Modulation électrooptique dans les guides diélectriques plans. Etude d'un guide..., PhD Thesis, University of Paris-Sud, (1975).

[Per 1993] Persegol D., Pic E. and Plantier J., "Experimental study of a ZnO modulator using guided wave resonance", *J. Appl. Phys*., 73(6), 2563-2565 (1993).

[Por 2000] Porte H., Jerome H., Pascal M., "Modulateurs electro-optiques large bande", Brevet FR 2 816 719 – A1 (2000).

[Ram 1982] Ramer O.G., "Integrated optic electrooptic modulator electrode analysis", *IEEE J. Quant. Elect*., QE-18(3), 386-392 (1982).

[Ran 1992] Rangaraj M., Hosoi T.and Kondo M., "A wide-band Ti:LiNbO3 optical modulator with a conventional coplanar waveguide type electrodes", *IEEE Photonics Tech. Letters*, 4(9), 1020-1022 (1992).

[Ree 1987] G.T.Reed and B.L.Weiss, "Electro-optic effect in He+ implanted optical waveguides in $LiNbO_3$", *Elect. Letters* 23 (.8), 424 (1987).

[Ree 2005] Reed G.T. and Jason Png C.E., "Silicon optical modulators", *Materials Today*, 40-50 (2005).

[Sab 1986] Sabatier C. and Caquot E., "Influence of a dielectric buffer layer on the field distribution in an electrooptic guided wave device", *IEEE J. Quant. Elect*., QE-22, 32-37 (1986).

[Sal 1991] Saleh B.E.A. and Teich M.C., *Fundamentals of Photonics*, John Wiley & Sons (1991).

[San 1999] Sanchez F., *Optique non linéaire*, Ellipse (1999).

[Shi 1994] Shiess M. and Carlden H., "Evaluation of the chirp parameter of a Mach-Zehnder intensity modulator", *Electronics Letters*, 30(18), 1524-1525 (1994).

[Sun 2002] Sunnerud H., Karlsson M., Xie C. and Andrekson P.A., "Polarization-mode dispersion in high-speed fiber-optic transmission systems", *J. Lightwave Technol*., 20, 2204- (2002)

[Suz 2003] Suzuki Y. and Toba H., "Recent research and development of all-optical wavelength conversion devices", Selected papers, *NTT Technical Review*, 1(1), 26-31 (2003).

[Swa 1995] Swalen J.D. and Thackara J.I., "Electro-optic measurements of poled polymeric films", *N-L.Optics*, 10, 371 (1995).

[Tam 1990] Tamir T., *Guided Wave Optoelectronics*, 2nd Edition (Springer series in electronics and photonics), Springer, (1990).

[Ten 1988] Teng C-C. and Stuetz D.E., Thin film waveguide electrooptic modulator, United States Patent no. 4, 787, 169 (1988).

[Tsa 1988] Tsai C.S., "Integrated-optical device modules in $LiNbO_3$ for computing and signal processing", *Journal of Modern Optics*, 35(6), 965-977 (1988).

[Tur 1966] Turner E.H., "High frequency electrooptic coefficients of lithium niobate", *Appl. Phys. Lett*., 8(11), 303-304 (1966).

[Van 1974] Vandenbulcke P. and Lagasse P.E., "Static field analysis of thin film electrooptic light modulators and switches", *Wave Electronics*, (1), 295-308 (1974/76)

[Vog 1987] Voges E., "Integrated electro-optic devices", in Günter P. (Ed.), *Electro-optic and Photorefractive Materials*, Springer, Berlin (1987).

[Won 1982] Wong K.K., De La Rue R.M. and Wright S., "Electro-optic waveguide frequency translator in $LiNbO_3$ fabricated by proton exchange", *Optics Letters*, 7(11) 546-548 (1982).

[Woo 1993] Wooten Ed.L., and Chang S.C., "Test structures for characterization of electrooptic waveguide modulators in lithium niobate", *IEEE J. of Quantum Electronics*, 29(1), 161-170 (1993).

[Woo 2000] Wooten E.D.L., Kissa K.M., Yi-Yan A., Murphy E.J., Lafaw D.A., Hallemeier P.F., Maack D., Attanasio D.V., Fritz D.J., McBrien G.J. and Bossi D.E., "A review of lithium niobate modulators for fiber-optic communications systems", *IEEE Journal of Selected Topics in Quant.Electronics*, 6(1), 69-82 (2000).

[Yar 1984] Yariv A. and Yeh P., *Optical Waves in Crystal*, John Wiley & Sons, New York (1984).

This page intentionally left blank

Chapter 6

Photonic Crystal Waveguides

Throughout this book, we have seen that it is possible to handle the light by successive total reflections on guiding structure interfaces. Under these conditions, we obtain a light confinement in the space of a few microns, which supports the radiation-matter interactions and increases the non-linear optical effects. This phenomenon of total reflection is at the foundation of many optoelectronic components which play a central role in various applications, and in particular in optical telecommunications. To carry out a total reflection, it is necessary to structure the refractive index of the material at a micrometric scale.

Moreover, micro-structuring the non-linear optical properties of the material ($\chi^{(2)}$) acts directly on the phase of the wave which is propagated there and reaches an artificial phase matching between the harmonic wave and the fundamental wave (see Chapter 4). This process makes it possible to reach high performances of frequency doubling. Structuring the linear and non-linear optical properties of a material on a micrometric scale makes it possible to develop miniature components to handle the light.

From this perspective, the essential question now is: can we structure these linear and non-linear optical properties on a sub-micrometric scale (nanometric), and what will be the consequences on the light manipulation? The answer to these two questions is the focus of this last chapter.

For more than ten years, the nano-structured materials, also called photonic crystals, have been the subject of increased interest, from the fundamental point of view of the comprehension of the physics which controls the light propagation in such mediums, or from the applications point of view of developing new

functionalities and designing new photonic components [Joa 1995, Lou 2003, Lou 2004, Mer 2003, Miz 2001, Kra 1999, Yab 1987, Yab 1993]. These new structures could be at the foundation of the future lasers, optical fibers or mirrors, etc. Moreover, the expected applications extend to many other fields of optoelectronics.

In this chapter, we will be interested in these structures, and will describe light propagation under such conditions (photonic crystals). This chapter is designed as an introduction to this field of photonics which is in full rise. Interested readers will be able to find many works and publications specializing in this field. Finally, we will give, at the end of this chapter, some examples of components based on photonic crystal structures.

6.1. Dispersion relation

Light confinement using the sub-micrometric structuring of the refractive index could been seen as a change of paradigm in the evolution of scientific ideas and concepts. As will be shown, this confinement is due to the existence of a photonic band gap structure (forbidden photonic bands). That is similar to what exists for semiconductor materials which have a forbidden band where the electrons with certain energies cannot exist [Joa 1995, Lou 2003, Lou 2004, Lou 2004b, Mer 2003, Miz 2001, Kra 1999, Yab 1987, Yab 1993].

Consequently, it is easy to understand that the duality between the photon and the electron will provide new possibilities for the handling of the photon. Indeed, from the optical point of view, the potential in which the photon moves is the material refractive index (or a function of n). It is the equivalent of the potential V for the electron. Moreover, from the optical point of view, modification of the "optical potential" is carried out using non-linear optical effects. This emphasizes the benefits of producing photonic crystals in non-linear optical materials.

In order to better understand the concept of the photonic bandgap, it would be necessary to reconsider basic concepts, such as the relation of dispersion and the electron-photon analogy.

6.1.1. *Dispersion relation of an isotropic medium*

Whatever the medium within which is the electromagnetic wave is propagated, its evolution is always described by the following Maxwell's equations:

$$\begin{aligned}
&\vec{\nabla} \wedge \vec{E} = -\mu_0 \frac{\partial \vec{H}}{\partial t} \\
&\vec{\nabla} \wedge \vec{H} = \frac{\partial \vec{D}}{\partial t} \\
&\vec{\nabla} \vec{E} = 0 \\
&\vec{\nabla} \vec{H} = 0 \\
&\vec{B} = \mu_0 \vec{H} \quad \text{and} \quad \vec{D} = \varepsilon \vec{E}
\end{aligned} \tag{6.1}$$

In the particular case of the isotropic mediums, the relation between the electric field displacement vector $\vec{D}$ and the electric field vector are linear, and the coefficient of proportionality ε (dielectric permittivity) is scalar. This relation translates the interaction between the electric field of the wave and the charges of the medium.

In the case of a plane wave, we have:

$$\begin{aligned}
&\vec{E}(\vec{r}, t) = \vec{E} e^{\,i(\omega t - \vec{k}\vec{r})} \\
&\vec{H}(\vec{r}, t) = \vec{H}\, e^{\,i(\omega t - \vec{k}\vec{r})}
\end{aligned} \tag{6.2}$$

Maxwell's equations become:

$$\begin{aligned}
&\vec{k} \wedge \vec{E} = \omega \mu_0 \vec{H} \\
&\vec{k} \wedge \vec{H} = -\omega \vec{D} \\
&\vec{k}.\vec{E} = \vec{k}\vec{D} = 0 \\
&\vec{k}\vec{B} = \mu_0 \vec{k}\vec{H} = 0
\end{aligned} \tag{6.3}$$

A simple calculation by using the first two equations of [6.3] led to the following relation of dispersion:

$$\vec{k} \wedge \left(\vec{k} \wedge \vec{E}\right) + \omega^2 \mu_0 \varepsilon \vec{E} = 0 \tag{6.4}$$

However from equations [6.3], $\vec{E}$ and $\vec{k}$ are orthogonals, thus the previous relation becomes:

$$\left(k^2 - \omega^2 \varepsilon \mu_0\right) \vec{E} = 0 \tag{6.5}$$

This equation makes it possible to obtain the dispersion relation of the medium, which is independent of the direction of propagation

$$k^2 - \omega^2 \varepsilon \mu_0 = 0 \qquad [6.6]$$

or:

$$\omega(k) = \frac{c}{\sqrt{\varepsilon}} k \qquad [6.7]$$

This relation represents a straight line as is schematically indicated in Figure 6.1.

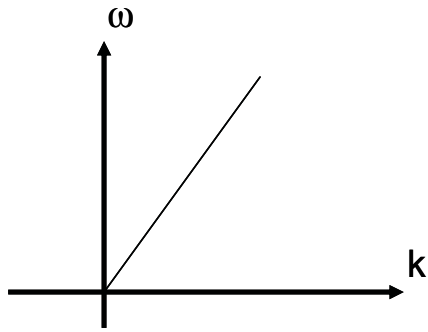

Figure 6.1. *The dispersion relation of a linear medium*

6.1.2. *Dispersion relation of an anisotropic medium*

In an anisotropic medium, light propagation is a little more complicated since ε becomes a tensor $[\varepsilon]$, and relation [6.5] is written [Sal 1991, San 1999]:

$$\left(\vec{k}\vec{E}\right)\vec{k} - k^2\vec{E} + \omega^2\mu_0[\varepsilon]\vec{E} = 0 \qquad [6.8]$$

This equation leads to a relation between the $\vec{k}$ and $\vec{E}$ components:

$$\begin{pmatrix} \omega^2\varepsilon_x\mu_0 - k_y^2 - k_z^2 & k_x k_y & k_x k_z \\ k_y k_x & \omega^2\varepsilon_y\mu_0 - k_x^2 - k_z^2 & k_y k_z \\ k_z k_x & k_z k_y & \omega^2\varepsilon_z\mu_0 - k_x^2 - k_y^2 \end{pmatrix} \begin{pmatrix} E_x \\ E_y \\ E_z \end{pmatrix} = 0 \qquad [6.9]$$

We obtain three linear and homogenous equations which determine the electric field components. To have a non zero solution, the determinant of the system must be zero. Moreover, it is necessary for the direction of the electric field to be specified. The solution of this equation gives the dispersion relation of the medium (the pulsation according to the wave number k). Actually, this problem was well-known during the study of uniaxial and biaxal anisotropic mediums; in particular making it possible to determine the index surfaces.

6.1.3. *Dispersion relation in waveguides*

The propagation of an electromagnetic wave in a guiding structure was covered in Chapter 1. In this part the equation of dispersion of the guided modes is to be reconsidered to transform it into a relation between ω (the wave pulsation) and β, the propagation constant. For simplicity, the superstrate and the substrate are called mediums 1 and 3 respectively. The guiding area will be regarded as medium 2.

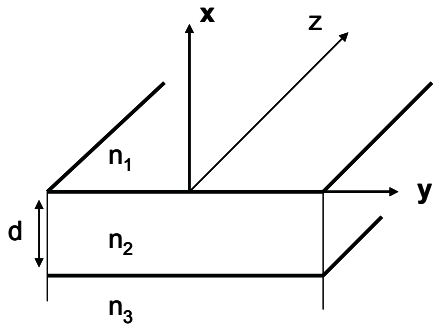

Figure 6.2. *Guiding structure representation*

Under these conditions, the equation of dispersion of the guided modes is written (see Chapter 1):

$$\begin{aligned} &2kd\sqrt{\left(n_2{}^2 - N_m^2\right)} = \Phi_{(n_2,n_a)} + \Phi_{(n_2,n_s)} + 2m\pi \\ &N_m = n_2 \sin\theta_m \end{aligned} \qquad [6.10]$$

$$\Phi_{(n_2,n_j)} = 2arctg\left[\left(\frac{n_2}{n_j}\right)^{2\rho}\left(\frac{\left(N_m^2 \quad n_j^2\right)}{\left(n_2^2 \quad N_m^2\right)}\right)^{1/2}\right]$$
$$j = 2, 3 \qquad [6.11]$$
$$\rho = \begin{cases} 0 \text{ for } TE \text{ polarization} \\ 1 \text{ for } TM \text{ polarization} \end{cases}$$

Knowing that:

$$\beta_m = kN_m$$
$$kn = \frac{\omega}{c} \qquad [6.12]$$

we can write the following dispersion relation [Sal 1991]:

$$2d\left[\left(\frac{\omega}{c_2}\right)^2 - \beta^2\right]^{1/2} = \Phi_{(n_2,n_a)} + \Phi_{(n_2,n_s)} + 2m\pi \qquad [6.13]$$

with:

$$\Phi_{(c_2,c_j)} = 2arctg\left[\left(\frac{c_j}{c_2}\right)^{2\rho}\left(\frac{\beta_m^2 \quad \left(\frac{\omega}{c_j}\right)^2}{\left(\frac{\omega}{c_2}\right)^2 \quad \beta_m{}^2}\right)^{1/2}\right]$$
$$j = 2,\ 3 \qquad [6.14]$$
$$\rho = \begin{cases} 0 & \text{pol. TE} \\ 1 & \text{pol. TM} \end{cases}$$

As an example, Figure 6.3 represents the calculation of the dispersion of the MEH-PPV guiding layer in space (ω, k), for the material transparency wavelengths.

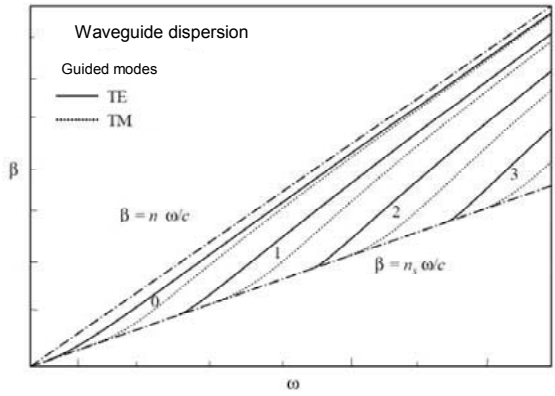

Figure 6.3. *Example of a dispersion relation: planar waveguide (MEH-PPV guiding thin film)*

In the following sections, it will be a question of finding the dispersion relation of mediums whose refractive index presents a spatial periodicity according to 2 dimensions (i.e. photonic crystals). We will also see the consequences of this periodicity on light propagation in such a medium.

6.2. Photonic crystals

6.2.1. *Definitions*

In this section, we will try to use a formal analogy which exists between the electron and the photon, in order to understand the physical nature of the photonic crystals. The photons and the electrons have similar characteristics; such as, the wave-corpuscle duality. In addition, there is a formal analogy between the Schrödinger equation for the electron and Maxwell's equations for the photon [Lou 2003, Lou 2004, Lou 2004b, Mer 2003].

According to quantum mechanics, in the stationary mode, the states of a system are given by Schrödinger's eigenvalues equation [Coh 1977, Kit 1983]:

$$H\Psi^{(n)} = E_n \Psi^{(n)}$$
$$\text{with } H = -\frac{\hbar^2 \Delta}{2m} + V \qquad [6.15]$$

where m is the electron mass, $\hbar$ Planck's constant divided by 2π, Ψ the wave function, E the electron energy and $V(x)$ represents the potential distribution.

In a crystalline material, the potential V has the same periodicity of Bravais's lattice of the structure.

Under these conditions, Bloch's theorem [Coh 1997, Kit 1983] announce that the solutions of Schrödinger's equation for such potentials have the shape of a product of a plane wave by a function $u(\vec{r})$, that has the same periodicity as the crystal lattice.

$$\begin{aligned} &\Psi(\vec{r}) = u(\vec{r})\ e^{ikr} \\ &\text{with}\ \ u(\vec{r}+\vec{R}) = u(\vec{r}) \\ &\vec{R}: \text{lattice vector} \end{aligned} \qquad [6.16]$$

Consequently, the essential properties of the crystal are described by its structure of energy bands which represent the variation of the eigenvalues according to the wave vector $\vec{k}$.

From the electromagnetic point of view, the state of an optical system is described perfectly by the Maxwell's equations [6.1]. By using relations [6.2] in the plane wave approximation, we can write:

$$\vec{E} = \frac{c^2}{i\omega\varepsilon}\vec{\nabla} \wedge \vec{B} \qquad [6.17]$$

we can also write:

$$\vec{\nabla} \wedge \left(\frac{1}{\varepsilon}\vec{\nabla} \wedge \vec{B}\right) = \frac{\omega^2}{c^2}\vec{B} \qquad [6.18]$$

This relation is written in a way similar to Schrödinger's equation [6.15]:

$$\begin{aligned} &\Theta\vec{B} = \left(\frac{\omega}{c}\right)^2 \vec{B} \\ &\text{with}\ \ \Theta = \vec{\nabla} \wedge \left(\frac{1}{\varepsilon}\vec{\nabla} \wedge\right) \end{aligned} \qquad [6.19]$$

The tensorial operator Θ is called Maxwell's operator. It is easy to show that the operator is Hermitian. Under these conditions, the solutions of the

electromagnetic problem are given by the eigenvectors and the eigenvalues of this operator. We will give some examples of solutions to this type of problem as well as the methods employed.

The following table points out the electron-photon similarity.

	Electron (Schrödinger)	*Photon (Maxwell)*
Field	$\psi(r,t) = \psi(r)\exp(-i\omega t)$	$\vec{H}(\vec{r},t) = \vec{H}(\vec{r})\exp(-i\omega t)$
Specific term	$V(r)$	$\vec{E}(\vec{r})$
Hermitian operator	$H = \frac{-\hbar^2\nabla^2}{2m} + V(r)$	$\Theta = \nabla \times \left(\frac{1}{\varepsilon(r)}\nabla \times\right)$
Eigenvalue equation	$H\psi = E\psi$	$\Theta\vec{H} = \left(\frac{\omega^2}{c^2}\right)\vec{H}$

Table 6.1. *Electron-photon similarity*

Ultimately, electronics is based on crystal properties in the field of solid state physics. The principal characteristic of crystals is their periodicity or more precisely the periodicity of their atomic potential V. This has direct consequences for the distribution of the electrons of this crystal. Indeed, in atoms, the electrons occupy discrete energy levels. However, when a certain number of atoms are laid out together in a periodic way, an energy bands structure appears replacing the discrete levels of the isolated atom. Moreover, for a certain interatomic distance, this band is divided into two parts separated by a zone empty of energy levels [Coh 1997, Kit 1983]. This zone is called the forbidden band (FB); see for example Figure 6.4.

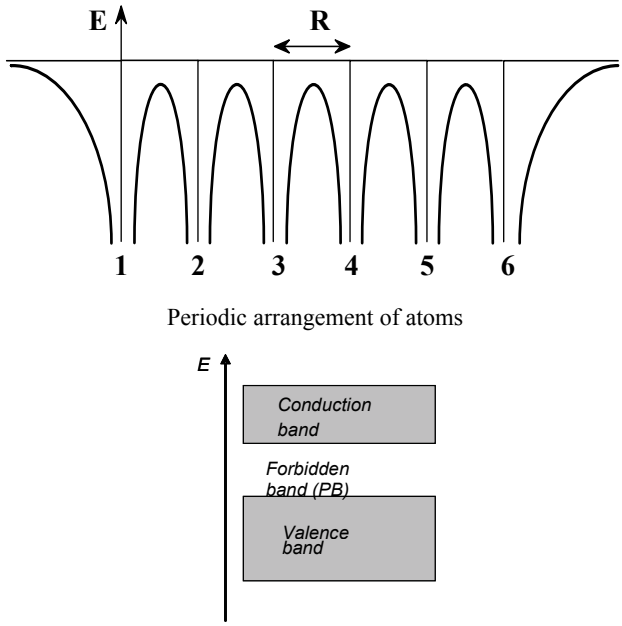

Figure 6.4. *Band structures in crystal*

By considering the same approach for photons, we can define the photonic band gap (PBG) as being the consequence of periodic structuring of the photon potential, i.e. the refractive index. However, the nature of the photon is different from that of the electron:

– photons are represented by vector quantities, whereas electrons are of scalar nature;

– photons do not interact between themselves;

– photon energy cannot be modified. The photon can be either absorbed or emitted. If not, its energy and its frequency are preserved;

– photons are regarded as bosons and thus they are governed by Bose-Einstein's statistics.

6.2.2. *Bragg's mirror*

To understand the photonic crystal concept, let us start with a unidimensional approach: Bragg's mirror. This component is made up of a succession of transparent material layers whose refractive indices are different. On each interface between two layers, the light is partially reflected and transmitted (see Figure 6.5).

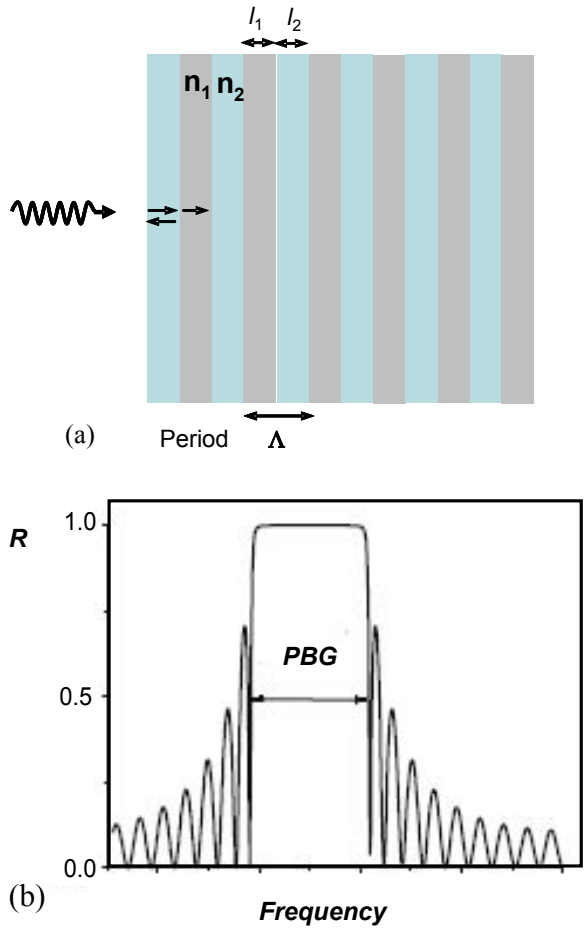

Figure 6.5. *Bragg's mirror: (a) Λ is the lattice period; (b) the reflected intensity indicating the PBG*

The emergent rays from the multi-layer structure each have a different optical path according to the number of reflections that they underwent. Indeed, the optical path δ is defined by (assuming normal incidence):

$$\delta = \sum_i n_i l_i \qquad [6.20]$$

where l_i is the *ith* layer thickness and n_i its index.

These rays, thus, each have a phase which depends on their trajectory throughout the various layers:

$$\phi = \frac{2\pi\delta}{\lambda} \qquad [6.21]$$

λ : wavelength

Note that phase mismatch between the emerged rays depends on the wavelength used. At the output of the device, the phase mismatch between the various transmitted waves gives rise to destructive or constructive interferences. More precisely, if the optical paths $n_1 l_1$ and $n_2 l_2$ are of the quarter wavelength considered, then the incident light is not propagated in the medium. We, thus, obtain a total reflection at the entry of the mirror which leads to a photonic band gap in frequency. The width of this PBG is a function of the index difference, as well as the angle of incidence of the beam. In this last case, the device behaves like a selective mirror for given wavelengths. Consequently, the refractive index periodicity creates a photonic band gap for this wavelength. This first approach illustrates the case of a 1D photonic crystal.

As a matter of fact, photonic crystals are the generalization of Bragg's mirrors to 2D and 3D.

6.2.3. *Photonic crystal geometries*

In this section, we focus on 2D and 3D photonic crystal structures; Figures 6.6a and 6.6b, respectively. The principle of Bragg's mirror based on the periodicity of the refractive index is applied to 2D and 3D in the case of photonic crystals. The benefit of producing 2D or 3D periodic structures is that they make it possible to obtain a total or PBG for all the directions of the beam propagation. Here are some simple examples:

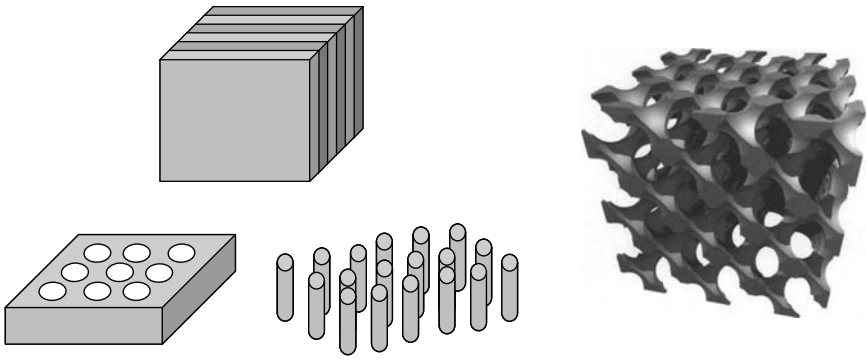

(a) (b)

Figure 6.6. *Examples of photonic crystals (a) 2D and (b) 3D*

The most interesting 3D configurations are based on diamond structures. There are two forms (see Figure 6.7): the first (a) known as "woodpile", and the second (b) known as "hexagonal" (resulting from two observation angles that differ from diamond) represented hereafter by the *Yablonovite*.

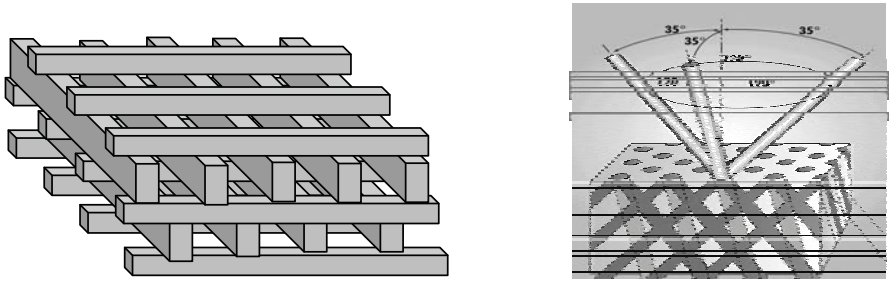

(a) Woodpile structure (b) Hexagonal structure (Yablonovite)

Figure 6.7. *Examples of 3D photonic crystals*

6.2.4. *2D photonic crystal cells*

Generally, photonic crystals are structured according to their lattice similarly to crystal lattices. We distinguish three principal families according to the PBG lattice form [Joa 1995, Lou 2003, Lou 2004, Mer 2003, Miz 2001, Kra 1999, Yab 1987,

Yab 1993]: the square, triangular and hexagonal lattice (see Figure 6.8). These cells can be of two forms: air holes in the material, or cylinders of the material in air.

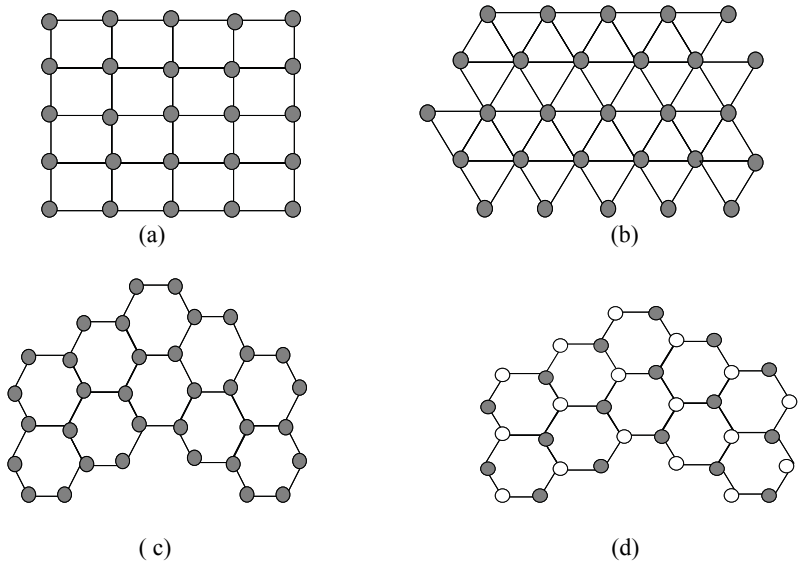

Figure 6.8. *Examples of 2D photonic crystal cells*

Square lattice: the elementary cell is a square of side *a* (see Figure 6.8a). This lattice is very sensitive to the angle of incidence and the polarization of the electromagnetic waves. Its first Brillouin's zone is a right-angle isosceles triangle (see Figure 6.9a). It was shown that this lattice does not make it possible to obtain a total band gap. In other words, it is difficult to simultaneously obtain a photonic band gap for polarizations TE and TM [Vil 1992a, Vil 1992b].

Triangular lattice: in this case the elementary cell is an equilateral triangle of side *a* (see Figure 6.8b). The first Brillouin's zone is a hexagon (see Figure 6.9b). This structure offers a better compromise when the filling factor is high, in other words when the holes diameter is close to the period of the grating. It is less sensitive to the angle of incidence than the square structure, however it remains difficult to obtain a total photonic band gap [Kua 2005].

Hexagonal lattice: this lattice can be obtained by removing some nodes of the triangular grating. It offers the best compromise between the technological constraints and the performances of the structure. We can distinguish two types of hexagonal lattice: the graphite structure (see Figure 6.8c) where all the nodes are

identical and are spaced of a – similar to the graphite structure – and the structure known as boron nitride (see Figure 6.8d) where a node differs from its neighbor by its nature or its dimension. This structure makes it possible to obtain broad PBGs [Cas 1996, Vil 1992b, Ye 2004, Zha 1997].

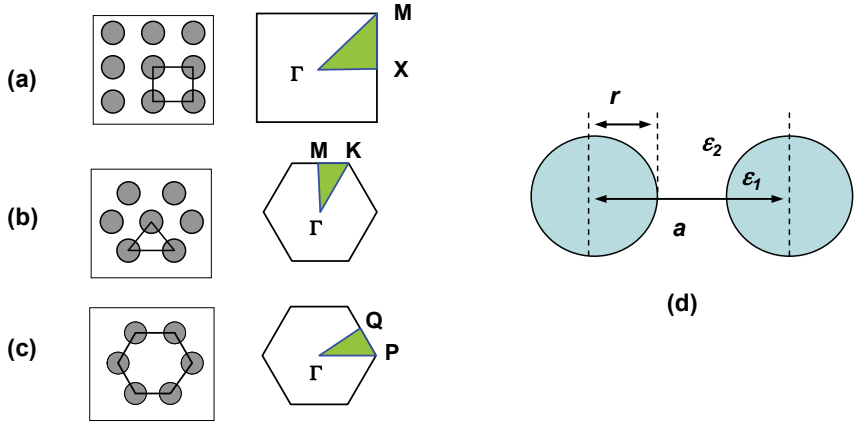

Figure 6.9. *Examples of 2D-PBG and their first Brillouin's zone: (a) square cell, (b) triangular and (c) hexagonal; and. (d) definition of the lattice radii r and period a*

The characteristics of PBG depend in particular on the grating parameters. The ratio r/a (see Figure 6.9d) as well as the difference in permittivity $\Delta\varepsilon = \varepsilon_1 - \varepsilon_2$ are the most influential parameters on the position and the width of the band gap [Joa 1995, Lou 2003, Lou 2004, Mer 2003, Miz 2001, Kra 1999, Yab 1987, Yab 1993].

Finally, only the 3D lattice provides a total PBG regardless of the direction of propagation [Ast 1997, Cas 1996, Cas 1997, Chu 2005, Rom 2003]. That allows, in particular, the complete inhibition of spontaneous emission, and the localization of the light on defects such as microcavities type. 3D-light confinement effects are also possible.

Although from the crystalline point of view there exist 7 types of cells and 14 types of Bravais's grating, the transposition of these structures to the photonic crystals remains technologically very difficult. However, the fabrication of "woodpile" [Lin 1999, Özb 1994] and Yablonovites [Yab 1993] structures presented above is well controlled for the microwaves field, but constitutes a major challenge for applications in the optical field.

6.2.5. *Electron-photon analogy*

Before developing the methods used to model 2D photonic crystals, we first point out some essential properties of the electrons in a crystal. A crystalline structure is considered to be a structure whose atoms are periodically arranged on a grating. Each atom has a mobile electron. As mentioned previously, the study of the properties of these electrons can be carried out using the Bloch's model based on the following assumptions [Kit 1983, Mer 2003]:

– the electrons are independent;

– the ions of the crystal are fixed on the grating;

– the electrons undergo the periodic potential resulting from a Coulomb interaction with the grating ions and interaction with the other electrons of the grating. This potential will have the same periodicity as the grating itself.

Within the framework of the Kronig-Penny's 1D-crystal model [Kit 1983], we consider a periodic square-well potential, which varies from 0 to V_0, with a period d equal to that of the grating itself (see Figure 6.10).

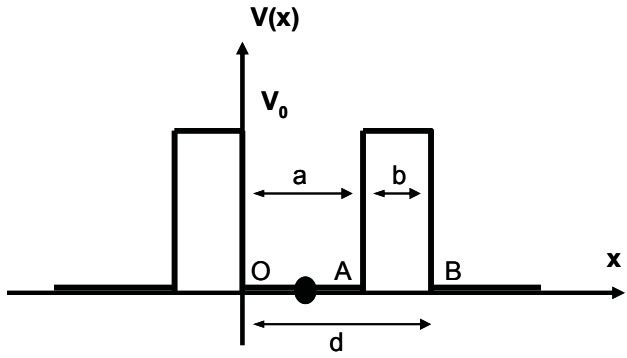

Figure 6.10. *1D periodic square-well potential*

In this case, Schrödinger's wave equation is written in the following form:

$$\frac{\partial^2 \Psi}{\partial x^2} + \frac{2m}{\hbar^2}\left(E - V(x)\right)\Psi = 0 \qquad [6.22]$$

where m is the electron mass, $\hbar$ is Planck's constant divided by 2π, Ψ is the wave function, E is the electron energy and $V(x)$ represents the distribution of the potential.

In the interval [O, A], we have $0 < x < a$ and $V = 0$, therefore equation [6.22] becomes:

$$\frac{\partial^2 \Psi_1(x)}{\partial x^2} + \frac{2m}{\hbar^2} E\Psi_1(x) = 0 \qquad [6.23]$$

In the interval [A, B], we have $a < x < a + b$ and $V = V_0$, then equation [6.22] is written:

$$\frac{\partial^2 \Psi_2(x)}{\partial x^2} + \frac{2m}{\hbar^2}(E - V_0)\Psi_2(x) = 0 \qquad [6.24]$$

with $E < V_0$.

Thus, the solutions of equation [6.22] within the interval O-A are:

$$\begin{aligned} \Psi_1(x) &= A\sin(px) + B\sin(px) && \text{zone [O, A]} \\ \Psi_2(x) &= Ce^{qx} + De^{qx} && \text{zone [A, B]} \end{aligned} \qquad [6.25]$$

with

$$p = \sqrt{\frac{2mE}{\hbar^2}}$$

$$q = \sqrt{\frac{2m}{\hbar^2}(V_0 - E)}$$

By using the continuity conditions at the edges of the potential-well and the periodicity conditions of Bloch's solutions we obtain four equations with four unknown factors A, B, C and D. The solution of this system (non-zero determinant not zero) leads to the following condition [Kit 1983, Mer 2003]:

$$\cos(pa)ch(qb) + \frac{q^2 - p^2}{2pq}\sin(pa)sh(qb) = \cos(k(a + b)) \qquad [6.26]$$

This can be written as:

$$F(p, q) = \cos(k(a + b)) \qquad [6.27]$$

The function F(p, q) is displayed in Figure 6.11. This highlights the existence of an energy band gap for the electron in the crystalline structure considered.

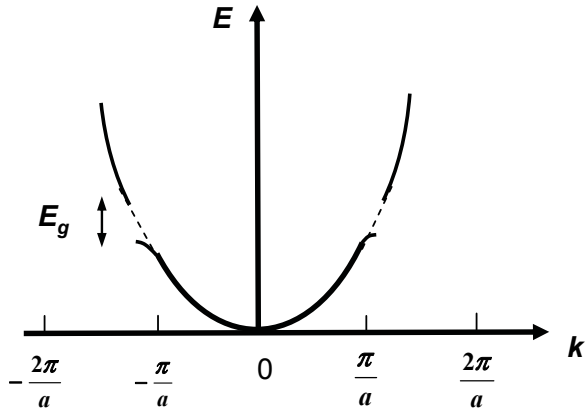

Figure 6.11. *Energy bands of electrons in a square-well potential*

6.2.6. *Dispersion relation and band structures*

In this part it will be a question of seeing how to transpose the preceding calculations in the case of the propagation of an electromagnetic wave in a periodic medium. Let us consider the case of a 1D perfect dielectric medium characterized by a periodic dielectric permittivity $\varepsilon_r(x)$ (refractive index) as indicated in Figure 6.12.

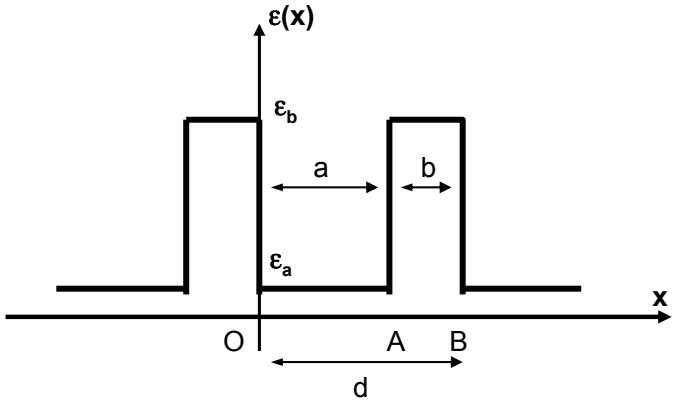

Figure 6.12. *Representation of a 1D photonic crystal*

$$\varepsilon_r(x+d) = \varepsilon_r(x) \qquad [6.28]$$

Helmholtz's equation derived from Maxwell's equation is:

$$\frac{\partial^2 E(x)}{\partial x^2} + \frac{\omega^2}{c^2}\varepsilon_r(x)E(x) = 0 \qquad [6.29]$$

As with the previous Schrödinger's equation, it is easy to identify the term $\frac{\omega^2}{c^2}\varepsilon_r(x)$ with q^2 and the electric field *E(x)* with the wave function *Ψ(x)*. By considering the same approach presented in the previous section, we can show that solutions of this equation can be written for 0<x<a:

$$\begin{aligned} E_1(x) &= A\sin(\alpha x) + B\sin(\alpha x) \qquad 0 < x < a \\ E_2(x) &= C\sin(\beta x) + D\sin(\beta x) \qquad a < x < a + b \end{aligned} \qquad [6.30]$$

with:

$$\alpha = \frac{\omega}{c} \text{ and } \beta = \frac{\omega}{c}\sqrt{\varepsilon_r}$$

Note that solutions of the propagation equation are Bloch's functions of the form $E(x) = u_k(x)e^{ikx}$.

$u_k(x)$ is a periodic function of the same period as the dielectric permittivity (period d). Using the pervious method, the field continuity and its derivative, as well as the periodicity of the function ε(x) and its derivative, make it possible to deduce the following equation of dispersion:

$$\cos(\alpha a)\cos(\beta b) - \frac{\varepsilon_r + 1}{2\sqrt{\varepsilon_r}}\sin(\alpha a)\sin(\beta b) = \cos(k(a+b)) \qquad [6.31]$$

According to this equation, the left member must range between -1 and +1. However it can take values higher than +1 or lower than -1. In this case, there are no wave vectors *k* fulfilling this relation. Thus, the electromagnetic waves with these wave- vectors cannot be propagated in this medium. We then refer to the photonic band gap.

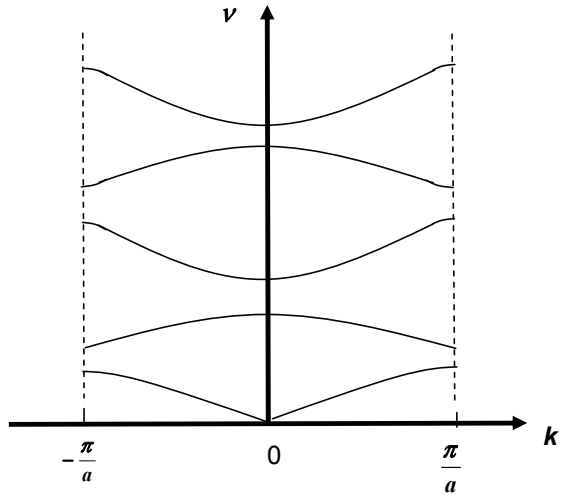

Figure 6.13. *Structure of 1D lattice photonic band gap*

We find the same behavior seen in the case of the electron. However, in this approach we did not take into account the vectorial nature of the electromagnetic field. Indeed, solving this problem becomes more complicated by taking into account the polarization of electric field.

6.2.7. *Simulation methods*

To solve this problem in particular with 2D or 3D, several theoretical simulation methods were developed [Cas 1995, Hes 2003, Lav 2004, Leu 1993, Rom 2004, Thé 1999, Wu 2003, Yee 1966], for example, the:

– finite momentum method;

– finite element method;

– plane wave method;

– finite difference in time division (FDTD) method.

In this section, we only point out the principles of the two last methods which are the most frequently used. The plane wave method makes it possible to determine the structure of the photonic band gap, whereas the FDTD method is used to study the distribution of the electromagnetic field which is propagating in the PBG structure. It also makes it possible to determine the reflection and transmission coefficients.

6.2.7.1. *Plane wave method*

This method is a reference method for calculation of the PBG. The basic principle consists of using Bloch's theorem [Kit 1983]. Thus, all the spatially periodic functions are developed into spatial Furrier's series. The objective is to solve the following wave equations:

$$\begin{aligned}&\vec{\nabla} \wedge \left(\vec{\nabla} \wedge \vec{E}(\vec{r})\right) + \frac{\omega^2}{c^2}\varepsilon_r(\vec{r})\vec{E}(\vec{r}) = 0\\&\vec{\nabla} \wedge \left(\frac{1}{\varepsilon(\vec{r})}\vec{\nabla} \wedge \vec{H}(\vec{r})\right) + \frac{\omega^2}{c^2}\varepsilon_r(\vec{r})\vec{H}(\vec{r}) = 0\end{aligned} \quad [6.32]$$

With Bloch's theorem, the electric field and the dielectric permittivity can be written in the following way [Lou 2003, Mer 2003, Kit 1983]:

$$E(\vec{r}) = e^{\,i(\vec{k}\,\vec{r})} \sum_{\vec{G}} E(\vec{G}) e^{i\vec{G}\,\vec{r}} \quad [6.33]$$

$$\varepsilon(\vec{r}) = \sum_{\vec{G}} \varepsilon(\vec{G})\, e^{i\vec{G}\vec{r}} \quad [6.34]$$

To release from the vectorial aspect of this equation, it is convenient to study the case of two principal polarizations TM and TE. Then, for a TM polarization the electric field which is propagated in the xOy plane is written:

$$E_z(x,y) = E(x,y) e^{\,i(k_x x + k_y y)} \quad [6.35]$$

where k_x and k_y are the components of the wave-vector along the x and y directions.

Helmholtz's equation becomes:

$$\frac{\partial^2 E_z}{\partial x^2} + \frac{\partial^2 E_z}{\partial y^2} + \frac{\omega^2}{c^2}\varepsilon_r(x,y)E_z = 0 \quad [6.36]$$

The electric field amplitude periodicity allows us to write:

$$E_z(x,y) = e^{\,i(k_x x + k_y y)} \sum_{\vec{G}} E(\vec{G}) e^{i\vec{G}\vec{r}} \quad [6.37]$$

with $\vec{G} = 2\pi\vec{g} = 2\pi\left(h_1\vec{g}_1 + h_2\vec{g}_2\right)$ a vector of the reciprocal grating.

In the same manner, the dielectric permittivity is:

$$\varepsilon(x, y) = \sum_{\vec{G}} \varepsilon\left(\vec{G}\right) e^{i\left(G_x x + G_y y\right)} \qquad [6.38]$$

By injecting the previous components of the plane wave into Helmholtz's equation, and after simplifications, we obtain:

$$\left[\left(G_x + k_x\right)^2 + \left(G_y + k_y\right)^2\right] E\left(\vec{G}\right) = \frac{\omega^2}{c^2} \sum_{\vec{G}} \varepsilon\left(\vec{G}\right) E\left(\vec{G}\right) \qquad [6.39]$$

This equation can be written in the form of a matrix system as:

$$AX_{\vec{G}} = \mathrm{v}BX_{\vec{G}} \qquad \left(\mathrm{v} = \frac{\omega^2}{c^2}\right) \qquad [6.40]$$

$$A = \left[\left(G_x + k_x\right)^2 + \left(G_y + k_y\right)^2\right]$$

$$B = \begin{bmatrix} \varepsilon\left(\vec{G}\right) & 0 & 0 \\ 0 & \varepsilon\left(\vec{G}\right) & 0 \\ 0 & 0 & \varepsilon\left(\vec{G}\right) \end{bmatrix}$$

This system makes it possible to obtain frequencies able to propagate in the crystal. The solution consists of finding the eigenvalues of matrix A.

Now, let us consider the case of a TE polarization propagating in the xOy plane. In this case, it is better to use the magnetic field equation:

$$\vec{\nabla} \wedge \left(\frac{1}{\varepsilon(\vec{r})} \vec{\nabla} \wedge \vec{H}(\vec{r})\right) + \frac{\omega^2}{c^2} \vec{H}(\vec{r}) = 0 \qquad [6.41]$$

The same preceding considerations, i.e. the decomposition in plane waves in a base of the reciprocal grating of all the spatially periodic functions (the magnetic field and the dielectric permittivity), lead to the following eigenvalues equation:

$$f_{\vec{G}}\left(k_x^2 + k_x G_x^{'} + G_x G_{x'} + k_y^2 + k_y G_y^{'} + G_y G_{y'}\right) H_{\vec{G}} = \frac{\omega^2}{c^2} H_{\vec{G}} \qquad [6.42]$$

with $f(x,y) = \dfrac{1}{\varepsilon(x,y)}$.

In this case as well, determination of the eigenvalues provides the frequencies allowed to propagate in the photonic crystal.

This method is usually employed to describe the PBG structure in particular in the case of semiconductor materials. However, as an example, we present here the modeling of PBG structures in dielectric materials such as $LiNbO_3$. Generally, we consider a dielectric medium of permittivity ε_b and a grating of holes of permittivity ε_a and radii r (see Figure 6.14). The grating period is a.

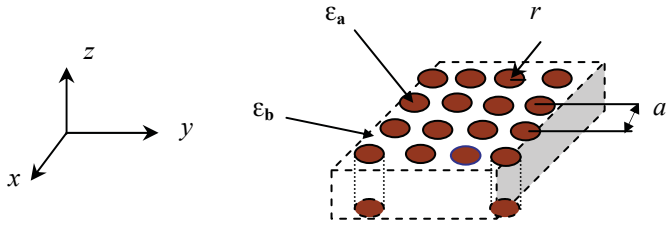

Figure 6.14. *Representation of a 2D grating*

Figure 6.15 displays results obtained for square and triangular hole lattices with lithium niobate (z-cut) for TE ($\varepsilon_b = 4.884$) TM ($\varepsilon_b = 4.584$) modes at $\lambda \quad 1.55\mu m$, and a ratio r/a = 0.41. The frequencies are given and in normalized units:

$$\frac{\omega a}{2\pi c} = \frac{v a}{c} = \frac{a}{\lambda} \qquad [6.43]$$

with ν the frequency and c the light velocity.

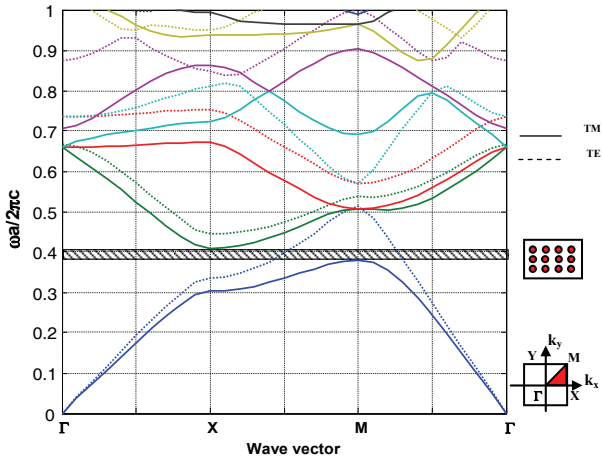

(a)

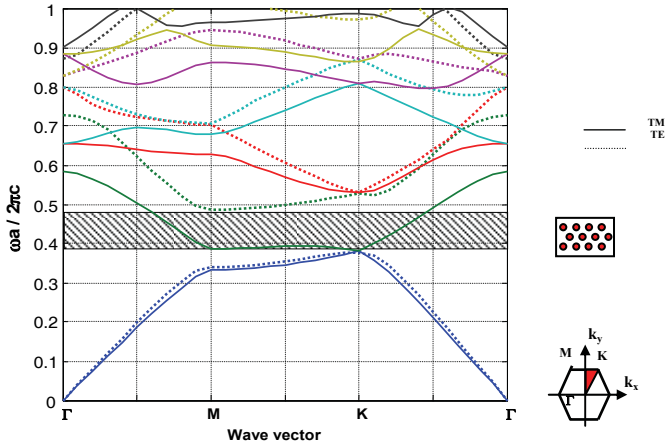

(b)

Figure 6.15. *Structure PBG of 2D grating in $LiNbO_3$: (a) a square lattice and (b) a triangular lattice [Beg 2007]*

For the square structure, we observe a PBG in TM mode. However, PBG is not possible in TE polarization regardless of the ratio r/a. For the triangular grating, we obtain a relatively broad TE PBG but in this case also no TM PBG.

The difference between the dielectric permittivity of the two mediums is an important factor. In the case of a grating of pillars (instead of holes) a larger difference favors the appearance of PBG, as indicated in Figure 6.16.

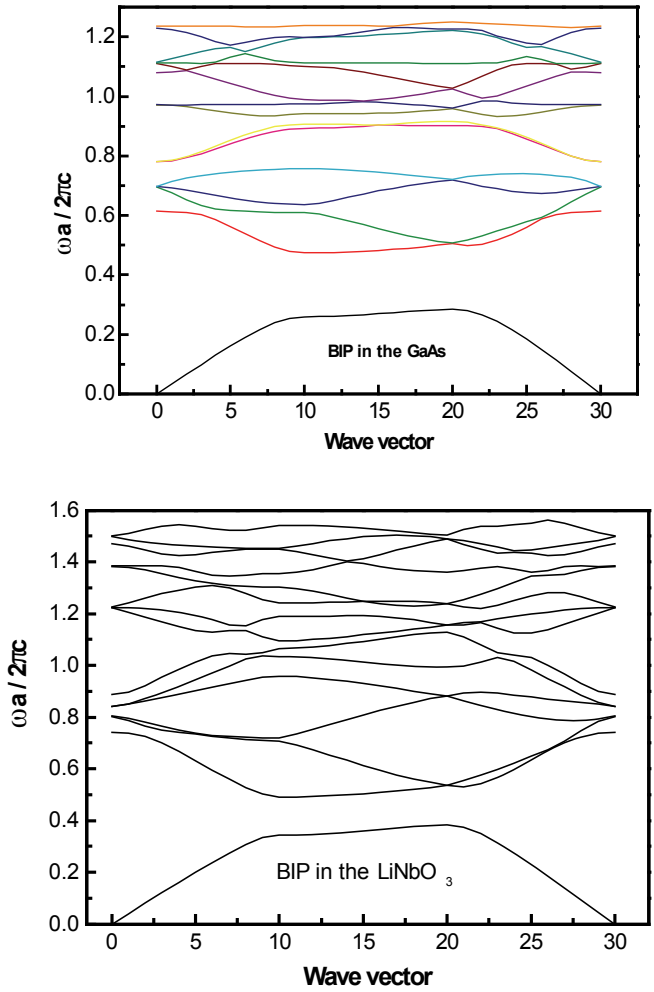

Figure 6.16. *PBG structures of pillar triangular lattice of GaAs, ε_o= 12.6 (a) and of $LiNbO_3$, ε_o= 4.884 (b), in air (TE mode)*

The second important parameter is the ratio r/a, which influences the position and the width of PBG. For example, Figure 6.17 reports the evolution of TE PBG

width for a triangular grating in $LiNbO_3$ and GaAs. Note that the maximum value corresponds to a ratio r/a of 0.41 and 0.46 in the case of $LiNbO_3$ and GaAs respectively.

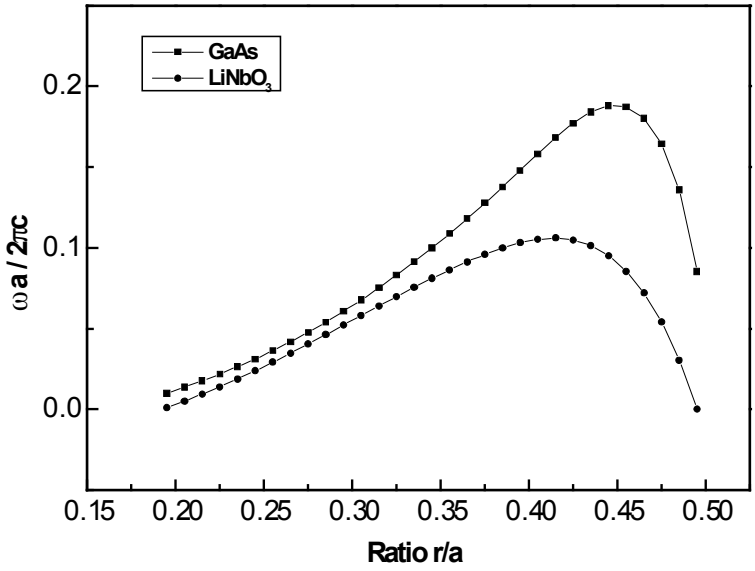

Figure 6.17. *Evolution PBG width as a function of the ration r/a for $LiNbO_3$, ε_o= 4.884 and GaAs, ε_o= 0.46 (TE mode)*

Moreover, the largest PBG is obtained for in case of GaAs thanks to the index contrast.

6.2.7.2. *Finite difference in the time division (FDTD) method*

The FDTD is a well known method of electromagnetic modeling. It is relatively easy to understand and belongs to the numerical methods based on temporal difference finite fields. The basic principle consists of solving the Maxwell's equations at a given time, then the field is found at the next time and so on. We start with a spatial and temporal grid with steps of Δx, Δy, Δz and Δt.

As an example, the Maxwell's equations for an isotropic medium are given by

$$\vec{\nabla} \wedge \vec{E} = -\mu \frac{\partial \vec{H}}{\partial t}$$
$$\vec{\nabla} \wedge \vec{H} = \sigma \vec{E} + \varepsilon \frac{\partial \vec{E}}{\partial t} \qquad [6.44]$$

These equations show that the temporal derivative of the field $\vec{E}$ depends on the curl of the field $\vec{H}$. In other words, variation in the time of $\vec{E}$ is related to that of $\vec{H}$ in space. This means that the current value of $\vec{E}$ depends on its previous value (the temporal difference), and the difference in the previous value of $\vec{H}$ on the two sides of space around the point of $\vec{E}$. Field $\vec{H}$ can be found in the same manner.

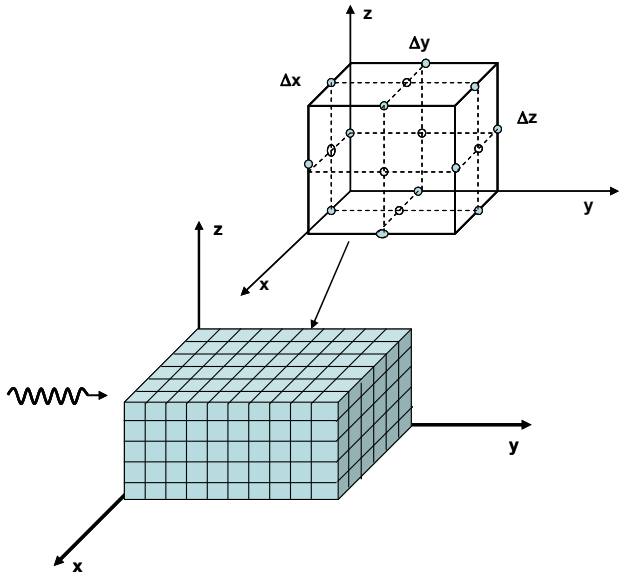

Figure 6.18. *Representation of Yee's cell [Yee 1966]*

From the mathematical point of view, the FDTD method is based on Yee's algorithm [Yee 1966]. This makes it possible to calculate at every discrete time, the components of the electromagnetic field in each parallelpiped cell of 3D volume (see Figure 6.18). The two previous equations can be written in the form of six equations using the Cartesian coordinates:

$$\begin{aligned}
\frac{\partial H_x}{\partial t} &= \frac{1}{\mu}\left(\frac{\partial E_y}{\partial z} - \frac{\partial E_z}{\partial y}\right) \\
\frac{\partial H_y}{\partial t} &= \frac{1}{\mu}\left(\frac{\partial E_z}{\partial x} - \frac{\partial E_x}{\partial z}\right) \\
\frac{\partial H_z}{\partial t} &= \frac{1}{\mu}\left(\frac{\partial E_x}{\partial y} - \frac{\partial E_y}{\partial x}\right) \\
\frac{\partial E_x}{\partial t} &= \frac{1}{\varepsilon}\left(\frac{\partial E_z}{\partial y} - \frac{\partial E_y}{\partial z} - \sigma E_x\right) \\
\frac{\partial E_y}{\partial t} &= \frac{1}{\varepsilon}\left(\frac{\partial E_x}{\partial z} - \frac{\partial E_z}{\partial x} - \sigma E_y\right) \\
\frac{\partial E_z}{\partial t} &= \frac{1}{\varepsilon}\left(\frac{\partial E_y}{\partial x} - \frac{\partial E_x}{\partial y} - \sigma E_z\right)
\end{aligned} \qquad [6.45]$$

We define a cell $\Delta x\Delta y\Delta z$ and Δt is the time step. Thus, the function of time and space is written:

$$F^n(i, j, k) = F(i\Delta x, j\Delta y, k\Delta z, n\Delta t), \qquad [6.46]$$

where n is the time index and (i, j, k) are integers that define the cell coordinates.

In these conditions, the spatial and temporal derivatives are:

$$\begin{aligned}
\frac{\partial F^n(i, j, k)}{\partial x} &= \frac{F^n\left(i + \frac{1}{2}, j, k\right) - F^n\left(i - \frac{1}{2}, j, k\right)}{\delta} \\
\frac{\partial F^n(i, j, k)}{\partial t} &= \frac{F^{n+\frac{1}{2}}(i, j, k) - F^{n\ \frac{1}{2}}(i, j, k)}{\Delta t}
\end{aligned} \qquad [6.47]$$

These two equations applied to the six preceding relations are the foundation of Yee's algorithm. Note that to have precise results, dimensions δ of the cell lower than the wavelength are generally necessary; normally $\lambda/10$. Moreover; the convergence criterion connecting the temporal and spatial steps is given by:

$$\Delta t = \frac{1}{\mathrm{v}}\left[\frac{1}{\Delta x^2} + \frac{1}{\Delta y^2} + \frac{1}{\Delta z^2}\right]^{\frac{1}{2}} \qquad [6.48]$$

where v is the wave velocity in the medium.

If the spatial period δ is the same in all cell directions ($\Delta x = \Delta y = \Delta z = \delta$), the stability criterion becomes:

$$v\frac{\Delta t}{\delta} = \frac{1}{\sqrt{N}}$$

where N is the number of the space dimensions (N=3, for instance).

Generally, the cells are characterized by different dielectric properties. While specifying $\varepsilon(i, j, k)$ and $\sigma(i, j, k)$ for each area, it is possible to determine the fields $\vec{E}$ and $\vec{H}$ in the considered area.

Once the spatial and temporal grid is carried out and the cells properties specified, the source should be determined. The latter can be a plane wave, a current or a potential difference, depending on the situation to be studied.

For a monochromatic plane wave v, the source field is written:

$$E^{inc}(x, y, z) = E_0(x, y, z)\sin(\omega t) \qquad [6.49]$$

Considering a pulse, the incident beam is turned off after a specific number of temporal periods. Thus, the incident plane wave is given by:

$$E_x^{inc}\left(i + \tfrac{1}{2}, j, k_s\right) = E_0\left(i + \tfrac{1}{2}, j, k_s\right)\sin(2\pi\upsilon\delta t) \qquad [6.50]$$

Here, it is considered that the incident field has only one E_x component and is in the $z = k_s$ plane. For each temporal step, the value $E_x^{inc}\left(i + \frac{1}{2}, j, k_s\right)$ is added to $E_x^n\left(i + \frac{1}{2}, j, k_s\right)$. To stop the algorithm, we use the boundary conditions to prevent an apparent indefinite extension of the solution. Among these conditions are absorption condition limits, which artificially surround the crystal of a perfectly absorbing area, making it possible to stop calculation as soon as the wave crosses the crystal.

The FDTD method has a certain number of advantages: it is an intuitive method making it possible to display the electromagnetic field propagation (see Figure 6.19). Consequently, comprehension of the phenomenon becomes easier.

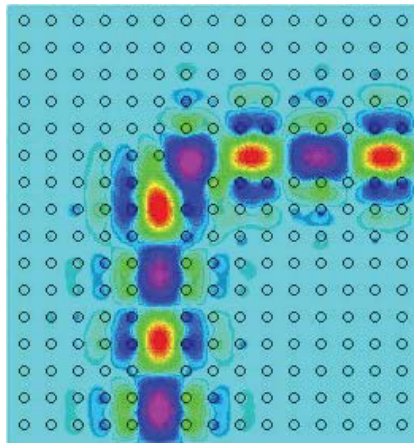

Figure 6.19. *Example beam propagation into 2D grating obtained by the FDTD method*

6.3. Photonic crystal fabrication techniques

This section does not detail all the photonic crystals fabrication techniques. However, it does describe the principal techniques with some examples. The use of these techniques with semiconductor materials is largely developed in the literature; thus we will give examples of the use of those techniques with dielectric materials such as $LiNbO_3$ (our reference throughout this book). In addition, we will concentrate on 1D and 2D photonic crystal fabrication techniques. We can classify these techniques in three categories: etching techniques, ion or electron beam lithography techniques and laser techniques [Joa 1995, Kam 2004, Lou 2003, Lou 2004, Mer 2003, Miz 2001, Nak 2002, Kra 1999, Yab 1987, Yab 1993].

6.3.1. *Etching techniques*

Wet etching techniques use chemical etching (by HF: HNO_3 acid) coupled with a physical effect to modify the etching speed in the zone to be structured. The description of these phenomena is provided in the second part of this section. Indeed, wet etching is generally used to reveal a structure already carried out by another physical technique.

Contrary to this, dry etching is directly involved in the structuring of a material. This technique requires several photolithographic steps to prepare the sample. For example, the mask fabrication is a crucial step which increases its cost. Moreover, it does not employ an acid liquid but a gas of ions in the case of reactive ion etching (RIE), or a plasma for plasma etching [Bou 2004, Hue 2005, Mil 2005, Par 2005] (see Figure 6.20). The ions of gases have the same role as the acid; to break the chemical bonds in order to remove matter.

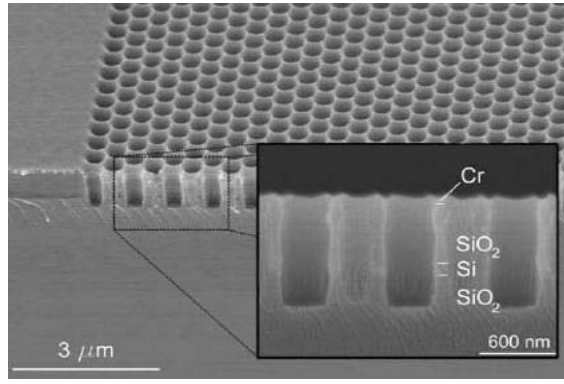

Figure 6.20. *Photonic structure obtained by RIE technique in a SiO_2 multilayer structure of 500 nm of SiO_2, 100 nm of Si and 1500 nm of SiO_2; the carbon layer is of 130 nm [Mil 2005]*

The plasma etching technique has recently been developed, in particular, for the structuring of dielectric materials [Hue2004]. For example, Park et al. [Par 2005] reported the fabrication of Bragg's grating in $LiNbO_3$ using this technique.

It was used to produce photonic crystals in various materials such as polymers (PMMA, BCB and Teflon), semiconductors (Si) and dielectric (Ta_2O_5, Nb_2O_5 and SiO_2) [Bou 2004, Hue 2005, Mil 2005]. The photonic crystal structures display perfect regularity of the shape periodicity; and the mask transfer is efficient and without defect, as indicated in Figure 6.21.

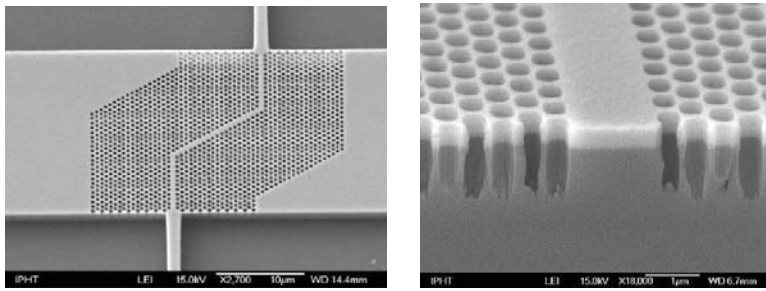

(a) Top view (b) Cross-section view

Figure 6.21. *A photonic waveguide with a triangular grating obtained on 500 nm thin film of Ta_2O_5 on 2.5 µm of SiO_2: hole diameter of 380 nm and period of 620 nm, over a depth of 1.5 µm [Hue 2005]*

The disadvantage of plasma etching is related to the number of intermediate steps necessary in order to obtain photonic structures on dielectric materials. This method requires four successive steps, therefore four different techniques which complicate its implementation:

– The first step uses the electron beam lithography (EBL) to fabricate a photonic mask on a polymer. PMMA is the polymer frequently used because it is easy to structure and it is very well adapted for nanometric shapes. We use an electron beam of about 40 keV. After the exposure, the zones of the PMMA which was sensitized are dissolved in a suitable solvent. This mask is used only for the creation of another metallic mask.

– In the second phase a metallic layer of NiCr type, for example, is deposited on the polymer, using the ion beam scanning (IBS) technique [Bou 2004].

– The third step is used to transfer the shape from the PMMA to the metallic layer by exposure to Ar ions, using ion bema etching (IBE). The polymer mask is etched by the acid and protects, for a short time, the covered parts of metal; whereas the unprotected zones are completely etched. In the case of a multi-layer metal, the part out of carbon must be treated with oxygen plasma [Hue 2005].

– The fourth step is related to etching plasma (EP). This step aims to structure the dielectric material. The plasma source can come from a cyclotron with electronic resonance (ECR) with a mixture of CHF_3 and/or CF_4 gas [Bou 2004, Hue 2005]: for example, the etching speed of Ta_2O_5 in a mixture of CHF_3+CF_4, to produce holes, is 90 nm/min. For the etching of $LiNbO_3$, carried out in a source with magnetic discharge, the gas used is a mixture of C_3F_8+Ar, and the etching speed is 150 nm/min [Par 2005].

The power of plasma etching lies in the ability to directly etch the guiding layer without damaging the layer-substrate contact. This makes it possible to etch more deeply than the layer thickness; so that the defects at the bottom of the hole do not play any role.

6.3.2. *Ion and electron beam lithography*

Two techniques are commonly used: the electron beam (EB) technique and the focused ion beam (FIB) technique.

The EB Technique is based on the use of an electron beam coming from a scanning electron microscope (SEM) [Res 2003]. Electron beam radiation makes it possible to locally reverse the spontaneous polarization of the crystal. Thereafter, chemical etching creates the expected holes grating.

One advantage of this technique is that the electrons are easy to direct and focus, thus giving a great flexibility and versatility to the reversed polarization grating realization. Moreover, a photolithographic intermediate step is not necessary.

Figure 6.22 presents the various technological steps using this technique to structure lithium niobate. Generally speaking, the electron beam radiation is carried out on the -z face of $LiNbO_3$. The accumulation of negative charges on this face causes a localized inversion of the spontaneous polarization of the material. Thereafter a chemical etching in a HF: HFO_3 acid makes it possible to reveal the structure produced. Indeed, it is known that in the case of $LiNbO_3$, the z- face is etched more quickly than the z+ face. Therefore, we must expect to obtain pillars on the z- face.

For instance, note the study carried out by the XLIM group (University of Limoges, France) which emphasized the experimental difficulty of obtaining the desired grating [Mas 2004].

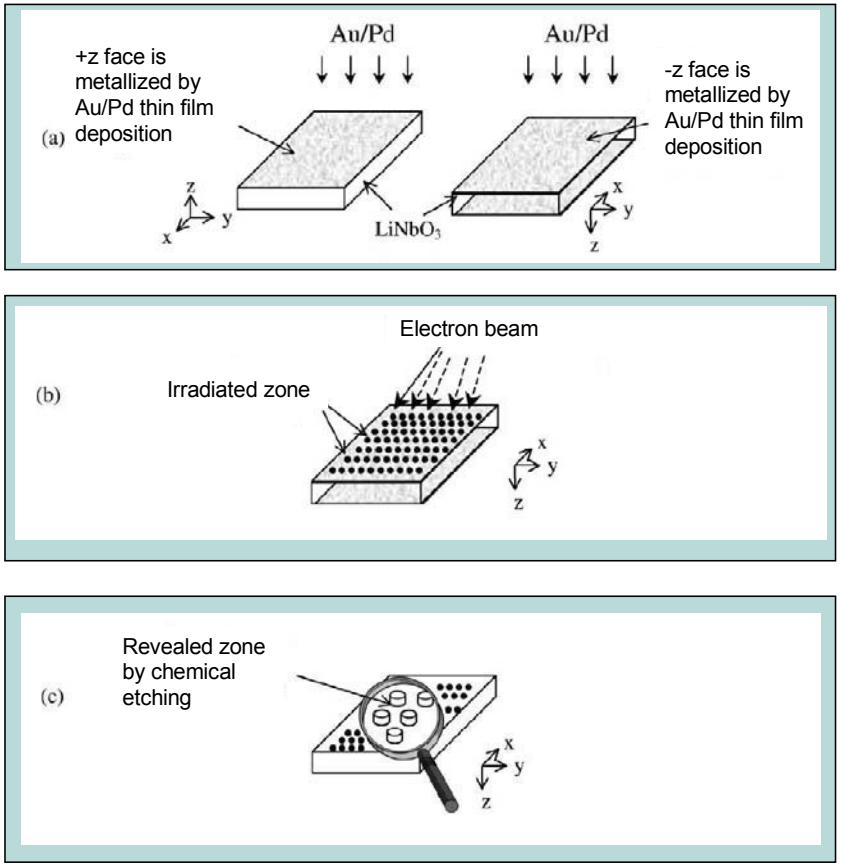

Figure 6.22. *1D and 2D structures of $LiNbO_3$ using the EB technique [Res 2003]*

Recently Massy et al. [Res 2000] showed that under certain radiation conditions the holes are obtained on the -z face of the lithium niobate. Moreover, XLIM group obtained hole diameters of about 690 nm by chemical etching after EB irradiation (these dimensions are necessary for applications in the field of telecommunications) (see Figure 6.23).

The studies undertaken to improve understanding of this phenomenon showed that the inversion of the crystal spontaneous polarization was not the cause of this process. Indeed, obtaining holes is attributed to an insufficient accumulation of charges to locally reverse the polarization but these charges selectively accelerate the chemical etching at the radiated zone [Beg 2008].

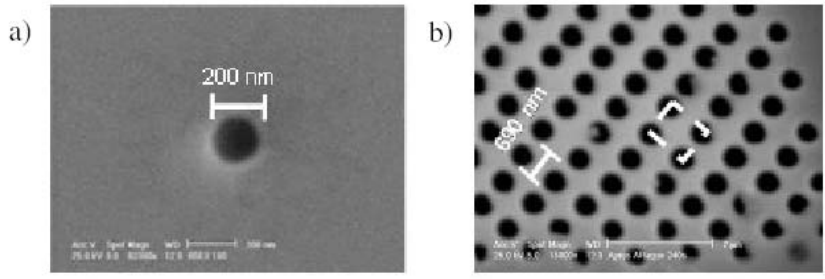

Figure 6.23. *Hole diameter of 200 nm in $LiNbO_3$ using pulsed EB radiation. Square lattice period of 690 nm [Beg 2008]*

The second technique is the FIB method [Ars 2005, Cab 2005]. This consists of radiating the surface of the sample with a Ga^+- ions beam, in a similar way to an electron beam. This technique developed for semiconductor technology at the beginning of 1980, appears to be a very promising method of materials nano-structuring with a resolution reaching 5-20 nm. It was recently employed to carry out a PBG grating in $LiNbO_3$ [Lac 2005]. The principal steps of this process are schematized in Figure 6.24 [Lac 2005]. For example, Figure 6.25 shows a triangular grating obtained in a $LiNbO_3$ crystal using this technique.

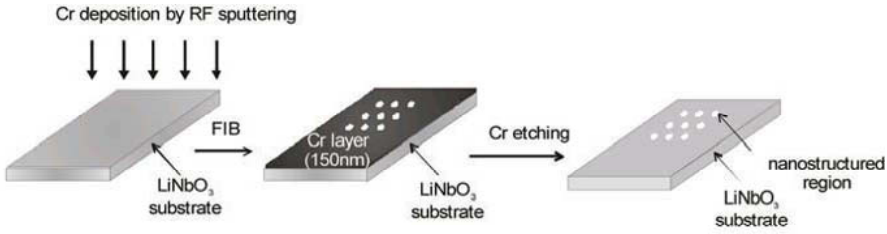

Figure 6.24. *Steps of the FIB process in order to fabricate a 2D photonic grating in $LiNbO_3$ [Lac 2005]*

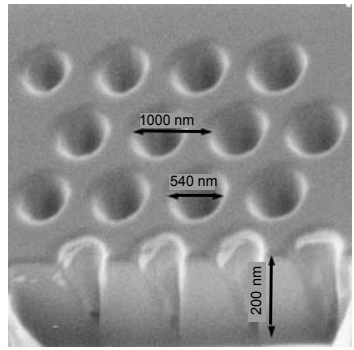

Figure 6.25. *2D grating in $LiNbO_3$ obtained using the FIB technique [Lac 2005]*

6.3.3. *Laser processing*

We can distinguish two approaches. The first is based on a direct laser machining, while the second combines UV laser radiation with chemical etching.

In the first approach, a high-speed laser is necessary to avoid the effects of cracks and distortion of the material [Per 2006]. The use of femto-second lasers based on the chirped pulse amplification (CPA) is recommended to obtain ablation processes based on athermic phenomena that is more interesting for the sub-micrometric structuring free from molten matter and deposited in the holes periphery [Cho 2002, Liu 1997, Per 2006, Pro 1995]. However, it is possible to positively carry out ablation with lasers in nanosecond mode, which is less expensive and easier than when using femto-second lasers [Bad 2005].

To carry out laser ablation, it is important to have an intensity higher than the ablation threshold of the material in energetic and temporal aspects. These two values are related to one another, and the pulse duration is small; also the energy necessary for ablation is weak. For example, the ablation threshold of $LiNbO_3$ is approximately 1 J/cm ² @248 nm in nanosecond mode and of a few tens of mJ/cm ² for the femto-second mode.

To limit the depositions on the surface, as shown in Figure 6.25 for the nanosecond mode, it is possible to use a SiO_2 layer on the top of $LiNbO_3$ [Cho 2002]. Silica has an ionization potential higher than $LiNbO_3$, making $LiNbO_3$ ablation possible without removing the SiO_2 layer. To use the protective coating, it is necessary to employ wavelengths in the range of silica transparency; a KrF laser @248 nm is perfectly adapted for this configuration. Figure 6.26 shows the difference with and without the protecting layer for the same conditions of exposure 512 pulses of 3.3 mJ/cm².

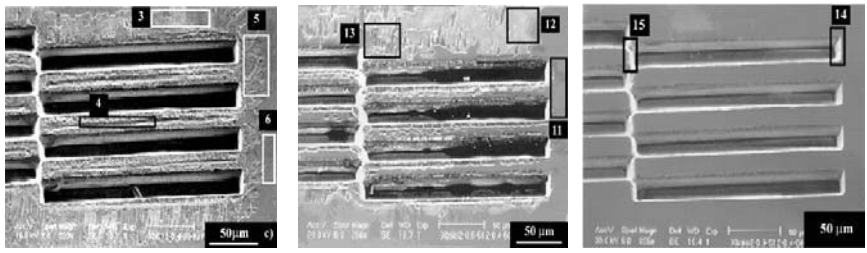

(a) (b) (c)

Figure 6.26. *Laser ablation: (a) without SiO_2 layer; (b) with SiO_2 layer of 0.5 µm and (c) 1 µm of SiO_2 [Cho 2002]*

The second approach combines UV laser radiation with chemical etching [Bar 1999, Bro 2002, Chr 1995, Mai 2003, Pis 2004, Sco 2004]. This technique was, in particular, used by the Eason team of the ORC (Optoelectronic Research Center, Southampton, UK) to engineer $LiNbO_3$ crystals (see Figure 6.27). This is called light induced frustration etching (LIFE), and includes two steps: illumination by a UV laser to modify the material resistance to the acid; and chemical etching in an acid bath to etch the material and to reveal the exposed structure. The exposure of the material to an intense light lower than the ablation threshold (threshold from which matter is directly removed) considerably modifies the material's resistance to the acid. In order to make this possible, it is necessary to use photovoltaic crystals because the beam moves the charges from doping to the surface of exposure. These charges modify the electrochemical interaction of the material with the acid. Illumination can be done in the continuous mode, with the acid etching at the same time or after exposure, or in the pulsed mode. It can also be made through a mask or directly on the crystal.

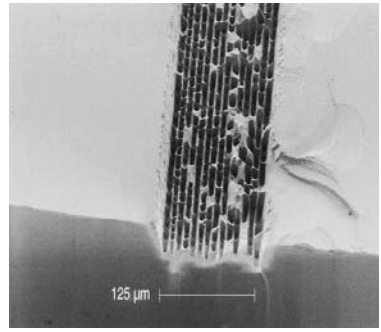

Figure 6.27. *Bragg's grating period of 10 µm and lines of 8 µm in $LiNbO_3$ [Chr 1995]*

It is possible to obtain a 2D grating directly by using an interferential set-up (see Figure 6.28). The principle consists of superimposing two Bragg's gratings perpendicularly, to obtain the 2D grating [Hir 2002].

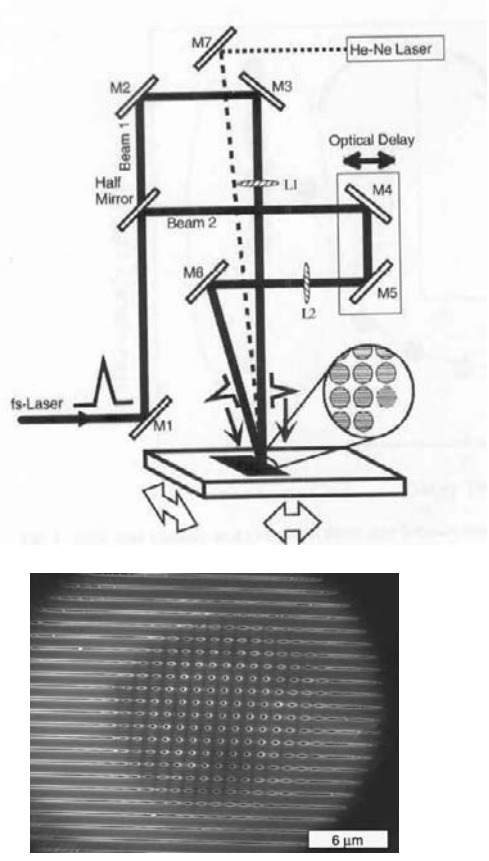

Figure 6.28.. *Photonic structure created using 40 µJ and 80 µJ for the first and second gratings, respectively: holes in the center have a diameter of 140 nm [Hir 2002]*

2D grating fabrication requires a very precise optical delay line and a short wavelength to have a small period Bragg's grating. The period of the grating is adjustable and is given by $d=\lambda/2$ (sin ($\theta/2$). The first grating must always be smallest in diameter and intensity to have a correct result.

To summarize this part of the chapter, we presented some examples of 2D photonic crystal fabrication techniques; in particular in dielectric materials. However, it is important to note that from the materials point of view, photonic

crystals mainly use III-V semiconductors. Indeed, photonic crystals components are mainly based on two-dimensional gratings fabricated in III-V semiconductor materials (GaN, GaAs, InP, etc.). The reason of this is that technologies of micro-electronics are easily transposable in the field of the photonics on those materials. Moreover, the fabrication of semiconductor thin layers is well controlled and makes it possible to obtain structures by electronic lithography and reactive ion etching.

It is worth noting that technologies based on membrane photonic structures seem to be more promising. In particular, structures on InP which is an important III-V material for optical telecommunications. To form a membrane, it is possible to use etching in an aqueous phase. The chemistry of wet etching composed of InP-type offers an enormous flexibility [Lou 2003, Lou 2004, Lou 2004b]. The advantage of semiconductor materials comes from their very high refractive index (~ 3) which makes it possible to obtain photonic crystals with a strong index contrast.

Another class of materials that is becoming of increasing interest is the Silicon on Insulator (SOI). The engineering of silicon being very well controlled, photonic crystals are fabricated in a single-crystal Si layer deposited on a substrate of SiO_2/Si [Not 2001]. These technologies will make it possible to extend the potentialities of the SOI components in the field of micro-and nano-photonics.

Polymeric materials are also of great interest for producing photonic structures. Although their refractive index is relatively weak, the implementation of these structures and the facility to obtain thin layers of good quality with low costs make these materials very attractive for use in producing photonic crystals with narrow band gaps but whose losses by diffusion are well controlled [Lig 2001].

Finally, many research activities concern the development of 3D photonic crystals with a total band gap. Among the technologies involved, we can highlight: electronic lithography [Nod 2000], the holographic lithography [Nod 2000] and the self-assembly of colloidal particles [Meg 2001].

As previously discussed, there are two principal 3D photonic crystal structures which present a total and omni-directional photonic band gap: the “Yablonovite” and the woodpile structure. The principle of Yablonovite fabrication consists of boring a material along three directions which correspond to the direction <110> of a diamond crystal [Pai 1999]. The difficulty comes owing to the fact that if we want to obtain a PBG in the IR regime, it is necessary for the pores dimensions to be sub-micrometric. In 2000, a team from the University of Orsay (France) used the FIB technique to carry out a drilling along two oblique directions (instead of three) to carry out a structure allowing an omni-directional PBG at $\lambda = 3$ μm [Lou 2004, Lou 2004, towards Cha 2000]. The same team also used x-ray lithography to produce a Yablonovite fabrication in a metal [Cui 2002].

In contrast to the Yablonovite structure, the woodpile structure seems to be easier to develop (see Figure 6.29). This structure consists of piling up several 1D gratings while turning them to 90° each time, and shifting by a half-period two consecutive parallel gratings [Fle 1999]. The creation of this type of structure uses the same processes developed for the structuring of silicon.

It is also important to discuss the self-assembled structures with partial PBG. In particular, the artificial opals and the self-cloned structures [Lou 2003, Lou 2004, Lou 2004.b, Xia 1999, Kaw 1997]. The opals are made of self-assembled silica balls by gravity or centrifugation. The grating obtained is of CFC (cubic with face cantered) type. In addition to the weak index contrast that these structures present, they are not flexible for introducing impurities that might enable the development of photonic components such as laser sources, for instance. The self-cloned structures are based on the deposition of thin layers by RF sputtering, which under certain experimental conditions makes it possible to reproduce exactly the topology of a previously structured substrate. This phenomenon is due to the ions of RF plasma allowing at the same time the deposition and the etching of the layers in the same sputtering chamber.

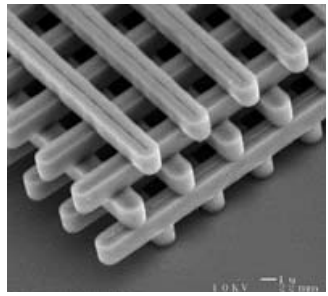

Figure 6.29. *Woodpile 3D structure [Lin 1999]*

6.4. Examples of photonic crystal applications

Generally, the components produced, containing structures with photonic band gaps, are obtained by voluntarily introducing defects into the PBG lattice. We find the same approach as with semiconductors, where a weak doping by impurities radically modifies the material properties and makes it possible to develop micro-electronic components such as the diode, transistor, amplifier, etc.

We can distinguish three types of defects: point defects, linear defects and heterostructures. The rest of this section is devoted to presenting some examples of these components.

6.4.1. *Optical micro-sources (point defects)*

These types of microcavity lasers can be formed either by a missing or deformed hole (see Figure 6.30). Then cavities with discrete modes can be obtained.

In the field of laser physics, according to Purcell [Pur 1946, Lou 2004], we can define a proportionality factor F of the spontaneous emission rate in the cavity mode (useful emission) and the emission rate in the leaky modes, by the following relation:

$$F_{\max} = \frac{3Q}{4\pi^2}\left(\frac{1}{V}\right)\left(\frac{\lambda}{n}\right)^3 \qquad [6.51]$$

Q: quality factor of the cavity

V: effective volume of the cavity

n: the index of the active medium

λ: wavelength

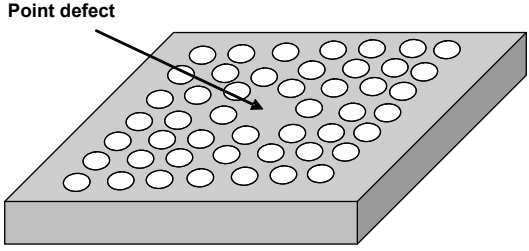

Figure 6.30. *Laser micro-cavity using point defects in photonic crystals*

According to relation [6.51], in order to increase the fraction of the useful spontaneous emission in the cavity, one of the possibilities would be to decrease the volume of the cavity (a volume about $(\lambda/n)3$). Under these conditions, for a very large quality factor, the useful spontaneous emission can reach 100%. The ideal would be to use a cavity with a 3D omni-directional photonic crystal. However, a 2D photonic crystal makes it possible to approach the 100% spontaneous emission and, thus, reduce the laser threshold of emission in particular in semi-conductors.

6.4.2. *Photonic crystal waveguides (linear defects)*

There is a large variety of waveguides based on photonic crystals. In the case of holes grating (the most frequently used configuration in contrast to pillars grating), the simplest way to create a waveguide consists of removing one or more lines of holes. Light guiding in these structures can be based on refraction and the existence of a photonic band gap as well. Generally the waveguide is designed at the time of the grating writing. For this reason, several guiding structures of different geometries can be introduced simultaneously. These guides are noted *W*n for *n* removed lines of holes. Figure 6.31 presents the case of a W1 guide containing a triangular network.

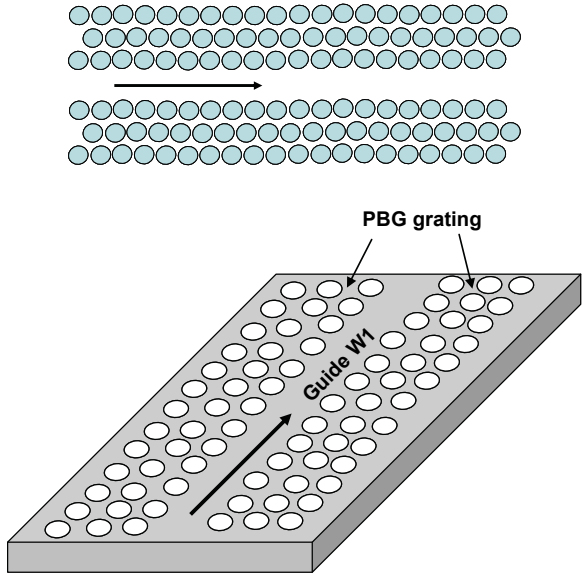

Figure 6.31. *Example of a W1 photonic crystal waveguide*

The nature of light guiding in these structures makes it possible to produce curved guides. Figure 6.32 reports a curved waveguide created by etching a thin layer of the GaAs semiconductor. The turn is obtained by omission of two lines of holes in the direction ΓK [Lou 2004, Lou 2004b]. This consists of two arms forming an elbow of 120°. Note that such a configuration is not allowed in the case of conventional waveguides. However, this type of component is not yet completely optimized and studies still continuing in this direction.

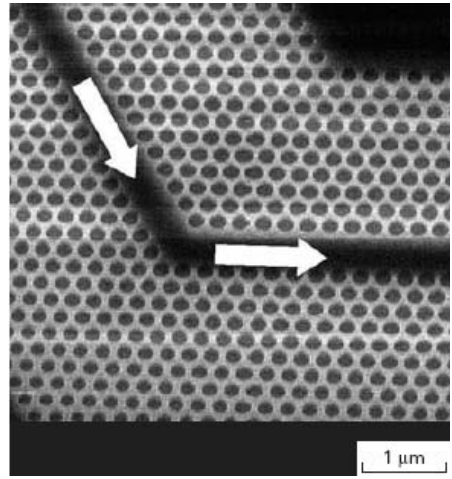

Figure 6.32. *Example of a curved waveguide based on photonic crystals [Lou 2004, Lou 2004b]*

While exploiting the number and the direction of the lines of removed holes it is possible to conceive and produce a multitude of components to guide the light, thus, we can produce mirrors, micro-optics elements and interferometers such as the Mach-Zehnder interferometer [Sha 2002, Cen 1999].

The creation of this type of waveguide should certainly allow development of high density photonic circuits similar to the integrated circuits of micro-electronics. However, there remains a major constraint related to the use of 2D grating combined with conventional planar waveguides. Indeed the optimization of light confinement in such structures is still a central motivation of many research and development activities.

6.4.3. *Optical filter*

The principle of the optical filter based on photonic crystals is to juxtapose a PBG grating on a waveguide as shown in Figure 6.33. Filtering is carried out by the existence of a forbidden band, which depends in particular on the characteristics of the grating geometry, dimensions and also on the number of the lines which is an important parameter. In the case of GaAs, a triangular grating of holes makes it possible to obtain a band gap for both TE and TM polarizations.

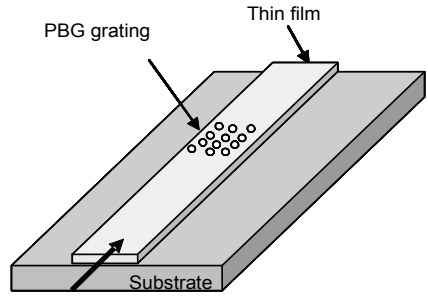

Figure 6.33. *Example of filter based on photonic crystal structure juxtaposed on a conventional waveguide*

In addition, optical filtering containing photonic crystals can be of great interest for optical telecommunications. Indeed, the "add and drop function" which consists of extracting or injecting a wavelength (a channel) into a optical fiber transmission line can be achieved using two waveguides with photonic crystals of W1 type connected by a cavity resonating at the working wavelength [Lou 2003, Lou 2004, Nod 2000] (see Figure 6.34).

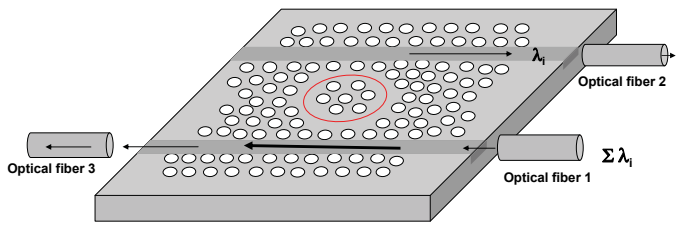

Figure 6.34. *Add and drop filter principle based on photonic crystals*

Fiber 1 makes it possible to inject several wavelengths. One of them corresponds to the resonance of the cavity which is extracted from the signal and is coupled with the second guide to be injected into fiber 2. The opposite process can also be carried out. Many research tasks are currently in progress to improve the performances of this type of add and drop filter, in particular in terms of the selectivity required for the future telecommunications network [Yos 2001].

6.4.4. *Hetero-structures*

These complex structures (see Figure 6.35) are also based on an approach borrowed from micro-electronics, for example, the engineering of band gaps while exploiting the composition of III-V semi-conductors. Also, the structures of photonic band gaps can be adjusted while exploiting the juxtaposition of several lattices or the various materials used.

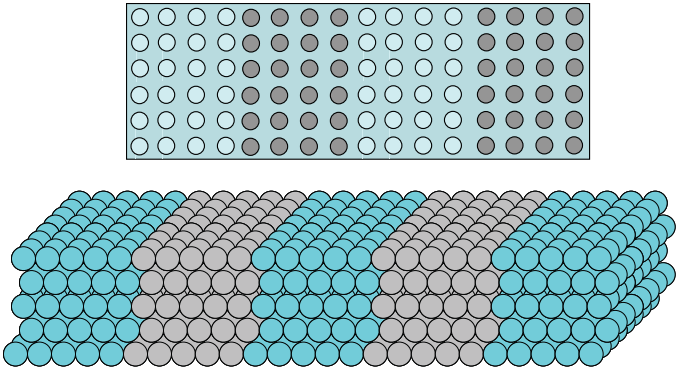

Figure 6.35. *Hetero-structure of 2D and 3D photonic crystals*

6.5. Photonic crystals and non-linear optics

The combination of photonic crystal structures and non-linear optics is related to two aspects: on one hand, the use of the non-linear optical effects for direct control of the PBG crystal response; thus, reconfigurable optoelectronic components can be developed for applications in the field of optical telecommunications. On the other hand, 2D structuring of the non-linear optical properties of the material allows the creation of ultra-short components for frequency conversion for integrated optics.

PBG structures allow the engineering of material dispersion in order to counterbalance its natural dispersion. For example, in the process of second harmonic generation (see Chapter 4), the photonic crystals make it possible to reduce the group velocities and to phase match velocities of waves ω and 2ω [Ang 2001, Bra 2004, Sca 2001] . Moreover, localization of the electromagnetic fields allows an increase in the non-linear optical interactions. For example, recent work [Dum 2002] showed that in the case of a PBG structure based on a III-V semiconductor ($AlGaAs/AlO_x$), the evolution of a second harmonic generation signal is no longer like the square of the sample length (as in common NLO interaction) but, rather, like power 6 of the length (see Figure 6.36).

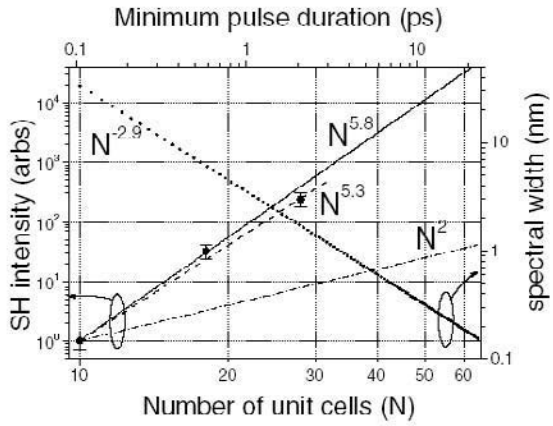

Figure 6.36. *Second harmonic generation in photonic crystal based III-V semi-conductor multi-layers (AlGaAs/AlO_x) [Dum 2002]*

Non-linear optics makes it possible to adjust the PBG response by controlling the refractive index or the absorption of the material, via the non-linear optical effects; such as the Kerr optical effect and the electro-optical effect. Thus, a fast optical reconfiguration can be obtained and reconfigurable photonic components may be developed. For example, the investigation of a membrane structure of InP incorporating 4 quantum wells was recently reported. The basic principle consists of using an optical excitation in order to modify the population of carriers in the quantum wells which enables change of the refractive index and, thus, shifting the PBG [Rai 2004]. The result of these technologies will certainly make it possible to design new components for optical signal processing [Min 2002].

In 1998, V. Berger [Ber 1998] proposed the idea of 2D or 3Ds periodic structuring of the non-linear susceptibility $\chi(2)$. This approach constitutes an extension of the theory suggested by Bloembergen et al. that has been reported in Chapter 4. As an indication, this theory is at the base of second harmonic generation by quasi-phase matching in PPLN materials (see Chapter 4).

The transition from theory to practice was carried out by a group from the ORC (Optoelectronic Research Centre) of Southampton (England) which, for the first time fabricated 2D periodically polarized structures in $LiNbO_3$ (2D-PPLN) [Bro 2000, Gall 2003]. This consists of fabricating PPLN periodic gratings in two directions x and y (see Figure 6.37). Such a structure produces the quasi-phase matching according to the angle of incidence of the pump beam, and thus, several wavelengths can be generated in the same 2D-PPLN crystal.

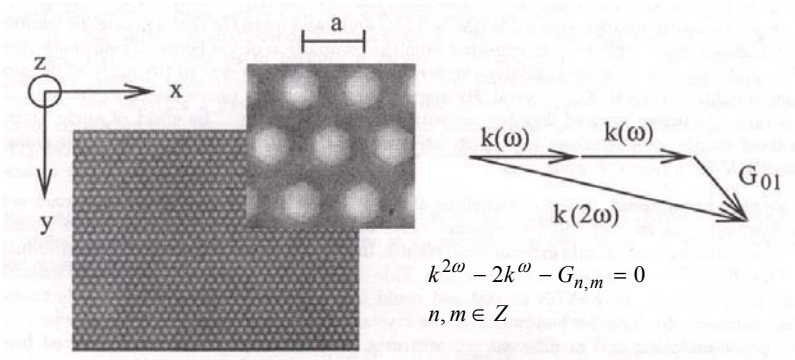

Figure 6.37. *QPM according to the propagation direction using a 2D-PPLN grating [Bro 2000]*

Other applications such as frequency commutation (see Figure 6.38) have also been reported by American group [Cho 2000].

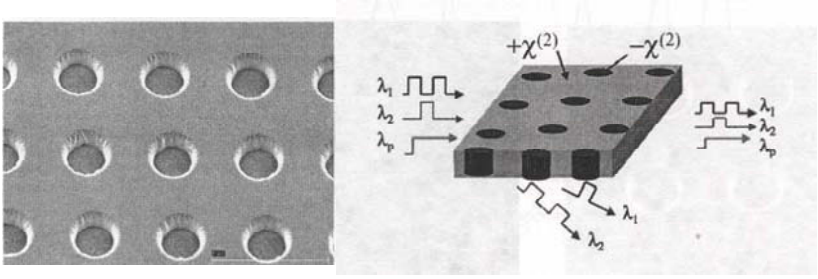

Figure 6.38. *Frequency commutation using frequency difference generation in 2D-PPLN gratings [Cho 2000]*

More recently, many teams were interested in the inscription of PBG structures in $LiNbO_3$ in order to benefit from the combination of the non-linear optical properties of this crystal with the PBG grating.

For instance, a team from Besançon (France) was interested in the inscription of a PBG structure with ionic exchange waveguides [Lac 2005]. As shown in the following photograph (Figure 6.39), 20 lines of holes were created perpendicular to a channel waveguide fabricated by protonic exchange in a x-cut sample.

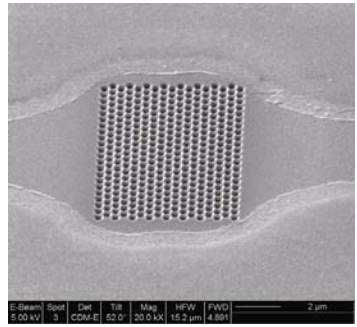

Figure 6.39. *PBG grating with a waveguide by proton exchange within $LiNbO_3$ [Lac 2005]*

The objective of this work is to prove the feasibility of a reconfigurable filter at telecommunication wavelengths, using the non-linear optical properties of the $LiNbO_3$ crystal; such as the electro-optical effect.

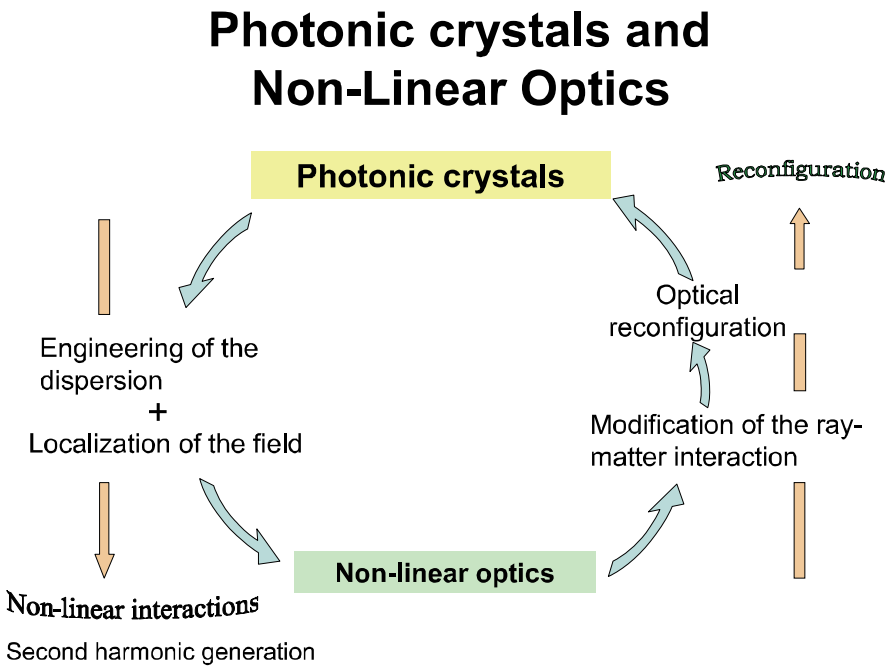

Figure 6.40. *Photonic crystals and non-linear optics*

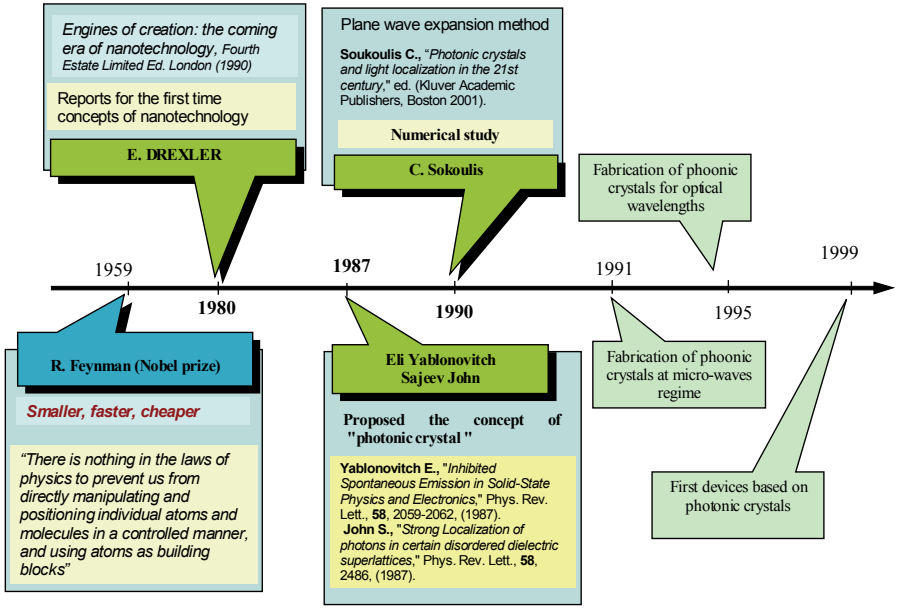

Figure 6.41. *Historical review of photonic crystal development*

6.6. Bibliography

[Ang 2001] De Angelis C., Gringoli F., Midrio M., Modotto D., Aitchison J.S. and Nalesso G., "Conversion efficiency for second-harmonic generation in photonic crystals", *J. Opt. Soc. Am. B*, 18(3), 348-351 (2001).

[Ars 2005] Arshak K., Mihov M., "State of the art of focused ion beam nano lithography", *J. of Optoelectronics and Advanced Materials*, 7(1), 193-198 (2005).

[Ast 1997] Astratov V.N., Vlasov Y..A., Z.Karimov O., Kaplyanskii A.A., Musikhin Y.G., Bert N.A., Bogomolov V.N., and Prokofiev A.V., "Photonic band structure of 3D ordered silica matrices", *Superlattices and Microstructures*, 22(3), 393-397 (1997).

[Bad 2005] Badi L., Beghoul M., Kremer R., Boudrioua A., Kilburger S., Millon E., Clauss E.and Fogarassy E., *Micro-structuration par ablation laser de $LiNbO_3$ sous forme de monocristal et de couches minces déposées sur silicium,* JNOG 2005 (2005).

[Bar 1999] Barry I.E., Eason R.W., Cook G., "Light-induced frustration of etching in Fe-doped $LiNbO_3$", *Appl. Surf. Sci*., 143, 328-331 (1999).

[Beg 2008] Beghoul M., Fougère B., Boudrioua A., Daraud C., Kremer K., Moretti P. and Vareille J. C., "Investigation of the inscription mechanism of 2D photonic band gap grating in $LiNbO_3$ by e-beam lithography using μ-Raman spectroscopy", *Optical Materials*, 31(2), 136-142 (2008).

[Beg 2007] Beghoul M., Fougère B., Boudrioua A., Daraud C., Lattrache S., Kremer K., Moretti P., "Photonic band gap grating in He^+-implanted lithium niobate waveguides", *Optical and Quantum Electronics*, DOI 10.1007/s11082-007-9082-8 (2007).

[Ber 1998] Berger V., "Nonlinear photonic crystals", *Phys. Rev. Lett*., 81, 4136-4139 (1998).

[Bou 2004] Boucher R.; Hiibner U.; Morgenroth W.; Roth H.; Meyer H.-G.; Schmidt M., "Etching of sub-micron high aspect ratio holes in oxides and polymers", *Microelectronic Engineering*, 73/74, 330-335 (2004).

[Bra 2004] Bratfalean R.T, Broderick N.G.R., Gallo K.,.and Peacock A.C., "Frequency conversion in a nonlinear photonic quasi-crysta", *Technical Digest of the Conference on Nonlinear Guided Waves*, Canada (2004).

[Bro 2000] Broderick N.G.R., Ross G.W., Offerhaus H.L., Richardson D.J.and Hanna D.C., "Hexagonally poled lithium niobate : a two-dimensional nonlinear photonic crystal", *Phys. Rev. Lett*., 84, 4345-4348 (2000).

[Bro 2002] Brown PT, Mailis S., Zergioti I.and Eason RW, "Microstructuring of lithium niobate single crystals using pulsed UV laser modification of etching characteristics", *Optical Materials*, 20, 125-134 (2002).

[Cab 2005] Cabrini S., Carpentiero A., Kumar R., Businaro L., Candeloro P., Prasciolu M., Gosparini A., Andreani C., De Vittorio M., Stomeo T., Di Fabrizio E., "Focused ion beam lithography for two dimensional array structures for photonic applications", *Microelectronic Engineering*, 78/79, 11-15 (2005).

[Cam 2000] Campbell M., Sharp D.N., Harrison M.T., Denning R.and Turberfield A.J., "Fabrication of photonic crystals for the visible spectrum by holographic lithography", *Nature*, 404, 53-56 (2000).

[Cas 1995] Cassagne D., Jouanin C., and Bertho D., "Photonic band gaps in a two dimensional structure", *Physical Review B*, 52(4), 2217-2220 (1995).

[Cas 1996] Cassagne D., Jouanin C., and Bertho D., "Hexagonal photonic-band-gap structures", *Physical Review B*, 53(11), 7134-7142 (1996).

[Cas 1996b] Cassagne D., Jouanin C.and Bertho D., "Hexagonal photonic band gap structures", *Physical Review B*, 53(11), 7134-7142 (1996).

[Cas 1997] Cassagne D., Jouanin C., and Bertho D., "Optical properties of two-dimensional photonic crystals with graphite structure", *Appl. Phys. Lett*., 70(3), 289-291 (1997).

[Cen 1999] Centeno E., Guizal B.and Felbacq D., "Multiplexing and demultiplexing with photonic crystals", *J. Opt. A : Pure Appl. Opti*., 1, L10- L13 (1999).

[Cha 2000] Chalnokov A., Wang K., Rowson S., Garoche P.and Lourtioz J.-M., "Near infrared Yablonovite-like photonic crystals by focused-ion-beam etching of macroporous silicon", *Appl. Phys. Lett*., 77(19), 2943-2945 (2000).

[Cho 2000] Chowdhury A., Hagness SC and McCaughan L., "Simultaneous optical wavelength interchange with a two-dimensional second-order nonlinear photonic crystal", *Opt. Letters*, 25, 832-834 (2000).

[Cho 2002] Chong H.W., Mitchell A., Hayes J.P.and Austin M.W., "Investigations of KrF excimer laser ablation and induced surface domage on lithium niobate", *Appl. Surf. Sci*., 201, 196-203 (2002).

[Chr 1995] Christensen F.K.and Mullenborn M., "Sub-band-gap laser micromachining of lithium niobate", *Appl. Phys. Lett*., 66(21), 2772-2773 (1995).

[Chu 2005] Chung Y.W., Leu I.C., Lee J.H., Hon M.H., "Fabrication and characterization of photonic crystals from colloidal processes", *Journal of Crystal Growth*, 275, 2389-2394 (2005).

[Coh 1977] Cohen-Tanoudji C., Diu B., Laloä F., *Mécanique quantique*, Hermann, (1977).

[Cui 2002] Cuisin C., Chelnokov A., Decanini D., Peyrade D., Chen Y.and Lourtioz J.-M., "Submicrometer dielectric and metallic structures fabricated from resist templates", *Optical and Quantum Electronics*, 34(1-3), 13-26 (2002).

[Dum 2002] Dumeige Y., Sagnes I., Monnier P., Vidakovic P., Abram I., Mériadec C.and Levenson A., "Phase matched frequency doubling at photonic band edges: efficiency scaling as the fifth power of the length", *Phys. Rev. Lett*., 89, 043901 1-3 (2002).

[Fle 1999] Fleming J.G.and Lin S.-Y., "Three-dimensional photonic crystal with a stop-band from 1.35 to 1.95 μm", *Opt.Lett*., 24(1), 49-51 (1999).

[Gal 2003] Gallo K., Bratfalean R.T., Peacock A.C., Broderick N.G.R., Gawith C.B.E., Ming L., Smith P.G.R. and Richardson D.J., "Second harmonic generation in hexagonally poled lithium niobate slab waveguides", *Electron. Lett*., 39, 75-76 (2003).

[Hes 2003] Hess O., Hermann C., and Klaedtke A., ''Finite-difference time-domain simulations of photonic crystal defect structures'', *Phys. Stat. Sol.(a)*, 197(3), 605-619 (2003).

[Hir 2002] Hirano M., Kawamura K-ichi and Hosono H., "Encoding of holographic grating and periodic nano-structure by femto-second laser pulse", *Appl. Surf. Sci*., 197/198, 688-694 (2002).

[Hue 2005] Huebner U., Boucher R., Morgenroth W., Kunert J., Roth H., Meyer H.-G., Glaser T.and Schroeter S., "Fabrication of photonic crystals in tantalum pentoxide films", *Microelectronic Engineering*, 78-79, 422-428 (2005).

[Joa 1995] Joannopoulos J.D., Meade R.D.and Winn J.N., *Photonic Crystals: Molding the Flow of Light*, Princeton University Press (1995).

[Kam 2004] Kamp M., Happ T., Mahnkopf S., Duan G., Anand S., Forchel A., "Semiconductor photonic crystals for optoelectronics", *Physica E*., 21, 802-808 (2004).

[Kaw 1997] Kawakami S., "Fabrication of submicrometre 3D periodic structures composed of Si/SiO_2", *Electron. Lett*., 33, 1260-1261 (1997).

[Kit 1983] Kittel C., *Physique de l'état solide*, Dunod (1983).

[Kra 1999] Krauss T.F.and De La Rue R.M., "Photonic crystals in the optical regime – past, present and future", *Progress in Quantum Electronics*, 23, 51-96 (1999).

[Kua 2005] Kuang W., Hou Z., Liu Y.and Li H., "The bandgap of a photonic crystal with triangular dielectric rods in a honeycomb lattice", *J. Opt. A: Pure Appl. Opt*., 7, 525-528 (2005).

[Lac 2005] Lacour F., Courjal N., Bernal M.-P., Sabac A., Bainier C., and Spajer M., "Nanostructuring lithium niobate substrates by focused ion beam milling", *Optical Materials*, 27, 1421-1425 (2005).

[Lav 2004] Lavrinenko A., Borel P.I., Frandsen L.H., Thorhauge M., Harpøth A., Kristensen M., Niemi T., "Comprehensive FDTD modelling of photonic crystal waveguide components", *Optics Express*, 12(2), 234-248 (2004).

[Leu 1993] Leung K.M.and Qiu Y., "Multiple-scattering calculation of the two-dimensional photonic band structure", *Physical Review B Condensed Matter*, 48(11), 7767-7771 (1993).

[Lig 2001] Liguda C., Bottger G., Kuligk A., Blum R., Eich M., Roth H., Kunert J., Morgenroth W., Elsner H.and Meyer H., "Polymer photonic crystal slab waveguides", *Applied Physics Letters*, 78(17), 2434-2436 (2001).

[Lin 1999] Lin S.-Y., Fleming J.G., Sigalas M.M., Biswas R., and Ho K.M., "Photonic band-gap microcavities in three dimensions", *Phys. Rev. B*, 59(24), R15579–R15582 (1999).

[Liu 1997] Liu X., Du, D., and Mourou, G., "Laser ablation and micromachining with ultrashort laser pulses", *IEEE Journal of Quantum Electronics*, 33(10), 1706-1716 (1997).

[Lou 2003] Lourtioz J.L., Benisty H., Berger V.and Gérard J.M., *Les cristaux photoniques ou la lumière en cage*, Hermes Science Publications (2003).

[Lou 2004] Lourtioz J.M., *Cristaux photoniques et gaps de photons: propriétés et applications*, Techniques de l'ingénieur AF 3 711, 1-17 (2004).

[Lou 2004b] Lourtioz J.M., *Cristaux photoniques et gaps de photons : aspects fondamentaux*, Techniques de l'ingénieur AF 3 710, 1-16 (2004).

[Mai 2003] Mailis S., Riziotis C., Smith P.G.R., Scott J.G.and Eason R.W., "Continuous wave ultraviolet radiation induced frustration of etching in lithium niobate single crystal", *Appl. Surf. Sci*., 206, 46-52 (2003).

[Mas 2004] Massy S., Contribution à la réalisation de fonctions optiques à base de cristaux photoniques sur $LiNbO_3$, PhD Thesis, University of Limoges, France, 2004.

[Meg 2001] Megens M.and Vos W.L., "Particle Excursions in Colloidal Crystals", *Physical Review Letters*, 86(21), 4855-4858 (2001).

[Mer 2003] Merle Y. Etude de la dispersion électromagnétique dans les matériaux périodiques diélectriques bidimensionnels, PhD Thesis, University of Limoges (2003).

[Mil 2005] Milenin A.P., Jamois C., Geppert T., Gösele U.and Wehrspohn R.B., "SOI planar photonic crystal fabrication: Etching through $SiO_2/Si/SiO_2$ layer systems using fluorocarbon plasmas", *Microelectronic Engineering*, 81(1), 15-21 (2005).

[Min 2002] Mingaleev S.and Kivshar Y., "Nonlinear photonic crystals: toward all-optical technologies", *Optics and Photonics News*, 49-51 (2002).

[Miz 2001] Mizeikis V., Juodkazis S., Marcinkevicius A., Matsuo S.and Misawa H., "Tailoring and characterization of photonic crystals", *J. of Photochemistry and Photobiology C: Photochemistry Reviews*, 2, 35-69 (2001).

[Nak 2002] Nakao M., Oku S., Tanaka H., Shibata Y., Yokoo A., Toshiaki Tamamura and Hideki Masuda, "Fabrication of GaAs hole array as a 2D-photonic crystal and their application to photonic bandgap waveguide", *Optical and Quantum Electronics*, 34, 183-193 (2002).

[Nod 2000] Noda S., Chuntinan A.and Imada M., "Trapping and emission of photons by a single defect in a photonic bandgap structure", *Nature*, 407, 608-610 (2000).

[Nod 2000] Noda S., Tomoda K., Yamamoto N.et Chutinan A., "Full three-dimensional photonic bandgap crystals at near-infrared wavelengths", *Science*, 289, 604-606 (2000).

[Not 2001] Notomi M., Shinya A., Yamada K., Takahashi J., Takahashi C.and Yokohama I., "Single mode transmission within photonic bandgap of width-varied single-line-defect photonic crystal waveguides on SOI substrate", *Electronic Letters*, 37, 293-295 (2001).

[Ozb 1994] Özbay E., Michel E., Tuttle G., Biswas R., Sigalas M., Ho K-M., "Micromachined millimeter-wave photonic band-gap crystals", *Appl. Phys. Lett*., 64, 2059-2061 (1994).

[Pai 1999] Painter O.J., Husain A., Scherer A., O'Brien J.D., Kimi.and Dapkus D., "Room-temperature photonic crystal defect laser at near-infrared wavelengths in InGaAsP", *J. Lightwave Technol*., 17, 2082-2088 (1999).

[Par 2005] Park W.J., Yang W.S., Kin W.K., Lee H.Y., Lim J.-W., Isshiki M.and Yoon D.H., "Ridge structure etching of $LiNbO_3$ crystal for optical waveguide applications", *Optical Materials*, 28(3), 216-220 (2005).

[Per 2006] Perriere J., Millon E., Fogarassy E. (Eds), *Recent Advances in Laser Processing of Materials*, Elsevier (2006).

[Pis 2004] Pissadakis S., Ikiades A., Tai C.Y., Sessions N.P.and Wilkinson J.S., "Sub-micron period grating structures in Ta_2O_5 thin oxide films patterned using UV laser post-exposure chemically assisted selective etching", *Thin Solid Films*, 453/454, 458-461 (2004).

[Pro 1995] Pronko P.P., Dutta S.K., Squier J., Rudd J.V., Du D.and Mourou G., "Machining of sub-micron holes using a femtosecond laser à 800 nm", *Optics Communication*, 114, 106-110 (1995)

[Pur 1946] Purcell E.M., "Spontaneous emission probabilities at radiofrequencies", *Phys. Rev.*, 69, 681-683 (1946).

[Rai 2004] Raineri, C.Cojocaru, P.Monnier, C.Seassal, X.Letartre, P.Viktorovitch, A.Levenson, Raj R., "Ultrafast dynamics of the third order nonlinear response in a 2D InP-based photonic crystals", *Appl. Phys. Lett.*, 85, 1880-1883 (2004)

[Res 2000] Restoin C., Darraud-Taupiac C., Decossas J.L., Vareille J.C., Hauden J.and Martinez A., "Ferroelectric domain inversion by electron beam on $LiNbO_3$ and Ti:$LiNbO_3$", *Journal of Applied Physics*, 88(11), 6665-6668 (2000).

[Res 2003] Restoin C., Massy S., Darraud-Taupiac C., and Barthelemy A., "Fabrication of 1D and 2D structures at submicrometer scale on lithium niobate by electron beam bombardment", *Optical Materials*, 22, 193-199 (2003).

[Rom 2003] Romanato F., Businaro L., Vaccari L., Cabrini S., Candeloro P., De Vittorio M., Passaseo A., Todaro M.T., Cingolani R., Cattaruzza E., Galli M., Andreani C., Fabrizio E.Di, "Fabrication of 3D metallic photonic crystals by X-ray lithography", *Microelectronic Engineering*, 67/68, 479-486 (2003).

[Rom 2004] Romo G.and Smy T., "Dispersion relation calculation of photonic crystals using the transmission line matrix method", *International Journal of Numerical Modelling: Electronic Networks, Devices and Fields*, 17, 451-459 (2004).

[Sal 1991] Saleh Bahaa E.A. and Teich M.C., *Fundamentals of Photonics*, Wiley Interscience, (1991).

[San 1999] Sanchez F., *Optique non linéaire*, Ellipse (1999).

[Sca 2001] Scalora M., Bloemer M.J., Bowden C.M., D'Aguanno G., Centini M., Sibilia C., Bertolotti M., Dumeige Y., Sagnes I., Vidakovic P. and Levenson A., "Non-linear frequency conversion", *Optics and Photonics News*, 12(4), 39-42 (2001).

[Sco 2004] Scott J.G., Boylan A.J., Mailis S., Grivas C., Wagner O., Lagoutte S. and Eason R.W., "Self-ordered sub-micron structures in Fe-doped LiNbO3 formed by light-induced frustration of etching", *Appl. Surf. Sci*., 230, 138-150 (2004).

[Sha 2002] Sharkawy A., Shi S.and Prather D.W., "Electro-optical switching using coupled photonic crystal waveguides", *Optics Express*, 10(20), 1048-1059 (2002).

[Shi 2005] Shi S., Chen C., and Prathe D.W., "Revised plane wave method for dispersive material and its application to band structure calculations of photonic crystal slabs", *Applied Physics Letters*, 86, 043104-043107 (2005).

[Thè 1999] Thèvenot M., Reineix A.and Jecko B., "FDTD approach for modelling PBG structures", *J. Opt.A: Pure Appl. Opt.*, 1, 495-500 (1999).

[Vil 1992a] Villeneuve P.R.and Piché M., "Photonic band gaps in two-dimensional square lattices: Square and circular rods", *Physical Review B*, 46(8), 4973-4975 (1992).

[Vil 1992b] Villeneuve P.R.and Piché M., "Photonic band gaps in two-dimensional square and hexagonal lattices", *Physical Review B*, 46(8), 4969-4972 (1992).

[Wu 2003] Wu N., Javanmard M., Momeni B., Soltani M.and Adibi A., Xu Y. and Lee R.K., "General methods for designing single-mode planar photonic crystal waveguides in hexagonal lattice structures", *Optics Express*, 11(12), 1371-1377 (2003).

[Xia 1999] Xia Y., Gates B.and Park S.H., "Fabrication of three-dimensional photonic crystals for use in the spectral region from ultraviolet to near-infrared", *J. of Lightwave Technol*., 17(11), 1956-1962 (1999).

[Yab 1987] Yablonovitch E., "Inhibited spontaneous emission in solid-state physics and electronics", *Phys. Rev. Lett*., 58, 2059-2062 (1987).

[Yab 1993] Yablonovitch E., "Photonic band-gap structures", *J. Opt. Soc. Am.B*, 10(2), 283-295 (1993).

[Ye 2004] Ye J-Y., Matsuo S., Mizeikis V.and Misawa H., "Silicon-based honeycomb photonic crystal structures with complete photonic band gap at 1.5 mm wavelength", *Journal of Applied Physics*, 96(11), 6934-6936 (2004).

[Yee 1966] Yee K.S., "Numerical solution of initial boundary value problems involving Maxwell's equations", *IEEE Trans. Antennas and Propagation*, 14, 302-307 (1966).

[Yos 2001] Yoshie T., Vuckovic J., Scherer A., Chen H.and Deppe D., "High-Quality slab photonic crystals slab cavities", *Appl.Phys.Lett*., 79, 4289-4291 (2001).

[Zha 1997] Zhang W., Hu A.and Ming N., "The photonic band structure of the two-dimensional hexagonal lattice of ionic dielectric media", *J. Phys.: Condens. Matter*, 9, 541–549 (1997).

This page intentionally left blank

Conclusion

Until recently all communication systems have relied on the transmission of information via electrical cables or have made use of radio frequency and microwave electromagnetic radiation propagating in free space. However, optical communication is now coming into its own and is becoming the preferred technology in many applications. In this way, integrated electronic circuits have defined the 20th century as the century of electronics, whilst the 21st century is emerging as the century of photonics – as a result of light wave technology. The success of this evolution will lead to the development of new optoelectronic devices, a field where innovations are progressing at "light velocity".

Thus, light (the photon) increasingly penetrates every aspect of our everyday lives.

The objective of this book is to provide readers with the basis of the integrated optics discipline, which made it possible to carry out this important technological leap. This didactic tool is appropriate for young researchers starting in the field, and could be used as a teaching support for a course at Master's degree level.

Work in integrated optics generally starts by considering two principal issues: the optimization of waveguide fabrication parameters and the characterization of the resulting structures as accurately as possible. Once the optimized conditions are found, the development of integrated optical components can be considered.

The principal aspects of planar waveguide theory were discussed in Chapter 1, allowing us to define the conditions necessary for light confinement in a three layer structure of step or graded index. Thereafter, the channel waveguide and propagation in anisotropic mediums were explained.

Chapter 2 presented the main fabrication techniques of waveguides. The guiding structures can be created either by modification of refractive index of a mono-crystal or by deposition of a thin layer on a low index substrate. This last process makes it possible to fabricate integrated optical components compatible with the already existing optoelectronics technology. However, we focused on $LiNbO_3$ waveguides. This crystal is one of the most important optical materials. It has virtually all the physical properties necessary to develop optoelectronic components of any kind. Generally, the two most frequently used fabrication techniques (with this material) are ionic exchange and diffusion. However, the extension of these techniques to other potentially interesting crystals is far from obvious. From this point of view, ionic implantation is an alternative that appears less disturbing for the crystalline matrix and which can be performed at ambient temperature. This technique has been developed for more than 20 years and is now matured and well established, emphasizing its practical use. The implantation technique has been given more attention within this chapter.

From the materials point of view, much remains to be created in order to meet the optoelectronics requirements. We can distinguish five families of optical materials usually used in the field of optoelectronics or integrated optics. The first, silicon-based materials, constitute the strong link between electronics and photonics: many photonic components took advantage from the development of Si-based electronics. The second relates to semiconductor materials in general: for example, III-V or II-VI semiconductors offer many applications for light emission and detection. The third is dielectric materials: these crystals generally have non-linear optical properties, which confer on them potential applications for optical signal processing via refractive index structuring and manipulating; for example, $LiNbO_3$ is the best-known dielectric material and has been used for many years for optoelectronic components fabrication. The fourth type of materials relates to organic or polymers: they are particularly interesting for electro-optic modulation or non-linear optics. Finally the fifth family relates to integrated optics on glass, which allows the development of various components at low cost.

Generally, the material must present a good compromise between its optical properties, its homogenity, its structure and its transparency. Moreover, the facility of growth (synthesis) of materials is also an important criterion. All these ideas were developed in the second part of Chapter 2.

Nevertheless, optical waveguide fabrication can be, in certain cases, prejudicial to the linear and non-linear optical properties of the guiding area. For this reason, it is of primary importance to control and test the waveguide features according to the fabrication parameters before the final use of the guide. The presentation of waveguide characterization techniques was addressed in Chapter 3. We mainly focused on m-line spectroscopy which uses prism coupling to excite the guided

modes of the structure. This method makes it possible to measure precisely, according to various parameters, the opto-geometrical properties of the guides. Losses within the guides are also an important factor in the realization of integrated optical components. A discussion of their origins and the techniques for their measurement are also presented in Chapter 3.

From the industrial point of view, two optoelectronic components, laser micro-sources and electro-optic modulators, are vitally important for any optical functional system. Fundamentally, electro-optic modulators and compact solid lasers lie at the foundation of the overall design of optical systems. From an economic point of view, the market for optoelectronics components has been recently estimated to be more than $23 billon, of which compact lasers and EO modulators constitute a very important part. A strong growth is also predicted for the next few years.

Consequently, these components are still subject to much research and development activity. Indeed, the laser industry has always been interested in the use of frequency conversion to widen the range of wavelengths available. In particular short wavelengths, which find many applications in several fields: high density optical data storage, the medical and biological field, data optical treatment and transmission on plastic fiber, etc. Infra-red wavelengths have applications in medical fields (zones of absorption of water) and in the military industry (windows of atmosphere transparency). It may be that frequency conversion-based systems play a very important role in producing efficient compact coherent light sources. For example, the use of a Nd^{3+} doped YAG crystal emitting at 1.06 μm with a non-linear crystal to obtain a visible light at 532 nm is a well-established system with an acceptable efficiency.

Moreover, employing optical waveguide configurations allows improvement of the conversion efficiency and provides a low pump light source power. In addition, it makes it possible to miniaturize laser devices, which is very convenient for practical large use. This is particularly realistic because pump sources in the range of 800 nm-1.6 μm are available at low cost since this technology already exists for optical fiber communication systems. Sources with power of 1 mW to 1 W can then be coupled with optical waveguides to generate visible light. Efficiencies of 200%/W to 500%/W based on this principle have already been reported with 1 cm waveguides. In addition, the coupling pump source to the waveguide problem which might influence the conversion efficiency is solved using the same technology of optical fiber connections.

Among other major advantages of frequency conversion within waveguides, is that we can use quasi-phase matching (QPM) processes to increase the efficiency of the system. Using QPM is also of great interest for generating all suitable wavelengths in the transparency range of the material depending on the period of

the reversed domain. Therefore, light ranging from UV to red can be produced. This hot topic of non-linear integrated optics was presented in Chapter 4.

The second link in the chain of optical communication systems concerns the modulation of light signals. This modulation could be internal, in the case of diode sources, or external, using physical phenomena such as the electro-optic or the acousto-optic effects. The most commonly used technique is of course electro-optic modulation which allows a high rate of modulation and enlarges the bandwidth. The use of guiding structures offers low power signal processing. Until now the common waveguiding structures employed for this purpose have been based on Ti diffused $LiNbO_3$ or exchanged $LiNbO_3$ guides; however, many problems remain unsolved and a better understanding of these difficulties is needed. Moreover, the use of implanted waveguides for EO modulation is a very likely alternative.

All these aspects were covered in Chapter 5.

With regard to photonic crystals, technological and theoretical projections allowed the emergence of several concepts of configurable components related to the changes of dimensionality or the variation of the index contrast, which we can induce using an optically active material. The principal ideas of this field were covered in Chapter 6.

The possibility of handling and machining materials on a sub-micrometric scale is a dream that is coming true. Since the first ideas were put forward by R. Feynman (Nobel Prize) in the 1950s, many achievements have showed the scientific, technological and economic viability of the nanotechnology concept. This also applies to the photonic field. Indeed, this new approach makes it possible to miniaturize the photonic components allowing for more effective photon molding. Under these conditions, new functionalities and new components will be possible.

Integrated optics appears today as a promising technology for the coming decades, in the context of the development that optoelectronics must take. This is especially due to the maturity of all the essential components needed for an optoelectronic complete chain at low cost. From this perspective, we easily understand the importance of the entire investigation chain: fabrication tools, characterization methods, test and control of guiding structures.

This approach (considering the entire investigation chain) makes it possible to carry out a return in “real time”, on the fabrication parameters, in order to adjust the characteristics of the material to better meet the integrated optics requirements. Under these conditions, it would also be easy to consider the development of components and functional devices containing these guiding structures. These problems are the principal motivation of this book.

Index